University of Trento
University of Brescia
University of Bergamo
University of Padova
University of Trieste
University of Udine
University IUAV of Venezia

ELVIS CESCATTI (Ph. D. Student)

# COMBINED EXPERIMENTAL AND NUMERICAL APPROACHES TO THE ASSESSMENT OF HISTORICAL MASONRY STRUCTURES

Prof. Claudio Modena (Tutor)

2016

UNIVERSITY OF TRENTO
Engineering of Civil and Mechanical Structural Systems - XXVIII Cycle

Prof. Paolo Scardi (Ph. D. Head's)

Final Examination 04/04/2016

Board of Examiners:

| | |
|---|---|
| Prof. Claudia Battaino | (University of Trento) |
| Prof. Herve Degee | (Hasselt University) |
| Prof. Andrea Vignoli | (University of Firenze) |
| Prof. Elizabeth Vintzileou | (National Technical University of Athens) |

**SUMMARY**

The assessment and the conservation of historical masonry structures are very challenging issues. According to the actual methodology, all the phases of the entire process of assessment require efforts and reciprocal comparison in order to understand reliably the structural behaviour and to design effective interventions.

This thesis goes through such phases (anamnesis, diagnosis and treatment), introducing some innovations in each step and connecting the experimental experiences to models with the support of some real cases. Three techniques are developed about the knowledge phase, namely sonic test, flat jacks and dynamic identification. Deeper studies have been dedicated to vault systems by means of an extended experimental campaign and a reverse analysis to better understand the behaviour of structures and, at the same time, the limits of models. Sometime this comparison suggests a lack between model parameters and physical meaning due to modelling approaches (mesh, element type) and parameters (material properties and constitutive laws) and this gap may be fulfil by both local and global tests.

From the experimental point of view this work presents a wide range of tests from the local to the global behaviour and varying among non-destructive, minor destructive and destructive tests. On the other hand for models, both linear and non-linear approaches have been adopted looking as well to local and global phenomena. Finally, about the deepest analysis on vaults even the scale of modelling was evaluated with the comparison between macro and meso-scale modelling. In this framework some proposal in kinematic analysis of strengthened vaults were provided.

The work carried out allows therefore to compare traditional and more used tools for structural assessment purposes with real and measured experiences helping to validate the current methodology in the safety evaluation of existing buildings.

**Tutor**
Prof. Claudio Modena

**Ph. D. Head's**
Prof. Paolo Scardi

**SOMMARIO**

La valutazione della vulnerabilità e la conservazione dei beni storici sono un intrigante e attuale tema di sviluppo. Seguendo l'attuale metodologia, tutte le fasi del processo di verifica richiedono un continuo confronto tra loro così da ottenere valutazioni di sicurezza efficaci e che intuiscano approfonditamente il reale comportamento strutturale col fine di progettare interventi efficaci e mirati che seguano le regole della conservazione.

La tesi si sviluppa attraverso ciascuna fase metodologica (conoscenza, diagnosi e intervento), introducendo alcune innovazioni in ciascuna di esse. In particolare nella fase conoscitiva si sono sviluppate le prove soniche, i martinetti e le identificazioni dinamiche.

A seguito delle osservazioni sugli elementi più colpiti dai terremoti e alla diffusa presenza di elementi voltati nell'edilizia storica, si sono approfondite le analisi e gli studi su questo elemento strutturale con una esaustiva campagna di indagine messa poi a confronto con i consueti strumenti e metodi di verifica al fine di comprendere limiti e vantaggi di questi ultimi. Successivamente, tramite l'applicazione di alcuni rinforzi, si è avuto un'ulteriore contributo sullo studio delle tecniche di intervento da adottarsi a seguito del giudizio di sicurezza.

Da un punto di vista sperimentale, il lavoro proposto presenta una vasta serie di prove sperimentali, sia a livello locale che globale e comprendendo prove con diversi gradi di invasività (non distruttive, parzialmente distruttive e distruttive). Al contempo, dal punto di vista dei modelli si sono considerati sia metodi lineari sia non lineari con analisi locali e globali. In particolare si sono anche potuti confrontare diversi tipi di modellazione.

Nel complesso quindi, il lavoro ha permesso di comparare e valutare i classici metodi di analisi della sicurezza strutturale con risultati sperimentali e reali contribuendo quindi a valutare la corrente metodologia di verifica degli edifici storici esistenti.

**Tutor**
Prof. Claudio Modena

**Ph. D. Head’s**
Prof. Paolo Scardi

A SERENA

*"If the designer can find a way*
*in which the structure behaves satisfactorily,*
*the structure itself certainly can"*
*Jacques Heyman*

*"la struttura è il miglior modello di se stessa"*
*Claudio Modena*

**ACKNOWLEDGEMENTS**

*Il mio primo e più sentito ringraziamento va al Prof. Claudio Modena per avermi dato la possibilità di seguire questo interessante e costruttivo percorso di ricerca e per avermi appoggiato nell'impegnativa avventura delle prove in cantiere. La grande esperienza, la profonda conoscenza, l'intelligenza e la sconfinata passione che lo contraddistinguono prima di tutto come ingegnere e poi come professore mi hanno trasmesso davvero tanto. Grazie anche a Maria Rosa e Francesca per avermi consentito di approfondire le ricerche nel campo della diagnostica.*

*Poiché l'intelligenza umana non è il prodotto di un cervello ma della collaborazione tra cervelli, che avviene dove i cervelli giusti si possono incontrare, un sentito ringraziamento va tutto il gruppo di ricerca, in particolare alla 'vecchia guardia' Massimo, Filippo, Enrico, Matteo, Paolo, Marco, Nicola e Giovanni con cui sono riuscito a discutere costruttivamente e che hanno speso tempo per darmi preziosi consigli utili sia sulla ricerca sia sul mio percorso e che hanno quindi contribuito in maniera sostanziale alla riuscita del lavoro e alla mia crescita personale.*

*Grazie a Fabio CiP, compagno di avventure e disavventure che non si tira mai indietro anche nelle esperienze di cantiere. A Michele, Luca, Diego e Mauro che hanno contribuito anche fisicamente alla parte sperimentale on-site ed ai tecnici di laboratorio. Un grazie anche a tutti gli amici: Sabrina, Marta, Claudie, Riccardo, Filippo, Nicolò, Alberto, Laura, Athanassios, Elena, Marco, Francesco e Giovanni per i consigli e i momenti condivisi.*

*Poiché la teoria senza la pratica è semplicemente pericolosa, un sentito grazie va a tutti gli amici e colleghi di SM Ingegneria, dai preziosi suggerimenti di chi sapientemente dirige a chi ha speso tempo per insegnarmi cose e condividere esperienze. In particolare a Mirko per avermi assistito già dai primi passi, a Massimiliano per la puntuale ed efficiente collaborazione in cantiere e a Daniele per la disponibilità, i suggerimenti e gli incitamenti nell'affrontare gli elementi finiti. Posso dichiarami veramente fortunato ad aver incontrato così tanti amici a cui devo molto.*

*Infine voglio ringraziare anche tutti i tesisti che hanno condiviso con me alcuni tratti di ricerca perché seguirli è stato un modo per imparare e crescere.*

*Thanks to all guys who attend the master SAHC because they always teach me a lot and because is inspiring to work with them. In particular I want to acknowledge Larisa for the time spent with me and to my friend Kacper, for the help, the interest and the passion in learning and teaching.*

*Ringrazio tutta la Fondazione Cariverona e in particolar modo l'Ing. Avesani per aver acconsentito e sostenuto la ricerca e a Kerakoll S.p.a., in particolare l'Ing. Paolo Casadei e l'Arch. Massimiliano Magagnoli, per aver contribuito alla realizzazione dei campioni.*
*La ricerca è stata possibile grazie al progetto PON-ProVACI (PON01_02324/7) e al Dipartimento Protezione Civile per il progetto ReLUIS Linea 1 Murature 2014-2016.*

*Un ringraziamento che va ben oltre questo dottorato va ai miei genitori Mario e Daniela e a tutti i miei famigliari perché mi hanno sempre appoggiato e aiutato incondizionatamente, devo a loro buona parte di quello che sono oggi.*

*Il più importante ringraziamento va alla persona che più di tutte scommette su di me in ogni istante, anche nei momenti più difficili o in quelli in cui le ho dato troppo poco spazio, per il supporto, l'incitamento e l'amore con cui mi ha accompagnato in questi anni e per la scelta di accompagnarmi da vicino per il futuro.*
*Grazie Serena che rendi speciale ogni momento.*

**TABLE OF CONTENTS**

## LIST OF FIGURES

## LIST OF TABLES

# 1 INTRODUCTION

## 1.1 BACKGROUND

The safety assessment of existing masonry buildings is one of the most fascinating topics in structural engineering because in their analysis the most advanced models are used despite they were designed without all the current knowledge and they are standing for centuries until nowadays.

Beyond the shadow of this paradox, some considerations and experiences on the capacity of Unreinforced Masonry (URM) and on the adopted analytical tools could provide a more understandable framework.

First of all it is worth to notice Heyman (see § 2.4.2) examination on design approaches in history where the analysis, especially for static loads, concerns geometrical proportions due to the typical behaviour of masonry which has a dramatic difference in resistance between the compressive and tensile field.

Two main issues characterize the demand of deepen analysis and research by means of sophisticated tools and experimental campaigns:

- the changing in behaviour for strengthened masonry sections compared with URM ones;
- the analysis of URM structures under seismic actions.

The earthquake which hit the Friuli region in Italy in 1976 strongly increases the attention on seismic issues and highlights some vulnerability of existing buildings. Moreover the next earthquakes occurred (i.e. Umbria-Marche 1997 and L'Aquila 2009) figured out how the refurbishment projects, carried out in following

years and mainly based on tools developed for new structures, were lack in estimations and sometimes showed worst damages than plain buildings. Such experiences, pointed out two crucial aspects:

- lack in knowledge of mechanisms, damages and vulnerabilities of masonry buildings under seismic action,
- lack in knowledge of predictive models, mechanical interpretations and effectiveness of intervention.

This aspects state a strong principle in restoring existing building which concerns the deep knowledge of structures based on constructive technique, load bearing mechanisms, material properties and historical development. The assessment procedure should look at the general meaning of the structural safety by the use of: investigation techniques, analytical model of structures, intervention techniques and structural health monitoring [Modena 2008]. Giuffré [2010], on the path of the Venice Charter [1964], concluded that the restoration process should pass through a multidisciplinary discussion able to draw together to the final solution which does not only matter the structural aspects.

In addition to this debate, an increase of interest in this field is international with the rise of several guidelines and standards [ASCE 41-13; Eurocode 8; LLGGBBCC 2010]. ISCARSAH [2005] has established a methodological procedure to assess historical structures by means of four main phases: knowledge, analysis, intervention and monitoring. The importance of the first phase is also stated in ISO 13882 [2010] which reports: "the establishment of principles for the assessment of existing structures is needed because it is based on an approach that is substantially different from design of new structures, and requires knowledge beyond the scope of design codes".

The second phase is also relevant and concerns the development of analytical tools and their verification. Tests on full scale existing elements allow to understand advantages and drawbacks of each computational tool. The monitoring phase (see § 2.1) will be here used as a continuous cross check among phases but was not implemented in a continuous way. The peculiar analysis on vaults also permitted to focus on some interventions on these elements looking at traditional and innovative purposes.

## 1.2 OBJECTIVES AND MOTIVATIONS

The aim of the thesis is to evaluate, improve and provide little innovations in each field of the safety evaluation methodological path of existing masonry buildings, moving in parallel between real cases and numerical applications.

To join this methodological aspect with experimental and detailed analyses a structural element has been selected. The wide diffusion on historical buildings of vaults and the analysis on earthquake damages pointed out the needs of deepen researches on this element. Moreover, the comparison between models and destructive tests is suitable for structural elements rather than entire buildings because of evident feasibility reasons.

Specifically for each phase the goals are:

- **Information and investigation**: three tests were focused to obtain more effective tools to increase the structural knowledge and to look by datasets at typical ranges in historical buildings. Specifically are:
  i. sonic test, that need an automatic and more objective procedure to detect the flight time,
  ii. the double flat jack technique, that needs a unified procedure in execution and interpretation,
  iii. dynamic identification in estimation of axial tension inside tie rods that need an evaluation of reliability.
- **Diagnosis and safety evaluation:** the comparison between the analytical tools and approaches commonly used in the structural assessment with an actual value of ultimate load, measured by an experimental campaign, aims to evaluate the current methodology.
- **Decision on interventions**: within the intervention on vaults looking at traditional and innovative solutions it is necessary to evaluate their effectiveness, their costs and their workability impacts;
- **Monitoring**: the evaluation of the dynamic tools involved in SHM to detect the rise of damage in a structural element with a controlled damage wish to confirm their effectiveness.

## 1.3 THESIS OUTLINE

The work was carried out in the framework of two national research projects: one commissioned by the Italian civil defence department to the Re.L.U.I.S. consortium and one called Pro.Va.C.I. which has the goals to protect, appraise and develop cultural sites in sustainable ways.

After the mandatory literature review to understand the current state-of-art, the thesis goes through the methodological phases (anamnesis, diagnosis and treatment), introducing some innovations in each step and connecting the experimental experiences to models with the support of some real cases. CH 2 describes also motivations which lead to select vaults as element to analyse in depth. The historical building typology defined by Violet Le Duc and confirmed by the study of pilot cases, selected for the ProVaCI project, pointed out that historical structures have horizontal diaphragms mainly made by timber floor or vaulted systems. In addition, the analysis of earthquake damages carried out through the database of the department of Civil and Environmental Engineering of the University of Padova shows that vaults are among the most highly activated mechanism during earthquake. Because of that, deeper studies have been dedicated to vault systems by means of an extended experimental campaign and a reverse analysis to better understand the behaviour of structures and, at the same time, the limits of models. Sometime this comparison suggests a lack between model parameters and physical meaning due to modelling approaches (mesh, element type) and parameters (material properties and constitutive laws), thus this gap may be fulfil by both local and global tests.

The parameters estimation in existing constructions not only allows to achieve better results on models but increases the reliability of the entire structural assessment. In this background, the knowledge phase became a fundamental stage of the assessment also looking at the retrofit with the goal of the minimum interventions. The diagnosis has to be combined with several techniques, both quantitative and qualitative. Many times the latter are not properly considered by practitioners but this work will highlight their importance especially if correlated among them. The three techniques more developed in this thesis are sonic test, flat jacks and dynamic identification presented in CH 3. The first one has been developed by the implementation of an algorithm which automatically figured out flight times and consequently controls the signal accuracy. The second one looks at how to define the masonry properties and how to interpret the test. On-site is difficult, expensive and sometime unfeasible, to obtain the exact material properties like the ones obtained by characterization tests made on lab. To overcome this is

necessary to develop MDT tests with proper procedures and interpretations. The use of an extended warehouse of data, herein shown, simplifies this work. The third technique is the dynamic identification which does not work locally on the material properties but it concerns the structural element or the entire structure and it helps to understand the dynamic global behaviour. Finally, some example will demonstrate how these techniques are also useful after the intervention, when needed, to control the efficacy of the intervention itself.

Thanks to these observations a more detailed analysis on vaults has been carried out in this work. To achieve this, one case study, chosen among the demonstration sites and presented in CH 4, is the St. Peter's Castle. The study was carried out from local to global aspects with both, models and experimentations. About the experimental campaign a first characterization of materials has been performed mainly on-site. In this case study it was possible to look at the element itself as well as to its contribution in the global behaviour of the entire structure. Some tests, in the tower and in the whole castle have been performed in order to carry out the influence of vault in the global dynamic response.

Thanks to a local demolition of one vault in a room of the castle, due to the refurbishment project, five full scale masonry vaults were obtained and tested. Experimental results are presented in CH 5. The aim of the experimental campaign was to evaluate the different response of several strengthening interventions. The selected interventions concern one reference vault (UR), one strengthened with the most used traditional technique which deal with the addition of diaphragm (DIA). The other three were strengthened by composite materials with an Externally Bounded Reinforcement (EBR) technique on the extrados by the application of: Carbon Fibre Reinforced Polymer (CFRP) on epoxy resin, steel wires in lime mortar called Steel Reinforced Grout (SRG) and Basalt net in a mortar matrix here called Basalt Textile Reinforced Mortar (BTRM). The test were executed cyclically in force control and performed until failure, this allows to highlight the whole vault behaviour for each step. The static unconventional test required a careful design of the test set-up composed by a dedicated counteract steel frame and some ties to constrain the trust on walls resulting by the applied load.

The test has the goal to analyse in detail the changing in failure mode due to the addition of composite and it considers the variation in maximum load and ductility. The state of art lacks indeed in experimental campaign on vaults strengthened with FRCM on existing structures. After this, some sensitivity analysis and models was carried out to understand and figured out the most relevant parameters and to manage the extension of results to similar situations.

CH 6 analyses current evaluation instruments namely limit analysis and FEM to compare these powerful tools, usually adopted at global scale, at the local scale where the comparison with experimental results is suitable. Some issues are hence pointed out in the field of strengthening with EBR techniques.

CH 7 focuses in the evaluation of the thrust acting on walls which is another problem of existing vaults. A very useful data in the assessment of the whole system could be given by the axial force acting in ties. In this work are presented the most typical ranges and a laboratory experimental campaign to evaluate this force and some purposes of tools to figure out reliably estimations. The modelling aspects are faced with a modal analysis which keeps into account the internal state stress that modifies the stiffness matrix usually adopted for the linear modal analysis.

Summarizing from the experimental point of view this work presents a wide range of tests from the local to the global behaviour and varying among non-destructive, minor destructive and destructive tests. On the other hand about models, both linear and non-linear approaches have been adopted looking as well to local and global phenomena. Finally, about the deepest analysis on vaults even the scale of modelling was evaluated with the comparison between macro and mesoscale modelling.

# 2 LITERATURE REVIEW

## 2.1 ASSESSMENT OF EXISTING BUILDING

The assessment of an existing building is a very challenging issue that requires a multidisciplinary approach based on an established methodology. This methodology is continuously developed in terms of conservative restoration and technical criteria.

The earthquake that strokes the Friuli region in Italy in 1976 strongly increases the attention on seismic issues and highlights some vulnerability of existing buildings. Moreover the next earthquakes occurred (i.e. Umbria-Marche 1997 and L'Aquila 2009, Emilia 2012) figured out how the refurbishment projects carried out in following years, mainly based on tools developed for new structures, where lack in estimations, and sometimes they showed worst damages than original buildings [Modena 2012].

Such experiences pointed out two crucial aspects that have to be analysed in depth:

- seismic actions, mechanisms and damages on existing masonry buildings and their vulnerabilities;
- predictive models, mechanical interpretations and effectiveness of interventions.

This paragraph aims to focus on such points by the review of the actual state of art to figure out the still open issues. The clever concept of capacity design, well established in new constructions is anyway effective in existing ones. The failure of

a structural system is concentrated on the weakest link of the chain. If on one hand the design of new constructions allows to decide which is this link, the tricky point on existing buildings is hence to proper evaluate the weakest mechanism.

For example many times earthquakes have showed that local vulnerabilities, related for example to overturn or to masonry crumbling, results in collapse without the activation of the global behaviour. Three levels are recognised and sorted by decreasing vulnerability are: material level, element level and global level.

Fig. 2.1 (left) shows the weakest mechanism which occurs at material level and it concerns the masonry crumbling. This occurs for low value of acceleration and results in the wall collapse. Giuffrè [1993] (see Fig. 2.2 left) analysed this effect also for static loads as a typical failure mode of the element in compression underlining the role of transversal connections. It is therefore crucial to underline the role of investigation, even qualitative, to point out such cases that are avoidable by means of local intervention.

Once the monolithically behaviour is ensured, failure can occur at the element level with the overturning of the façade (Fig. 2.1 right). Giuffrè [1993] divided local mechanisms in "*first damage mode*" if involves the out-of plane and "*second damage mode*" if involves the in-plane failure. The division in two levels stressed the order in which such damages occur. Also many other authors working on such aspects (Doglioni [1994], Lagomarisino [1997; 2004], Borri [1999]) observed and analysed possible mechanisms activated in buildings. Fig. 2.2 (right) shows some typical first damage modes which can occur in constructions [D'Ayala 2002]. About the knowledge on the prediction of these events, Tom Paulay and Nigel Priestley wrote in their textbook [Paulay 1992],

*"The response of masonry walls to out-of-plane seismic excitation is one of the most complex and ill-understood areas of seismic analysis."*

*Fig. 2.1 Material failure in San Michele Arcangelo, Celano (left)*
*local collapse, via Arrischia, L'Aquila (rigth)*

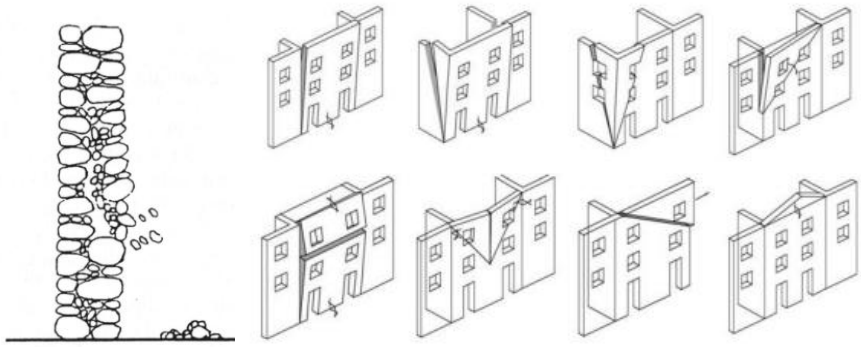

*Fig. 2.2 Crumbling in masonry wall [Giuffré 1993] (left)*
*damage mode collapse mechanism [D'Ayala 2002] (right)*

Despite considerations on analytical predictions of these mechanisms, considered later on, from simple evaluations on vulnerability it clearly appears that seismic risk mitigation can be severely reduced by avoiding first damage mode and crumbling that lead to tragic collapses, sometimes of the entire structure, and that can be avoided by local intervention. Once all these vulnerabilities do not occur the global box behaviour is activated. Fig. 2.3 shows the enrolment of the entire structure which bears seismic action in plane. The earthquake that strokes Emilia in 2012 highlighted the performances of structures acting globally [Modena 2012].

The proper maintenance or installation of connection between elements in order to achieve the *box behaviour* could improve significantly the seismic response of the entire structure. At this stage the second abovementioned point raises it role. If in on hand the intervention could be local (promoting its practical feasibility) the design of it should be carried out at the global level analysing the effects of it on the other structural elements. The experience accrued after strokes highlights also wrong approaches or unbalanced interventions.

*Fig. 2.3 Global behaviour of S.Agostino city council (Ferrara)*

In this framework is therefore crucial to underline that a careful design of intervention should look to the proper definition of the bearing mechanism involved in either unreinforced or reinforced conditions. The intervention criteria should also follow the restoration principle of: minimum intervention, reversibility, compatibility (in physical and chemical terms), durability and safety operated by distinctive and cutting edge interventions. ISCARSAH [2005] guidelines reports that: *qualitative judgements will play a role in these decisions which may be as important as quantitative data whole drawing a balance between ensuring structural stability and preserving the cultural values of the fabric taking into account social and economic factors as well.* Therefore analysis and interventions require an intense evaluation in the entire design process which is therefore a crucial phase where intense efforts should be spent.

The methodology was reported in international guidelines as presented in CH1. In literature Binda [1999] presented an important contribution with a multilevel approach to the damage assessment and seismic improvement of masonry buildings in Italy. Casarin [2006] showed a path to follow in the seismic assessment of buildings. Fig. 2.4 shows this process which underlines the need of a cross-check between the knowledge phase and the analysis phase and stresses the comparative evaluation between limit analysis and non linear modelling.

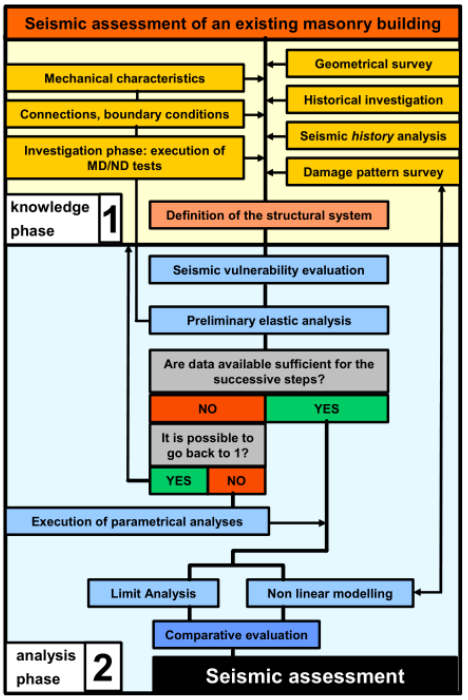


*Fig. 2.4 Methodology adopted: phases for the seismic assessment of an existing masonry building, Casarin [2006]*

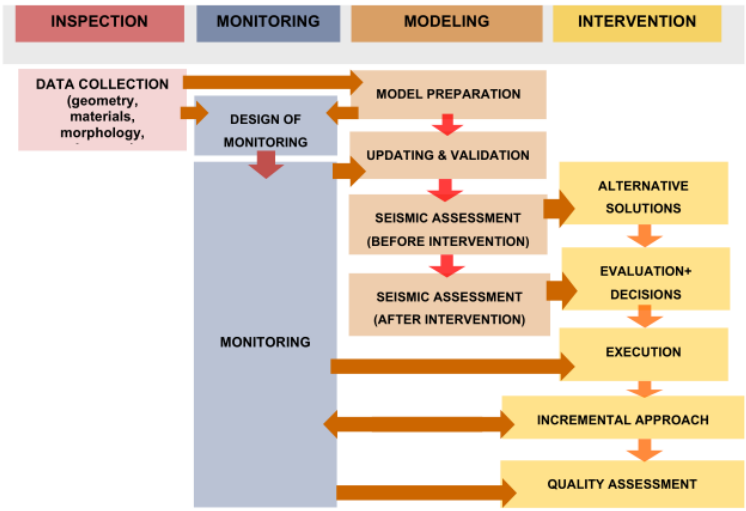


*Fig. 2.5 Methodology for the study and assessment of CH buildings [9.4, NIKER 2012]*

A further improvement of the methodology was given by the NIKER [2012] research project (Fig. 2.5) that introduces the intervention and monitoring phases. Because continuous monitoring is not always affordable, such phase could be related to the testing and diagnostic phase that can be applied as well pre, during and after interventions in order to obtain also a quality assessment, nevertheless, when possible the use of continuous monitoring is surely an optimal solution. For the point of view of the minimum intervention, the incremental approach and the prediction reliability are two key issues.

About the latter an emblematic work has been carried out by Lourenço [2015] who analysed collapse predictions of a masonry wall provided by 25 of the world's leading experts in the field. The first outcome concerns the basic steps followed by experts (Fig. 2.6) which agrees at least with the path presented by Casarin [2006] (Fig. 2.4). The second more important conclusion is that when all steps are carried out correctly the final response would be correct as well.

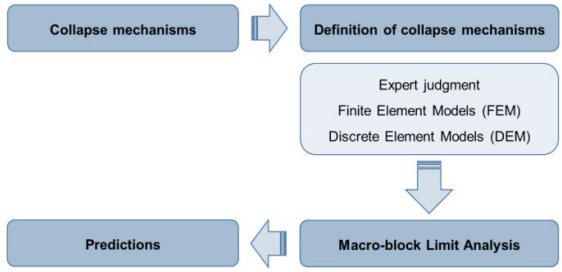


*Fig. 2.6 Predictive methodology currently adopted by experts [Lourenço 2015]*

This study provides a very interesting contribution because looked at the current cutting edge in this field and the average response demonstrated to be affected by a significantly variation. From the positive side generally predictions

were on the safety side leading to over strength structures but at least without causing life losses.

The key issue was related to the effective evaluation of the damaged condition and thus to the activated mechanisms. The ways adopted to achieve this were: DEM and FEM in static and dynamic non linearity. The relevance to select the actual mechanism was demonstrated and analysed by Casarin [2006] who quantified the error raised by an incorrect collapse mode selection (Fig. 2.7).

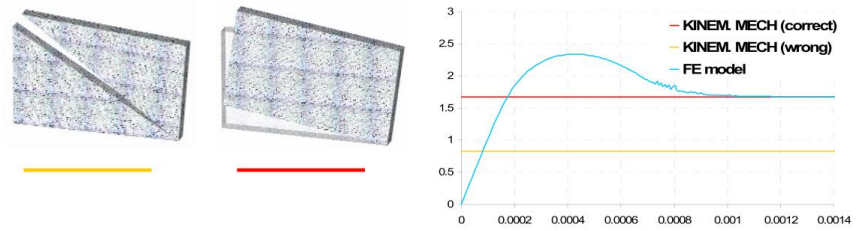


*Fig. 2.7 Influence of mechanism identification in the analysis of capacity [Casarin 2006]*

In addition to the analysis of URM, where the limit analysis is chosen for the numerical outcome, in reinforced masonry element this could not be still used without modification and the role of stiffness and strength distribution increases its effects.

After this review on model predictions the deep understanding on bearing mechanism acting on the structure, the masonry quality, the connection between elements and their interaction must be summarized by means of a serious knowledge phase and on the judgment to evaluate and calculate the correct collapse mechanisms.

In conclusion, quoting Lourenço [2015] :*Simple intuitive visualization of crack patterns for a three-dimensional structural system acknowledging effects of vertical compressive stress and overturning moment on rocking and sliding of piers or gables can lead to more accurate results than nonlinear dynamic analyses.*

## 2.2 MATERIAL LEVEL

This paragraph aims to present the current state-of-art about studies on two materials: masonry, the constitutive material of nearly all historical buildings in Europe; and composites, the innovative materials developed to provide tensile contribution to masonry. As it will be highlighted in the following, depending on the involved mechanism the knowledge of constitutive laws and failure modes of these

materials become crucial. About timber, the other typical material of historical buildings is not herein treated. The studies on metallic elements in this work do not regard directly the deepen analysis of material characteristics but it will be based on common literature assumptions.

### 2.2.1 *Mechanical characteristic of masonry*

Although masonry was the most used material in constructions the definition of its mechanical characteristics is still an open issue. First of all because this name refers to a material composed by units (clay brick, stone ...) and mortar (lime, cementitious...) arranged with several organized or irregular textures creating in fact any time a different material. Then, the material design is a current paradigm and masons who constructed buildings in centuries did not refer to this aspect. Finally historical masonries are there since a long time and hence suffer of ageing, damages, reworks and they also have a stress loading history that, in non linear materials is relevant.

In this apparently mess it has to be accounted that aside the considerations on the element safety which concern the sensitivity to each parameter, the scientific community deeply investigated the field recognising that, if properly classified by typologies, there are suitable typical ranges. Therefore the key issues are:

- to classify the investigate masonry,
- to establish its quality,
- to directly perform tests on it.

About classification Carbonara [1996], at least in Italy, is considered a reference manual in this topic with some mechanical interpretation by Giuffré [1990]. The classification is made looking at unit material and arrangement in plane and in the cross section. The Italian scientific community also works, in the framework of the GNDT, to define a survey instrument [GNDT, AA. VV., 2000] to objectively classify each typology referring to: general quality, regularity, unit material and shape; providing to the editor some examples.

In the international framework, guidelines provide mechanical ranges only for specific masonry categories (i.e. Solid clay brick, hollow brick) [EC-06, ACI 530-08 ASCE41-13]. The Italian masonry building stock represents a relevant percentage of existing buildings and the use of stone masonry is also significant part.

In the current Italian Technical Code for constructions [NTC 2008 and Circ. 617/2009] the approach defined concerns the masonry's typology classification. The code provides ranges (max and min) of mechanical characteristics for 11 typical masonry categories of existing constructions, observed in the Italian territory (see Tab. 2.1). It represents a strongly relevant tool for practitioners involved in the

assessment of existing masonry structures, and can be considered “innovative” with respect to other international guidelines. Moreover the CNR [203/2013] document provides a statistical interpretation of those data using a lognormal distribution with the mean value in the average of the range and with a standard deviation which provides the 13$^{th}$ percentile for the lower bound of the range. Due to the number of data collected for the table a statistical treatment seems to be premature. A revision is currently on-going to improve the contained information [Vignoli 2016]. A table shortcoming is the qualitative definition of stone categories by the standard that is not precisely specified yet, and not related with some objective tools. A possible tool to overcome this issue could be the quality index which refers to material properties, unit features and arrangement.

*Tab. 2.1 Figures proposed by Italian technical standards and documents*

| Masonry Type | $f_m$ [a] [N/mm$^2$] | $\tau_0$ [a] [N/mm$^2$] | E [a] [MPa] | G [a] [MPa] | $\sigma^{b*}_{ln,fcm}$ [N/cm$^2$] | $\sigma^{b}_{ln,Ec}$ [MPa] |
|---|---|---|---|---|---|---|
| Strongly irregular stone masonry - I | 1,00<br>1,80 | 0,020<br>0,032 | 690<br>1050 | 230<br>350 | 0.20 | 0.21 |
| Ashlars roughly worked rubble masonry - II | 2,00<br>3,00 | 0,035<br>0,051 | 1020<br>1440 | 340<br>480 | 0.20 | 0.17 |
| Squared stones masonry with good texture - III | 2,60<br>3,80 | 0,056<br>0,074 | 1500<br>1980 | 500<br>660 | 0.19 | 0.14 |
| Ashlars of soft stone masonry - IV | 1,40<br>2,40 | 0,028<br>0,042 | 900<br>1260 | 300<br>420 | 0.27 | 0.17 |
| Stone blocks squared masonry - V | 6,00<br>8,00 | 0,090<br>0,120 | 2400<br>3200 | 780<br>940 | 0.14 | 0.14 |
| Brick masonry and lime mortar - VI | 2,40<br>4,00 | 0,060<br>0,092 | 1200<br>1800 | 400<br>600 | 0.26 | 0.20 |
| Hollow brick masonry with cementitious mortar (% holes < 40) - VII | 5,00<br>8,00 | 0,240<br>0,320 | 3500<br>5600 | 875<br>1400 | 0.24 | 0.24 |
| Hollow brick masonry (% holes < 40) - VIII | 4,00<br>6,00 | 0,300<br>0,400 | 3600<br>5400 | 1080<br>1620 | 0.20 | 0.20 |
| Hollow brick masonry with dry joints (% holes < 45) - IX | 3,00<br>4,00 | 0,100<br>0,130 | 2700<br>3600 | 810<br>1080 | 0.14 | 0.14 |
| Hollow concrete or expanded clay masonry (% holes = 45/65) - X | 1,50<br>2,00 | 0,095<br>0,125 | 1200<br>1600 | 300<br>400 | 0.14 | 0.14 |
| Hollow concrete masonry (% holes < 45) -XI | 3,00<br>4,40 | 0,180<br>0,240 | 2400<br>3520 | 600<br>800 | 0.19 | 0.19 |

[a] figures from the Italian tecnical code [Circ. Min, 617/2009]
[b] values reported from [CNR DT 203/2013]

Binda [2009b] provides also practical guides and examples to define the Masonry Quality Index (IQM) which is a qualitative indication of the quality of masonry looking at seven features namely:

- (MA.) mortar / joints between units
- (P.D.) transversal connections
- (F.EL.) units shape
- (D.EL.) units dimension
- (S.G.) presence of staggered joints
- (OR.) Presence of horizontal joints
- (R.EL.) Resistance of units.

For each of this categories three possible judgments are possible namely: fulfilled, partially fulfilled, not fulfilled. Finally, with some point attribution an overall result is pointed out. This qualitative tool demonstrates to be useful and suitable showing a relationship between the IQM figures and the mechanical properties (Fig. 2.8) [Borri 2011].

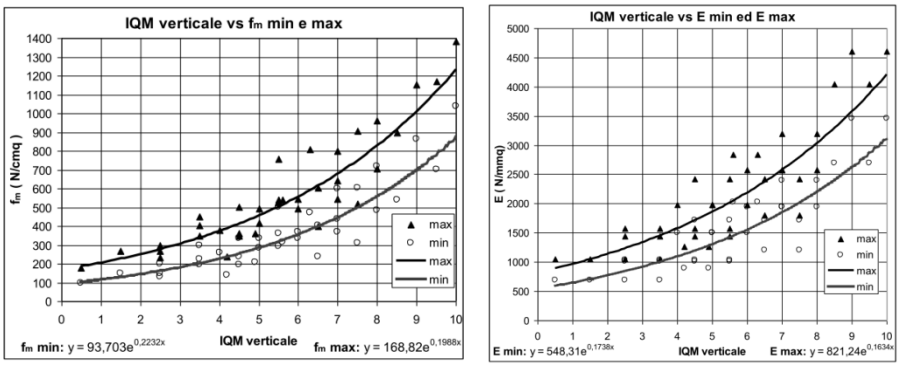


*Fig. 2.8 Correlation between IQM and mechanical properties [Borri 2011]*

It can be notice that the ranges are widespread and recent works demonstrate an high dispersion of data [Vignoli 2016], moreover § 3.3 shows a similar outcome. In order to perform the assessment the knowledge phase, which tests and understand the mechanical behaviour (stress-strain curves, integrity, cross-section) with unlike levels of destruction are fundamental to characterise masonry.

In this work a special attention, due to the experimental applications on brick masonry, will be given.

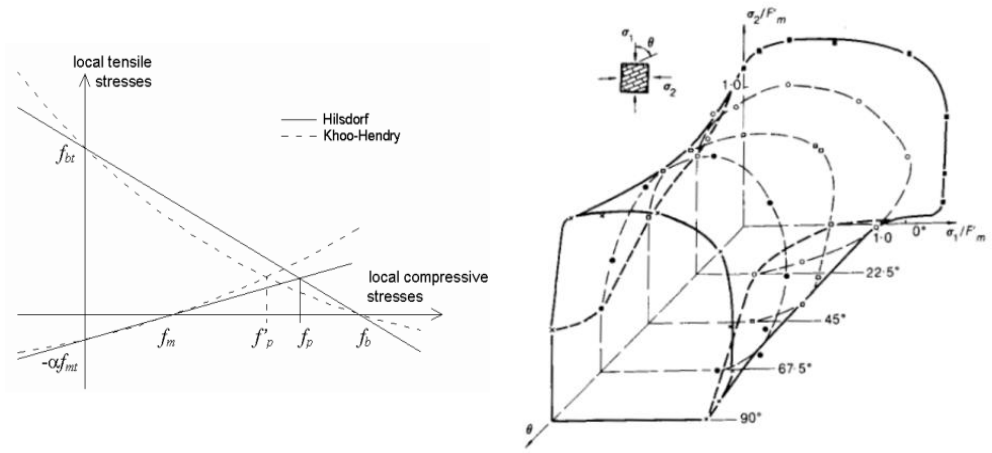


*Fig. 2.9 Failure criteria of Hilsdorf [1969] and Khoo and Hendry [1973] (left) and biaxial compression strength [Page 1981] (right)*

Compared with irregular stone masonry where the arrangement influence, as remarked above, strongly affects the overall behaviour, in brickwork masonry this effect is limited due to its regular texture. The mechanical characteristics of the constitutive materials and their thickness are in this case the key parameters. The awareness on these aspects from researchers is since sixties when Hilsdorf [1969] first, and Hendry [1973] later (Fig. 2.9 left), pointed out some equations to figured out the masonry behaviour starting from material constitutive laws. Also other authors and the two international standards (EC 6 and ACI 530-08) provides this type of equations. Another important work is from Page [1981] who analysed the anisotropic inelastic behaviour of masonry due to mortar joints, which are plane of weaknesses, for different angle of action and combinations. He presented a failure surface in terms of the two principal stresses for several stress ratios (Fig. 2.9 right).

Although these studies give a deep knowledge of this typology many issues on actual figures are steel open and in some aspect and this appears also in the Drougkas et al. [2015] work. In the paper are reported the compressive characteristics of thirty brick masonry specimens with also the properties of each component and compared in the strength prediction (Tab. 2.2).

From the analysis of this data by the two formulations provide by the European and American standards (eqs. (2.1) ,(2.2)) the modulus of elasticity seems to be overestimated since the average value estimated from the collection of literature reported in Tab. 2.2 gives an average ratio between modulus and compressive strength of 413 with a very high Coefficient of Variation (CoV) (99%). About this, the estimations given by the Italian technical standard (see Tab. 2.1)

figured out an average ratio of 523, calculated for all typologies, and of 475 for masonry brick with lime mortar which appears more accurate.

ACI 530-08 $$E_c = 700 \cdot f_m \quad (2.1)$$

EC 6 / NTC $$E_c = 1000 \cdot f_m \quad (2.2)$$

*Tab. 2.2 Collection of masonry and its constitutive material properties Drougkas et al. [2015]*

| Case | Ref.* | $E_u$ [MPa] | $f_{cu}$ [MPa] | $f_{tu}$ [MPa] | $h_u$ [mm] | $E_m$ [MPa] | $f_{cm}$ [MPa] | $f_{tm}$ [MPa] | $h_m$ [mm] | $f_{cexp}$ [MPa] | $E_{cexp}$ [MPa] |
|---|---|---|---|---|---|---|---|---|---|---|---|
| S01 | [41] | 9900 | 44.0 | 1.8 | 55.0 | 1750 | 6.2 | 0.6 | 7.5 | 19.7 | – |
| S02 | [32] | 4200 | 23.0 | 3.1 | 45.0 | 125 | 1.3 | 0.2 | 10.0 | 12.0 | 729 |
| S03 | [33] | 976 | 5.7 | 0.6 | 75.0 | 1500 | 1.2 | 0.1 | 12.0 | 1.7 | 467 |
| S04 | [15] | 14500 | 11.5 | 0.7 | 80.0 | 6450 | 3.5 | 0.4 | 10.0 | 6.2 | – |
| S05 | [33] | 3370 | 23.0 | 2.3 | 75.0 | 8570 | 5.1 | 0.5 | 12.0 | 6.7 | 2393 |
| S07 | [32] | 4200 | 23.0 | 3.1 | 45.0 | 250 | 1.9 | 0.4 | 10.0 | 13.7 | 1181 |
| S08 | [14] | 5500 | 12.0 | 0.9 | 113.0 | 2770 | 4.6 | 0.5 | 30.0 | 4.7 | 4200 |
| S09 | [33] | 3370 | 23.0 | 2.3 | 75.0 | 5450 | 4.4 | 0.4 | 12.0 | 7.4 | 3135 |
| S10 | [33] | 976 | 5.7 | 0.6 | 75.0 | 238 | 0.6 | 0.1 | 12.0 | 1.3 | 379 |
| S11 | [15] | 14500 | 11.5 | 0.7 | 80.0 | 6450 | 3.5 | 0.4 | 7.0 | 6.3 | – |
| S12 | [15] | 14500 | 11.5 | 0.7 | 80.0 | 6450 | 3.5 | 0.4 | 20.0 | 5.0 | – |
| S13 | [16] | 2000 | 13.8 | 3.3 | 55.0 | 1700 | 9.2 | 2.4 | 10.0 | 14.6 | 1936 |
| S14 | [13] | 7500 | 30.0 | 1.3 | 65.0 | 220 | 1.7 | 0.1 | 20.0 | 4.5 | 878 |
| S15 | [37] | 12000 | 62.6 | 6.3 | 45.0 | 4200 | 6.2 | 0.6 | 10.0 | 28.6 | 10000 |
| S16 | [14] | 5500 | 12.0 | 0.9 | 238.0 | 2770 | 4.6 | 0.5 | 12.0 | 8.8 | 5517 |
| S17 | [40] | 16700 | 66.0 | 1.2 | 52.0 | 2100 | 3.0 | 0.2 | 13.0 | 11.7 | 6800 |
| S18 | [41] | 9900 | 44.0 | 1.8 | 55.0 | 8600 | 21.0 | 2.1 | 7.5 | 34.7 | – |
| S19 | [38] | 5760 | 19.8 | 2.5 | 55.0 | 5490 | 2.6 | 0.4 | 10.0 | 8.2 | 2132 |
| S20 | [41] | 15000 | 58.9 | 2.7 | 57.0 | 11600 | 31.1 | 3.1 | 7.5 | 48.2 | – |
| S21 | [33] | 976 | 5.7 | 0.6 | 75.0 | 8570 | 5.1 | 0.5 | 12.0 | 1.8 | 365 |
| S22 | [41] | 15000 | 58.9 | 2.7 | 57.0 | 8600 | 21.0 | 2.1 | 7.5 | 40.9 | – |
| S23 | [7] | 8000 | 8.3 | 0.4 | 100.0 | 6600 | 3.5 | 0.4 | 30.0 | 3.1 | 5900 |

* reference to tests are according to Drougkas [2015]

For the deformability point of view, from the concrete analysis an ultimate strain of 0.0035 is purposed whereas Hendry [1981] suggested 0.003. Its magnitude appears, form the collection presented, slightly higher, in the order of 0.005-0.006 strains confirmed also in Briccoli Bati [2007a]. These considerations are relevant depending on the type of model used.

In conclusion the sliding capacity of brick masonry is calculated according to the Coulomb law. The law need the definition of initial shear strength (c or $\tau_0$ in NTC) and a friction coefficient ($\mu$). In Tab. 2.3 are reported a series of five experimental campaigns on clay brick masonry with friction values lying between 0.47 and 0.85 that is a relevant variation. The American and European standards specify respectively 0.45 and 0.40 instead Heyman [1996] suggests 0.6. In conservative terms, looking at S2 and to the guidelines a value of 0.40 seems reasonable. It has also to be accounted that this values could be calibrated on site when sliding occurs accounting for the normal action acting.

*Tab. 2.3 Average values of five campaign of sliding tests at UniPd*

| ID | $f_{c.u}$ [MPa] | c [MPa] | $\mu$ [MPa] |
|---|---|---|---|
| S1 | 1.8 | 0.17 | 0.54 |
| S2 | 6.3 | 0.09 | 0.44 |
| S3 | 6.5 | 0.66 | 0.73 |
| S4 | 17.6 | 0.88 | 0.85 |
| S5 | 2.5 | 0.24 | 0.47 |

### 2.2.2 *FRP*

The first traces of FRP development emerged after World War II, and during the Cold War to improve and advance the aerospace branch; than the industry increased the use of composites as well. Moreover in the field of civil engineering, problems in concrete structures related to exposure to aggressive environments required researchers to find new solutions. CFRP had been tested but was not considered as a viable commercial solution until 1980s.

This technology was implemented in Japan more so than any other country, and up to the mid-1990s Japan had the largest use of FPR reinforcement. China has recently become the largest user of composites in new constructions. In addition, Canadian civil engineers have developed provisions for FRP reinforcement. The role of Europe in this field began in Germany with the construction of a prestressed FRP highway bridge in 1986 [Maier, 1992].

In the field of assessment and retrofit of existing structures several advantages of these materials increased their use especially on concrete and masonry applications mainly by limited thickness, light weight and immunity to corrosion. On the other side, as disadvantages there are lack of ductility and sensitivity to UV rays and temperature (e.g. fire condition). The development and the use of these materials increase the research in the field and the rising of guidelines and technical standards. Composite could be applied in two ways:

externally to the element EBR (Externally Bond Fibre-Reinfocement) or inside the material by means of slots NSM (Near surface mounted). The mechanical properties varying among different fibre used (e.g. carbon, aramid, glass) and are related also to the fibre volume with respect to the organic matrix. There are some codes available in the North America [ACI 440-7R] and in Europe [CNR-DT 200 R1/2012].

The increased number of applications on real cases, sometimes before enough experimental testing, helped also to recognise some problems of the technique in the field of restoration. The main problems figured out are: compatibilty, removability, moisture [Valluzzi 2011, Ghiassi, 2012] and limitation of transpiration in the substrate. [Valluzzi 2014]. Recent developments about restoration and sustainability issues bring also to other solutions based on inorganic matrices, cementitious or lime mortar based, and to other reinforcements such as steel fibre (also called Steel Reinforced Polymers) [Borri et al. 2006-2009, Prota et al. 2006] and Textile Reinforcement Mortar (TRM) [Papanicolaou et al. 2007]. The latter group is called FRCM (Fabric Reinforced Cementitious Matrix) even if on restoration purposes lime based mortars are preferred. In the North American community it is already available a technical standard [ACI 549.4-13].

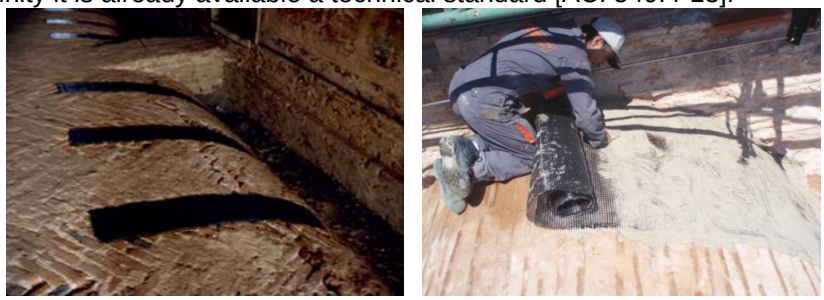

*Fig. 2.10 Example of FRP application [Valluzzi 2014] (left) and FRCM application [ACI 549.4-13] (right)*

The interest in the use of this strengthening technique is relevant in particular on vaulted structural element, the element focused in this thesis (Fig. 2.11), and on churches [Panizza, 2010].

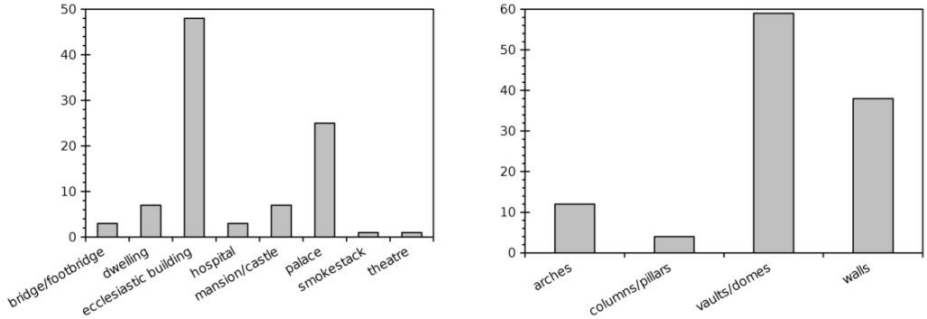


*Fig. 2.11 FRP intervention on building (left) and structural element (rigth) [Panizza 2010]*

The applications of design calculations on masonry come from the adaptation of some models on concrete elements although in last decades some models were presented about masonry. All models have to take into account the different failure modes which can occur. The fibre application, for both FRP and FRCM, deals with three parts: the substrate, the matrix and the fibre itself. It is thus evident that each component could bring to a failure inside the material (called choesive failure) or to a failure within the interface between them (called adhesive failure). The presence of cohesive and adhesive failure is called mixed failure. Form this, the bond between the strengthening and the substrate plays a key role in the overall resistance of the system.

In this framework the scientific community is carrying on two efforts: to define reliable models to calculate the bond and to standardize a common procedure in material and bond characterization.

**OUT OF PLANE BEHAVIOUR**

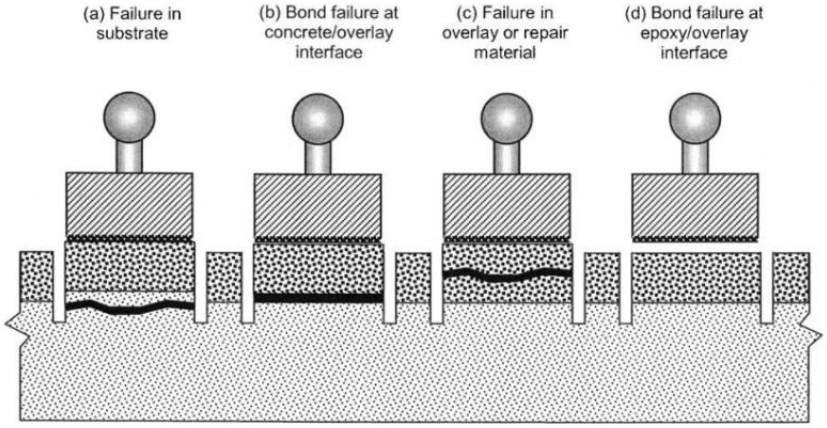


*Fig. 2.12 Pull-off possible failures, [ASTM C1583, 2013]*

One tests used to evaluate the bond between fibre and substrate is the pull-off test standardised by the American standard [ASTM C1583, 2013]. The standard is dedicated only to concrete substrate and epoxy resin application but widely use for research purposes on masonry. The test provides the tensile strength for load perpendicular to the applied layer. In addition to the load another information concerns the recognised failure modes that are four (Fig. 2.12) and related to the failure position as introduced before and summarized in the caption above the drawing.

Although the test gives limited information of the overall bond behaviour because applied perpendicular to the fibre direction, it is useful to have a preliminary overview of the interface behaviour and hence is wide used to analyse

the influence of different actions on bond as well moisture effect and ageing [Valluzzi 2011, Ghiassi 2012, Cardani 2015]. Moreover the method is simple and thus very useful onsite to identify the proper application of the reinforcement [Borri 2006, Olivito 2008] looking to the failure mode and to indicate, referring to the application on laboratory, the quality of the bond.

From several experimental tests available in literature there is a evident difference in behaviour between composites glued with organic or inorganic matrix. This is confirmed by the tensile strength of the two matrixes.

For the organic resins, usually epoxy, the most frequent failure is A. Panizza [2012] showed the influence of the primer in the fibre application with an overall result of 99.1% of failure A for CFRP with primer and 72% of failure A for GFRP. Olivito [2008] confirmed that also on-site the tests performed on carbon and glass reinforcement with organic matrix gave a 100% of failure A. Giradello [2012] tested 198 specimens of six fibre types (steel, carbon, basalt) bonded with 8 lime mortars. The exhaustive campaign pointed out about a 60% of failure A for steel reinforcement with low and medium densities instead for high density steel fibres the mortar cannot well penetrate into the reinforcement giving a percentage of 75% C failure. About basalt and carbon net the 60% of cases gave failure B and 33% of C. Another outcome concerns the agreement between the tensile strength of the matrix compared to the pull-off results. In those cases of failure B the pull-off tension agreed with the mortar tensile strength.

Finally, also in studies based on durability and ageing aspects [Borri 2006; Cardani 2015] there is the confirmation that organic matrices give a major number of failure A compared to inorganic one that present a major number of failure B. In organic matrix the FRP-masonry interface is weakened by moisture or temperature effects increasing the number of failure B [Valluzzi 2011].

**ON PLANE BEHAVIOUR**

The FRP is generally used to confine structural elements or to add tensile resistance. In the latter case the tensile stress undergoes by the composite is transferred by means of tangential stresses. The characterization of this bond law is the key issues accounting for types of: substrate, matrix and fibre.

In the field of concrete the bond between EBR composites with epoxy matrix has been deeply investigated by a large amount of authors. Lu et al. [2005] provided an overview of bond-slip laws adopted by analytical models which in general are based on bi or tri linearization or on exponential curves. An interesting approach, also adopted in the Italian CNR, is based on an overall fracture energy balance. Liu and Wu [2012] in their work collected a wide number of contributions in

experimental terms and they also provide a proposal of bond-slip. Finally, in order to standardize the test and its execution a round robin has been done [Guadagnini et al. 2012].

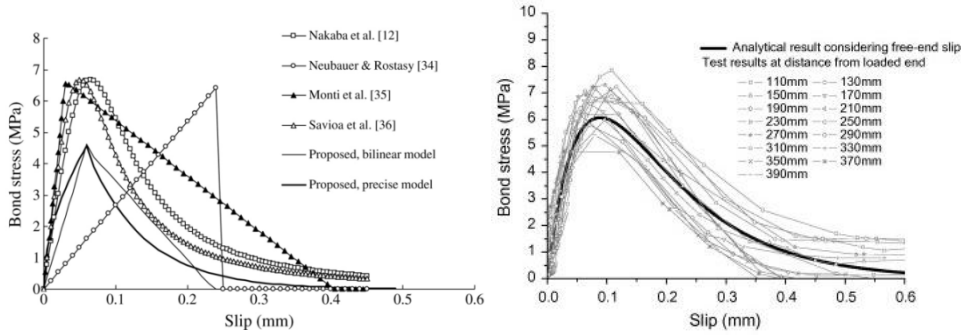


*Fig. 2.13 Curves adopted in different models [Lu et al. 2005] (left) and analysis on an high number of test and relative proposal [Liu and Wu 2012] (rigth)*

The models presented before were also used for masonry applications with some comparisons [Panizza 2012] and with some proposed calibrations. About masonry same efforts have been done with a large investigation, similarly to concrete studies, looking at: (i) standard tests method and procedures; (ii) to give typical ranges based on empirical experiences; (iii) to highlight the critical aspects of the technique with predictive model application; (iv) to fix procedures to check the intervention in terms of execution quality and durability problems.

The first point is defined by means of reference Round Robin Tests (RRT) [Valluzzi 2012] where common tests procedures and methods are defined (see Fig. 2.14). The RRT was focused on organic matrixes (epoxy resins) with four fibres materials: steel, carbon, basalt and glass. With results were figured out some ranges curve of the load-displacement behaviour of each material (Fig. 2.15, left). From those curves is possible to notice different effective lengths and force developments.

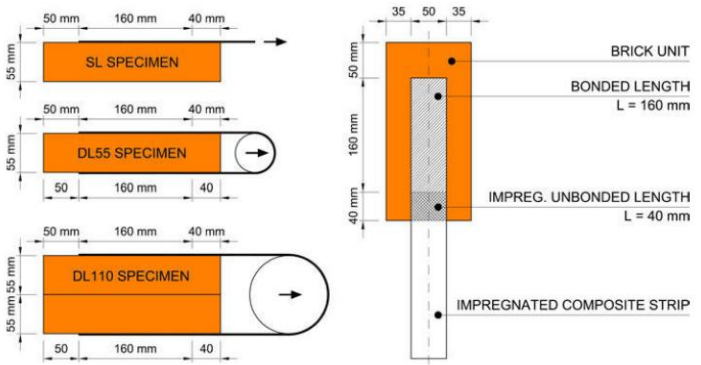


*Fig. 2.14 Configurations for shear bond test in round robin [Valluzzi 2012]*

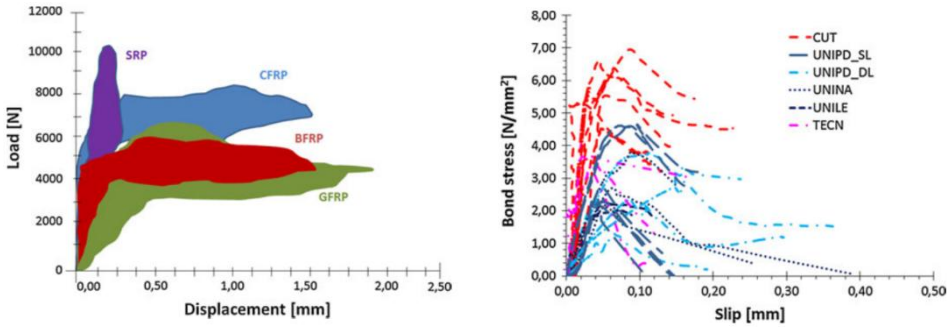


*Fig. 2.15 Typical ranges in load-displacement curves (left) bond slip curves of CFRP application (right) [Valluzzi 2012]*

The RRT reported also the experimental curves for each application. The curves of Carbon fibres (used herein in the experimental campaign) are shown in Fig. 2.15 (right). It is possible to select from here, according also CNR [DT-200], the ultimate slip in this application as $s_u$ equal to 0.4 mm.

In the field of inorganic matrix, according to out of plane there are different behaviours and mechanisms. Fig. 2.16 shows the failure mechanisms which can occur in the interface of these applications. Moreover the failures on substrate or fibre have to be considered. Meanwhile failure A and B are common also for FRP the slipping of the textile from the matrix (C) is typical of these applications.

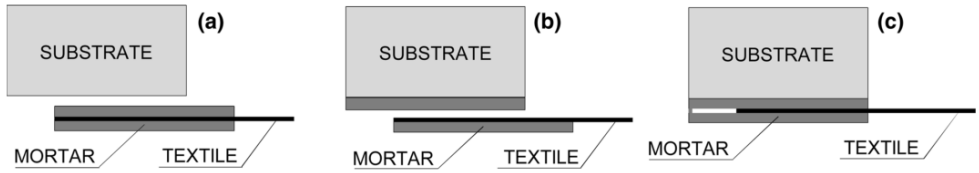


*Fig. 2.16 Possible failure modes in FRCM applications [de Felice 2014]*

The observed failure modes differ with the fibre material as reported with the 43 tests by de Felice [2014] The highest number of C failures were for carbon applications. Other interesting data and typical curves are reported in Giradello [2012].

About the third point, many interpreative models may used based on literature. The proposal here chosen is based on the CNR [DT-200] according to some observation of Cerroni [2014]. The application of the bond law will be presented later.

The two problems herein not considered are the influence of curvature in the bond behaviour where some jobs, mainly numerical, are available [de Lorenzis 2009, Milani 2014], and the influence of mortar joints actually present in real applications alhough shear tests are carried out only on brick. About the latter,

some authors in literature faced the problem providing observations and proposals [Panizza 2012, Carloni 2016].

In conclusion, about the check in filed (iv), an adaptation of the laboratory SL test was proposed by the Italian technical standard [C.S.LL.PP. 24/07/2009] (Fig. 2.17). The document mentions the limit of 24 kN to accept the test result but it seems difficult to achieve such tension, especially with a strip width of 5 cm. In CNR [DT-200] this limitation has been removed.

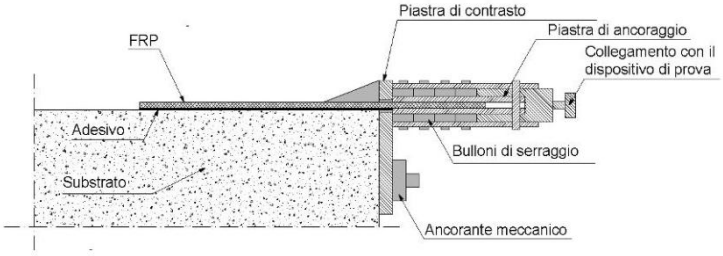


*Fig. 2.17 Direct shear tearing test [C.S.LL.PP. 24/07/2009]*

Some examples of this kind of application are reported in literature [Olivito et. al. 2008, Borri et al 2006] and an example of the instrumentation and the failure mode are reported in Fig. 2.18.

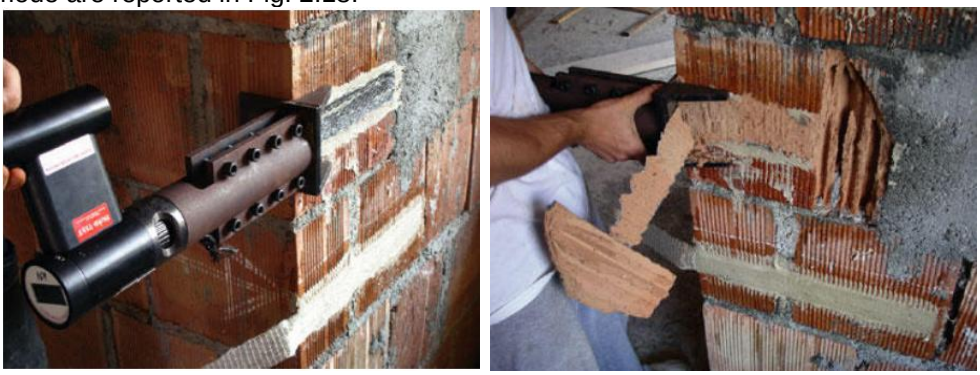

*Fig. 2.18 In-situ shear test, instrumentation (left) and failure mode (right) [Olivito et. al 2008]*

## 2.3 KNOWLEDGE PHASE

The knowledge phase plays a crucial role in the assessment of existing buildings in order to comply reliably with all the structural verifications needed to the goal. Since the development of ISCARSAH [2005] guidelines, concerning the structural restoration of heritage structures, and in the framework of the most

developed methodology to the restoration of cultural heritage, the knowledge phase is considered as a compulsory step which is directly related to the overall safety of the structure [ISO 13882:2010]. In this framework, an attempt of quantitative definition of this influence is provided by standard [NTC:2008, LLGGBBCC:2010, EC8:2004, ASCE 41-13:2014]. The degree of knowledge of a structure concerns mainly four aspects:

- Historical, structural and architectural investigation
- Survey of the structure
- Field research and laboratory testing
- Monitoring

The definition of these phases slightly varies among standards but all looks at the historical evolution, the characterization of materials and details of the constructions. The aim of this chapter is to present the different typologies of suitable tests, some of them also cited in standards, to characterize the structure and highlighting the actual state of art of each techniques.

Binda [2005] presented an overview of testing techniques applied on existing building depending on the moment of application, the investigated parameter and the methodological step. (Fig. 2.19)

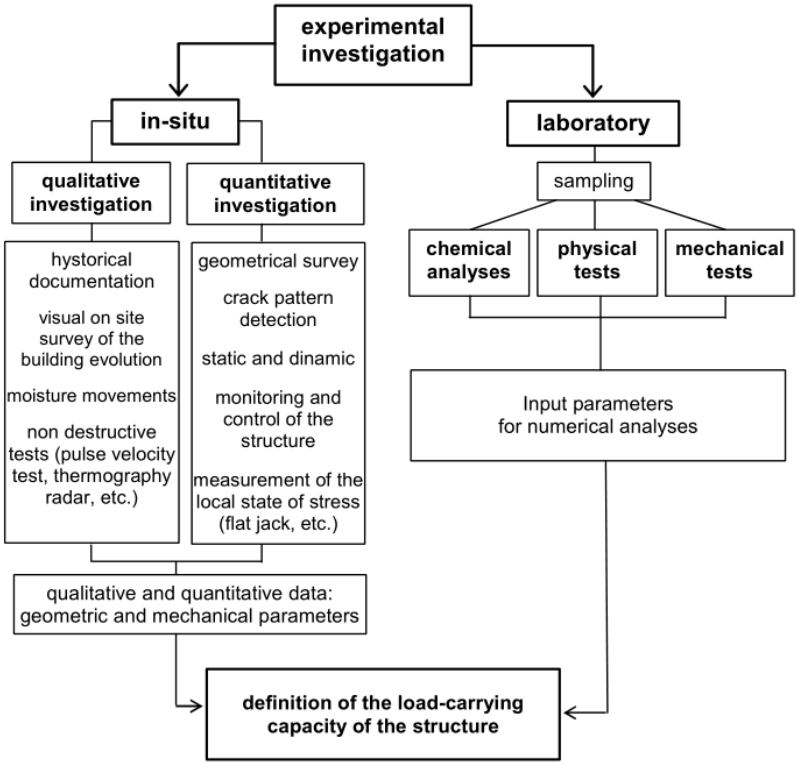


*Fig. 2.19 Finalisation of the experimental survey to the structural analysis [Binda 2005]*

Testing techniques can be applied on site and on laboratory by means of sampling. The mechanical characterization of extracted specimens of existing masonry in laboratory is indeed quite unfeasible in real applications, due to the dimension of samples, which should be representative of masonry, and to the needs of recreate “undisturbed” conditions that - following the transportation - are very difficult to preserve.

Another division of tests is related to the disturbance on the structure in terms of non-destructive techniques (NDT), minor destructive techniques (MDT) and destructive techniques (DT). The first types, does not damage the structure and historical material by could not provide quantitative results. On the other hand the DT tests provide quantitative results, related to the mechanical properties used in the final structural assessment, but the tested portion has to be later demolished. The intermediate categories aim to balance this shortcoming in order to increase the reliability of tested parameters without relevant damages.

### 2.3.1 *Sonic test*

The sonic test, also called mechanical pulse velocity, is a NDT test which does not damage the tested sample. The test is suggested by some standards [NTC 2008; ASCE 41-13] and it consists of impacting a wall with an instrumented hammer and measuring the travel time of a longitudinal stress wave (sonic wave) across a specified gauge distance (Fig. 2.20).

*Fig. 2.20 Direct sonic test execution, instrumented hammer (left) and accelerometer (right)*

The measure refers to the time that the stress wave generated and recorded by the hammers takes to travel in masonry and to be recorded by an accelerometer. The flight time, once divided by the path length, represents the pulse velocity.

The measure does not directly concerns any mechanical properties. The dynamic elastic modulus is theoretically proportional to the density and quadratic of speed as shown in eq. (2.3).

$$E_{dyn} = \rho \cdot v^2 \tag{2.3}$$

This formulation is reliable in isotropic and homogeneous materials and hence not suitable to masonry. Nevertheless although there are not suitable formulations to derive mechanical properties, the test provides interesting qualitative information.

Mechanical pulse velocity is suitable on masonry due to its wave length and energy rather than ultrasonic method. The test is a well established technique in scientific community, it was suggested by Abrams [1989], a standard is present ASTM C597 and many authors refer to this technique [da Porto 2003, Binda 2005, 2009a, Bosiljkov 2004, Péres-Garcia 2013]. Moreover in many European research projects (i. e. ONSITE-FOR-MASONRY, NIKER) and Italian projects (ReLUIS DPC 2005-2008 and 2014-2016) this technique was investigated.

The test is suitable to give information in terms of:

- morphology evaluation: detecting holes, wide cracks, lack of material or difference in material properties,
- masonry quality: the sonic velocity can qualitatively describe a good or poor quality of the investigated panel,
- intervention efficacy: for instance in case of grout injection, the execution of the test before and after can indicate an effective filling of voids.

The test, depending on receivers numbers and corresponding position, can point out different information.

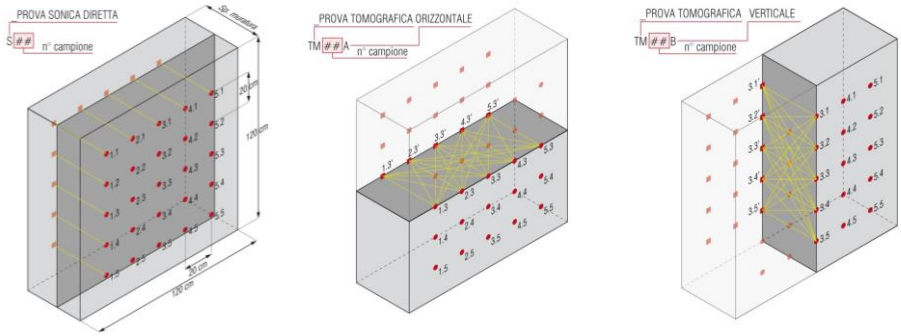


*Fig. 2.21 Acquisition schemes and methodology for sonic tests [Cescatti 2015]*

Fig. 2.21 (left) shows the direct sonic test where there is only one accelerometer which measures directly beyond the hammer position in the depth of the wall hence acquiring an orthogonal wave. This measure is repeated many times following a grid. The punctual response is then interpolated in the investigated area and the results is a distribution of speed on the wall surface.

The evaluated velocities are hence an average value of the wall section and do not give information about different leafs. In order to characterize anomalies of different material in the transversal direction it is possible to use tomography where the acquisition is made with multiple accelerometers measuring all possible paths among points inside the inspected area (see Fig. 2.17 centre and right). In this case the result is a ray tracing matrix which has to be elaborated in order to provide a speed maps. The speed distribution on the cross-section can identify the internal morphology.

Another application is the indirect sonic test where the hammer and the accelerometer are located on the same surface. The measure looks at the wave velocity of propagation throughout the surface and does not give information of the whole section.

### 2.3.2 *Ground penetrating radar and electrical techniques*

The Ground Penetrating Radar, also called Georadar, is a suitable technique in the field of diagnosis which is based on the analysis of dielectric properties of materials. It is a promising technique in masonry applications because does not become from homogeneous material application that always demonstrates some limits [Binda 1998].

The systems can use different antennas (200-500 MHz 1 GHz) depending on the investigated details and depth. A more deep analysis needs a low frequency and thus also a low resolution. The information provided are distributed in a section of acquisition position and depth, for example acquiring a squared grid on the wall the elaboration figured out all the investigated volume of the wall with a continuous set of information with also a good resolution (in the order of mm). The technique, compared with other NDT, is faster and permits to recognise void, damages, presence of humidity and different layers. The combined use with sonic test permits a good reconstruction of the wall morphology as shown in Fig. 2.22 where a chimney on the right was detected and further information on damaged zone are available.

The disadvantages of this technique are the sensitivity to metallic layers that could disturb the test and the non geometric reconstruction of thickness which is based on flight time of the wave and need expert calibration. Moreover the resulting

image is affected by reflections, shadows and the humidity should not be confused with different materials, therefore many skills in interpretations are required in order to avoid misunderstanding of results.

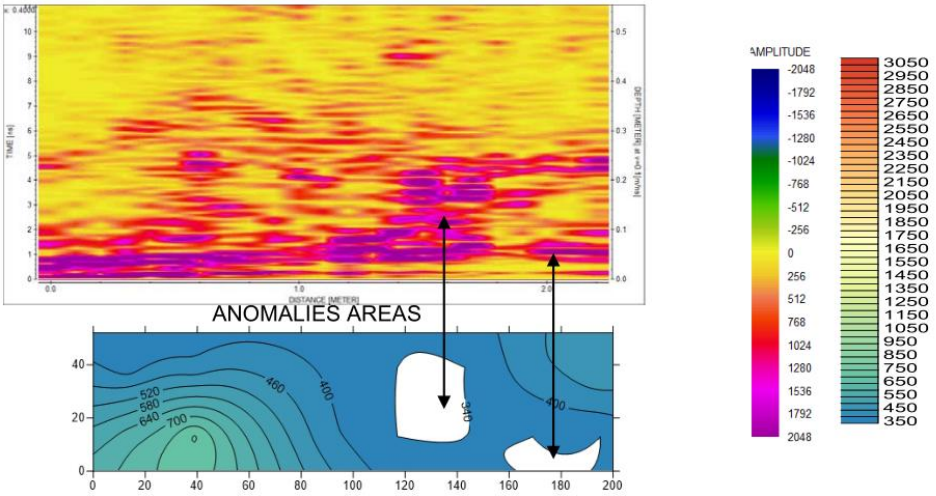


*Fig. 2.22 Comparison between results of radar (above) and sonic test (below) [Cescatti 2015]*

Another technique used in geophysics and then adopted to restoration purposes is the geo-electrical test based on the Ohm's law and with a series of dipole electrodes is possible to create a map of resistivity. The test is carried out form one side of the wall and to investigate a defined depth the acquisition area should be in the order of five times longer. Some authors report interesting results [Keersmaekers 2004] but so far it is a technique often difficult to apply because of low level of humidity, high level of damage or void index.

### 2.3.1 *Video endoscopy*

The survey of masonry section and of some construction details, which cannot be visually inspected, can be overcome by means of coring and video endoscopies which are minor destructive techniques (some example in CH 4). The test could be performed in association with coring, in order to analyse the section or in existing small holes to recognise structural details and understand some connections. Video endoscopy is also very useful drilling small diameters just to recognize the thickness of elements (i.e vaults) and eventually understand the stereotomy. The inspection by means of a fibre optic is an important tool, especially if guided by other test as e.g. sonic, to evaluate and confirms results on the transversal section and to evaluate the efficacy of grouting intervention.

### 2.3.2 *Infrared images*

The infrared thermography is based on the analysis of infrared rays with a IR camera. Each element emits electromagnetic radiation depending on its temperature (T), the emissivity coefficient (e) and the constant s ($5.67 \times 10^{-8}$ W/m$^2$K$^4$) according to the Stefen-Bolzmann equation (2.4). The energy distribution in frequency is given by the Rayleigh-Jeans law and at normal ambient temperature it corresponds at the infrared range.

$$E = e \cdot s \cdot T^4 \qquad (2.4)$$

This technique is therefore based on the measurement of superficial temperature of building and due to the different conductivity to each material it is indirectly possible to recognise different materials. The IR vision does not analyse temperature in depth and for this reason a careful interpretation of superficial resulting temperature have to be done. The instrumentation gives quantitative results and can be associated to transmittance but in term of structural analysis the technique is qualitative because associate to the definition of different structural parts and materials.

The technique has to be carefully interpreted because it suffers of reflection problems (i.e. glass behaves as a mirror in IR field) and illumination problem. In some cases lights illuminate but also heat surfaces leading to recognise areas with a different temperature do not associated to a different material. The same effects could be faced in case of moisture.

IR thermography can be applied in two ways: passive and active; the two rely on conductivity and thermal capacity respectively. The passive application does not require any action on the investigated element but the simple observation of it. In this case, to be efficient, the investigated element needs a gradient of temperature by the two side in order to have a heating flow going across the wall. The different conductivity of materials leads to observe different temperatures on the surface.

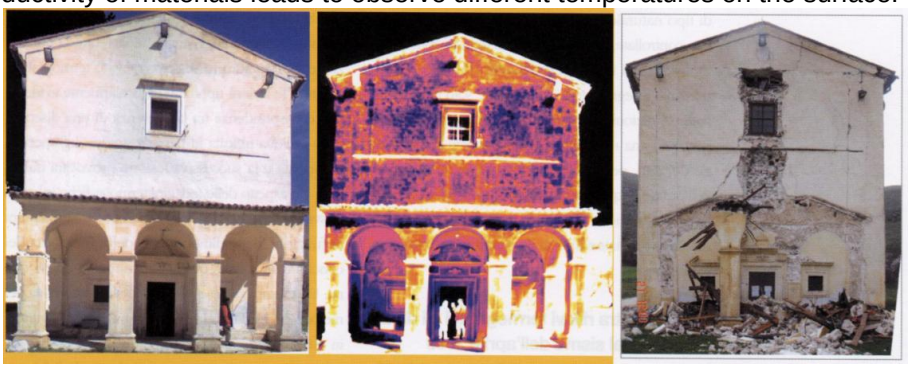

*Fig. 2.23 Comparison between IR termography and damages occurred on the façade of S. Stefano di Sessanio's church [Grinzato 2009]*

Grinzato [2009] (see Fig. 2.23) shows an example of the performance of IR technology that helps to analysis vulnerability in buildings.

The active use of IR vision requires to heat the element rising the superficial temperature. After the heating, a series of IR images are taken with a sampling period and due to the different thermal capacity of materials the external temperature drop differently. This method allows an investigation of 15-20 cm depending on material and only on the warm part, it is thus more difficult to use it in overall analysis of the structure. This approach, efficiently works in localized portions and is also used to check efficacy of the FRP application as reported in Fig. 2.24 [Niker 2012].

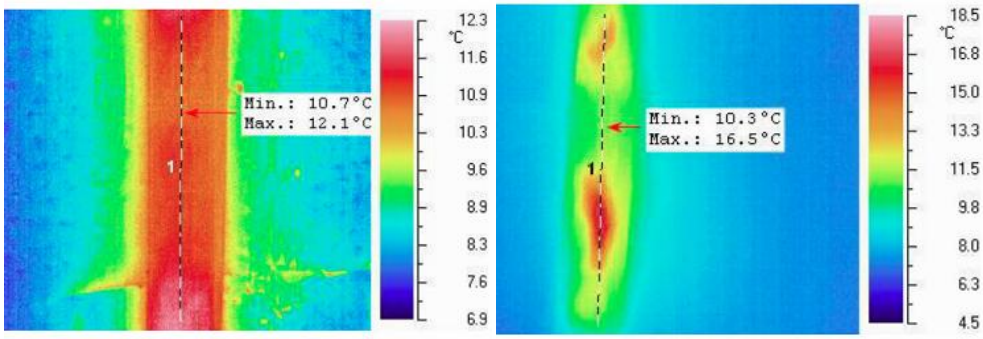


*Fig. 2.24 Termography profile, fairly uniform (left) and non uniform (rigth) temperature [Niker 2012]*

### 2.3.3 *Dynamic identification*

Similarly to analytical and numerical tools, also testing techniques could refer to local or global characterization. As presented before, often tests are focused on limited portions of material with DT, MDT or NDT. In the previous paragraph IR thermo vision, used in passive conditions, looks at the global structural location of elements but does not characterize the structure in mechanical terms. A powerful NDT tool that proves to be effective in the analysis of the global structural behaviour is dynamic identification.

Chopra [2001] deeply focused on free vibrations of system with single degrees of freedom (SDOF) or multiple degrees of freedom (MDOF) of undamped systems that demonstrate to have intrinsic deformations (mode shapes) and frequencies. This analysis could be carried on by means of an eigenvalue problem solution of the homogenous differential equation of motion (2.5) with the aforementioned hypothesis that led to the solution of the system (2.6) where the eigenvalue vector $\boldsymbol{\omega}_n$ represents mode frequencies and the eigenvectors matrix $\boldsymbol{\Psi}_n$ represents mode shapes.

$$\mathbf{M}\ddot{\mathbf{x}}(t) + \mathbf{C}\dot{\mathbf{x}}(t) + \mathbf{K}\mathbf{x}(t) = \mathbf{f}(t) \tag{2.5}$$

$$(\mathbf{K} - \boldsymbol{\omega}_\mathbf{n}\mathbf{M})\boldsymbol{\Psi}_\mathbf{n} = 0 \tag{2.6}$$

where **M** is the matrix of masses of each DOF, **C** the damping matrix and **K** the stiffness matrix.

The actual problem has always a external excitation in time **f**(t). Peng [1987] highlights this solution as considerably important in the area of mechanical systems, but some interesting applications are available also for historical building [Gentile 2004, 2015, Casarin 2006, Ramos 2007, Ceravolo 2010, 2013]. An interesting example of first application of combined estimations of elastic modulus by means of flat jack and dynamic identification was presented by Modena [1997].

This topic was widely investigated in last decades by many authors who analyse the mathematical problem and different estimations techniques. It is hence suggested to look at Caetano [2000], Ramos [2007], Vincenzi [2007], Brownjohn [2010] where a board analysis and a complete overview is given.

In this work is relevant to remind that on the structure are applied, for each DOF of interest, accelerometers which records time history in acceleration. It is possible to analysis them in time and frequency domain.

The time history is in time domain and to move on a frequency domain, the Fast Fourier Transform is used. In this domain, a peak can be associated to a Dirac delta function which represents an harmonic response as for example the aforementioned eigenvalues. In order to move from frequency to time domain is also suitable to use the inverse Fast Fourier Transform. The acquisition of accelerations by means of electronic devices is a discrete approach that is based on a sampling frequency that can lead to aliasing problems. In order to avoid such problems a recommended factor of 5 is suggested and herein followed.

Looking at hypotheses of system in eq. (*2.6*) it is practically impossible to obtain a free vibration (with **f**(t) null) due to vibrations and environmental excitations. Therefore dynamic identifications are subdivided in Input-Output techniques where the input is known and generated by dedicated instruments (impacts hammer, shakers etc.) and output-only techniques that rely on a reasonable simplification.

Fig. 2.25 shows schematically how the Operational Modal Analysis work and remarks its limitations. Looking at this scheme, the structural system should be linear and time-invariant and the ambient vibration $\boldsymbol{u}_k$ is assumed as a stationary Gaussian white noise stochastic process. This means that the Power Spectral Density (PSD) of the excitation should be constant. Due to the nature of the measurement data, the response $\boldsymbol{y}_k$ includes the modal contributions of the ambient forces, the contribution of the structural system and the contribution of the noise

signals from undesired sources. Nevertheless, if $u_k$ is constant, the measured response is only function of the linear structural system.

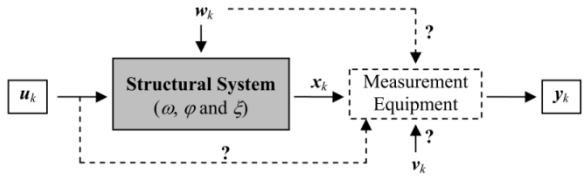


*Fig. 2.25 Output-only identification techniques scheme [Ramos 2007]*

Although such hypotheses are theoretical, in practical terms this could be reasonable considered without large errors and approximations. Obviously this should be verified on site. The use of such methods allow, especially in existing and massive building, to perform the dynamic identification without any input source that is a decisive simplification.

Tab. 2.4 presents an overview of the main methods used. In this work particular interest is given in the frequency domain analysis such as FFD and in particular on Enhanced Frequency Domain Decomposition (EFDD) [Brincker 2001] which is based on peak peaking in and it allows also to estimate damping ratios. The method is user-friendly and easy to apply. In order to check the quality of the identification is always applied, on at least one reference case a time domain method. In this work was used the Stochastic Subspace Identification Methods [Peeters 1999].

*Tab. 2.4 Classification of relevant output-only identification algorithms [Caetano 2000]*

| | Method | Characteristics |
|---|---|---|
| Frequency Domain | Peak Picking (PP) | Classical SDOF method |
| | Frequency Domain Decomposition (FDD) | MDOF method; application of SVD to reduce noise |
| | Enhanced Frequency Domain Decomposition (EFDD) | MDOF method; application of SVD to reduce noise |
| | Polimax | MDOF method |
| Time Domain | Random Decrement (RD) | Operates on time domain series, leading to a free decay curve analysis |
| | Recussive Techniques (ARMA) | Time series modelling using recursive algorithms |
| | Maximum Likelihood Methods | Stochastic methods based on the minimization of a covariance matrix |
| | Stochastic Subspace Identification Methods (SSI-DATA) | Stochastic methods based on the project of state vector on a vector of past realizations |

In conclusion the dynamic identification is an effective tool in the evaluation of the global behaviour of entire structures or elements and hence it could be adapted to many uses as:

- calibration of mechanical models (see CH 4)
- detection of main frequencies related to internal state stress (CH 7)

- stiffness evaluation to check strengthening intervention (§ 0)
- damage identification in structural element (§ 0).

### 2.3.4 *Estimation of axial force acting on ties*

In the knowledge phase many testing techniques are available and the main aim is usually to characterise material or building properties in terms of strength and response. Nevertheless there are testing techniques that aim to evaluate the action bearded by elements. The availability of tools to estimate stresses beard by structural elements is a powerful way to understand the whole actual behaviour.

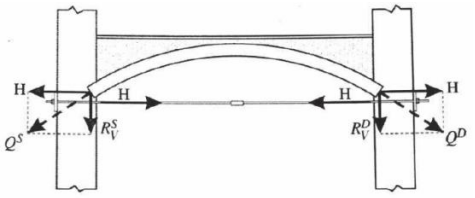


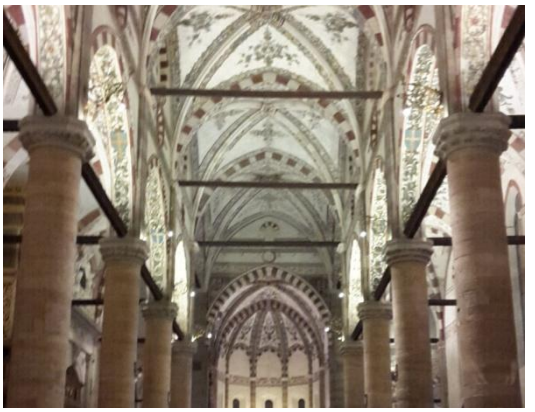

*Fig. 2.26 Schematic example of tie-rod Pisani [2008] (L), timber ties in S. Anastasia (VR) (R)*

In vaulted system two solutions are suitable to counteract the acting thrust, the use of buttresses or the introduction of tie rods. First examples and studies on the latter approach date back to the XV century when Leon Battista Alberti in *De re Aedificatoria* suggested the use of metallic ties with flat arches.

From a structural point of view, the stability of vaults, and in general of structures, relies on their geometrical features. The use of buttresses or walls was primarily based on such aspects while ties are related to resistance criteria which were less used in past centuries (see § 2.4.2). Despite those aspects the use of timber (see Fig. 2.26 rigth) or metal tie-rods in vaults and arches was quite common in Italy. Many churches and palaces, with cloisters and porches, adopted this solution which was reported also in the main manuals of the time (see Fig. 2.26 left). Facing a vaulted system, if statically determinate, (e.g. Fig. 2.26 left) the magnitude of the horizontal thrust of the arch can be assessed by knowing the tension inside the tie rod.

In this framework, to employ reliable methods for the estimation of the axial tension in ties is of a paramount importance for a correct assessment of the real behaviour of the investigated structure. To do so, in the following (Tab. 2.5) is reported a general overview on the existing models divided by two different

approaches: static and dynamic techniques. Each model than can account for the sole axial force (N) or also for the Boundary Conditions (BC). In case of models based on the dynamic response, the table reports if the analysed parameter is frequency rather than mode shape.

*Tab. 2.5 Overview of the reviewed models (in bold methods further analysed)*

| Author | Approach | UNKN. | | METHOD | | FREQ | MODES |
|---|---|---|---|---|---|---|---|
| | | N | BC | ANA. | NUM. | | |
| Briccoli Bati [1993] | STATIC | ● | | ● | | | |
| Beconcini [1996] | STATIC | ● | ● | ● | | | |
| **Briccoli Bati [2001]** | STATIC | ● | ● | ● | | | |
| **String theory** | DYNAMIC | ● | | ● | | ● | |
| Dardano [2005] | DYNAMIC | ● | ● | ● | | ● | |
| Lagomarsino [2005] | DYNAMIC | ● | ● | | ● | ● | |
| Park [2006] | DYNAMIC | ● | ● | | ● | | ● |
| **Tullini [2008]** | DYNAMIC | ● | ● | ● | | | ● |
| Garzera [2009] | DYNAMIC | ● | ● | | ● | ● | |
| **Amabili [2010]** | DYNAMIC | ● | ● | | ● | ● | |
| **Luong [2010]** | DYNAMIC | ● | ● | ● | | ● | |
| Rebecchi [2013] | DYNAMIC | ● | ● | ● | | | ● |

First three models are static methods, indeed each model is the upgrade of the previous one, and hence in the following, only Briccoli Bati [2001] will be focused.

Static models use the relationship between the theoretical deflections of the beam, in the absence of tensile stress and subjected to a generic transversal load P applied in any section of its length, and the experimentally measured beam deflection corresponding to the presence at the same time of an unknown axial force N, and a given applied load P.

It is well known that deflection of beams is affected by the rotational stiffness of supports. For example the method proposed by Briccoli Bati [2001] correctly requires the definition of restraint conditions, which for historic buildings is a complex problem whose evaluation is quite uncertain. The restraint conditions are clearly decisive for both, the expression of the theoretical deflection and the determination of the corresponding critical load. To overpass this, the use of strain gauges in mid-span which measure the actual bending moment due to the punctual load helps to simply estimate the moment beard by supports, allowing hence solving the problem.

From a practical point of view, the static approach requires to install a number of sensors, involving at least three LVDT transducers (for measuring

vertical displacements) and three strain gauges, therefore it becomes a relevant time consuming procedure with a possible rise of uncertainties in measures, especially on-site.

Since the practical issues related to the static approach are relevant in usual cases the investigation of the dynamic behaviour represents a viable solution. Also in the dynamic case, in addition to the tensile action, BC are additional unknowns. To detect and fix the response caused by BC, it is possible to operate by two quantities: eigenvalue (frequencies) or eigenvectors (mode shapes) (see Tab. 2.5).

The dynamic response of a linear structural element subjected to tensile forces is function of both its geometry and its state of stress. The governing motion equation (eq. (2.7)) is then related to stiffness, internal state of stress and density.

$$EJ\frac{\partial^4 w(x,t)}{\partial x^4} - N\frac{\partial^2 w(x,t)}{\partial x^2} + \rho A\frac{\partial^2 w(x,t)}{\partial t^2} = 0 \qquad (2.7)$$

To obtain a valid solution of a complex problem from an engineering point of view, it is in general requested to simplify some aspects which are negligible with reference to the obtainable result. For example, without simplifications differential equations like (2.7) could not be solved in closed form. First applications in this field focused on bridge cables. In this case a strong hypothesis was proposed, neglecting the stiffness of the cables. Hence, the eigenvalue of eq. (2.7), are given in eq. (2.8), with ω = 2πf:

$$\omega_n = \frac{n\pi}{l}\sqrt{\frac{N}{\rho A}} \qquad (2.8)$$

In this equation, the frequencies are function of: mode number, length, axial force and density. This string linear theory used for cable-suspended bridges, demonstrated in years to work properly. Some authors [Belluzzi 1941, Mastrodicasa 1981] suggested to extend this method to historical ties, where the initial hypothesis of negligible stiffness has to be verified. A further optimization of the method, considering both the cross section stiffness and BC was carried out by Luong [2010]. The BC estimation plays a relevant role in the assessment of the axial force, considering that in string theory, assuming pinned restraints for the tie rod, gives an estimation actually four times higher than the one with fixed restraints.

Eq. (2.6) can also be solved by using numerical approaches in which - starting from guessed parameters and minimizing the error between guessed and actual values measured (e.g. frequencies) - is possible to define the tensile stress inside the element. Those models have shown to manifest problems of hill conditioning [Lagomarsino 2005] where slight differences in input strongly affect the

final result or sometimes the non convergence of the error. In another case the iterative procedure is not clear and repeatable following the paper [Park 2006].

Dardano [2005] also tried to base his model on higher frequency but in many practical cases the models does not provide a solution.

In general, the dynamic methods rely on relations based on stiffness and mass rather than on those which accounts for the internal state of stress. However in some fields where the effect is not neglegible, as the aerospace industry, the problem of estimating internal state stress in beams by means of modal parameters (i.e. frequencies and mode shapes) permitted to analyse in depth the problem [Shaker 1975]. Based on this work a rigorous analytical model developed by Tullini [2008] takes into account all the three terms of eq. (2.7) analysing stiffness, of both boundary condition and beam, tension, which is the unknown, and density.

The core of this model is based on eq.(2.9) that finds the matching of the experimental amplitude of mode shapes, measured at each quarter of the tie-beam span, with the related analytical values based on Shaker [1975] theory.

$$\frac{\nu_1 + \nu_3}{\nu_2} = \frac{1 + 2\cos(q_1/4) \cdot \cos(q_2/4)}{\cos(q_1/4) + \cos\mathrm{h}(q_2/4)} \tag{2.9}$$

where $\nu_1$ and $\nu_3$ are the nodal amplitudes of the first mode shape at intermediate quarters and $\nu_2$ is in mid-span whereas $q_1$ and $q_2$ are defined as:

$$q_1 = \frac{1}{2}\left(\sqrt{n^2 + 4\lambda^4} - n\right), \quad q_2^2 = q_1^2 + n \tag{2.10}$$

$$n = \frac{NL^2}{EJ} \tag{2.11}$$

$$\lambda^4 = \omega^2 \frac{\mu L^4}{EJ} \tag{2.12}$$

where n is a normalized axial stress and λ a parameter to take into account the angular velocity (ω), the linear mass (μ) and the stiffness properties. An extension of this method was carried out by Rebecchi [2013] where the model tries also to adopt an unknown length of the element. In case of historical tie rods this problem is less relevant and Tullini [2008], for a known length, provides better results.

As suggested by Garzera [2009] and then improved in Amabili [2010] a further numerical approach could be based on dynamic identification with the development and the calibration of a finite element model (FEM). Some issues related to this calibration will be discussed in CH7.

### 2.3.5 *Flat Jack*

The development and experimentation on the reliability of flat jack test start from Faiella [1983] on rock mechanics and then adapted to brick masonry by Rossi [Maier 1983, Rossi 1985]. Already in those experimental campaigns and in particular in Rossi [1987] (see Fig. 2.27) many considerations, especially about the single flat jack were already carried out in order to analyse the influence of the flat jack shape or the sensitiveness on eccentric loads. The 20x40 jack presented good approximations (10% of overestimation) meanwhile the 12x24 cm might be too small to test a representative masonry samples. About the elastic modulus, increasing the load the confinement increases as well, thus overestimating the modulus. The double flat jack curve, compared with the axial compression, is higher of 10-15 %.

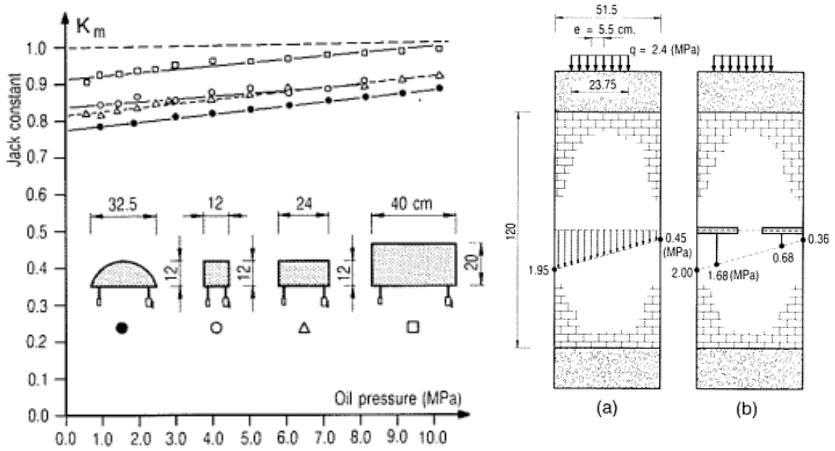


*Fig. 2.27 Calibration of different flat jacks (left) and calibration under eccentricity (right) [Rossi 1987]*

Other relevant contributions came from Abrams [1989] and Nolan [1990]. In these works, some considerations on transducers position and number are pointed out. By the comparison with destructive tests on laboratory for the single flat jack a 5% of error was estimated whereas for the modulus of elasticity of the double flat jack and error that lies between 1.70 and 0.90 was figured out.

More recent attempts to correlate the flat jack test with classical laboratory compressive tests were provided also by Gregorczyk [2000], Valluzzi [2003]. Such contributions indicated that the double flat jack test seems to give a slight overestimation of the Young modulus. Differences between the two methods are around 15-20%.

Dalla Benetta [2012] performed a calibration of single and double flat jack on a brick masonry wall and on irregular stone masonry in a three leaf wall (Fig. 2.28). The author stressed that these figures apply for brick masonry, instead in case of stone masonry the uncertainties increase due to the different distribution of stresses in the loaded area. Similar conclusion was also drawn by Binda [2007] comparing the different response of four transducers.

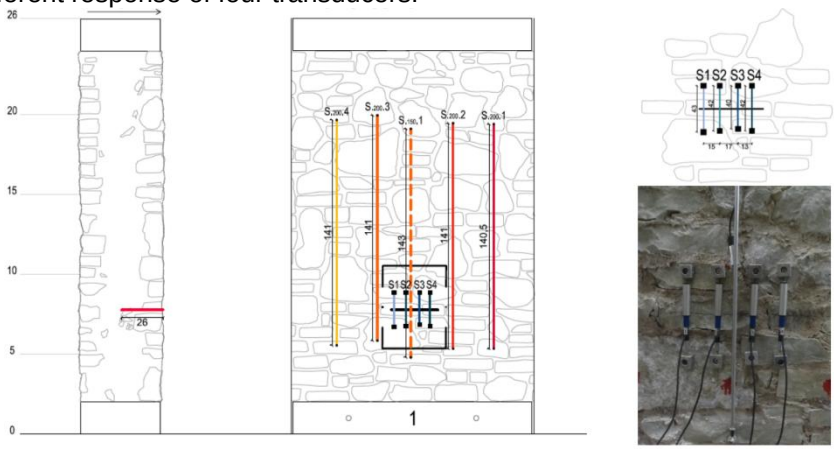


*Fig. 2.28 Dalla Benetta [2012], calibration of the single and double flat jack on stone masonry*

The scientific community nowadays accepts this test methodology as the reference technique for the on-site testing of masonry panels (in compression). Technical standards are available in the European [RILEM MDT.4:04, RILEM MDT.5:04] and American community [ASTM C1196:09, ASTM C1197:09] for the single and double flat jack respectively. These guidelines are a valuable support in the execution of the test, but a lot of work still has to be done in terms of test interpretation.

The Italian structural code [NTC 2008], as well as the American one [ASCE 41-13], suggest this test with clear references and quantitative significance. It is worth to notice, in the framework of the knowledge levels and confidence factors, as the intermediate FC equal to 1.2 assigned to flat jack agrees with the experimental outcomes and hence seems to be adequate.

After all these considerations, the present research does not aim to confirm or compare flat jack with laboratory test, even if a wider number of such measures could provide a statistical meaning of these coefficients. This work aims, looking to a wide sample of executed tests, to evaluate advantages and drawbacks of this technique in real applications also highlighting that the significant scatter among samples is mainly due to the material and not the technique itself. In addition some considerations are drawn in terms of test interpretation which should be a key issue.

## 2.4 LOCAL LEVEL

The safety assessment of a building has to consider also the assessment of each structural element inside its structure. There are many types of structural elements and thus only one of them is here chosen. This paragraph aim to highlight, by means of literature review and real cases, why is important to deepen research on vaults. Three main reasons will be presented: the widespread of this element, its vulnerability to earthquake, the lack of knowledge in the analysis of the strengthened element.

### 2.4.1 *Arches and vaults in masonry building, historical aspects*

The first human constructions were based on the easiest structure which is the trilithon where the horizontal stone bears its selfweight. This system was adopted for a very long time and was used also for temples. The space between columns was established on geometrical proportions to avoid any resistance problem to the architrave. An interesting example of this is reported in Ezekiel book of Bible were a sort of manual of temple construction is described by means of geometrical proportion.

The needs to overpass higher span, and sometimes for the lack of massive stones, conducted to seek a construction technology which allows to achieve the goal. The usage of arch or vaulted structure was adopted in Mycenae (Fig. 2.29 left) to built tombs or after in Babylon to built the door of Ishtar (Fig. 2.29 right).

*Fig. 2.29 Treasury of Atreus, Mycenae, Bronze age 1250 bC (left)*
*Ishtar door at Babylon, VII-VI bC, Staatiliche Museen, Berlin (right)*

The great affirmation of vaulted system was due to Romans who looked at Greek and Etruscan techniques and after then they widely deepen the knowledge on this structural element. Romans well understood limits and advantages of arch,

they improved materials and constructive techniques. The effect of thrust was well known using very rarely flat arches. Romans were also confident with the weight distribution in vaults by means of clay vases (e.g. in Baths of Caracalla, [Lancaster 2005]) in some locations to create lighter portions or with the use of different aggregates in the *opus caementicium* as skilfully demonstrated in the Roman Pantheon (118-128 AD) which, with a diameter of 43.3 m, is actually the largest unreinforced concrete dome in the world (Fig. 2.30, left).

There are several books and researches on these aspects since their age (Vitruvio), throughout the history (Palladio), and nowadays [Watkin, 1996, Adam, 1984].

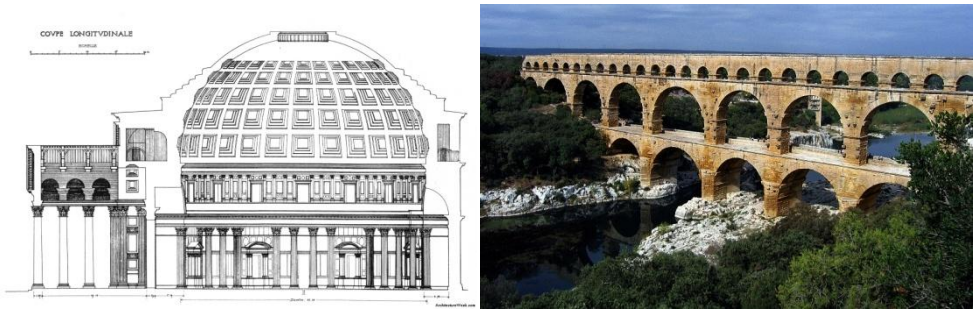


*Fig. 2.30 Pantheon's cross-section, Rome (left). Aqueduct of Pont du Gard, France (right)*

A special attention should be given to Roman Aqueduct that are impressive structures well constructed. In the Aqueduct of Pont du Gard (Fig. 2.30) is possible to recognise that arches with longer span, necessary to reduce the number of pillars on ground, were chosen only in lower levels. In higher level short span arches were preferred in order to stabilize, with a distributed load, the lower levels. Finally in the upper part that carries water, the height of wall is higher to stabilize also smallest arches with a distributed load. The cutting edge and the skills of Romans are here well demonstrated and from some point of view never recovered.

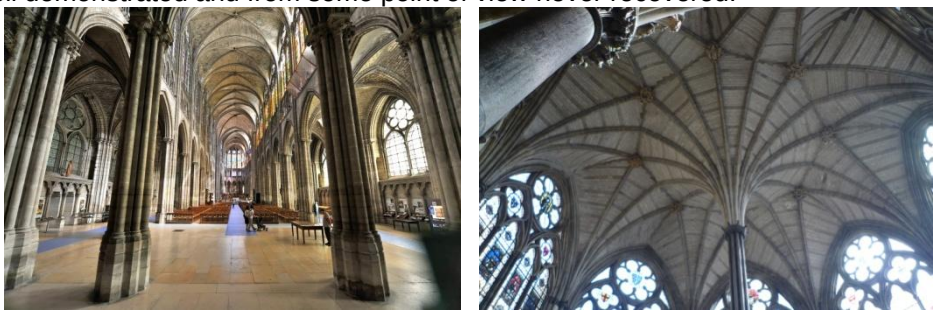

*Fig. 2.31 Basilica of Saint Denis, 1144 Paris (left) Vaults in Westminster, 1556 London (right)*

The use of barrel vaults was intensive in Romanesque style while it starts to be substituted by groin vaults and by pointed arches, or in some cases by more complex systems as fan vaults or Tudor arches, with the arrival of the gothic style in

the Northern Europe that led to the construction of some awesome architectures such as for instance Saint Denis and Westminster abbey (Fig. 2.31).

The use of domes is also an historical constructive technique which allows to cover wide spaces. An epitome of Byzantine architecture, considered with the Parthenon and the Pantheon the three top heritage of the history of architecture [Watkin 1996], is Hagia Sofia (Fig. 2.32 left), erected in 537 with a diameter of 31.5 m. The whole complex is 71x77 m wide and characterized by a system of minor vaults to counteract the thrust of the main dome in order to avoid the use of massive walls under the dome itself.

*Fig. 2.32 Hagia Sofia 537AD, Istanbul(L) Dome of S. Maria del Fiore, 1296-1436 Florence(R)*

Another example is dome of the Santa Maria del Fiore cathedral in Florence which actually is the largest masonry dome the world has never known. The way in which this construction was erected is not clear yet because it was built without internal scaffolding. This dome is emblematic from a structural point of view because it helps to show how a sophisticated use of geometry in a very precise way together with a carefully stereotomy and a balanced weight distribution could bring to construct this heritage without the analytical tools available nowadays.

The interest in vaults is not only related to paramount heritage but is strictly related to common structures. Masonry buildings are the most common type of constructions and they are present in all historical city centres. An interesting drawing by Violet-le-Duc [1854] (see Fig. 2.33) represents a typical cross section of a medieval building that are representative also of other periods such as Renaissance and modern age, until the introduction of steel and concrete.

In this section is possible to recognise all the structural elements that should be analysed in a masonry building. The vertical elements are walls with different sections and the horizontal elements are vaults for the lower storeys, and timber floors and roof for the higher elements. In addition to palaces, in the major part of churches, structural vaults are used to cover naves and chapels with a timber roof above. Only sometimes due to economic reasons light system with wattle ceiling

was built. The use of a sole timber roof was frequently adopted in Romanic churches but due to its vulnerability to fire was progressively abandon.

Hence, the massive presence of vaults requires a deep study of them in order to reliably understand their behaviour and their influence on the whole construction.

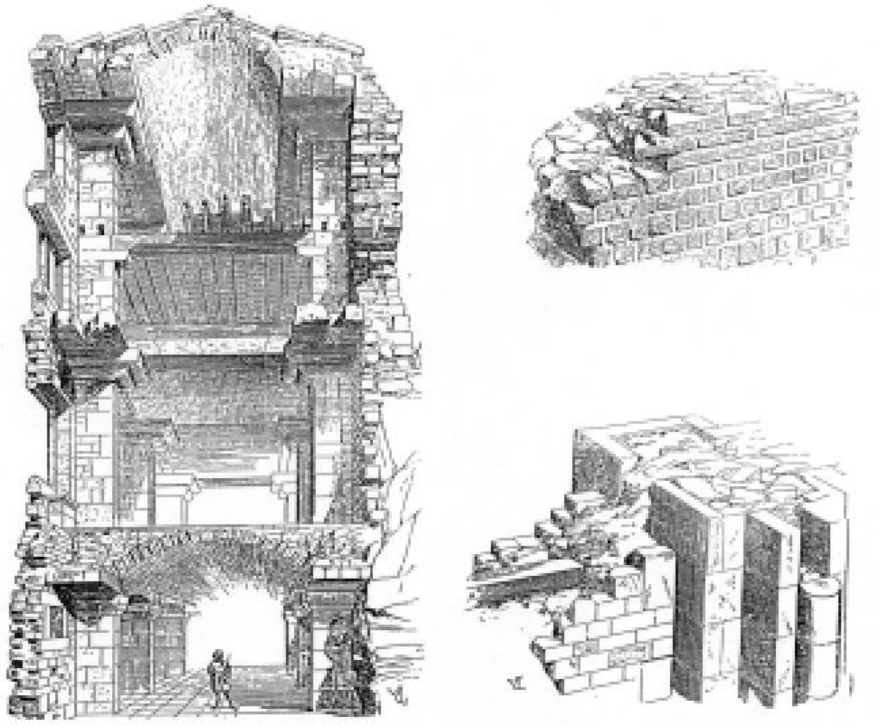

*Fig. 2.33 Section of a medieval building and of roman wall (Viollet-le-Duc 1854)*

An example of the vault widespread is also related to the pilot sites studied in the ProVaCI research project in which from the Roman age, with the Roman Theatre, going through the medieval age, with cloisters in S. Fermo and the Archeological museum, to modern age with the St. Peter Castle all buildings are dealing with vaulted systems (see Fig. 2.34 and Fig. 2.35).

*Fig. 2.34 Arch in the Roman Theatre (left), groin vaults in S. Fermo's lower church (right)*


*Fig. 2.35, groin vaults of the museum cloister (left), barrel vaults in St. Peter Castle (right)*

### 2.4.2 *Structural assessment of masonry arches*

From the brief introduction about possibilities, historical background and distribution of vaults, the major question which rises is about how those structures were calculated, because about safety, the time has already answered. To figure out this question Santiago Huerta [2001] concluded that on one hand is matter of geometry, based on equilibrium approach; and on the other hand, engineers and architects are lack in experience and cutting edge faced to cutting masons or master builders which built indeed cathedrals.

In his speech for the *Doctor Honoris Causa* in Madrid, Jacques Heyman faced this topic summarizing in a very clear way such aspects defining three main branches: geometry, mechanics and analysis.

Thanks to this division is here presented the current state of art in vaults analysis following the flowchart of Fig. 2.37.

The meaning of historical proportions in architecture becomes not only from aesthetic reasons but are strictly linked to structural issues that guarantee the whole stability. To use defined proportion in structure allows to achieve those results.

Vitruvio in *De Architettura* and than Leon Battista Alberti in *De Re Aedeificatoria* expresses those roles of proportion that are needed to achieve stable structures. A first intuition about the modern analysis on arches where by Leonardo Da Vinci (1452–1519) that wrote (translated) "*The arch is nothing else than a force originated by two weaknesses, for the arch in buildings is composed of two segments of a circle, each of which being very weak in itself tends to fall; but as each opposes this tendency in the other, the two weaknesses combine to form one strength.*" Then, he understood that for ensure its stability for any type of action the geometry should permits to draw a line from abutments toward the keystone. This could be defined a geometrical rule about thrust line antelitteram.

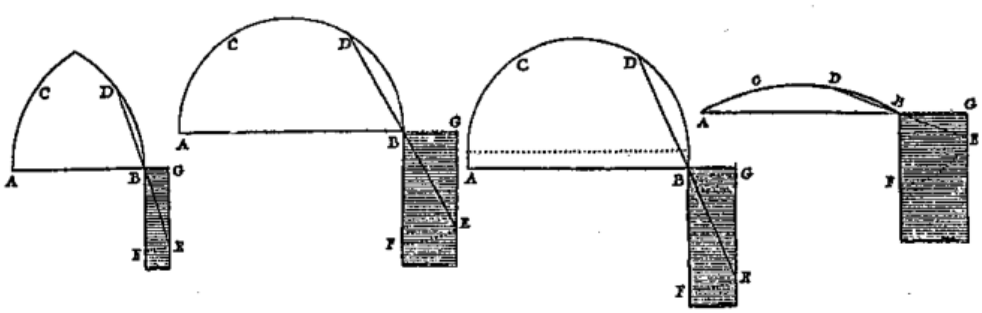

*Fig. 2.36 "Course d'Architecture" on butresses proprotion [Blondel 1683]*

Moreover, two hundred years later, a similar concept used to build abutments was given by Blondel's [1683] lectures note (Fig. 2.36). Based on the arch shape, he taught how width should be abutments or pillar bearing arches. In this drawing is nowadays possible to see and insight of thrust line. However it has to be noticed that geometrical roles work because forces were based only on selfweight.

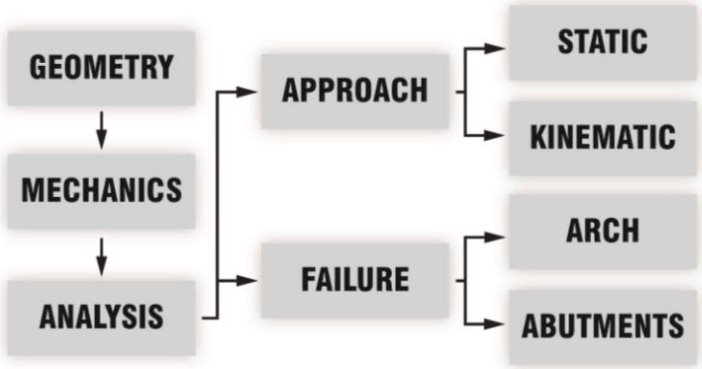


*Fig. 2.37 Flowchart of the structural assessment of arches*

Two main reasons conducted to introduce the branch of mechanics where equilibrium conditions were evaluated by means of calculations: wish of changing those proportions and damages on existing structures. The need of changing geometrical proportions was for example used to built nave and aisles vaults with different spans by the introduction of some additional weight on the smaller vault to properly counteract the thrust [Rubiò, 1912].

It was obviously possible thanks to improving in mechanical science such as the introduction of parallelogram of forces [Straub, 1952] and first resistance definitions [Galileo, 1638]. After those first progress a scientific method on vault calculation was introduced with the concept of thrust line by Hooke [1670] who stated: "*as hangs the flexible line so but inverted will stand the rigid arch*". Although he was unable to give a mathematical description of this theorem, this concept is

the base of the thrust line analysis. Inverted chain assumption will have led interesting innovation and architectures after centuries with Gaudì who used this concept, with the addition of a mirror, to create his architectures.

This idea was fixed by the definition of a graphical method by De La Hire (1712) who introduced the funicular polygon to define the thrust line. The use of this tool to assess arches was than fixed with the introduction of the current failure modes by Coupelet [1730] who introduced the concept of hinges (Failure 1 and 2 Fig. 2.38 left) and after by Coulomb [1773] who defined sliding between voussoirs (Failure 3 and 4 Fig. 2.38 left). Coulomb was also aware that this type of failure rarely occurs. Therefore also in branch of mechanics first insights of failure modes were known. In this field also Mascheroni (1785) gave an interesting contribution with the idea of plastic hinges and the structural system of equilibrated beams.

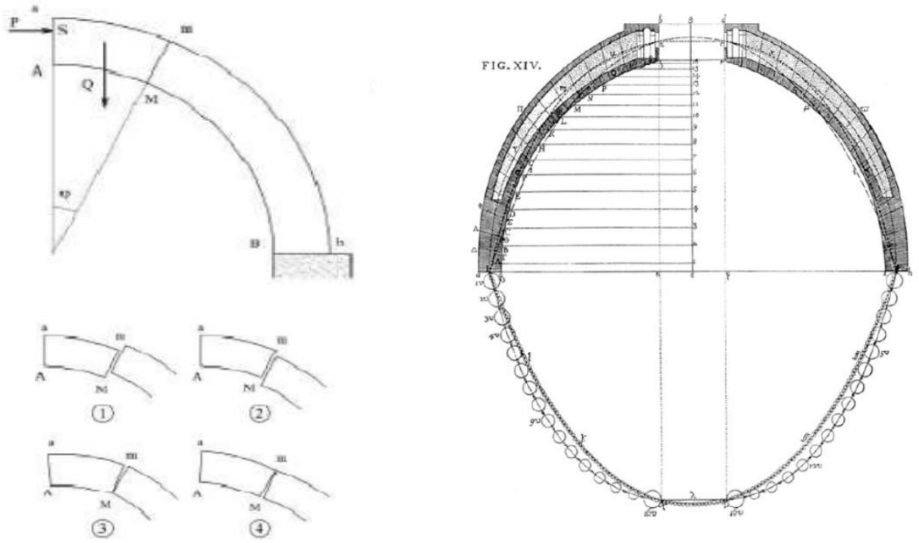


*Fig. 2.38 Failure mode by Coulomb [1773](left)*
*Analysis of the cross section of the St. Peter's Dome made by Poleni [1743] (right)*

An application of Hooke principle was by Wren in the calculation of the St Paul's Cathedral in London. Another important application on a real case was made by Poleni [1748] (Fig. 2.38 right) that demonstrated a rigorous scientific application of the idea of inverted chain which has always to remain inside the dome thickness. He studied the Michelangelo's dome after some damages and meridional cracks concluding, thanks to the inverted chain method, that the dome was safety in cracked conditions but cautiously he designed three hooping levels demonstrating to be confident with safety of arches and with the behaviour of domes.

Analysis, although introduced in theoretical terms by Galileo [1638] with the problem of the cantilever beam, was rigorously considered starting from Navier

[1826] who tried to define the actual position of thrust line. He used the modern statements of elastic theory in stress terms compatibility conditions. Further development was carried out by Mery [1840] with the implementation of a rigorous graphical method to calculate the position of the thrust line by means of the funicular polygon.

The use of elastic theory on arches requires to fulfil both compatibility and equilibrium. On arches, that are indeterminate structure (hyperstatic), this means that a slight change in boundary conditions dramatically changes the internal solution. Castigliano [1879] constrained the thrust in the middle third to avoid crack or then he developed his approach with also iterative solutions to account of part in tension and thus cracked. Heyman [1996] underlined that the challenge to evaluate the actual state-stress was impossible because it is too sensitive to external conditions. Therefore the question moves from actual stress distribution to safety, that means: does exist a thrust line that is in equilibrium with the given geometric and load distributions?

Barlow [1846] demonstrated experimentally (Fig. 2.39) that in an arch not only exist a defined thrust line, but also that there are infinite allowable lines inside the arch.

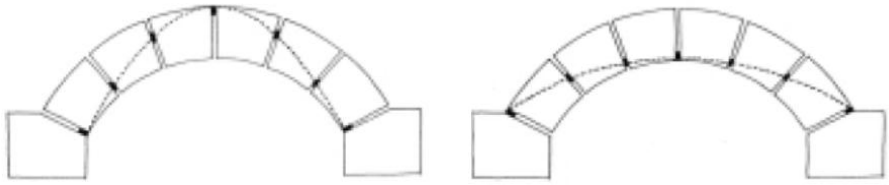

*Fig. 2.39 Barlow (1846) experimental demonstration of different allowable thrust lines*

This demonstration should be considered a practical example of formally summarizing by the implementation of the master safe theorem [Heyman 1966] in masonry with the following hypothesis:

i. masonry has no tensile strength;
ii. stresses are so low that masonry has effectively an unlimited compressive strength;
iii. sliding failure does not occur.

A deep analysis of this is reported in Heyman [1996] with some important conclusions here summarized:

1. a slight movement of abutments does not significantly change the arch safety due to the 'natural morbidity' of masonry;
2. it is possible to evaluate the stability of the arch even if in the internal state could change time to time;

3. thrust line and hence the trust on abutments can lie between to boundaries define by two extreme lines (Fig. 2.40);
4. if exist an equilibrated thrust line within the arch, then, it is safe even if the line does not represent the actual stress state;
5. from a practical point of view the arch is safe when the thrust line could be contained in an arch of half the real depth.

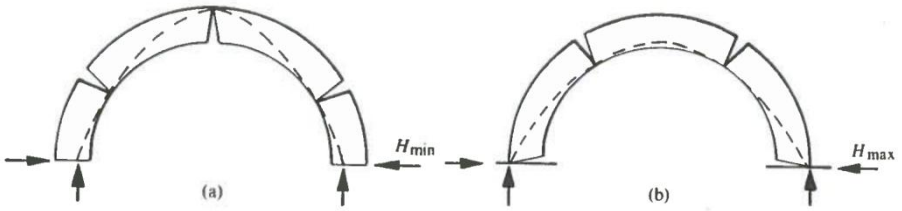


*Fig. 2.40 Heyman (1966), minimum and maximum abutment thrust*

From the static side about analysis the field was deeply investigated by the scientific community. The other approach (Fig. 2.37) is the kinematic analysis which is based on find a load multiplier $\lambda$ which gives positive plastic energy dissipation. Plastic theory is based on theorems demonstrated by Gvodzev [1936, 1960] and using the principle of virtual work. This model is faster and applies a sufficient number of releases to transform the structure into a mechanism.

In order to theoretically demonstrate which is the safer and easier way to approach the problem a great innovation is given by the three theorems of lower bound, the upper bound and their uniqueness. The limit analysis is hence based on three powerful theorems.

In the lower bound, an equilibrated state for which the yield condition is respected in any point is a statically admissible configuration.

In the upper bound, any potential failure mechanism for which the external power is positive is a kinematically admissible configuration.

The uniqueness theorem state that, the load factor $\lambda$ for which mechanisms, yield and equilibrium conditions are satisfied is the unique collapse load factor.

Yield condition is satisfied when the stresses in material are everywhere lower than the material strength while the equilibrium condition is satisfied when the internal and external actions are equilibrated. The graph in Fig. 2.41 summarizes this concept.

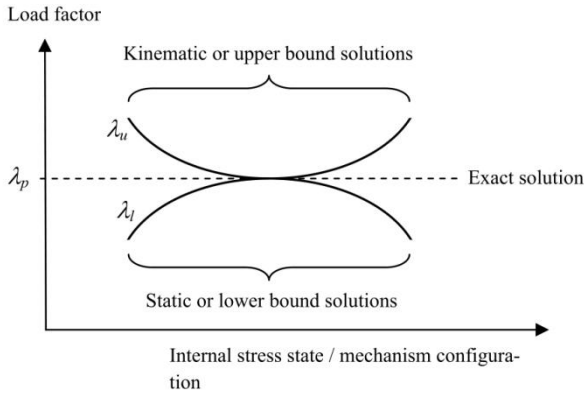


*Fig. 2.41 Relationship between upper and lower bound solutions [Gilbert 2007]*

Summarising, to date three main approaches are available, two based on static equations and one based on kinematic. About static is possible to use the approach based on the thrust line calculation with already mentioned safe theorem which guarantee the stability of the arch if it is possible to draw at least one curve inside the section. From an analytical point of view equations (Fig. 2.42) [Heyman 1996] have three unknowns based on the thrust position on supports and its magnitude.

Heyman faced also the problem of the resisting domain for an uncompressive material (black line) and for a material with finite compressive strength (dash line).

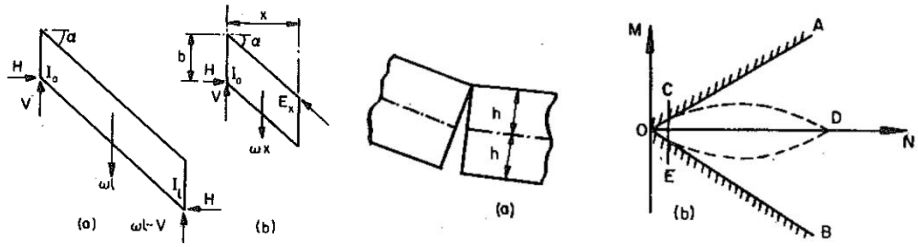


*Fig. 2.42 Example of equilibrium of a flying buttress with the thrust line (left) and resistance domain (right) [Heyman 1996]*

The other static approach is suggested by Orduna [2003] and is based to equilibrium and compatibility equations of several blocks which should represent the arch voussoirs. Also here the definition of a resistance domain was carried out (Fig. 2.43)

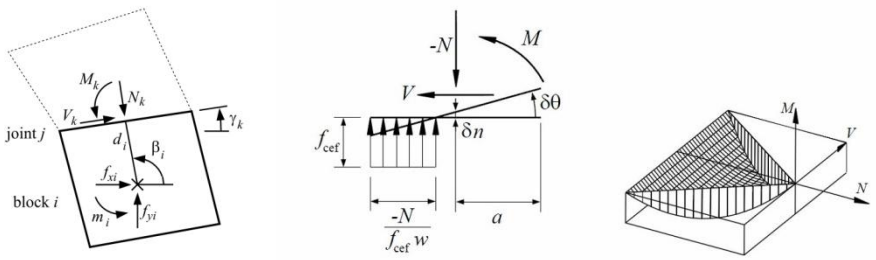


*Fig. 2.43 Equilibrium between two blocks and forces definition (left and centre), half resistance domain (rigth). [Orduna 2003]*

The third approach is based on a kinematic approach and the principle of virtual work (Fig. 2.44). The use of kinematic analysis is hence easier but a careful positioning of hinges is required whereas the thrust line is a conservative approach. The proposal of Chen [2007] looks also to possible reinforced conditions which really improve the possible use of the presented method.

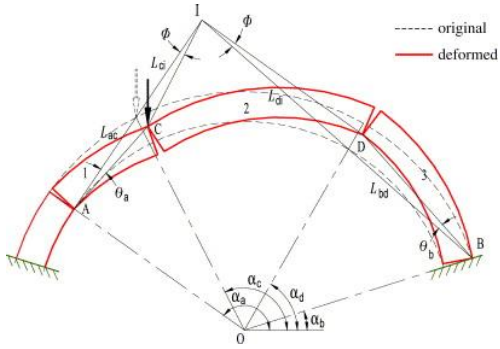


*Fig. 2.44 Limit analysis with kinematic approach [Chen 2007]*

Finally there are two simplified methods, used mainly in railway engineering which are: MEXE and SMART [Melburne 2007].

The MEXE method (Military Engineering eXperimental Establishment) was a semi-empirical method used during the World War II by military engineers to quickly determine the load bearing capacity. The method is based on Pippard's elastic method and is the analytical solution of the problem based on the Navier's formula [Navier 1824]. The model is thus conservative and related to some geometrical correlations (rise/span ratio, shape of intrados) based on nomograms to figure out some correction factors. The model was update several time and there is a current version given by the UK Department of Transport.

The SMART model is based on geometry, material properties, loads and failure mode with the goal to assess the long term behaviour of the structure by means of limit states.

Back to Fig. 2.37, masonry arches, here considered as unreinforced, are governed by rules of proportion and for this reason their construction in stable conditions was possible thousands of years ago. The use of mechanics and evaluation of acting forces allows a better understanding and the uniqueness theorem is the keystone of the theoretical approach.

About the failure modes of an arch a brief analysis is presented. Rather than sliding which occurs rarely a focus on possible mechanisms is herein taken into account.

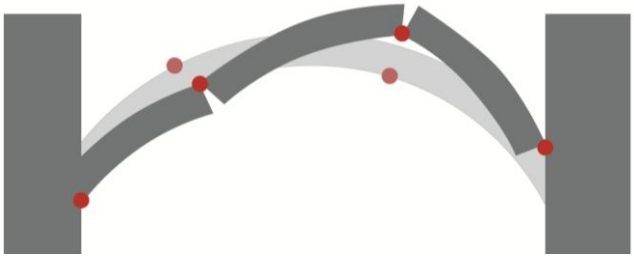

*Fig. 2.45 Typical mechanism failure mode for an arch*

Mechanisms can be activated involving the abutments or not and this is an important separation. In Fig. 2.45 a typical mechanisms involving only the arch is presented. From a theoretical point of view the number of hinges is 4 for asymmetric conditions of load or geometry and 5 for symmetric conditions but in practical terms the latter condition is unlikely. Hinges positions are always alternately on extrados and intrados and their position is the key issue of the problem.

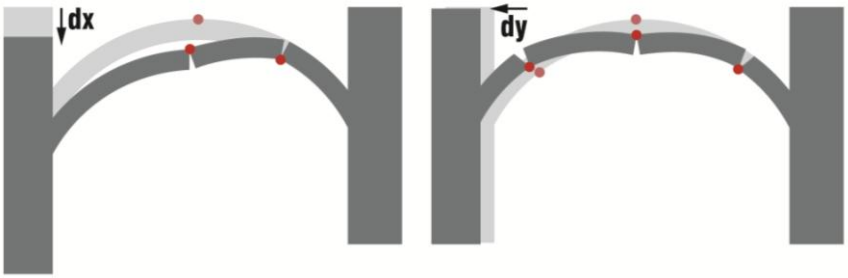


*Fig. 2.46 Hinges formation after abutments settlements*

Another possibility of damage in arches is related to the interaction of the arch and its abutments. Therefore its stability is also influenced by supports which could cause its collapse. In Fig. 2.46 mechanisms associated to differential settlements are reported. For small displacements, as suggested by Heyman [1966] there are not unstable conditions. The number of hinges is still lower than four but the load factor is decreased. Moreover if that displacement becomes too large the structure fails. In conclusion, especially the mechanism on the right is frequent and could involve in the mechanism the entire pillar with the fourth hinges at the base.

The thrust on abutments enhance this problem especially with pillars or walls. A possible solution to avoid this horizontal differential displacement is the introduction of a tie rod.

### 2.4.3 *Arches and vaults in recent earthquakes*

From the previous chapter, arches and vaults in historical constructions seem to be well constructed and safe. Moreover the analytical tools were properly developed to be reliable but an environmental action which was not evaluated in past is earthquake. This doesn't mean a necessary vulnerability or collapses for all structures, for example in Rome, between the year 1000 and 2000, 8 earthquakes occurred with a macroscale intensity equal or major than 6 with a maximum of 7.5 and the Pantheon does not collapse. The same for the Brunelleschi's dome which bears in the same period 13 quakes in the same intensity range [DBMI11_INGV]. In the case of Hagia Sofia it suffered more about earthquakes with three collapses after earthquakes.

The interest in topic is great and a first analysis on damages of this action is considered in order to practically demonstrate the need of research in that field that rises in the scientific community in last decades.

As presented in §2.1 about the safety of masonry structures the Friuli earthquakes in 1976 has strongly increased the attention on seismic action, at least in Italy. In earthquakes severe and extent damages were observed on many buildings and elements, and vaults are one of these (Fig. 2.47). It is possible to analysis two possible limit states about vaults and the event on Umbria-Marche 1997 which hit the vaults of the San Francesco Maggiore church (Fig. 2.47) is an example. The major one of course is the collapse related to safety and one, introduced in Italian guidelines about cultural heritage, is related to damages on artistic parts. In this case for instance some Giotto's frescoes have been lost.

*Fig. 2.47 Vault collapsed after Friuli earthquake 1976 (left),*
*S. Francesco d'Assisi vault collapse 1997 (right)*

The aim of this paragraph is to evaluate and highlight, with the respect to other mechanisms, the vulnerability of vaults. In practical terms is interesting to understand which are, in a building, the most vulnerable parts. To figure out this from a numerical point of view the attention is focused only on churches where data are available

After a Italian seismic event, the University of Padova is involved in emergency phases to evaluate, by means of expeditious tools, the buildings safety. It is mandatory for authorities, after extreme events, to immediately deal with the evaluation of damages also to plan emergency facilities. There are several levels, depending on the detail of the survey, and herein only one is faced and concerns the data coming from the evaluation form called "Scheda chiese" (D.P.C.M. n.55/2006) [Modena, Binda 2009] which actually is related to the second of three levels. The survey changed several times in past and a first draft was elaborated by GNDT and than revised from the University of Genova [Lagomarsino 2004]. The number of mechanisms considered increased from 16 to 18 and finally to 28 (Fig. 2.48). The final form became law by the prime ministerial decree of above. In the same national law there is also another form about "palazzi" (large town houses) but is not similarly developed and hence less useful for the goal. Summarizing, the data gathered from the present analysis are related only on churches and only on earthquakes occurred later the law, namely Abruzzo 2009 and Emilia 2012.

The form collects several information about: building, localization, site, infrastructures, artistic assets, function and maintenance state. The damages on churches are evaluated with the respect to possible mechanism in the structure (Fig. 2.48). The final part is related to required first interventions, their costs estimation and aims to give a whole judgment of the structure.

The data gathered in the first database [da Silva 2012] are the survey of Abruzzo 2009 earthquake and it has been enlarged with the available forms collected in Emilia 2012. The two events showed a different response by the structures of the two regions, mainly due to typologies of building and masonry quality [Modena et al. 2012]. For this reason the data will be treated separately. The overall number of cases analysed is 419, 241 cases concerning Abruzzo and the other 178 Emilia.

The data reports the possibility of occurrence of each mechanism and the actual activation. Moreover for each one a damage level, from 1 to 5 is assigned. These levels should be chosen based in the macroseismic scale EMS98 [Grünthal, 1998] ( 0-no damage, 1-minor damage, 2-moderate damage, 3- medium damage, 4-severe damage, 5-collapse).

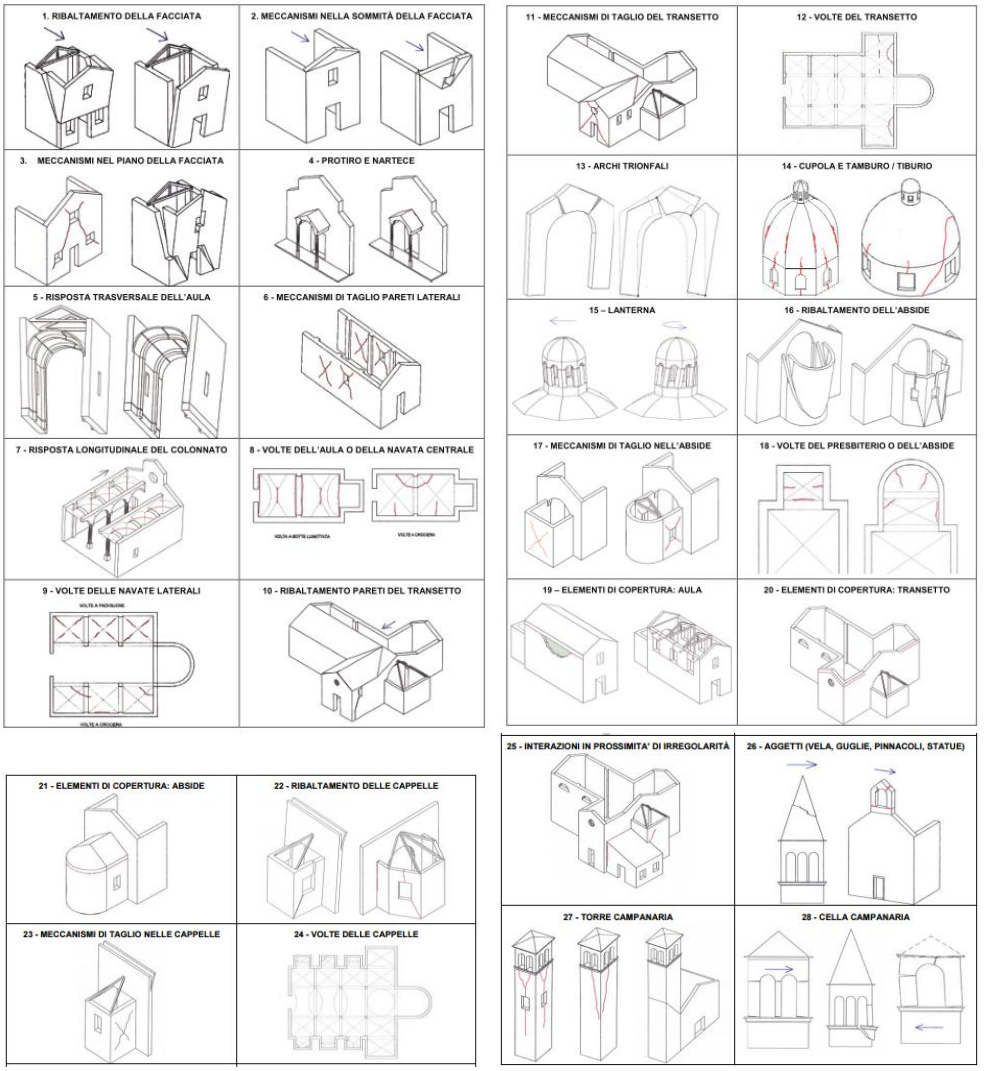


*Fig. 2.48 List of the 28 damage mechanisms in the current form*

In the evaluation of possible cases some are always present because related to essential elements (1,2,3,5,6,19) other could give interesting information on structural typologies such as presence of nave, transept and domes.

It has to be accounted that the collected data are surveys of the building structural response to the seismic action and therefore describes demand and capacity together. Due to the variability of action, affected by distance to epicentre or by local soil effects, it is not possible to obtain an effective vulnerability measure. It seems anyway reasonable to analyse the observed effects due to a random distribution of the action among churches.

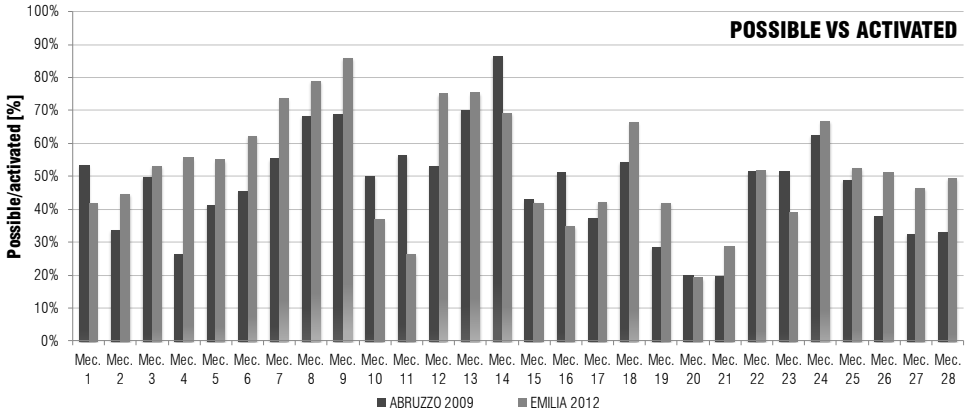


*Fig. 2.49 Histogram of the percentage of mechanisms in fact activated*

The ratio of the possible mechanisms to the number of those in fact activated, is a relevant parameter to understand which are the mechanisms more affected by the seismic action and somehow their vulnerability. In Fig. 2.49 are presented these percentages where is possible to see that the most common mechanisms associated to the facade are activated in about the half of all cases. Highest percentage of activation are related to mechanisms 8,9,13,14 which actualy regards arches and vaults. The possibility of these four is related to the building typology but when possibile are activated with ranges lying between 70 and 90% confirming the high vulnerability of those elements.

Fig. 2.50 shows the average level of damage associated to each mechanism calculated with eq. (2.13):

$$i_d = \frac{d}{5n} \tag{2.13}$$

Values varys around 2 and 3 because average does not properly represent the distribution of damages. The mechanisms most damaged (over 2.5) are 8,9,15,26,28 and only for Emilia 2012 19,27. This shows high damages of small isolated portion as lantern, belfry and pinncles when occured but the attention is given to the high damage related to mechansims 8 an 9 that envolve the entire structure and stress a significant role in reducing the vulnerability of vaults.

Fig. 2.51 presents the number of damage indexes for each mechanism giving a overall idea of damage distribution. Mechanisms 26 has the higher occurance of collapses but is related to the overturn of smal portion which does not involve the overall behaviour. Mehanism 8 is the second and it presents a constant number

among damages wheras in general there is a decreasing of cases form minor to major levels. This means that this is a dangerous mechanism with high occurancy of collapses. The observation on field demostrated (Fig. 2.52) that also high damages related to bearing walls cause the collapse of upper structures such as vaults and roofs increasing the number of collapse cases even if not directly related to the vault vulnerabilities.

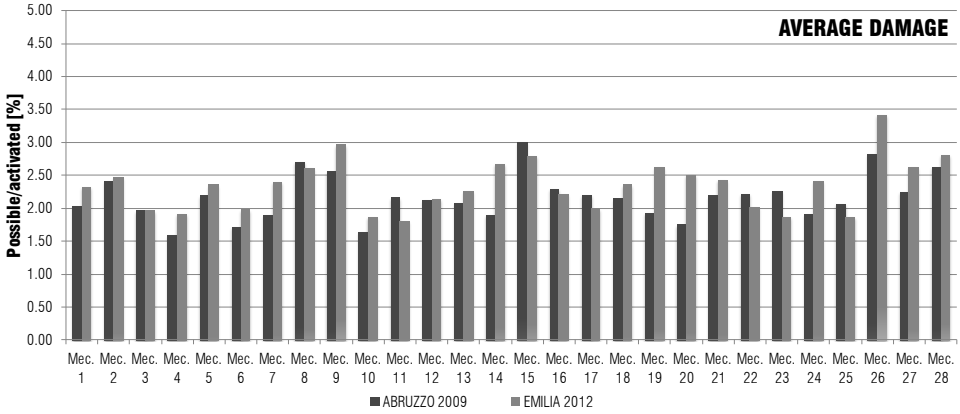


*Fig. 2.50 Average damage index for each mechanism*

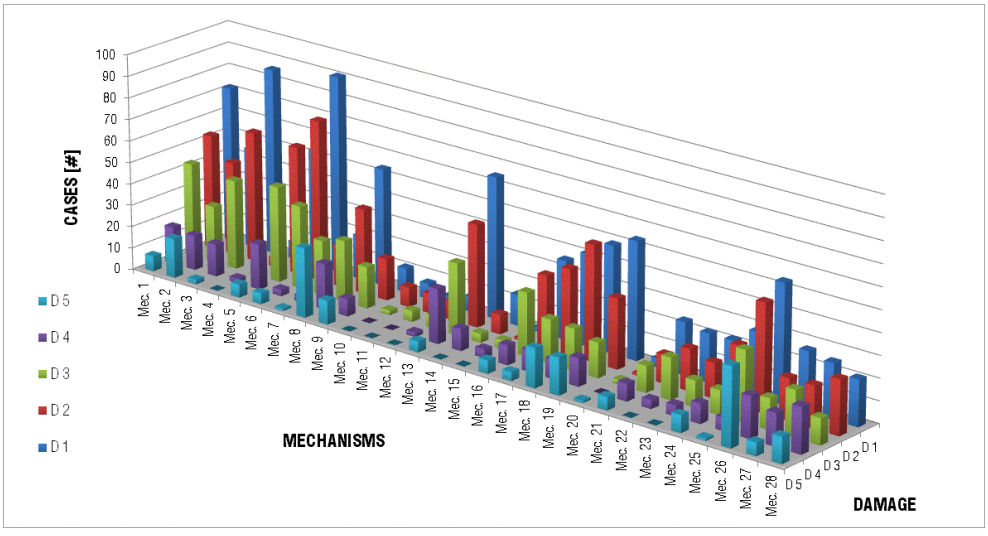


*Fig. 2.51 n of damage indexes for each mechanism*


*Fig. 2.52 S. Martino Buonacompra - BO (left), San Francesco, Carpi - MO (right)*

A conclusive evaluation is reported with the attempt to relate the two normalized indexes, namely possible vs activated and damage index. A risk factor $r_i$ is introduced in eq. (2.14) to take into account on one side the frequency of occurrence of one mechanisms and on the other side its average damage when it occurs indeed.

$$r_i = \frac{n_{activated}}{n_{possilbe}} \cdot i_d \tag{2.14}$$

In conclusion is possible to figure out that, to ensure the safety of a church, attention on vaults should be carefully evaluated. To obtain this, reliable tools have to be studied and the research should be deepened.

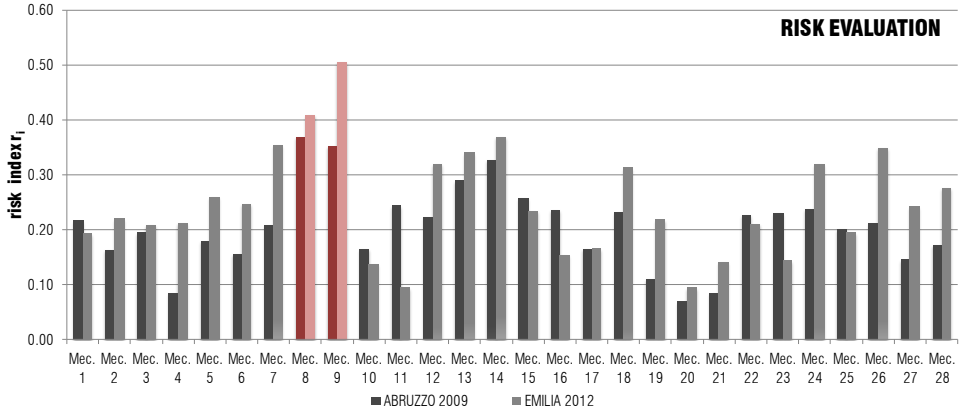


*Fig. 2.53 Summarize of risk factor for each mechanism (vaults of naive and aisle are in red)*

The survey of earthquake damages gave an opportunity to test also the reliability of interventions. The introduction of fibre reinforced polymers, as presented in § 2.2.2, allows to strengthen arches increasing considerably their strength and deflections. The application in some cases of these in churches before the Abruzzo earthquake allows to have a proof of major problems such as the debonding of fibre applied at the intrados (Fig. 2.54).

*Fig. 2.54 Carbon fibre detachment after the opening of an hinge in the arch (L'Aquila)*

### 2.4.4 *Structural assessment of strengthened arches*

Although the knowledge of vaults in unstrengthened conditions has been well developed from an analytical point of view with the safety theorem, the introduction of a material bearing tensile stresses changes completely the hypothesis. Moreover some parameters with negligible influence in unreinforced conditions become more relevant in the new configuration. This is basically due to the evaluation of stress distribution based on materials stiffness and strength less significant before. In next paragraphs some considerations on this will be illustrated.

#### *2.4.4.1 Existing models on literature*

A first important contribution in the calculation of masonry cross sections strengthened by composites material was by Triantafillou [1998] with the definition of the resistance domain of strengthened cross sections (Fig. 2.55).

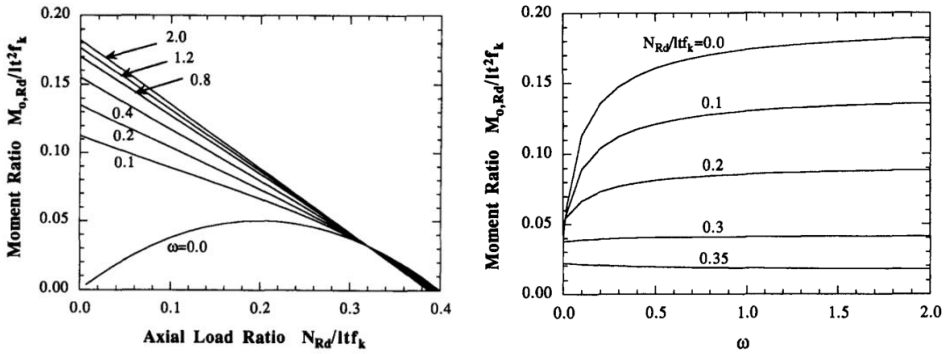


*Fig. 2.55 Triantafillou domains varying $\omega$ (left),*
*out-of-plane moment capacity vs $\omega$ for several axial loads (right)*

To operate with a homogeneous material, Triantafillou [1998] adopted two parameters defined in eq. (2.15) based on the composite area fraction of the cross section $\rho$ and on the normalized area fraction of FRP $\omega$.

$$\rho = \frac{A_{frp}}{l\,t} \qquad \omega = \frac{\varepsilon_{m,u} E_f}{f_m} \cdot \rho \tag{2.15}$$

Masonry is defined with a stress block law, with $\varepsilon_{m,u}$ and $0.2\,\varepsilon_{m,u}$ as boundaries, neglecting the reduction parameter $\alpha$ and acting only on compression. The constitutive law of the FRP is linear until $\varepsilon_{f,u}$ and acting only in tension (Fig. 2.56). The approach was general for a distributed number of reinforcements and it was adapted to a vaulted system by Valluzzi [2002].

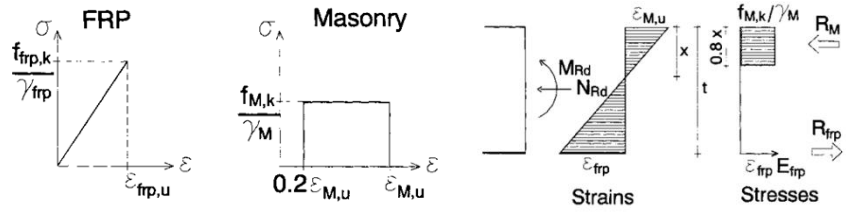


*Fig. 2.56 Constitutive laws of materials (left) stress distribution (right) [Valluzzi 2002]*

To draw the resistance domain an equation calculating the resisting bending moment for a determinate axial load is need. To do determine this, equilibrium conditions are defined as:

$$N = R_{frp} + R_m \tag{2.16}$$

$$M = \frac{t}{2} \cdot R_{frp} + \left(\frac{t}{2} - \frac{0.8x}{2}\right) \cdot R_m \tag{2.17}$$

$$\frac{\varepsilon_f}{\varepsilon_m} = \frac{t - x}{x} \tag{2.18}$$

To draw a general resistance domain without a reference to specific dimensions or strength two normalized quantities are defined as follow:

$$N^* = \frac{N}{f_{m,k}\,l\,t} \tag{2.19}$$

$$M^* = \frac{M}{f_{m,k}\,l\,t^2} \tag{2.20}$$

where :

$f_{m,k}$ is the design compressive strength of masonry,

$l$ is the width of the cross section,

$t$ is the thickness of the cross section.

Like presented in Fig. 2.56 the relationship between $R_{FRP}$ and $R_m$ is based on compatibility equation of strain which relates both terms by means of the position of

the neutral axis defined by x (see eq.(2.18)). The substitution of (2.15) and (2.18) into (2.16) and (2.17) and further normalized with (2.19) and (2.20) bring to equation (2.21) in order to define the position of the neutral axis for a defined value of axial force. After this, eq. (2.22) gives the resistant bending moment.

$$\frac{x}{t} = \frac{\gamma_m}{1.6}\left[\frac{N^*}{\gamma_m} - \omega + \sqrt{\left(\omega - \frac{N^*}{\gamma_m}\right)^2 + \frac{3.2}{\gamma_m}\omega}\right] \tag{2.21}$$

$$\frac{M^*}{\gamma_m} = \frac{1}{2}\omega\frac{\left(1 - {}^{x}/_{t}\right)}{{}^{x}/_{t}} + \frac{0.4}{\gamma_m}\frac{x}{t}\left(1 - 0.8\frac{x}{t}\right) \tag{2.22}$$

Form this formulation is possible to notice that no conditioning was introduced for the compression acting on the FRP. With high values of ω the domain reaches the abscissa axis for lower value than 0.4.

$$\omega_{lim} = \frac{\varepsilon_{m,u}E_f}{f_k}\cdot\rho_{lim} = \frac{\varepsilon_{m,u}}{\varepsilon_{f,u}}\cdot\left[\frac{0.8}{\gamma_m}\frac{1}{\left(1 + \frac{\varepsilon_{f,u}}{\varepsilon_{m,u}}\right)} - \frac{N_{Rd}}{ltf_k}\right] \tag{2.23}$$

Moreover this approach looks only to masonry crushing because it is not suitable for $\omega < \omega_{lim}$ calculated according eq. (2.23) and therefore for low values of $\rho$ a strange behaviour rises for low values of N*. This behaviour is present for example in the experimentation carried out in this work (see § 6.1.1).

Another method to calculate the flexural capacity of a strengthened cross section was purposed by Foraboschi [2004] where, based on experimental testing, he assumes a fixed position and magnitude of the compression acting in masonry.

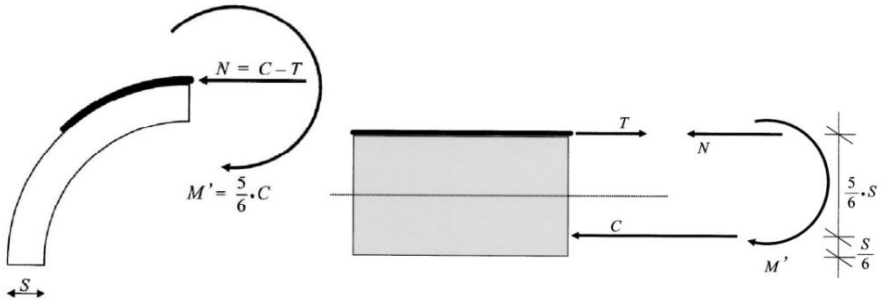


*Fig. 2.57 Foraboschi [2004] model for strengthened arches*

As illustrated in Fig. 2.57 the compression of masonry at the ultimate stage is located at a fixed location of 1/6 of the thickness and with a dimension of the stress block of 1/3 of the overall thickness. The model appears easy applicable without many calculations because of the constraining of the compressive component which is indeed a strong hypothesis. The formulation seems to lack in theoretical formulation with missing of a compatibility equation less rigorous than the previous model. Moreover the definition of a maximum compression force limited to one third of the entire thickness limits the overall capacity of the cross-section for high the

domain part higher than N* equal to 0.5. Form the consideration of the paper it seems that the maximum moment M' should be calculated despite the evaluation of the acting axial force which does not bring also to equilibrium condition.

A careful analysis of the model with some additional considerations based on the highlighted problems, presented in § 6.1.1, demonstrates an adaptation of the model. For the fibre rupture there is an overall agreement with the more complicated case whereas the limitation of the compressive force completely neglects a portion of the domain.

An interesting approach is suggested by Roca et al. [2007] where a similar approach to the unreinforced arch is used by means of the thrust line. The limits of the thrust are not the material thickness of the arch but some strength boundaries (see Fig. 2.58) calculated from the cross section. In this case the reinforcements are steel bars and hence the formulation uses a constant stress of bars given by yielding but it is possible to use a resistance domain to detect those strength boundaries.

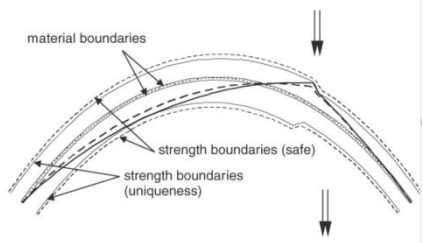


*Fig. 2.58 Thrust line and its limits for a strenghtned arch [Roca et al. 2007]*

The last reference here reported is on the proposal of D'Ambrisi [2013] who develops an analytical model, based on limit analysis, to calculate the ultimate load capacity of an arch strengthened by an unbonded tendon. The model is similar to Chen [2007] and Gilbert [2007] because considers the upper bound theorem to estimate the critical load. The model accounts for a linear elastic material also in the virtual work formulation and therefore suitable to composites application. Conversely it does not account for masonry compressive strength and due to hypotheses on friction, it is suitable only for this kind of intervention and not for typical FRP applications.

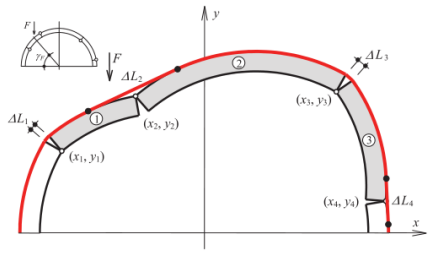


*Fig. 2.59 Generic configuration of a strengthened arch by unbonded tendon [D'Ambrisi 2013]*

#### *2.4.4.2 Tension distribution in curved beam*

The analysis of a cross-section resistance domain, with the calculation of each field, distributes the internal stresses linearly. In term of stress, considering the presence of materials which bear tension and compression, a strengthened vault requires to evaluate effects of curvature. Curved beam does not fulfil Navier [1826] and de Saint-Venant [1864] hypothesis and equations and hence new equation should be considered.

In order to describe formulations that governing this case, an infinitesimal cross-section with an angle of $d\theta$ is considered with the geometrical parameters reported in Fig. 2.60.

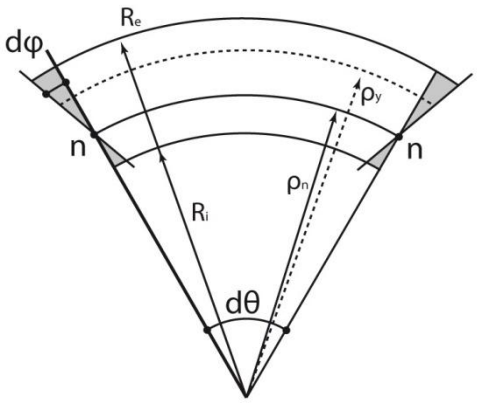


*Fig. 2.60 Infinitesimal cross-section of a curved beam*

First of all the equilibrium equations, in both translation and rotation, are described as:

$$N = \int_A \sigma_y dA \tag{2.24}$$

$$M = \int_A \sigma_y \cdot y \, dA \tag{2.25}$$

Let use in this case a pure bending action with a null axial action. Hence eq. (2.24) is equal to zero.

The moment M applied at each end is evaluated by an imposed infinitesimal rotation of $d\varphi$ with the hypothesis of a linear distribution of strains. Deformations are thus related to stresses by Hooke's equation (2.26) and referring to parameters of Fig. 2.60 is possible to define:

$$\sigma_y = E\varepsilon_y = E\frac{\Delta l_y}{l_y} \tag{2.26}$$

$$l_y = \rho_y \cdot d\theta \tag{2.27}$$

$$\Delta l_y = (\rho_y - \rho_n) \cdot d\varphi \tag{2.28}$$

Now eq. (2.27) and (2.28) are substituted in eq (2.26), that inside (2.24) becomes:

$$N = \int_A E \cdot \frac{d\varphi}{d\theta} \cdot \frac{\rho_y - \rho_n}{\rho_y} dA \tag{2.29}$$

Solving the integral, and keeping in mind that the overall axial force is null, $\rho_n$ remains the only unknown and hence:

$$N = E \cdot \frac{d\varphi}{d\theta} \left( \int_A dA - \rho_n \int_A \frac{1}{\rho_y} dA \right) = 0 \tag{2.30}$$

Considering the finite integral of the area with the two internal and external radiuses as limits eq. (2.30) gives:

$$\rho_n = \frac{A}{\int_A {}^1/_{\rho_y}\, dA} = \frac{R_e - R_i}{\ln\left({}^{R_e}/_{R_i}\right)} \tag{2.31}$$

In case of bending moment, similarly to the axial force where $\sigma_y$ is define as (2.26), starting from (*2.25*) is possible to obtain.

$$M = E \cdot \frac{d\varphi}{d\theta} \cdot \left( \int_A y\, dA - \rho_n \int_A \frac{y}{\rho_y}\, dA \right) \tag{2.32}$$

Remembering the definition of centroid the first integral is solved as:

$$\int_A y\, dA = A \cdot y_g \tag{2.33}$$

meanwhile the second integral is null in the same way of (2.30), and therefore, the final definition of the bending moment is:

$$M = E \cdot \frac{d\varphi}{d\theta} \cdot A \cdot y_g \tag{2.34}$$

From (2.26) and (2.34) is possible to calculate the stress value for each fibre of y for a given bending moment M.

$$\sigma_y = \frac{M}{A \cdot y_g} \cdot \frac{\rho_y - \rho_n}{\rho_y} \tag{2.35}$$

Form this simple demonstration is possible to conclude that the hypothesis of linear relationship between strain and stress is here not accurate. The position of the neutral axis does not meet the geometrical centroid but is always closer to the curvature centre. The stress-strain relationship in strengthened cross sections is relevant to properly evaluate the actual resistance and thus such considerations on hypothesis where figured out (see example in Fig. 2.61).

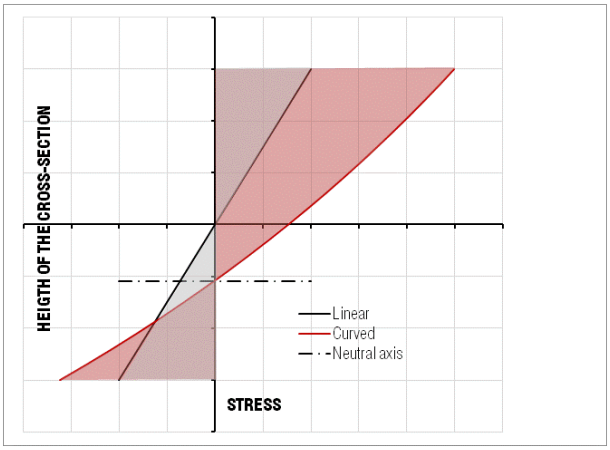


*Fig. 2.61 Example of different stress distribution for a curved beam and a straight one*

To assess the actual influence of this stress distribution in real arches an analysis on the stock of masonry arch bridges of the Italian Railway Network [Zampieri, 2013] has been carried out. The parameters which affect the disagreement with the linear distribution are the internal and the external radius that in practical terms are related to the curvature and the thickness of the arch.

The effect starts to be considerable when the thickness has the same order of magnitude than the internal radius. In other word the influence becomes bigger when the difference between neutral axis and centroid is considerable. In eq. (2.31) the position of $\rho_n$ is defined by the numerator that actually is the thickness and the ratio $R_e/R_i$ function of thickness and span. The considered values of f/L (rise over span) lie between 0 and 0.5 and the values of t/L (thickness over span) reach a maximum of 0.06 in the whole stock. The differences between stresses calculated accurately and neglecting the curvature effects reach a maximum of 5.9%.

In particular in the case of the vaults tested in this work the percentage difference is of 3.55%. Due to this consideration it seems reasonable to keep valid, in this work the hypothesis of linear relationship between strains and stresses.

### 2.4.5 *Strengthening interventions*

Usually arches or vaults are subjected to strengthening interventions manly due to: lack in existing conditions or because of an actions upgrade.

For instance the latter is usual in masonry bridges where service loads and requirements are increasing. Another example is given by seismic assessment where the action was not considered yet in the construction phase. In these cases the element itself is in good conditions but the demand increases. Other times,

damages observed in the crack pattern, for example caused by material deterioration, can lead to an unsafe situation even without variation in the action.

In both cases the solution is to operate by strengthening interventions. Their design and execution, especially in cultural heritage restoration, need a multidisciplinary approach and several issues has to be considered as described in § 2.1. In the following are pointed out only the structural issues and each intervention are classified according Fig. 2.62.

Mastrodicasa [1981] and Cangi [2012] divided failures by:

- damage due to abutment movement,
- damage due to vaults,
- combined damage in vault and abutment.

It is author opinion to refer at different vulnerability and causes. Intervention goals are hence the base to their evaluation and classification. The strengthen could be provide on indirect vulnerability (related to supports) or direct one related to vaults itself.

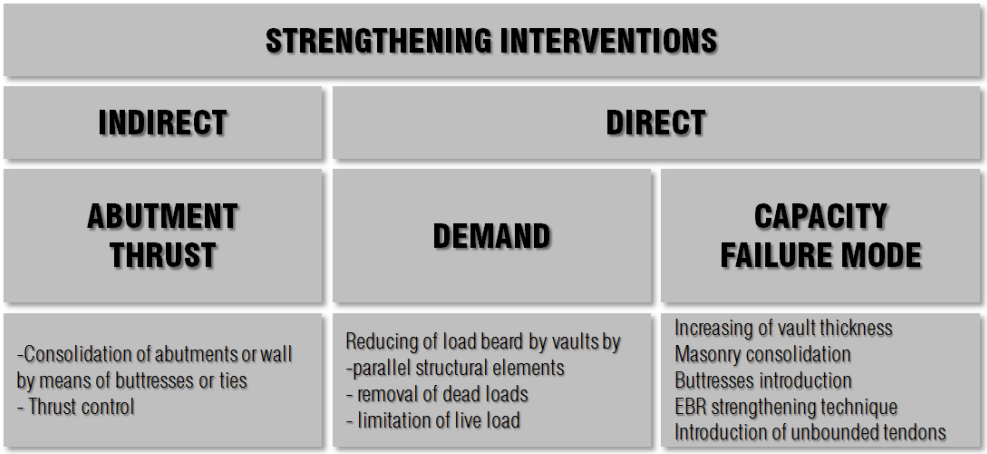


*Fig. 2.62 Schematic classification of strengthening interventions*

#### *2.4.5.1 Indirect intervention*

As indicated above (see Fig. 2.40), the masonry arch mechanism relies on the thrust development within the element. A first possible failure is hence due to the vanishing of thrust caused by a settlement in abutments or by mutual movement of bearing walls as can happen in churches. This intervention category aims to avoid this mechanism constraining abutment or bearing walls. The failure is not hence due to vault fault but caused by the changing in boundary conditions.

The two most representative cases are the introduction of buttresses or tie rods under the vault (Fig. 2.63). In particular for aesthetic reasons other possibilities, less efficient and that need of proper cautions, are tie rods above

vaults or inclined in the backfill. Finally in groin vaults it is possible to insert ties above the diagonal direct to bear the thrust of groins.

*Fig. 2.63 Buttresses in Chartres (FR) (left) ties in S.Fermo's Cloister (right)*

It is worth to notice that although damages related to failure on supports are not directly linked to vault capacity this is one of the most frequent problems, especially for vault in tall buildings and in case of earthquakes.

In conclusion an interesting proposal to control the thrust in bearing walls is by Cangi [2012] (see Fig. 2.64). He purposes to add masses on floor and by a tie system the weight is transferred on bearing wall and thus the force composition results in a vertical thrust (see the green vector).

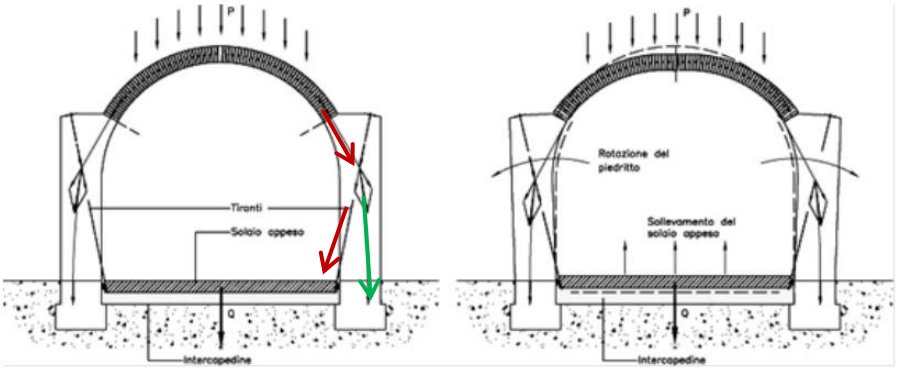


*Fig. 2.64 Mass addition to reduce thrust (left) ties to support the vault (right) [Cangi 2012]*

### *2.4.5.2 Direct interventions on demand*

The vault vulnerability could be reduced operating on the demand by limiting actions on the element. For example for static load is possible to limit live loads by regulated access to the structure. Another possibility is to reduce dead loads especially by backfill removal. This operation needs careful evaluations because could have advantages in limiting stresses and seismic actions acting on the structure (proportional to masses) but on the other hand could decrease the critical

load for asymmetric condition. Indeed the backfill dead load helps the thrust line to remain in the cross section.

The demand can be limited also by the addition of new structural elements which bear the increased action or help the vaults to do that. This may be accomplished, in barrel vaults, by the introduction of new bearing arches in the intrados, as Carbonara [1996] defines for traditional intervention, or with new rib elements on the extrados as Giuriani [2006] suggested (see Fig. 2.65)

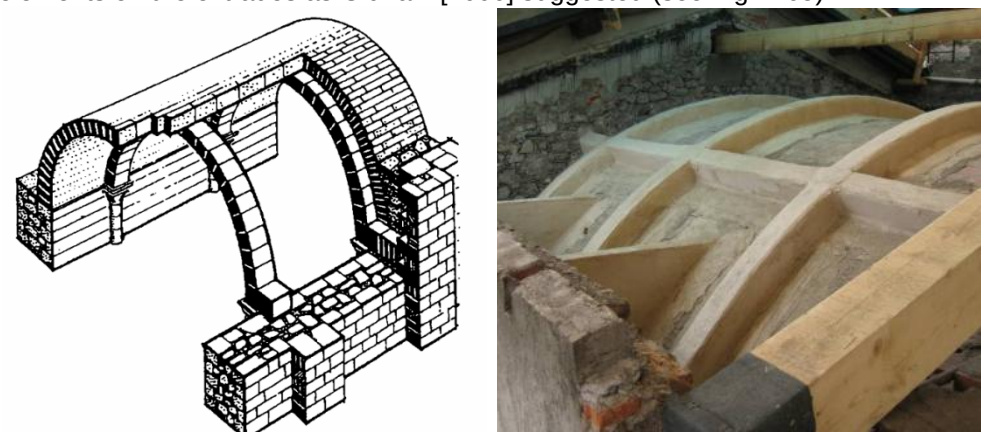

*Fig. 2.65 Introduction of masonry arches under vault [Carbonara 1996] (left) addition of ribs in the extrados [Giuriani 2006] (right)*

Another element which unloads a masonry plain vault is the creation on the extrados of a reinforced concrete vault (Fig. 2.66 left). This system increases significantly the stiffness, adds tensile strength to the vault and resistance to bending moment. On the other hand is invasive and actually substitutes the function of the masonry vault which became a secondary element. Moreover a severe unloading can result in brittle shear mechanisms or elements relaxation which causes voussoirs fall, in particular in case of dynamic actions. In case of irregular curvature Cangi [2012] also suggested to unload the vault by a parallel system. In this case it was a steel frame which holds steel ties sustaining the vault in several positions (Fig. 2.66 right).

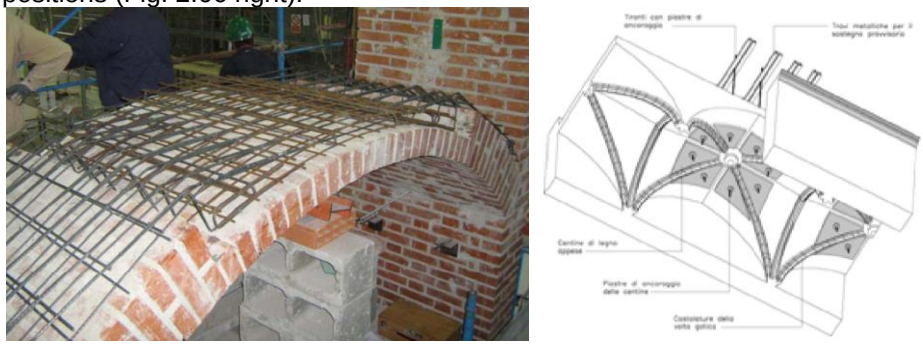

*Fig. 2.66 Addition of R.C. vault [ReLUIS 2008] (left) suspension by ties [Cangi 2012] (right)*

### *2.4.5.3 Direct interventions on capacity*

The capacity increases of a structural elements is more coherent whit this definitions because aims to increase the strength of the element working on constitutive materials or mechanisms. From the overview on analyses the common failure mode of vaults is the mechanism activation which occurs for limited stresses.

To increase this load the addition of new layer of brick provides an higher thickness and hence a greater load. If the vault suffers by material deterioration or lack in mortar joints, repointing or micro injection may be suitable operations.

Another set of solutions aims to avoid this mechanism, for instance with the introduction of diaphragms (Fig. 2.67) that avoids or at least change the hinge position therefore increasing the load bearing capacity. Modena [2009] suggested to provide tensile resistance to the diaphragms to be effective in both directions. The intervention is hence reversible and compatible.

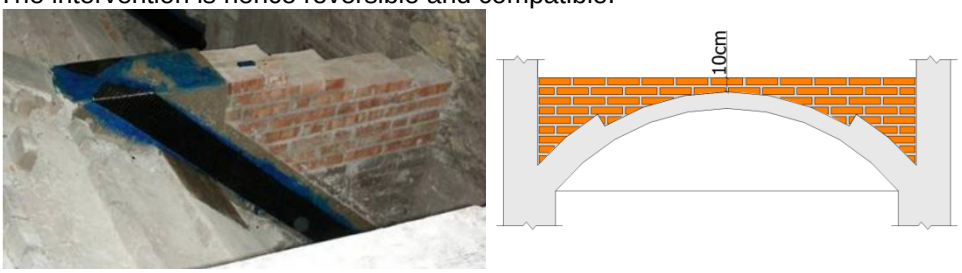


*Fig. 2.67 Diaphragm with FRP [Modena 2009] (left) Diaphragm [ReLUIS 2008] (right)*

Looking at Heyman [1996] analysis on unreinforced vaults, one of the key hypotheses is the zero tensile strength of masonry. Many interventions aim to solve this shortcoming by the introduction of elements able to bear the tensile action.

A widely adopted solution is the External Bonded Reinforcement (EBR) with composites material or textile. Many possibilities on fibre materials and matrixes are possible. As presented in Fig. 2.11 the development and the use of FRP is focused, in masonry applications, on vaults and domes. Details on these applications were already presented in previous paragraphs.

An interesting solution for the introduction of tensile strength was presented by Jurina [1999] whereby the introduction of a cable on the vault extrados. The cable first of all increases tension against the hinge opening and avoid the mechanism activation although it does not act in the same way of a flexural strengthened cross section because the cable is unbonded. Moreover it has a active role if pre-stressed. Indeed, the application of a pre-stress in the cable results in a distributed normal pressure orthogonal to the arch which increases the stability of the thrust line within the cross section.

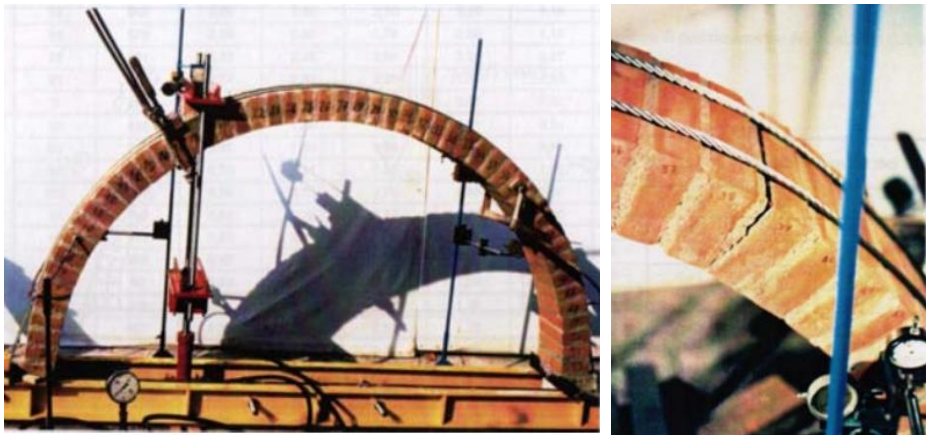

*Fig. 2.68 Insertion of unbonded tendon [Jurina 1999]*

### 2.4.6 *Previous experimental campaigns on strengthening arches*

Since the early 2000s, the attention on vault testing rises within the scientific community. Developments and new possibilities brought by composites demonstrate to be a valuable solution in vault strengthening and therefore many researches were carried out.

Valluzzi [2001] drawn first evaluations on the effectiveness of this intervention and Briccoli Bati [2000] focused the attention on intrados strengthening with detachment issues. In the same period Foraboschi [2001] tested a significant number of specimens with different shapes and reinforcement geometries. In particular he tested 12 vaults with the typical greater thickness on springing (Fig. 2.70) and 6 barrel vaults.

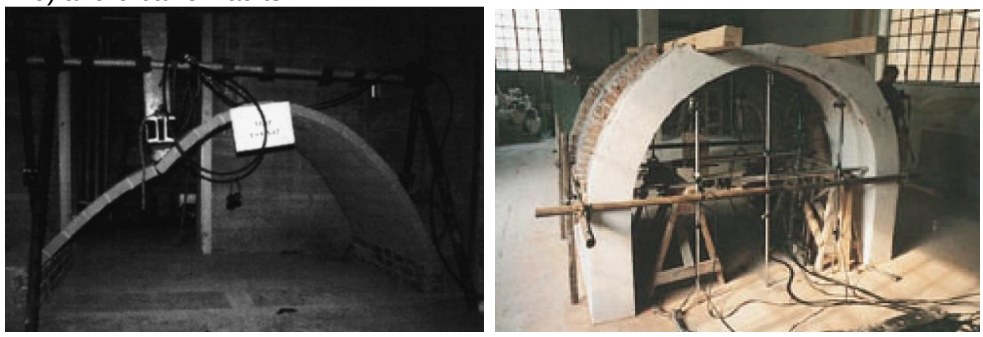

*Fig. 2.69 Vaults with CFRP EBR composites in Valluzzi [2001] (L) and Foraboschi [2001] (R)*

Other relevant contributions are by Ricamato [2007], Basilio [2007] and Badalà [2008] where small barrel vaults were tested with different configurations of reinforcement. The adopted reinforcements were carbon or glass fibres in epoxy resins. The first use of mortar based reinforcement was by Castori [2006] and Borri [2009] with the comparison among CFRP and steel fibres glued on epoxy resin

(SRP) and grouted on mortar (SRG). The same author ([Borri & Castori 2011b]) focused the attention also on intrados strengthening with the evaluation of anchors number to avoid detachment. The first adoption of diffuse net reinforcements was by Garmendia [2010] who selected a Basalt Textile Reinforcement on Mortar to strengthen small arches.

Tab. 2.6 shows a summary of experimental campaigns available in literature. The table does not report unreinforced vaults but at least one for campaign was tested. It is possible to notice the wide number of tests carried out (87). Despite such number of specimens it is tough to figured out general conclusions or calibrate analytical models. The reasons of this are related to the variability of configurations and dimensions but above all due to the mechanism failure. In fact the most frequent failure mode recorded concerns joint sliding. This occurs many times on support as Valluzzi [2001] underlined or in the hinge under the load application point. It seems therefore useless to seek for numerical correlations. From all these tests is possible to conclude that the most effective intervention is the EBR application on the extrados with an efficient anchorage on supports.

*Tab. 2.6 Experimental campaigns on vaults with composites intervention*

| Author | Year | Spec. N | Shape | t [mm] | L [mm] | width [mm] | rise [mm] | Strengthening | Load pos e type |
|---|---|---|---|---|---|---|---|---|---|
| Briccoli Bati | 2000 | 6 IN | CIR | 10 | 1500 | 100 | 433 | CFRP | 1/2 MN |
| Valluzzi | 2001 | 4 EX + 2 IN | CAT | 55 | 2000 | 1020 | 730 | CFRP GFRP | 1/4 MN |
| Foraboschi | 2001 | 12 (comb of EX+ IN) | CIR* | 260/ 130 | 2000 | 1000 | 1000 | CFRP | 1/4 MN |
| | | 4 IN + 2 EX | CIR | 250 | 4350 | 2000 | 2175 | CFRP | 1/4 MN |
| Ricamato | 2007 | 2 EX | CIR | 120 | 900 | 225 | 510 | CFRP | 1/3 MN |
| Basilio | 2007 | 4 EX + 4IN +2EX-IN | CIR | 50 | 1413 | 450 | 562 | GFRP | 1/4 MN |
| Badalà | 2008 | 1 EX | CIR | 70 | 1497 | 550 | 398 | CFRP | 1/4 MN |
| Castori** | 2009 | 4 EX + 4IN + 1EX-IN | CAT | 100 | 1980 | 200 | 480 | CRFP SRP SRG | 1/4 MN |
| Garmendia*** | 2010 | 3 EX + 3IN +3EX-IN | CIR | 120 | 1130 | 250 | 330 | BTRM | 1/4 MN |
| Castori | 2011 | 14 IN | CIR | 125 | 2000 | 250 | 1000 | CFRP GFRP | 1/4 MN |
| Girardello | 2013 | 7 EX | CIR | 120 | 2980 | 770 | 1340 | BTRM SRG BTRP SRP DIASRP DIASRG | 1/4, 3/4 CY |
| Giamundo | 2014 | 1 EX | CIR | 120 | 2980 | 2200 | 1340 | MORT | - DY |
| Garmendia | 2015 | 4 EX | CIR | 120 | 2980 | 770 | 1340 | BTRM SRG BTRP SRP | 1/4 MN |

*two thickness at springing and crown; ** concrete brick; ***sandstone
MN (Monotonic load), CY (Cyclic test); DY (Shaking table test)

Solutions partially reinforced moves hinges but lead to mechanism activation in UR section, the lack of anchorages reduce the shear capacity and lead to debond on the vault end. Finally, even if in some case for practical reasons is the only applicable solutions, the intrados reinforcement confirmed its vulnerability to detachment.

An interesting and meaningful series of tests, started with Girardello [2013], Garmendia [2015] (see Fig. 2.70) and Giamundo [2014]. The worth of these tests is the possibility to their mutual comparison. The selection of the same geometry and the strengthening application in the extrados with anchorages allows to find similar results for a qualitative point of view.

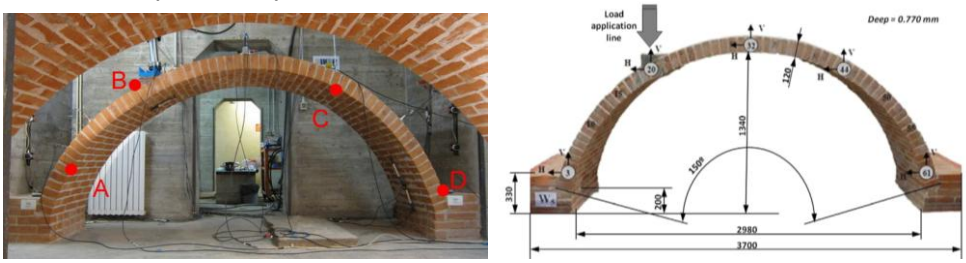


*Fig. 2.70 Girardello [2013] (left) and Garmendia [2015] (right)*

The load application was different because Girardello [2013] chosed a cyclic test with load alternating application on both quarters meanwhile Garmendia [2015] adopted a monotonic load application on a sole quarter. Finally Giamundo [2014] applied, for the same vault configuration, a dynamic time history with a shaking table. Failure modes observed in these campaigns are useful because involved the mechanisms with fibre failure or masonry crushing. The involvement of FRP and FRCM allowed also to underline differences on EBR technique. The mortar base reinforcement seems to involve better the mechanism behaviour, probably due to the lower stiffness. By this example seems advisable, at least on laboratory test with reconstructed vaults, to operate always with similar conditions to improve and compare results as usually happen with tests on beams.

The shaking tests program had been carried out in the framework of ProVaCI project by the University of Naples. Specimens were, unreinforced, reinforced with mortar and by diaphragms (see Fig. 2.71). The latter case, shown on the right, helps to understand the meaning of vulnerabilities related to support shift. The lack in buttresses or ties under the vault involves the entire structure to the failure. As is possible to notice form the picture, the vault develops only three hinges and hence is inner ultimate capacity was surly higher.

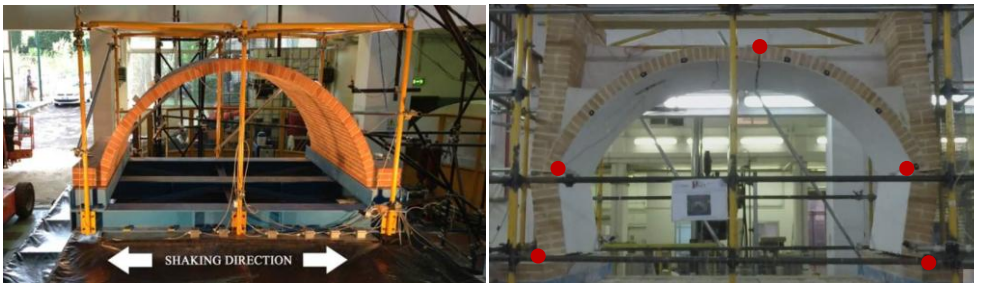


*Fig. 2.71 Shaking table tests in the framework of ProVaCI research project*

Anania [2013] considered, together with the extrados EBR reinforcement the introduction of a Ω-Wrap technique.

Other experimental campaigns on vaults were carried out, for instance Tao [2011] (Fig. 2.72 left) tested vaults strengthened by CFRP on the extrados and Hojdys [2012] vault reinforced with glass grid grouted in mortar. Both cases account for backfill interaction and hence with the addition of other uncertainties.

Ferrario [2010], in the framework of ReLUIS project, introduced the analysis of horizontal actions in the combine structure of vault and bearing walls in order to analyse the abutment rocking (Fig. 2.72 right). Also in this case backfill is considered and several reinforcements adopted. By an overall consideration on interventions Ferrario [2010] stated that the traditional introduction of diaphragms (see Fig. 2.67 right) provides the better response because increases the global stability of the structure but at the same time the original vault keeps its structural role.

*Fig. 2.72 Tao [2011] (left) and Ferrario [2010] (right)*

In conclusion it has to be noted that there are not available tests performed directly on historical existing vaults but are always performed on reconstructed vaults and in most cases with a scaled geometry.

## 2.5 FINITE ELEMENT ANALYSIS AND NOLINEARITIES

With the rising of computational tools, in the second half of the last century, a promising alternative to analytical models, sometimes very complex to solve, came from numerical solutions.

Bathe [1982], which is a milestone reference in this fields, argues that FE represents a most general analysis tool and is used practically in all fields of engineering analysis. The FE method applied to solid and structural mechanics is based on the numerical solution of basic equations of discrete elements referring to nodal displacements. Internal stress are then calculated in specific points, called Gauss points, within integration of defined interpolation functions based on the element type selected. Typically elements rely on linear or quadratic interpolation functions. Because of the numerical being, the method is strongly related to computational mathematical iterative solution methods.

The first issue for the creation of a model is related to the mechanical idealization of the actual physical problem. The development of specific finite elements and nonlinearities which on one hand improved the power of this tool on the other hand needs a careful evaluation of the physical problem and the related critical issues. Therefore this phase plays a crucial role in the definition of the model.

The basic steps of the methods are:

- Geometrical definition
- Creation of a mesh (looking at element typologies and nodal topology)
- Load definition (in terms of imposed displacements, forces or inertial forces)
- Boundary conditions (constrain equations of some DOF)
- Material properties
- Solution method

The method could be carried out linearly with holonomic constrains in an indeterminate system therefore overcoming a relevant problem of analytical analysis.

In this work major interest is in masonry structures. The material, as described in § 2.2.1, presents a strongly non linear behaviour in compression, tension and shear with also a brittle behaviour. Masonry composition, made of units and mortar, brings also to deal with interface problems. Finally, the behaviour of masonry in cracked conditions develops high displacements that may not be still considered only referring to the undeformed condition, thus introducing geometrical

issues. The attempt to deal with all these aspects in an analytical way leads to strong assumptions and simplifications mainly based on empirical formulations that could be overcome by this powerful tool.

Nonlinear finite element analyses will always be helpful for the validation of the design of complex masonry structures under complex loading conditions [Lourenço 1996]. Research on post-peak behaviour demonstrated softening and dilatancy properties of masonry that play a crucial role in the nonlinear process. The possible different types of non-linear behaviour associated to the main issues will be focused in next paragraphs.

It has to be noticed that (see Fig. 2.73 left), beside the use of analytical tools as linear elastic and plastic analyses, the FEM could properly follow the real structural response in each stage namely elastic, cracking, crushing and complete failure. Nevertheless is important to know that this is unquestionable in theoretical terms but in real application it might happen only partially, depending on the assumed values (looking in example to the peak behaviour of ft 0.2 N/mm$^2$ in Fig. 2.73 right).

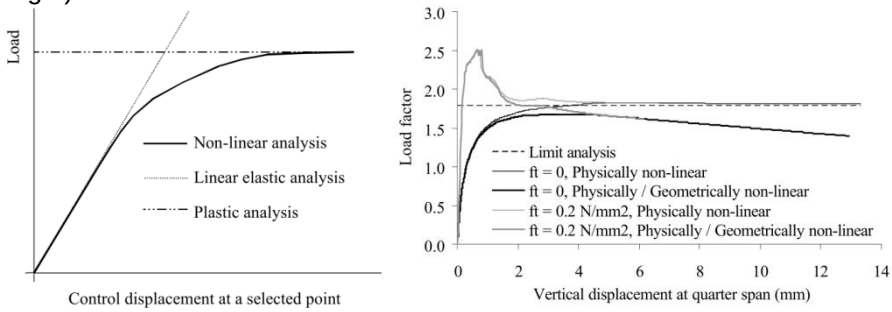


*Fig. 2.73 Comparison between analytical and numerical tools in general (left) and on a semicircular arch (right) [Lourenço 2001]*

Although many researches and validations have been done on these tools, the high complexity of such non linear mechanical behaviours deal with an high number of parameters that in many case are unknown or indeed scattered in existing structure that the overall analysis could be compromised. It is therefore crucial for the user to be deeply aware of the adopted analysis tools and of their agreement with the sought results in order to reach reliable outcomes. According to Lourenço [2001], more complex analysis tool does not necessarily provide better results than a simplified tool. This conclusion is also drawn in the following in this work.

### 2.5.1 *Material Non Linearity*

The mathematical description of the material mechanical behaviour is called constitutive law [Casarin 2006]. The key point of the material non linearity is

focused on the definition of this domain. First attempts to describe this different behaviour in tension came from concrete applications. Deep analyses of the state of art and new proposals were performed by Rots [1988] with the contribution of practical and analytical observations of Reinhardt [1986]. Within these researches a load/unloading mode for the elastic-softening mode was defined in order to properly described the concrete behaviour in cracked conditions.

The main concept concerns the wide deformations actually lumped in cracks after their opening. To account of this the total strain considered is a combination of: the elastic strain and the strain associated to the non linear behaviour eq. (2.36). In compression field $\varepsilon_{cracking}$ is substituted with $\varepsilon_{crushing}$.

$$\varepsilon \quad = \varepsilon_{elastic} + \varepsilon_{cracking} \tag{2.36}$$

By this application the crack opening is smeared within the mesh (Fig. 2.74 left). Another solution could be the discrete crack approach (Fig. 2.74 right) that is more coherent with local actual behaviour but requires the re-meshing after each iteration. Rots by Fig. 2.74 states that the simplification of the smearing is acceptable.

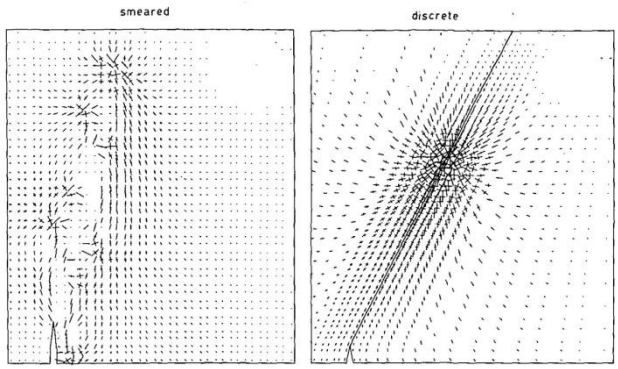


*Fig. 2.74 Smeared crack approach (left) and discrete crack approach (right)[Rots 1988]*

This stress-strain relationship, in the software Tno-DIANA herein used, is called total strain crack model [DIANA 2012] (Fig. 2.75 left). The model could be rotating of fixed according to Feenstra [1993]. The definition of the softening branch is based on fracture energies $G_c$ and $G_f$ in compression and tension respectively. Such energies are the integral of the stress-strain curve in the non linear branch. A wide contribution in the experimental characterization of such figures is in van der Pluijm [2002] and followings. Moreover, in order to relate the energy to the mesh the crack band width has to be calculated according the element area (plate) or

volume (brick). Further details and references are available in Rots [1988] and DIANA [2012].

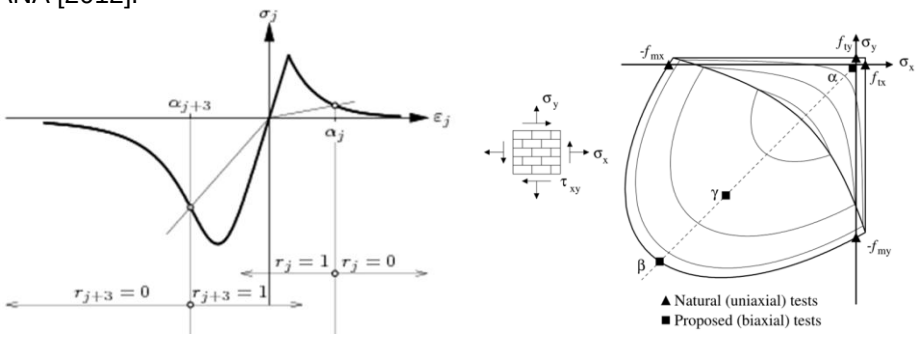


*Fig. 2.75 Total strain crack model [Diana 2012] (L) Rankine-Hill criterion (R) [Lourenço, 1996]*

Another interesting model more accurate for the masonry behaviour was the Renkine-Hill criterion [Lourenço, 1996]. Rankine type yield criterion was adopted for tensile failure and a Hill type yield criterion for compressive failure (Fig. 2.75 right). That model fulfil the experimental observation on masonry as reported in §2.2.1 (see Fig. 2.9). As drawback, the model requires an extensive definition of the domain that may lead to adopt total strain models.

### 2.5.2 *Geometrical Non Linearity*

A common structural analysis deals with infinitesimal deformations and always refers to the undeformed configuration. In the field of linear elastic analysis this is a suitable simplification for the FEM which does not update nodal position and all displacements refer just to deformations. In some structural cases, because of particular configurations of loads and boundary conditions, or for high deformations (e.g. cracking material), the second order effects are no more negligible.

In addition, looking at seismic analysis also made with simple capacity curves in out-of-plane mechanisms (Fig. 2.76), the ultimate displacement $d_0$ can be derived by solely geometrical considerations on rigid body motion. Furthermore the Ultimate Limit States considered are usually in the downward branch.

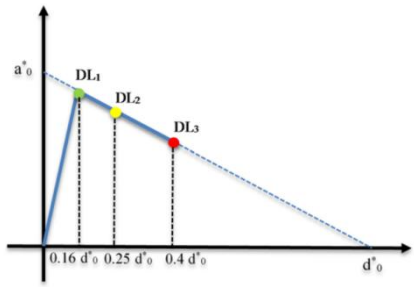


*Fig. 2.76 Example of capacity curve for different limit states [Zampieri, 2013]*

Therefore is worth to remind that geometrical non linearity plays a crucial role in seismic and capacity analysis and consequently has to be carefully evaluated in FE modelling in order to achieve reliable results.

### 2.5.3 *Contact Non Linearity*

The adoption in masonry constitutive laws of concrete material non linearity by means of a smeared crack approach considers masonry as a homogeneous material. The advantage of this simplification, especially in modelling entire structures, is a good compromise between computational efforts and final results [Lourenço 2001]. This approach is defined macro-modelling.

The actual physical problem is strictly related to a complex interaction of effects on unit, mortar and in the interface between the two. Such phenomena cannot be described by a homogeneous material, but requires a more detailed analytical and geometrical description.

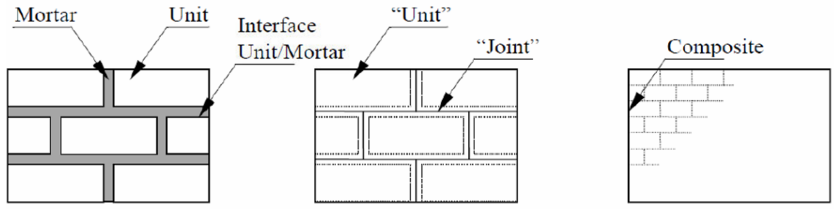


*Fig. 2.77 Micro (left) meso (centre) and macro (right) modelling [Lourenco, 2002]*

An exhaustive treatment concerning such problems is given in Lourenço [2002-2009]. There are interesting contributions in micro-modelling in literature [Drougkas 2015] but is clear that is suitable to limited elements and is also severely time consuming. An intermediate solution is provided by the mesoscale-modelling (or simplified micro-modelling) (Fig. 2.77 centre) where mortar joints are considered as interfaces between units. This approach demonstrate to be effective because despite less complex analytical descriptions of micro modelling it accounts for all the main problems related to mortar joints. Back to material non linearity the simplified modelling is close to a discrete crack approach because, especially in tension or sliding the failure planes are typically located on interfaces.

Lourenço [1997] and later developments defined a typical interface model called combined crack-shear-compression interface. The law considers all three failures with a mohr-coulomb law for shear and by tension and compression caps, based on fracture energy assumptions.

In conclusion all constitutive models, starting from the simplest to those most complex, are idealization of the actual physical problem, therefore to obtain reliable results are the user's engineering skills which have to guide the choice of the best compromise between model simplification and model parameters definition.

### 2.5.4 *Dynamic Issue*

A brief observation is herein reminded about FE modal analysis. Regardless any non linear problem, the usual approach looks only at the solution of the eigenvalue problem described in § 2.3.3 in eq. (2.6) thus accounting only for stiffness and masses distributions. Nevertheless, in some physical dynamic problems the internal state stress affects the overall dynamic response in a non negligible way (see §2.3.4).

Therefore, it is has to noted that to properly analyse this phenomenon the eigenvalue problem has to considered the initial conditions of state stress that updates the stiffness matrix even calculated with a linear static analysis.

# 3 KNOWLEDGE PHASE AND DATABASES

## 3.1 INTRODUCTION

The role of diagnosis, as underline in introduction, is the compulsory step towards the development of reliable and accurate numerical models which cannot be performed without a material description and a proper evaluation of behaviour provided by experimental results. In the following chapter are presented analysis and improvements on tests introduced in the literature review. The first step was to collect a significant number of real cases for each test to assess problems, typical ranges and potential improvement on them. The other step was to analyse and improve the test methodology on both procedures and interpretations.

## 3.2 SONIC TESTS

As introduced in the literature review the sonic test is qualitative and useful in comparison with MDT or DT tests to understand and widespread on all the building the collected information. An example of this is provide in the following where two diagonal compression tests were carried out on two unreinforced masonry specimens (UR1 and UR2) of a squared shape 1.2x1.2 m and 58 cm thick.

Before the execution of the destructive test a direct sonic test with a grid of 6x6 points with a spacing of 20 cm (black dots in Fig. 3.1) was performed and the pulse velocity recorded are illustrated in Fig. 3.2 where is easy to recognise how the second panel (UR2) shows higher velocities for all point and has an average value significantly higher. UR2 has an average of 2143 m/s with a C.o.V. of 14.13 % instead UR1 has an average of 968 m/s and a C.o.V. of 34.76 %. From the C.o.V. is also possible to notice how the UR2 is significantly more homogeneous than the other one.

*Fig. 3.1 Diagonal compression test of one specimens, the black dots refers to the sonic grid*

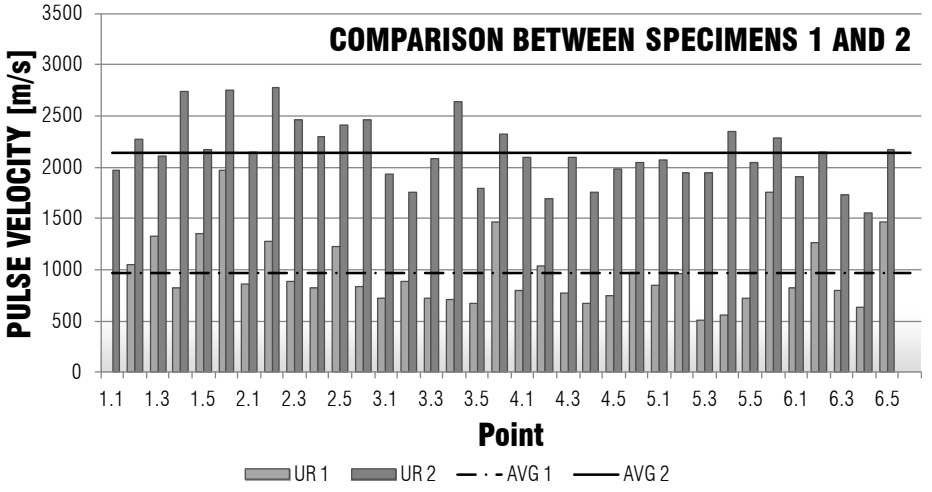


*Fig. 3.2 Histogram of pulse velocity for both specimens*

Fig. 3.3 shows the two velocity maps about the investigated surface highlighting the differences about the two panels.

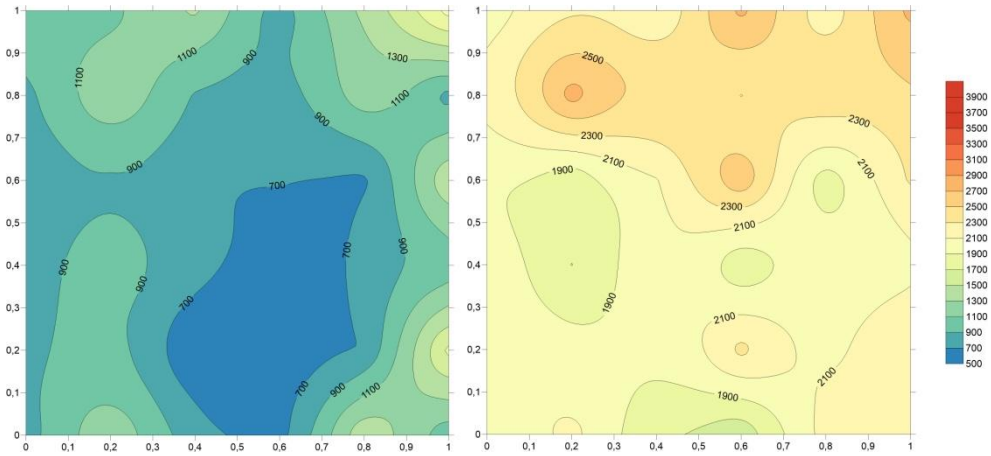


*Fig. 3.3 Map of pulse velocity in specimens UR1 (left) and UR2 (right)*

After the execution and elaboration of the direct sonic test a shear compression test was carried out on both panels obtaining the shear stress strain curve reported in Fig. 3.4 and obtaining a final value of shear strength of $\tau_0$ = 0.029 MPa for UR1 and $\tau_0$ = 0.089 MPa for UR2.

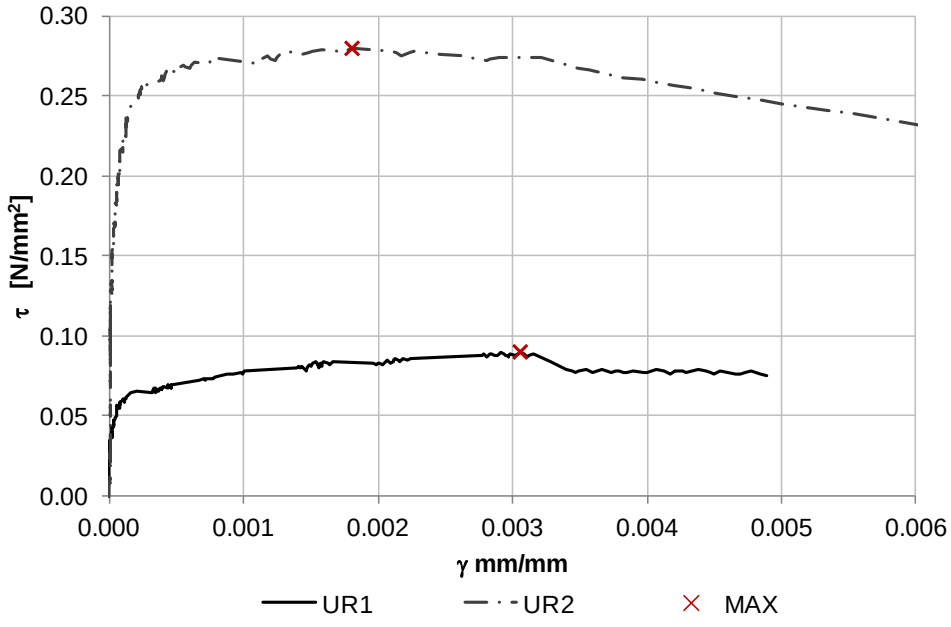


*Fig. 3.4 Shear stress-shear strain diagrams of wall specimens UR1 and UR2*

It is evident from this example and according to many authors [Binda 2005, Casarin 2006, Silva 2012] how the sonic test is very useful and permits to recognise vulnerable portions within the structure. It is interesting also to notice that tests were performed in the same building and is evident that DT tests are not repeatable in many portions of the structure and hence the widespread of information could be provided by the use of sonic test.

### 3.2.1 *Analysis*

Looking at the above mentioned results the comparison of sonic tests with MDT or DT tests to characterise the compressive elastic modulus of masonry has been done. The first step was to collect the data available in literature, 36 from simple compression test (C) [Valluzzi 2000, Riva et al. 2003, Silva 2012, Mazzon 2010] and 69 from double flat jack test (FJ), in detail: 46 in [Binda 2009a] and 23 form the database created in this work (see § 3.3.1). All the collected data are plotted in the graph of Fig. 3.5, the DT and MDT tests are coloured in gray and red respectively. Fig. 3.5 shows also the curves of models proposed by some authors [Binda et al 2007, Binda 2009a, Silva 2014] to give a relationship between elastic modulus and velocity.

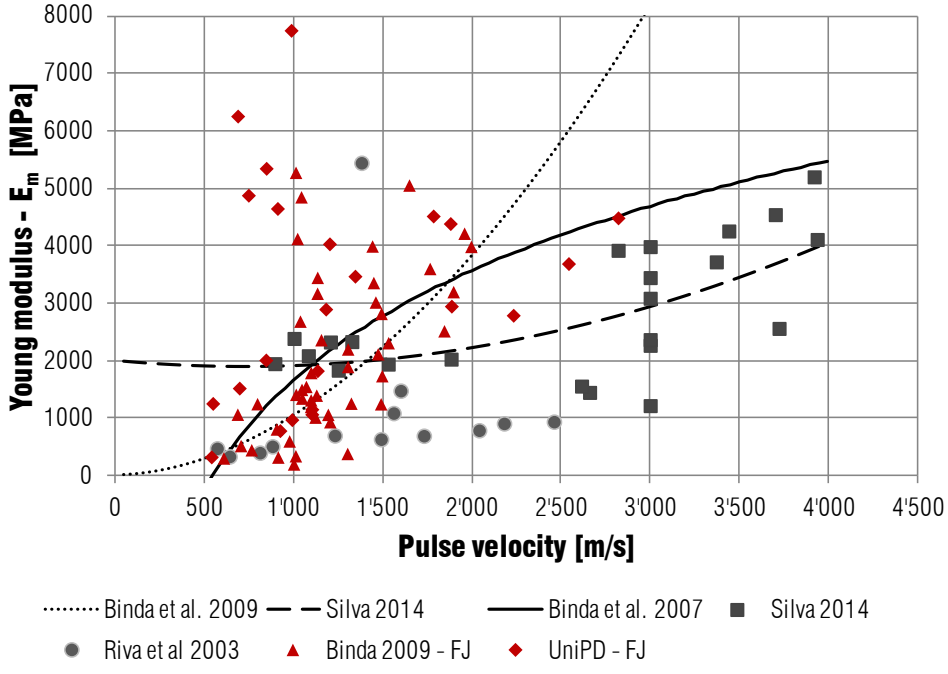


*Fig. 3.5 Measured pulse velocity versus tested elastic modulus*

The graph clearly shows a difference between FJ and C figures where the first provide higher moduli of elasticity than the other one. Moreover deep

differences are visible also in curves. Binda's proposals where calibrated on FJ and it might be due to this the second proposal (2009). Anyway, looking at eq. (2.3) a parabolic fitting, as suggested to Silva [2014] seems more near the physical problem. In conclusion about the DT tests and the overall panel capacity the Silva's equation seems to be suitable although the regression factor $R^2$, only considering DT, is still low (0.286).

About the FJ test, so far not suitable solutions are available and this could basically due to the intrinsic limits of the two tests. On one hand the FJ measures the elastic modulus of only the external leaf and usually overestimates the modulus of the entire panel and on the other hand the direct sonic test provides an average of the entire panel with significant speed drop due to internal voids.

### 3.2.2 *Database*

In order to qualitative guide the definition of masonry quality for the selection of material properties in mechanical ranges suggested by the Italian technical standard (Tab. 2.1) [NTC 2008] the sonic test might be a suitable tool. The implementation of a database collecting the tests performed by the University of Padova, divided by typology (Roman numbers Tab. 2.1), is a useful task to obtain a overall point of view on typical ranges of velocity for each category. The database collects only the categories (I,II,III,VI).

The whole number of cases is 154 and collected both laboratory and on-site cases. Fig. 3.6 shows the number of data divided by Italian region on the left and the number of test for each masonry typology on the right. The number of data will be increased in next years but it already represents a first description of a typical range for some categories (in particular CAT II and VI) the most diffused in Veneto region.

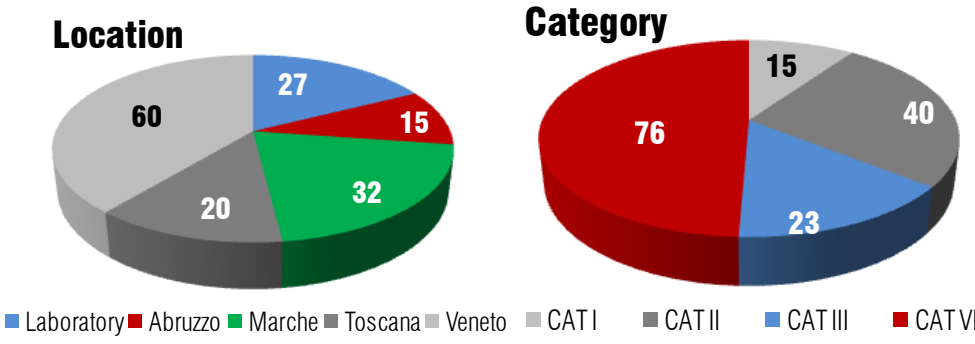


*Fig. 3.6 Distribution of the collected data by location (left) and masonry category (rigth)*

The information collected in the database are:

- Identification code
- Masonry typology (according to NTC 2008)
- Thickness of the investigated panel
- Range of the recorded pulse velocity
- Average value
- Standard deviation of the panel
- Author of the test and year of execution
- Building information as typologies (bridge, church, palace) and period of construction;
- Location of the test
- Eventual annotation

The investigated thicknesses lie between 0.25 and 2 m but the greatest percentage (49%) is in the range 0.25-0.50 m, the second most frequent range (31%) is between 0.5 and 0.75 m whereas the other 20 % is about wall thicker than 0.75 m. Analysing each typology, with the increasing of thickness the quality seems to increase as well. This might mean that monumental buildings with great dimensions were in general built with a good masonry quality with the respect of normal building.

Fig. 3.7 shows the velocity distribution for each category. It appears that CAT I, related to irregular stone masonry has very low values of velocity and there are not data up to 1500 m/s. Categories II and III show homogenous response with a wide number of case in the range 1000-1500 m/s. Finally brick masonry demonstrates higher velocities but also a more widespread behaviour and this could be directly associated to the material quality

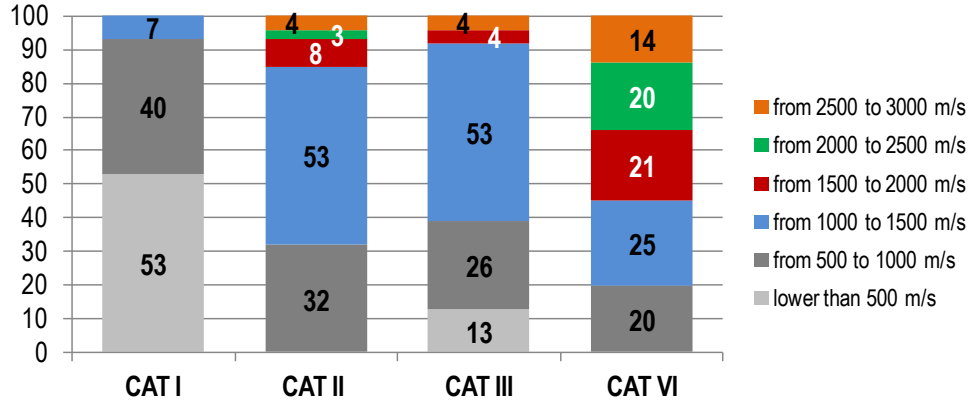


*Fig. 3.7 Detected range distribution (for each categories)*

Fig. 3.8 shows a summarizing graph of the inspected masonry's typologies with relative ranges. It has to be noted that CAT I presents a scatter value compared with graph in Fig. 3.7. This graph could become a useful tool in comparison with the selected typology. For example once recognise the typology of masonry, and thus the speed range, the measure pulse velocity could be compared in order to evaluate its position and hence its quality, confirmed by the DT test.

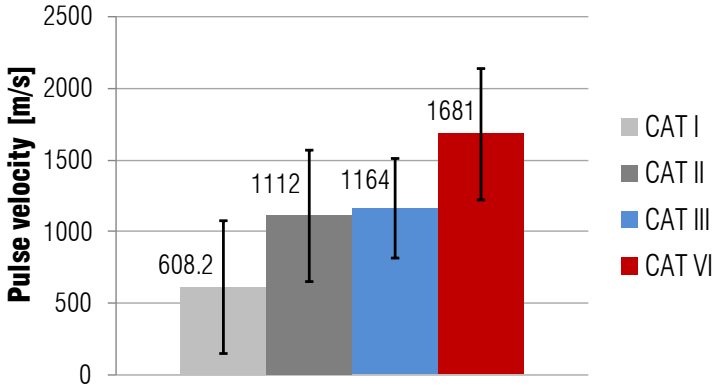


*Fig. 3.8 Average velocity in panels for each type of masonry*

For example, with the results obtained before the specimens UR1, which is of II type, is fairly above the range and it provides very high strength (compared with the typology range) whereas UR2 that recorded an average speed of 968 is in the normal range of its type with hence a medium quality.

### 3.2.3 *Operators' influence in estimation of flight time*

In case of tests complex to execute, time consuming and affected by subjective evaluations, their application from practitioner is limited and could discourage the execution of deepen knowledge phases properly calibrated, even if the sonic test demonstrated its efficacy. These motivations led primarily to evaluate the error introduced by subjectivity of operators and then to optimize and improve tools to reduce efforts in acquisition and elaboration.

The typical response in the time domain recorded by instrumented hummer (in green) and the accelerometer that receives (in yellow) is presented in Fig. 3.9. The flight time is the time gap (on the abscissa) between the two points which correspond to first moment of the hammer hit (in red) and the first arrival of the perturbation (in blue) where sudden increase of acceleration takes place. The detection of the two instants was usually carried out by an operator who manually record flight time.

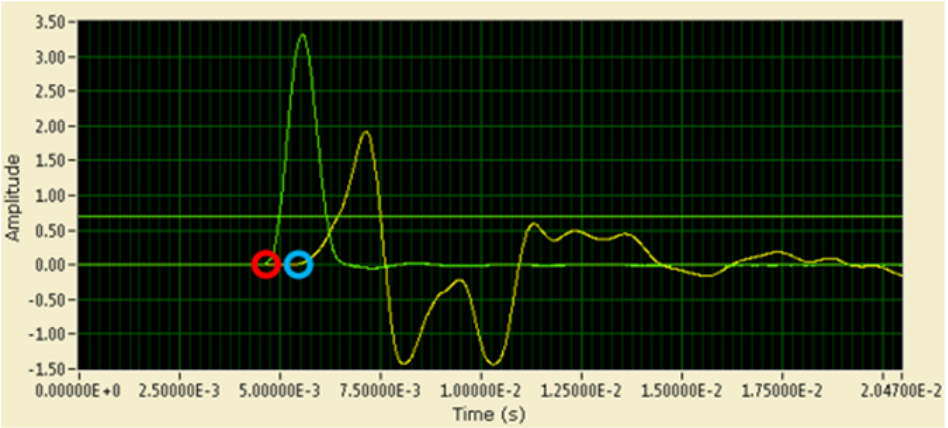


*Fig. 3.9 Recorded signals from hammer (green) and accelerometer (yellow)*

To each point three signals are usually recorded hence providing a total number of 225 signals. The time estimation was carried out by 7 expert operators who were not aware of masonry typology and wall thickness to avoid any external influence.

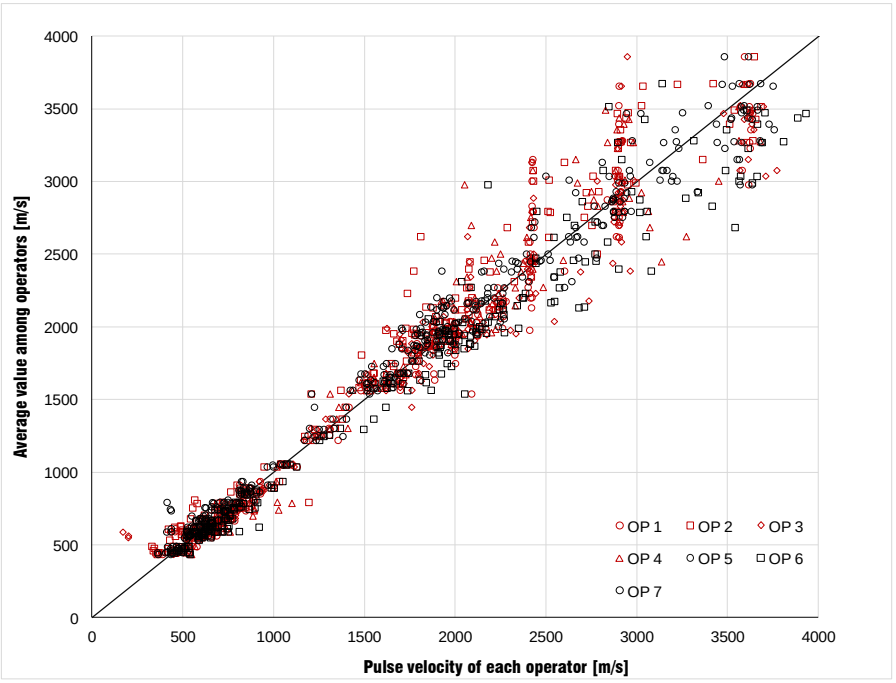


*Fig. 3.10 Pulse velocity estimated by each operators versus the average value of signals*

Fig. 3.10 shows in abscissa the pulse velocity estimated by each operators versus the average of them. This was used to see the scatter of human interpretation of the same signal and the graph shows a large scatter increasing the velocity. To give a numerical estimation of this scatter an error of each signal was

calculated with eq. (3.1) and then the frequency of occurrence in defined intervals was accounted.

$$\xi_i = \left| \frac{v_{op} - v_{avg}}{v_{avg}} \right| \tag{3.1}$$

Fig. 3.11 shows this error distribution for intervals and it is possible to estimate a possible human error in estimation of maximum 15 % considering that the error increase with higher speeds.

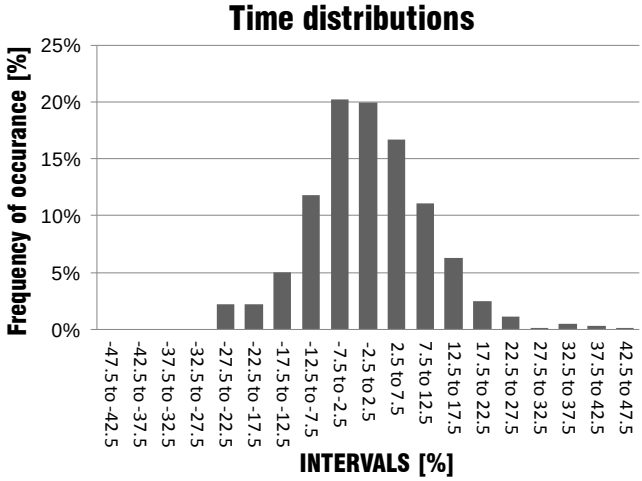


*Fig. 3.11 Frequency distribution of error for all signals*

In conclusion the manual detection of times could affect the sonic measurement depending on operators and an automatic algorithm which standardized flight time detection could erase this additional error to the measure.

### 3.2.4 *Software for the automatic detection of flight time*

In addition to reduce errors in estimation of flight time, the implementation of the automatic time detection considerably reduces the time consumption caused by the post processing phased carried out by operators. The execution of test in two moments leads to recognise and erase outliers only during elaboration losing some measurements. The implemented software allows to control measurements point by point during the test execution. The new software indeed, once the whole series of measures on one point has been acquired, calculates the C.o.V. of detected saves relative measures and results in a specific file.

The signals observation highlighted the difficulty of using thresholds fixed 'a priori' due to the variability in amplitude of signals. If on one hand a very small threshold can help to recognize the first variation in signals, on the other hand this can mean a wrong detection due to noise of electrical disturbances. This problem was observed in both hammer and receiver. Moreover the accelerometer exhibits a

variable response in shape and amplitude because affected by the masonry properties and by other external constrains.

Fig. 3.9 shows the typical shapes of the two curves and the point that should be automatically considered. In real applications the impact shape of hammer is often similar, therefore a geometrical approach based on a linear intersection was used. The algorithm is iterative and looks at the minimum error between the acquired signal and the intersection of two interpolations representing the undisturbed part and the rising part of the hammer peak. Because of the shape variability of receiver, the algorithm used for the accelerometer was based on a statistical approach which aims to fix automatically the correct triggering value.

In the set-up parts, software allows to calibrate two relative coefficients that increase the sensibility of detection but can gain the algorithm instability. To overcome this, in the GUI the two signals and the two detected points are shown, in order to help the user to recognise detection errors due to disturbances.

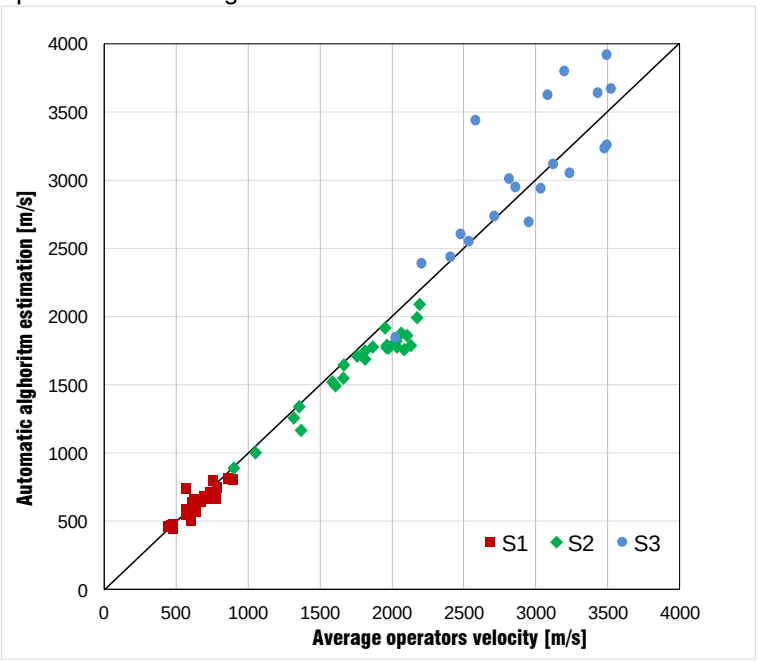


*Fig. 3.12 Average pulse velocity estimated by operators versus the automatically detected*

Software has been tested within the evaluation of operators sensitiveness before mentioned. Acquisition was carried out with the new algorithm which automatically detects flight times. Many tests were carried out but, only the three mentioned in § 3.2.3, that uniformly cover the investigated pulse velocity range, were used. Comparison between the average velocity estimated by seven expert operators and the velocity by the algorithm is reported in Fig. 3.12.

Comparing all samples, the average ratio between the automatic velocity and the average detected by users is 0.98, with a C.o.V. of 10%. This could be considered a good result to confirm the reliable estimation of the developed software. Anyway, it has to be noted that the differences between methods, might be associated to the different level of zoom that users adopt during the elaborations.

### 3.2.5 *Graphic User Interface (GUI)*

The new sonic tests software has a rich graphic interface divided in two different sections:

- General commands bar;
- Tabs menu composed by “Setup” and “Graph” tabs.

General commands bar, positioned in the upper side of interface, contains useful buttons and indicators which allow to set test parameters, acquire and elaborate signals and display final results.

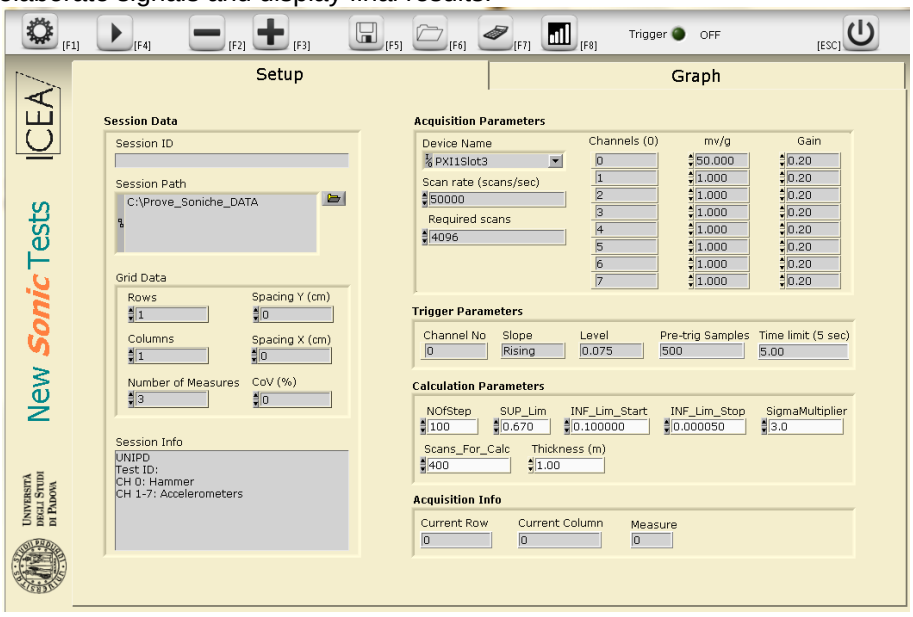


*Fig. 3.13 Set-up GUI where the session information are fixed*

“Setup” tab is composed by controls for managing test parameters values. Controls characterized by grey background cannot be edited during signals acquisition, therefore it is very important set them correctly before starting the test. “Setup” commands are grouped in five different categories depending on their functions:

- Session Data: Start a new session, set geometrical test parameters and control acquired signals quality;

- Acquisition Parameters: Manage acquisition adaptor cards and control signals sampling parameters;
- Trigger Parameters: Set up acquisition trigger;
- Calculation Parameters: Control new automatic algorithms for identification of flight time and calculation of propagation velocity;
- Acquisition Info: Specify current test grid position and running measurement. The latter is essential because it is necessary acquiring at least three signals for every couple of points.

"Graph" tab allow to manage and control measures and to evaluate their quality during the acquisition phase. "Graphs" commands and indicators are located in three different interface areas depending on their functions:

- Current Acquisition Data: Indicate the progress of the test and display generated signals parameters;
- Control Parameters: Display results relative to signals acquired in a particular grid point;
- Graphs: Display the generated signal and its flight time calculated by automatic algorithms. In this interface section there are two graphic windows, one is used for signal visualization only, while the other is useful for better analyzing it.

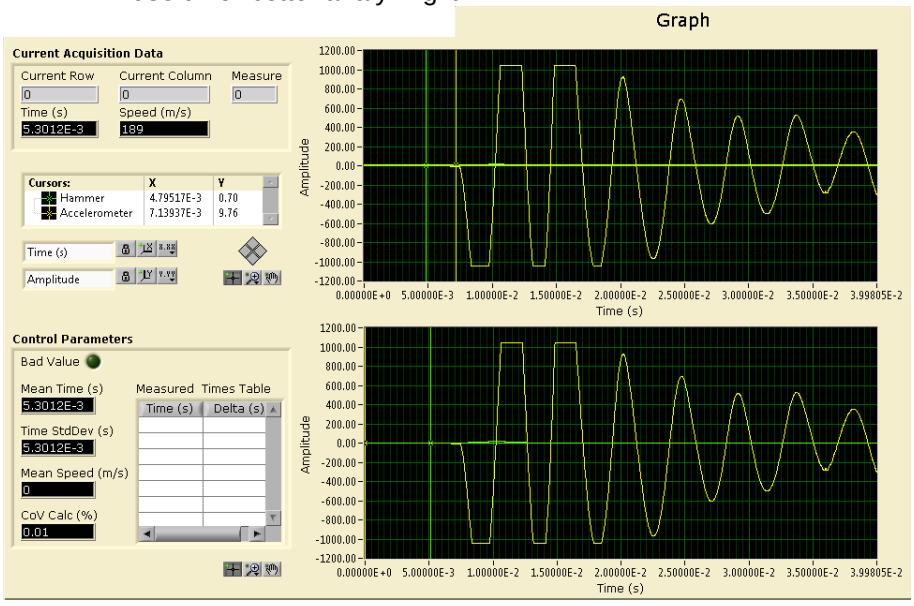


*Fig. 3.14 "Graph tab" Acquisition GUI with indication of selected point and acquired times*

## 3.3 FLAT JACK

The following paragraph aims to underline possibilities and limits of the double flat jack technique, in addition to the review carried out in § 2.3.5. By means of the collection of wide dataset it is possible to recognise the significant parameters that have to be considered in the test and typical ranges of brick masonry, the typology herein selected to deep analysis.

### 3.3.1 *Database*

The dataset of double flat jacks presented concerns the collection of all the tests carried out in the last decade by the department of Civil, Architectural and Environmental Engineering of the University of Padova [Cescatti et al. 2016b]. An overall number of 103 specimens have been tested in 40 buildings. The investigated typologies of masonry correspond to categories I, II, III and VI of Tab. 2.1 as for the sonic dataset. The cluster analysis of the wide number of data, proposed indeed consistent information on the mechanical ranges of each parameter and typologies and helps to understand how to improve the test execution and interpretation.

Tested buildings were located in five Italian regions, namely: Abruzzo, Emilia Romagna, Lombardia, Toscana and Veneto. Number of specimens, their location and typology are shown in Fig. 3.15:

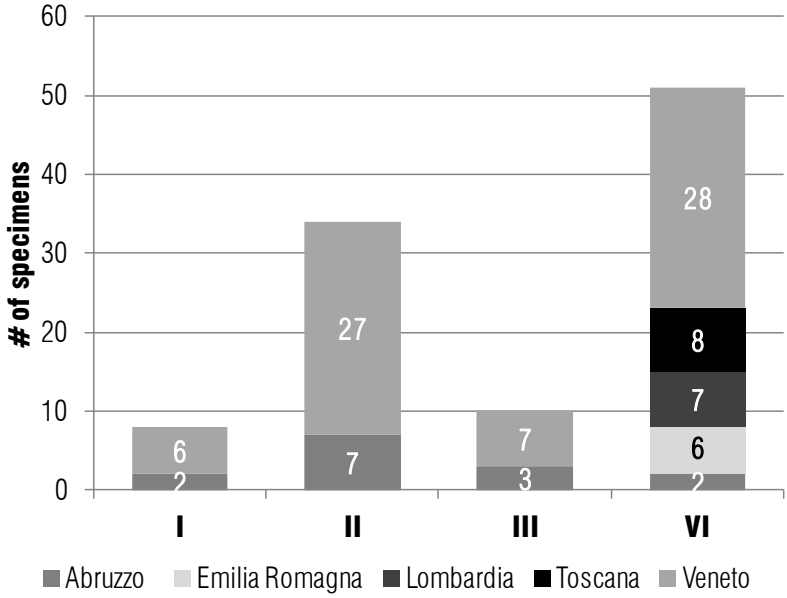


*Fig. 3.15 Number of samples divided in each typology and region*

The attributions of tested specimens to the different categories, similarly to the sonic database, were based on subjective choices. The database tries to collect all the suitable information to find some correlations, with relevant difficulty due to the high variability of the measured parameters.

The general collected information consists in:

- Masonry typology and relative corrective factors (according to NTC 2008);
- Location: municipality, province, region;
- Building information as typologies (bridge, church, palace) and period of construction;
- Additional tests to be compared (chemical test on mortar, pulse velocity, inspection through video endoscope, etc).

The gathered information are:

- Step of pressure for each loading cycle;
- Measured strain at each step;
- Tangent modulus at each step;
- Secant modulus of unloading phase at each step;
- Average tangent and secant elasticity moduli;
- Range boundaries of the two moduli;
- Local stress (coming from single flat jack, if available);
- Maximum load reached in the test;
- Loads related to onset of cracking (based on modulus variation and to residual displacement of horizontal transducer).

These information together with the consistent number of tests in the case of categories II and VI allowed to reach some conclusions, although an increased set of measures is desirable. Also about flat jacks the attention is hereafter given to the brick masonry typology, within the studied case, even if similar considerations are possible for the other categories.

### 3.3.2 *Test procedures*

The use of a consistent execution procedure for the whole tests in the database allowed an objective and uniform evaluation among parameters and data. In order to extend the database and hence the reliability of data analysis, a comparable testing procedure should be considered. Due to these simple reasons, a unified and shared methodology on test is needed. The procedure used in for these cases was consistent with RILEM recommendations [RILEM MDT.5:04]. Tests were performed always using four vertical and one horizontal transducers.

The sensors positioning and the ratio between tested area height and width of the flat jack meet the technical standards provisions. The acquisition was electronic and continuous, allowing a possible evaluation on modulus in post processing phase. To this aim, the secant unloading modulus was chosen after the test, selecting the elastic branch of unloading, being this very hard to obtain without electronic data record. The use of load cycles (loading-unloading) in the test proved to be quite relevant, with limited stress-steps, since a increased number of cycles helps to get much information in unloading and a detailed load envelope. As a drawback, an higher number of cycles increases considerably the time of execution. In most cases a stress-step value of 0.3 N/mm$^2$ seems to be a valid compromise between relevant data collection and test effective feasibility.

As a reference example, a double flat jack test carried out on a stone masonry belonging to category III and tested in Verona, will be presented.

Fig. 3.16 shows the stress-strain curve, expressed as the average of the four vertical displacement transducers. The “tangent” stiffness modulus is calculated at each load step between the maximums of each cycle. All tangent lines graphed together give the envelope curve of the cyclic test. It is possible to appreciate, from the visible changing in the tangent stiffness, the masonry cracking onset at the load of 1.5 N/mm$^2$.

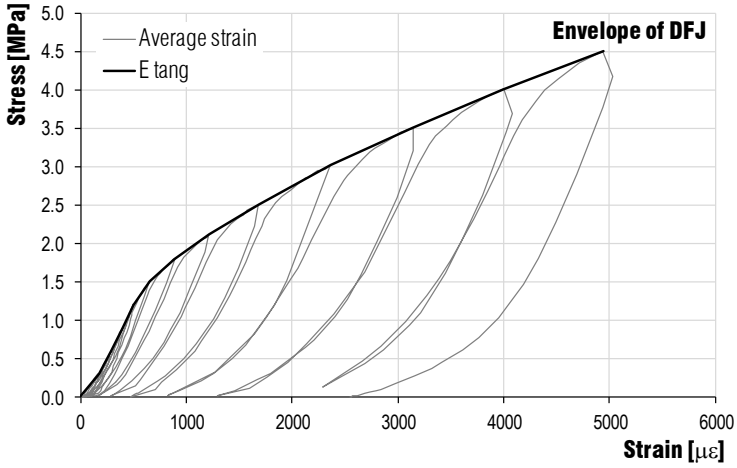


*Fig. 3.16 Tangent elastic modulus and FJ average curve*

At the same time, from the test it was also calculated the secant modulus in the unloading phase, as reported in Fig. 3.17. This stiffness is selected tangent to the unloading branch of the cycle. During the test, for loads lower than the local stress (in the case of Fig. 3.16 equal to 0.5 N/mm$^2$) the unloading phase has a marked non linear behaviour, considering thus this stress was the reference lower value for the calculation of the secant stiffness moduli.

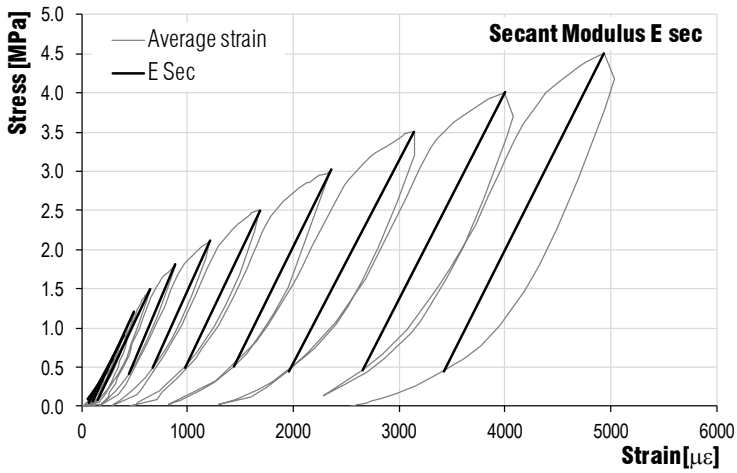


*Fig. 3.17 Secant elastic modulus in unloading phase.*

The analysis of the two calculated moduli throughout the whole test referring to the applied stress is drawn in Fig. 3.18. It seems clear how until the stress of onset of cracking the two moduli are similar whereas later on, the tangent modulus drops instead the secant modulus remains almost constant.

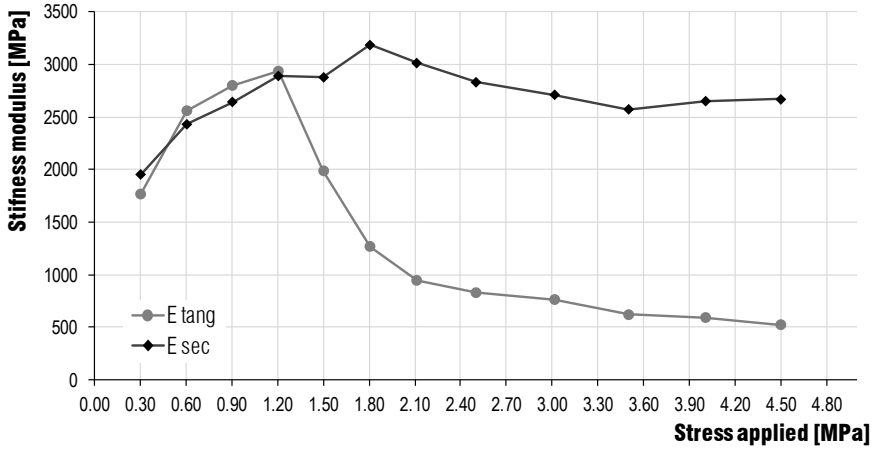


*Fig. 3.18 Tangent and Secant stiffness for each stress level*

### 3.3.3 *Data analysis*

From the database and the selected information, it is possible to create the envelopes of all curves as presented in Fig. 3.19 for brick masonry. Although all graphs belong to the same category it is evident the spread of mechanical behaviour in the stress-strain relationship. This indicates the relevant difficulty in defining a specific range of mechanical characteristics only based on the masonry typology.

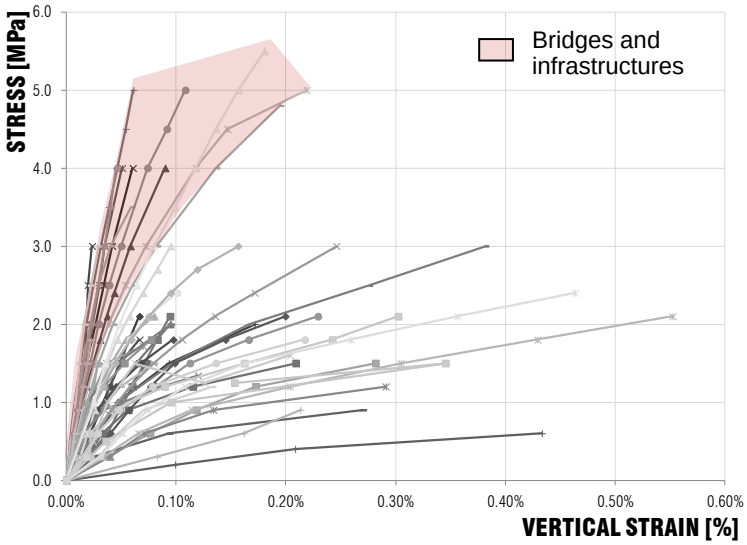


*Fig. 3.19 Envelope of the tested specimens of brick masonry [Cescatti, 2016b]*

Looking at Fig. 3.19 the scattered distribution of results suggests to find other correlations in order to try to reasonably cluster the actual ranges of mechanical properties. The modulus lies between 1028 and 12454 N/mm$^2$ which is a too wide range. As the analytical models for this typology suggests (see pag 16), the overall influence might be due to mortar properties. Unfortunately there is a lack of information on mortar and therefore is advisable to add mortar physiochemical characterization in the standard flat jack test procedure. To overpass this, some indirect correlations on masonry quality have been chosen. The considered parameters were location (region) and building information (typologies and ages).

To date, the regional analysis does not provide fine results and it might be due to the lower influence on brick masonry characteristics related to regional aspects whereas it might be more significant with stone masonry where the construction technology and the material itself varying throughout cities. The number of data and their geographical distribution on the other categories (I,II,III) is not suitable for this kind of analysis (see Fig. 3.15).

The analysis carried out considering building typology and age proposed instead more interesting results as showed in the hatched part of Fig. 3.19 and in Fig. 3.20.

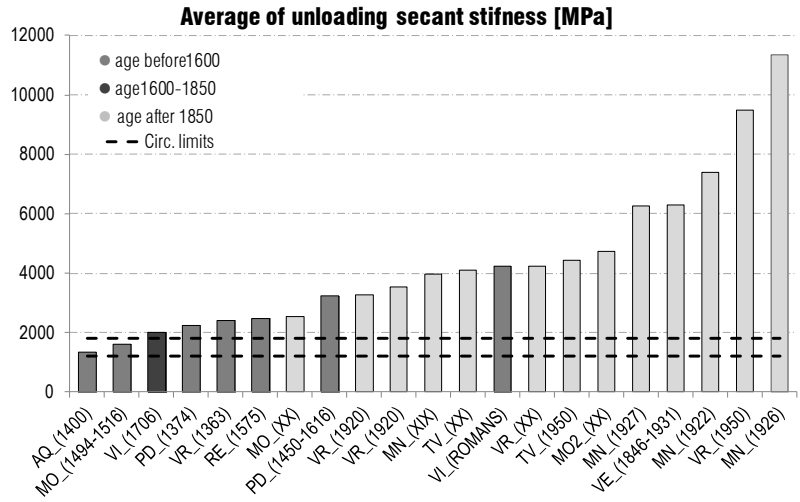


*Fig. 3.20 Average secant modulus in unloading phase for different building ages*

The division in building typology/relevance, such as: bridge, infrastructure, church, palace, common building, pointed out some aspects. An increased importance of the structure means a more accurate execution and material selection than in normal buildings. In Fig. 3.19 the first two listed types are coloured with a red hatch emphasizing their good quality with a pseudo-elastic behaviour still at 4-5 N/mm$^2$. In Fig. 3.20 different colours represent different construction ages. The ancient constructions showed lower values of stiffness usually lower than 4'000 N/mm$^2$. The use of cementitious mortar in the last century is directly related to good performances as in the case of a school VR-(1950). The other four values exceeding 6'000 N/mm$^2$ are all infrastructures. Despite the case of relevant structures, the influence of construction period is still confirmed for normal building (from VR-1920 to MO2-XX). The exception of VI-ROMANS refers again to a bridge.

In addition to the stiffness analysis, some considerations on the "allowable" stresses (i.e. elastic limit) have been carried out.

The analysis was based on the onset of cracking load rather than on the material ultimate strength, also considering the fact that the flat jack test usually does not allow to reach such limit conditions.

In order to select the stress value related to the onset of significant cracking in masonry, two main approaches were followed. One is based on the variation of tangent modulus which should suggest a changing in behaviour (from elastic to non-linear phase). The other is related to the definition of the cracking onset analysing the residual horizontal strains after the unloading phase. The searched "elastic limit" load should correspond to the threshold between two different magnitudes of residual strains.

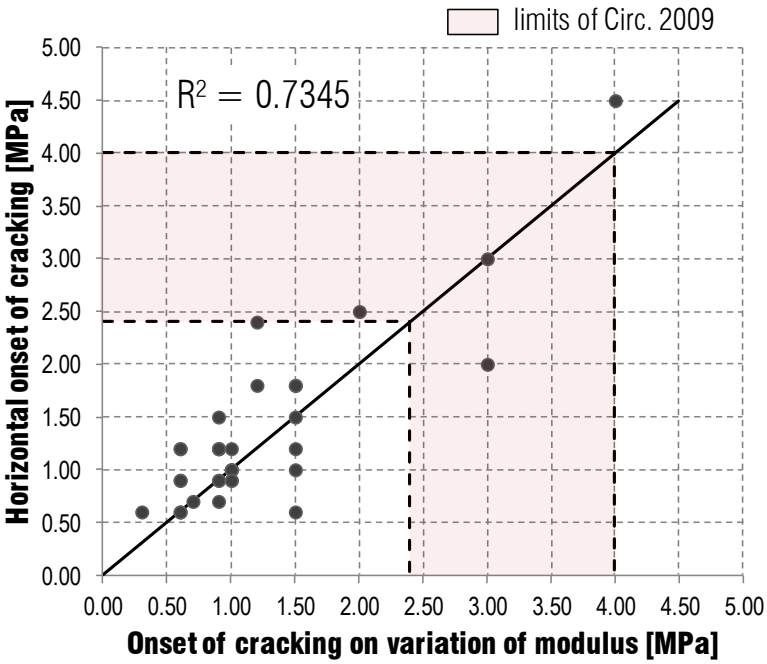


*Fig. 3.21 Comparison between the onset of cracking with the two adopted method*

Fig. 3.21 shows a comparison between the two approaches showing a reasonable agreement. The red hatch refers to the strength limits suggested by the Italian standard (Tab. 2.1). As it possible to notice, the magnitude of these stresses is quite low, even with the respect of the limits.

It is noted that the changing in slope or the rise of vertical cracks in the specimen, recognized by the horizontal transducer, does not refer to the ultimate strength used for calculation, which is actually further.

In the same experimental campaign of pag.80, where two flat jacks were executed, there was the possibility to reach the post peak phase and hence to recognise the ultimate compressive strength (see Fig. 3.22). This example was given to notice how the value of the cracking onset, at about 2.0 N/mm$^2$, is at one half of the ultimate strength. This is an example and it is not possible to give a relationship between the two stresses but it is useful to recognise this difference.

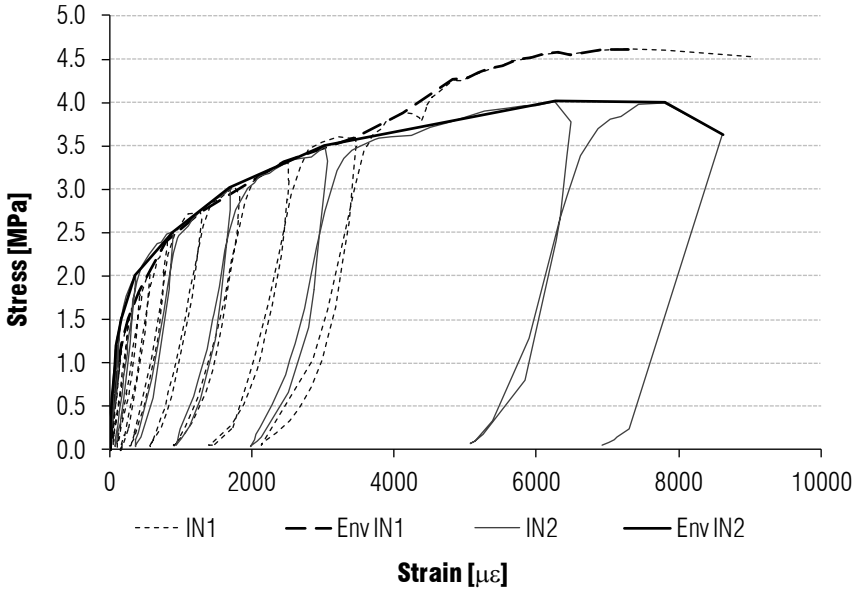


*Fig. 3.22 Flat jack stress strain curve with post peak phase for two injected panels*

A comparison between Fig. 3.22 and Fig. 3.23 highlights how from the moduli analysis the two samples showed a significantly different behaviour instead in the stress strain curve this is less emphasized.

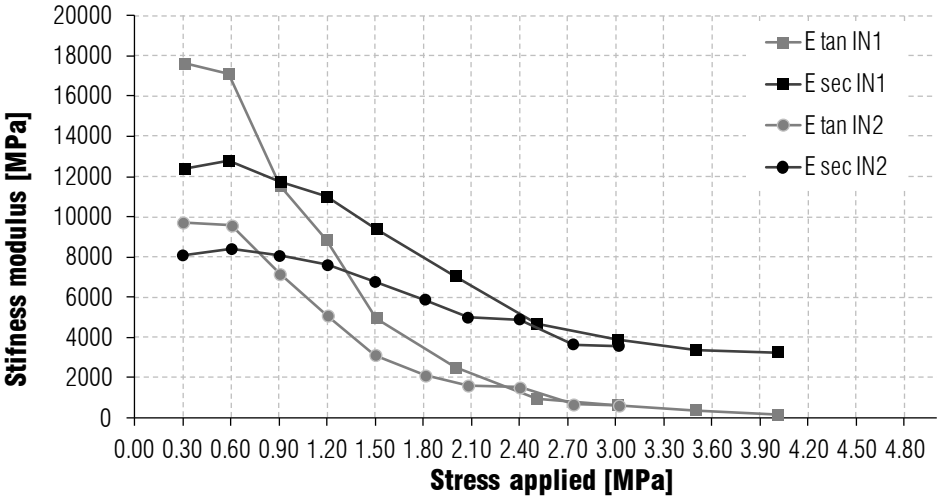


*Fig. 3.23 Tangent and Secant stiffness for each stress level for both cases*

Tab. 3.1 shows a comparison between the ultimate strength and the onset of cracks and also the modulus calculated according the compression test and the

average value of secant modulus. It has to be noted that the latter reduce the difference between the two.

*Tab. 3.1 Figures of onset of cracks, ultimate stregth and elastic moduli*

| | $f_{cracking}$ [MPa] | $f_{c,u}$ [MPa] | $E_{30\ \%}$ [MPa] | $E_{avg,sec}$ [MPa] |
|---|---|---|---|---|
| IN1 | 2.00 | 4.61 | 6247 | 7946 |
| IN2 | 1.50 | 4.01 | 12199 | 6185 |

### 3.3.4 *Methodological aspects*

In order to compare univocally the tests results, also aiming at updating the properties ranges given in the standard, only one reference value should be selected.

To solve this trouble the use of areas (e.g. Fig. 3.19 and the case study of Fig. 3.22) seems to be more suitable instead of numerical ranges, describing better masonry typology by means of stress strain areas. Further work will be desirable in this field. To figure out a representative value of the elastic modulus a study on the whole database was carried out.

The trial to estimate parameters by the use of predetermined stress-state or based on a percentage of the maximum load, as for the Young modulus in uniaxial compressive test, do not seem to give solution mainly because for flat jack the initial state stress is variable and the maximum load, related to the material ultimate strength, is usually unknown also after the test. A more viable solution proposed is to refer to values that are constant as much as possible during the whole test, hence not being related to specific stress conditions.

In order to extend to the whole dataset the comparison among the two elastic moduli, a normalized modulus of tangent ($E^*_{t,i}$) and secant stiffness ($E^*_{s,i}$) at each step is introduced in eq (3.2) as follow:

$$E^*_{s,i} = \frac{E_{s,i}}{\overline{E_s}} \qquad E^*_{t,i} = \frac{E_{t,i}}{\overline{E_t}} \tag{3.2}$$

where $E_{s,i}$ and $E_{t,i}$ are the secant modulus in unloading phase and the tangent modulus respectively and $E_s$ and $E_t$ oversigned are the average values of both moduli throughout all steps.

Similarly to Fig. 3.18 and Fig. 3.23, the values of (3.2) are plotted versus the stress achieved in each step and in Fig. 3.24 (secant modulus in unloading phase) and Fig. 3.25 (tangent modulus) are shown for all the cases. Those curves considered the trend of the modulus throughout the whole test.

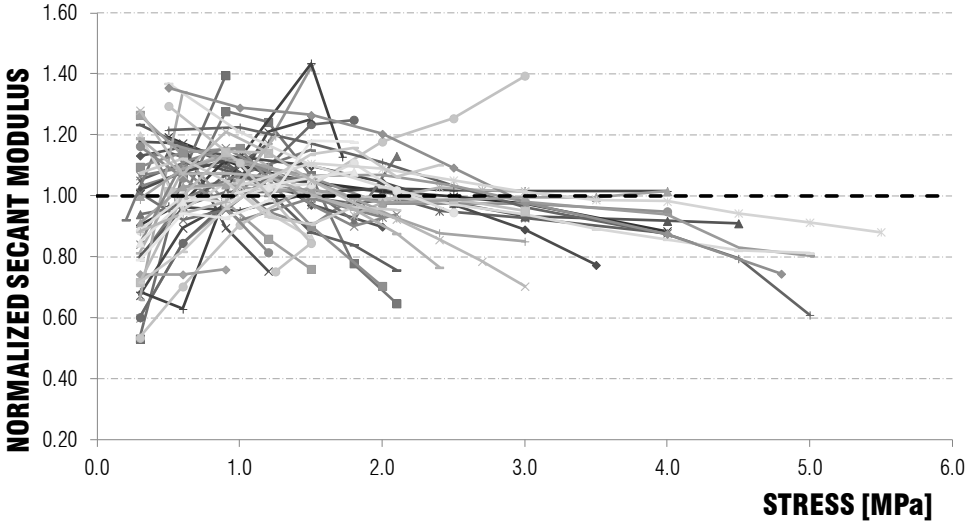


*Fig. 3.24 Normalized unloading secant modulus vs the applied load for the whole dataset*

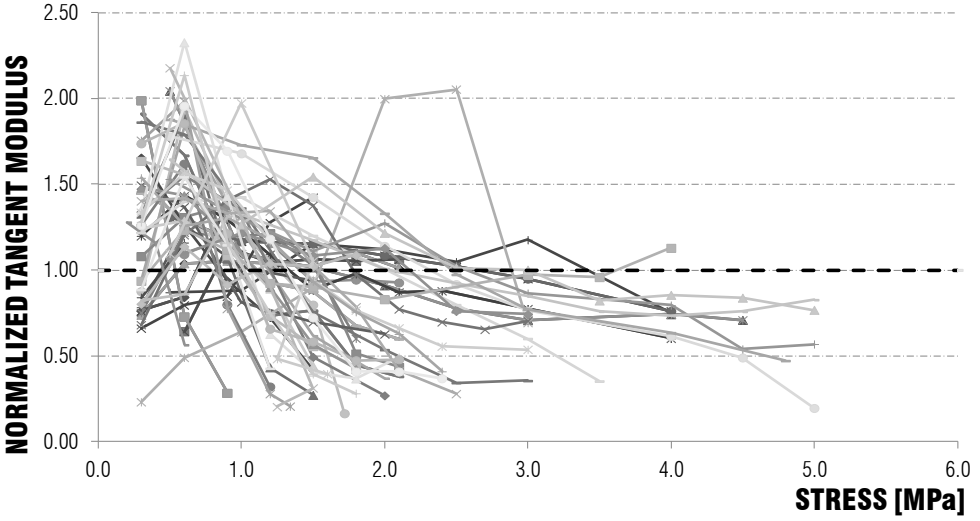


*Fig. 3.25 Normalized tangent modulus vs the applied load for the whole dataset*

From a theoretical point of view the tangent stiffness of a parabolic or elasto-plastic behaviour should decrease with the rise of stress meanwhile the secant modulus should follow an elastic branch, even in the plastic phase of loading, besides any damage. It is possible to notice how the behaviour of those two parameters is in accordance to the theoretical meaning of both.

In Fig. 3.24 the values of the modulus lies between 1.4 and 0.6 the main value and the average, equal to 1, agrees with the global behaviour. An opposite behaviour is shown in Fig. 3.25 where the measures majority decreases from 2 to

0.5 times the main modulus with in some cases an high gradient. Moreover it is clear that this measure is very sensitive to step position and stress conditions.

The generalization of the two cases illustrated before on the whole dataset agrees with the observation before mentioned. Because of these considerations the average of secant stiffness in unloading phase seems to be an adequate solution to summarize results. This is valid when only one value is required. It is clear that when the numerical analysis uses a constitutive law more sophisticated the envelope could be more suitable. This procedure of interpretation will be applied to the experimental cases study presented in CH. 4.

In conclusion the FJ test confirms to be a valid technique on site for the characterization of the mechanical characteristics of masonry. The general outcome about the interpretation of stiffness behaviour is related to the proposal of the average secant modulus in unloading phase as a summarizing value of the masonry stiffness. The analysis of the database highlights an intrinsic high variability on the material properties according to conclusions about the sonic dataset although in this case the figures are related to quantitative values. In these terms the FJ test is a very suitable tool in order to understand the actual masonry behaviour within the proposed range and helps to get reliable results.

To update the Italian technical ranges [NTC 2008] a lot of work is still needed in order to find other parameters to be evaluated together (e.g. mortar properties). Moreover, to do that, the test procedure should be defined and shared with the scientific and professional community to allow comparison among the testing procedures.

## 3.4 INFRARED IMAGES

In the following paragraph a brief series of examples of the infrared thermovision are presented according to the experimentations carried out on the pilot cases.

In practical cases, the use of active or passive techniques is mainly related to the dimension of the inspected element. In general, in order to control or to understand structural parts or elements, which are extended portions, the passive thermovision is the only affordable solution. Because of this limitation, it is relevant to remember, according to §2.3.2, how an high gradient between the two sides of the inspected element is crucial and many times restrictive.

The most interesting and useful information could be summarised as:

- Detection of different materials and structural elements in wall such as reinforced concrete stringcourses or existing infill doors. In terms of vulnerability analysis those information are relevant to increase the level of knowledge(Fig. 3.26)
- Detection of materials and structures of floors and roofs such as wattle ceilings or concrete slabs (Fig. 3.27). This allows a proper estimation of possible loads and structural elements and point out where to perform deep analysis.
- Both in walls and vaults is sometime possible to recognise the unit shape and texture. In case of wall this allows to identify the masonry typology without plaster removal and in case of vaults can help to understand stereotomy (Fig. 3.28).
- Form an overview is also possible to detect and localize buttresses or thicker part in the vault that help to reduce coring. In this case was also possible to detect plaster detachments. (Fig. 3.29)

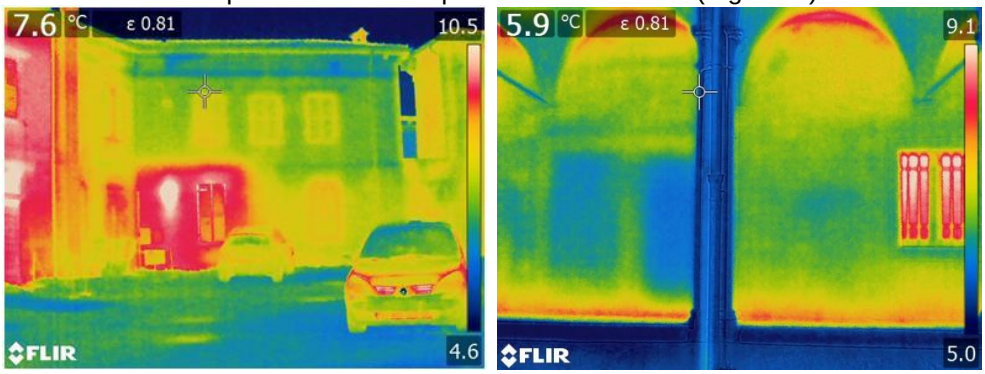


*Fig. 3.26 Identification of different structural elements, concrete stringcourse (left) and infill door (right)*

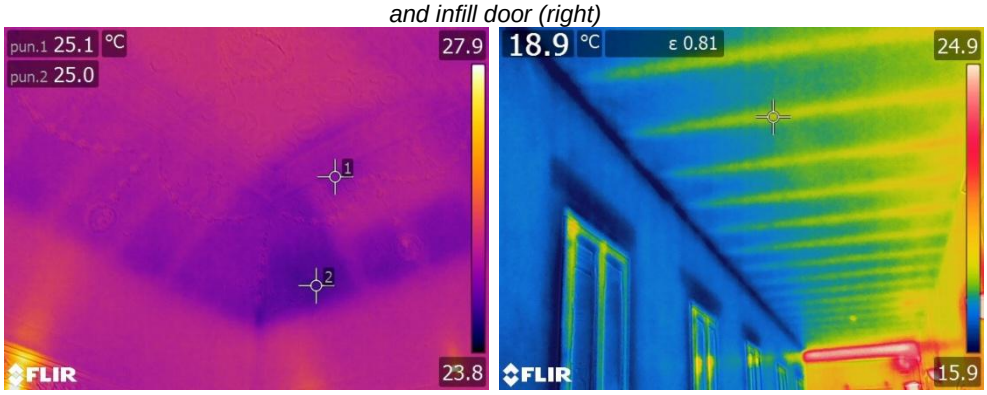


*Fig. 3.27 Identification of material and typologies: ceilings (wattle, L) and roofs (concrete, R)*

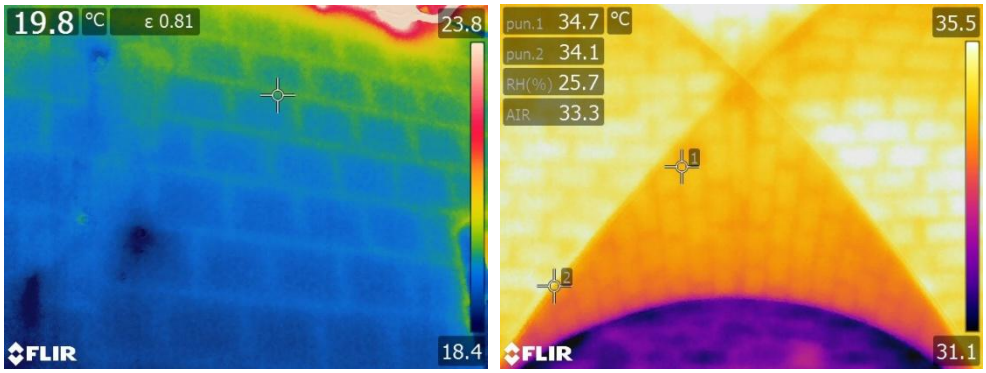


*Fig. 3.28 Identification of unit texture on walls (left) and vaults (right)*

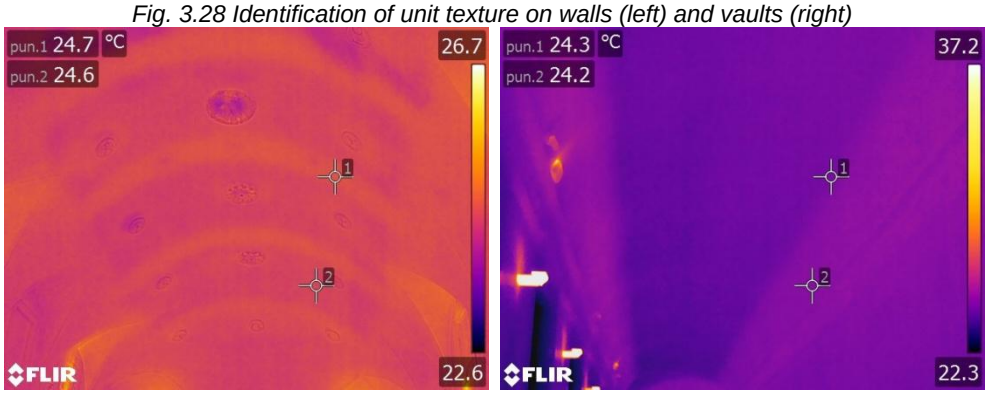


*Fig. 3.29 Identification of thickness distribution and detachements*

As is possible to understand from these cases, thermovision is a suitable solution, easy and fast to perform on wide surfaces and areas. Information are purely qualitative but fundamental to address minor destructive tests as well coring to measure thicknesses in vaults, or to be aware of possible failure mechanisms (detachment of plaster) or unexpected contributions (presence of stringcourses or buttresses).

## 3.5 TENSION ESTIMATION IN TIE RODS

Consistent with the work carried out for sonic tests and flat jacks, also in this case the first step was the gathering and the organization of data acquired in previous years in order to understand the possible lack in procedures and test interpretation. Moreover, the analysis of typical ranges and dimensions was the base to design and perform and experimental campaign.

CH 7 reports tests, elaborations and analysis performed to improve the method.

### 3.5.1 *Database*

The on-site experience gained by the University of Padova in past years permitted to gather an overall number of 353 ties “extracted” from several cases studies.

The database collection had three principal goals:

- to develop a data management coming from different cases, for revising the methodology;
- to analyse modal parameters, at least the first frequency to evaluate and compare different estimation models;
- to characterize common tie rods typologies related to geometrical features and usual rate of work.

The database is composed of four sections: the first one with the general data regarding the location of tie rod, the supposed dating and its ID. The second section has the specification of the vault typology where the tie rod is located, and the characterization of that vault for each tie. The third section includes the geometrical features such as the type of cross section (rectangular or circular) and its dimensions, the specification of material; including density, Young Modulus, and the span. The final section reports the dynamic identification of the tie rod with the first frequency gathered. Due to the application of the string linear theory in past years, requiring the only measurement of the frequency, for a wide number of surveys information about highest modes and in general about mode shapes is lacking. The database was subsequently widened in the last section with the addition of data describing the first three frequencies and mode shapes. Such data are only available for 50 cases.

The proposed dating of elements relied on possible variations in time of proportions, material properties and tension rate of elements. Even if construction’s age has been evaluated and goes from V-VII century (Santa Maria Assunta di Vobarno, BS) and XVII century (Seminary of Venice), unfortunately it was not possible to exactly understand if tie rods were consistent with such periods or if they were added or modified later. A parameter which affects the static and dynamic behaviour in operational condition is the young modulus. In this work it has been considered at 200 GPa. The tensile strength is the other relevant parameter although the estimated stress rate is usually far less than 200 MPa.

Form a geometrical point of view the database gives many indications about the typical area and cross section.

A first analysis considered a classification based on the tie length, trying to define different geometrical proportions related to this parameter. The analysis of data suggested a division in long and short ties, arbitrarily defining the length of 5 m as threshold. Short ties have an average length of 3.70 m with a CoV of 20%: 59 elements of the population lies between 3.50 and 4.00 m, considered as representative of arches and vaults of cloisters and palaces. Longer ties have an average length of 6.98 m and a CoV of 27%. In this class values are less uniform and are mainly related to nave of churches.

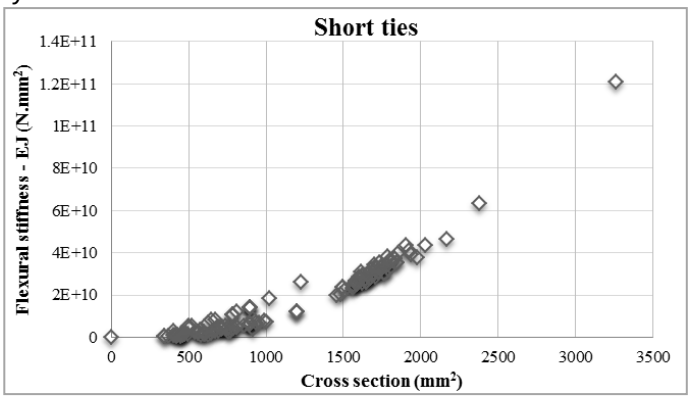


*Fig. 3.30 Area distribution versus flexural stiffness of short ties*

In addition to this first classification, the database was used also to evaluate the sensitiveness to stiffness in the first frequency.

Starting from eq. **(2.8)** where frequency is related to the root square of the linear density the graphs in Fig. 3.31 shows the squared frequency for different groups of moment of inertia.

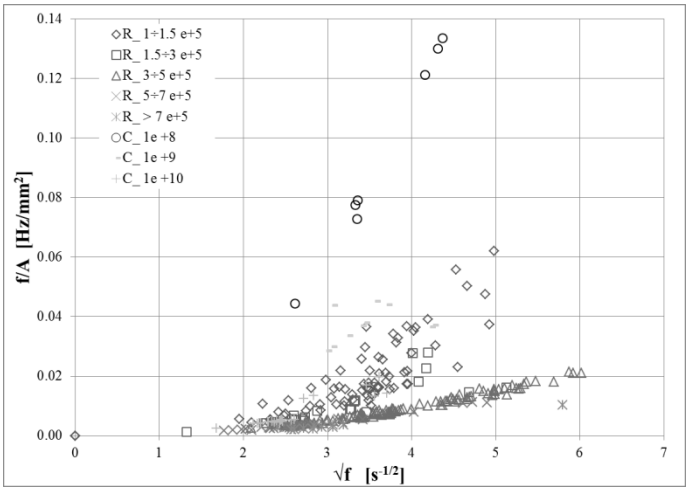


*Fig. 3.31 Square rooted frequency versus ratio frequency and area. Data are grouped in different classes of moment of inertia*

The graph highlights that the flexural stiffness is not negligible and strongly affects frequencies. Indications obtained by initial analyses of tie rods in historical constructions database hence suggest behaviour closer to beams than cables, with stiffness of the element deeply affecting the overall behaviour. The experimental available data refers to the tie-rods dynamic behaviour.

Due to the lack of a complete vibrational analysis (e.g. modes of vibration, higher frequencies), the axial force estimation is necessarily related to the use of the sole first frequency.

The equation given in eq. (2.8) was used to this aim, generally overestimating the axial force, since the pinned condition at the extremities was taken into account. Cumulative values of the tensile axial stress in ties belonging to the database, obtained through this simplified approach, are presented in Fig. 3.32. The tests carried out in the laboratory, whose results will be shown in CH 7, indicate that the actual force is closer to this formulation rather than its adaptation to the fixed restraints conditions.

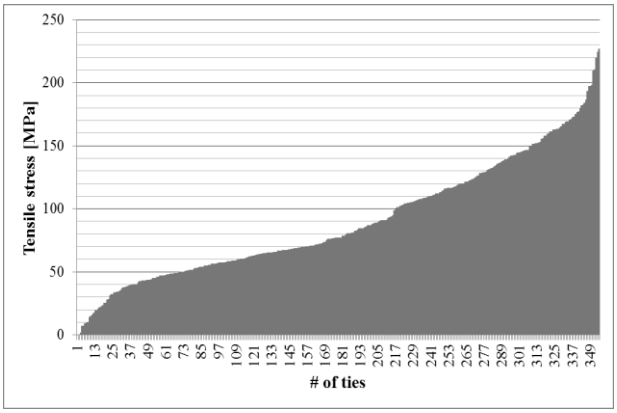


*Fig. 3.32 Working stress of each tie (sorted increasingly), estimated with string theory*

Fig. 3.32 shows that the estimated tensile stress inside elements is lower than 100 MPa for the 61% of ties, and lower than 150 MPa for the 86% of cases.

The analyses carried out indicate a stress level which is generally compatible with the material strength. This observation is consistent with the lack of available theoretical models at the time of construction, and then the related relatively conservative stress/strength conditions found.

On the other hand, it was noted that it is in general not possible to correlate – for example – the span with the axial force, or this last with the cross-sectional values, given the highly scattered data collected.

# 4 CASE STUDY

## 4.1 INTRODUCTION

This chapter aims to present some practical applications of what developed and presented in other chapters in a more theoretical way as mentioned in the thesis introduction. The entire research has been developed in the framework of the Pro.Va.C.I. project in which the selected pilot cases were two sites inside the city namely the San Pietro's Hill (Fig. 4.1) and the ex San Fermo's monastery [Cescatti 2015b/c]. In this work are reported only the aspects related to the Castle, closer to the experimental campaign presented. About the relevance of the historical analysis it is suggested to look at the project's deliverables in particular about San Fermo's cloisters. The castle was involved in a restoration project, which allows many tests and interventions for its future usage as a museum.

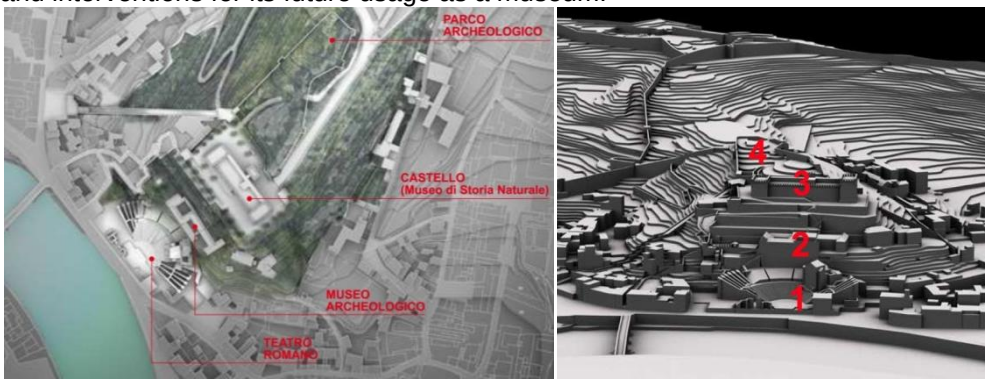


*Fig. 4.1 San Pietro's Hill over the city of Verona*

## 4.2 INFORMATION AND INVESTIGATION

The city of Verona was founded by Romans inside the natural inlet of the Adige River. Before current buildings, other constructions were present on the hill over the city. This location has been played an important role during centuries and currently inside the area there are (looking at Fig. 4.1):

1. Roman Theatre
2. a medieval convent
3. Asburgic Castle - San Pietro's Castle
4. Green archaeological park

Varying among such different constructions, in term of functions but also in terms of structural concepts, these set of cultural heritage represents a unique opportunity to look at the assessment methodology, the preservation approach and the interaction with the city. In particular in this work are shown the analysis and the tests carried out on San Pietro's Castle.

The history of the settlements in this area dates back to the 7th c. BC (Pinali 1834), but the existing structure was raised in the second half of the 19th c. on the remains of the former church. On top of the hill traces of pre-Roman settlements which date back to the Iron-Age were found suggesting the existence of a castle. In 89 BC Verona became a Roman's colony. On top of the hill the sacred and strong place called *Arx* was built to guard via Postojna on the passage on Adige. This was also confirmed by the recent works inside the Castle which reveals some medieval and roman settlements under the current building. Moreover, despite the ancient memories, in 1914 it was demonstrated that the Roman *Capitolium* where not located on the hill.

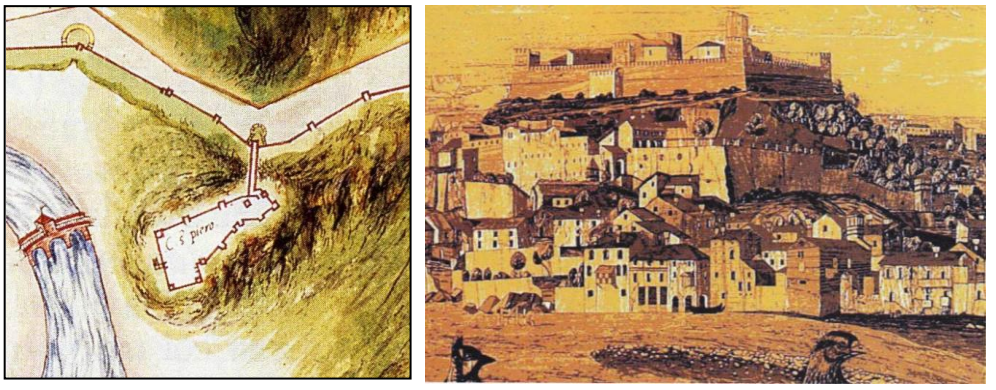


*Fig. 4.2 General Plans of fortresses in Verona (1550-1560) State Archive, Turin (left) Wooden inlay by Fra Giovanni (1519-25) (right)*

After the end of the Western Roman Empire, during Teodorico kingdom's Verona was the favourite city of the king who constructs and built palaces, fortress and thermal baths. He built his palace on the hill. Form the 8th centuries in the tops was built a church dedicated to San Pietro. In 1393 the Visconti Castle was constructed on top of the hill around the church by Gian Galeazzo Visconti (1387-1405), the first Duke of Milan. After this, from 1407 to 1797 Verona was dominated by Venetians, from the sixteenth documents and representations (Fig. 4.2) clearly appears the S.Pietro Fortress on the hill.

This symbol of the city, during the Venetians' age, was completely destroyed and blown up by Napoleon's army in 1801. After that event the ruins of the Castle and the internal church stand until the Habsburgs Empire took the control of Verona.

The first documented project of an Habsburgs' barrack date back to 1852 on the ruins of the previous church (see Fig. 4.3 left). Slightly different from the architectural point of view (Fig. 4.3 right) form the actual structure, the general concept remains also in the final version (Fig. 4.4). The influence on design by the previous castle is evident from the lateral towers volumes with a typical architectural composition. After several observations by the Vienna's civil engineering department the project was modified in two versions and sent to Vienna on 28th of January in 1853. The actual building had a military function of a barrack for 452 soldiers and 9 officials [Bolza 1853] and was constructed in a Neo-Romanesque style. With the architectural appearance of the building the goal was to give a new architecture of the Habsburg Empire for the city.

The main mass of the building is composed of three parts in a line. The number of floors follows the slope of the ground. The barrack has three stories in the East side and four in the West side. The two towers, located at each side, are standing with one additional floor.

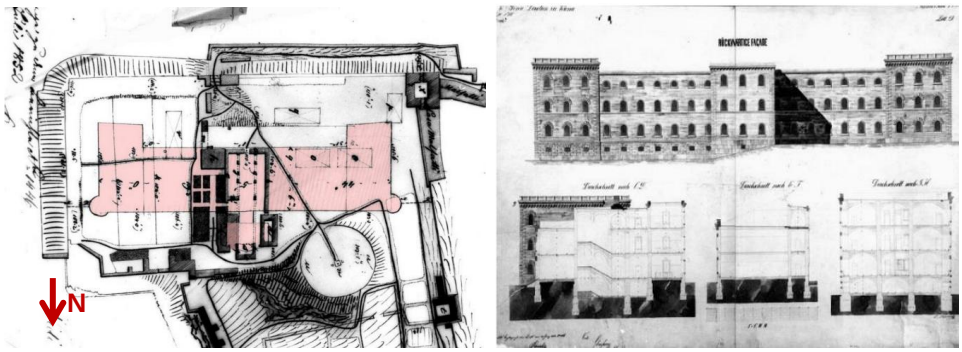


*Fig. 4.3 "Situations Plan des Castelles S. Pietro" (1852), Kriegsarchiv, Wien*

*Fig. 4.4 View of Verona form the River Adige in 1866, upon the hill the Castle*

The internal distribution is based on big modular spaces, 13.6 m long and 6 m wide, all covered by barrel vaults and connected by a long corridor in the back part of the building. The vaults direction is orthogonal in the two towers.

The lavatories where all located at each floors in an additional tower in the Northern part of the Castle, connected to the main building by a small corridor.

### 4.2.1 *Modification and intervention until now*

There is a lack of documentation about the building but from a carefully survey is possible to recognise few interventions on the structure. Some drawing stored in the city hall archive goes from 1931 to 1970. Other documentations about maintenance works without any graphical restitution go from 1976 to 1995. Starting form 1937 and until 1941 some works were carried out by fascists to use the barrack as headquarter.

The most relevant works from a structural point of view were done in order to use the building as a school. In particular modifications were focused on the second floor of the west branch where the windows in the north facade were enlarged and vaults of the corridor were demolished and reconstructed according to the direction of the main rooms (see Fig. 4.5).

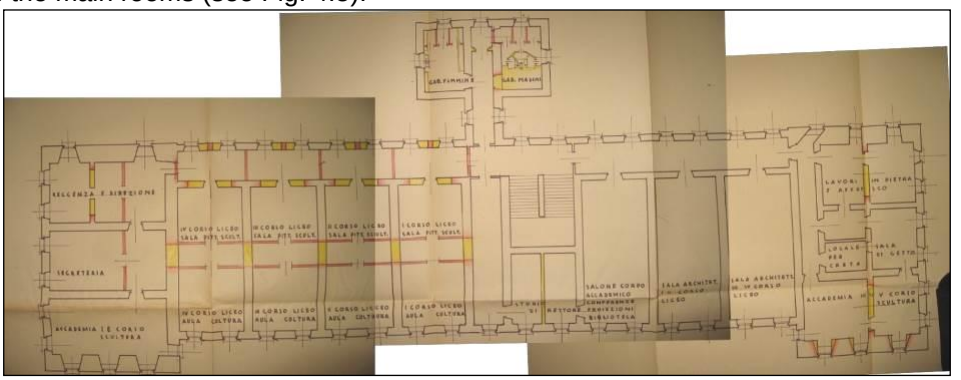

*Fig. 4.5 Plan of level C, 1948, demolished parts (in yellow) and new structures (in red)*

### 4.2.2 *Geometrical survey*

The structure is composed by three masonry typologies namely:

1. brick masonry
2. stone masonry with brick stringcourses
3. stone masonry (using the hill's rock as unit) for foundations

The distribution of each type is regular (Fig. 4.6). The brickwork masonry (1) with lime mortar was used to build all the external walls and vaults, with the only exception of the ground floor where are made with the second type. The internal bearing walls were built with stone masonry (2) which was finely shaped following the typical Habsburgs' texture. Finally for the foundation wall a stone masonry less regular (3) and with soft stones was used. The definition of those typologies allows to design the material characterization and to define the structural geometry.

Especially in towers the walls thicknesses are considerable high where dimensions varying between 1.97 at the bottom and 1.60 m at the top. The other perimeter walls lie between 1.15 m at level A (bottom) to 0.64 m at level D (top). Internal bearing walls vary in thickness between 0.80 and 0.85 m in the whole castle.

After the geometrical survey and the definitions of masonry typologies the crack pattern and the damage survey was carried on.

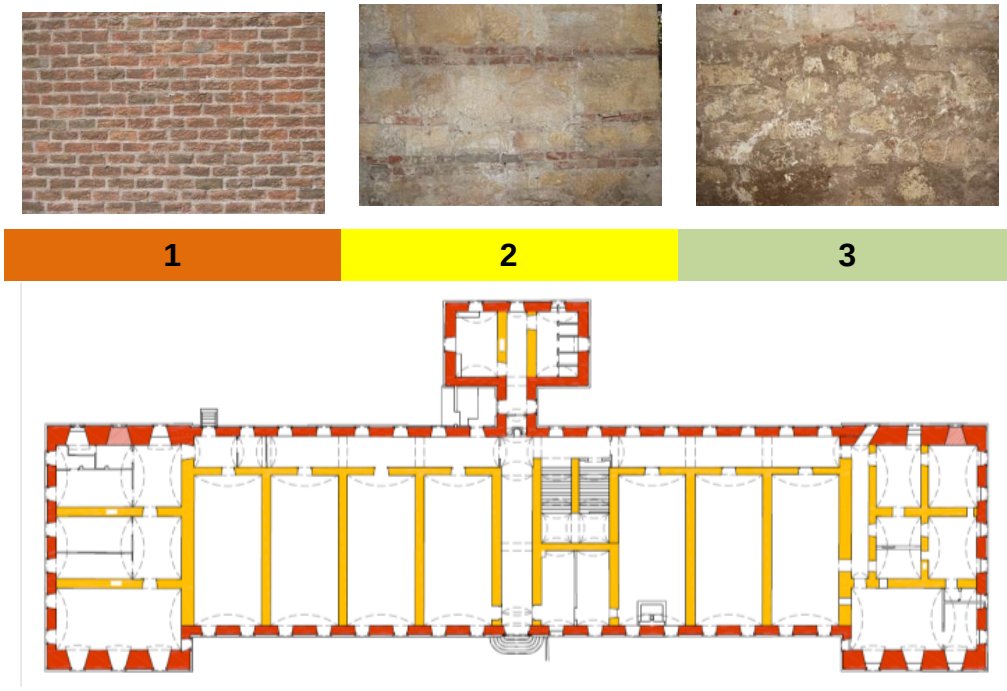


*Fig. 4.6 Masonry typologies (above) and plan distribution (below)*

Fig. 4.7 and Fig. 4.8 show the crack pattern in which are evident in some positions mortar deterioration and salt crystallization in particular in the upper level and next to the drain pipes inserted in walls. In terms of structural cracks the worst portion is related to the Northern tower where during refurbishment works some cut iron ties were found. Finally in the two towers, in particular in the higher level, some diagonal cracks are located in the spandrel walls.

In general is possible to conclude that, despite the northern tower where some structural problems caused by some reworks were recognised, the damage survey highlighted a good state of the structure but also a deep lack of maintenance that rise many problems that led to material degradation.


*Fig. 4.7 Crack pattern and damage survey of the North (above) and South (below) façade.*

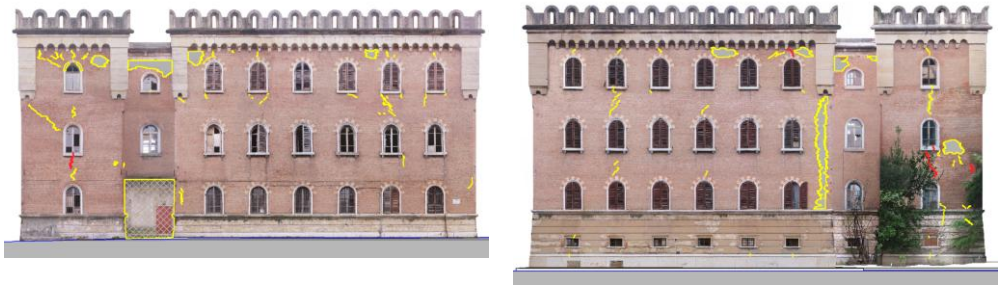

*Fig. 4.8 Crack pattern and damage survey of the West (left) and East (right) façade*

### 4.2.3 *Coring and video endoscopy*

In order to identify wall transversal section, presence of voids, connections, aggregation and regularity a series of eleven coring, with the addition of video endoscopy were performed in several positions (Fig. 4.9). These tests highlighted

(Tab. 4.1) a very good quality of walls that are compact and without voids despite their wide thicknesses (1.97 m). The endoscopy on brick masonry also showed a strict regularity among courses.

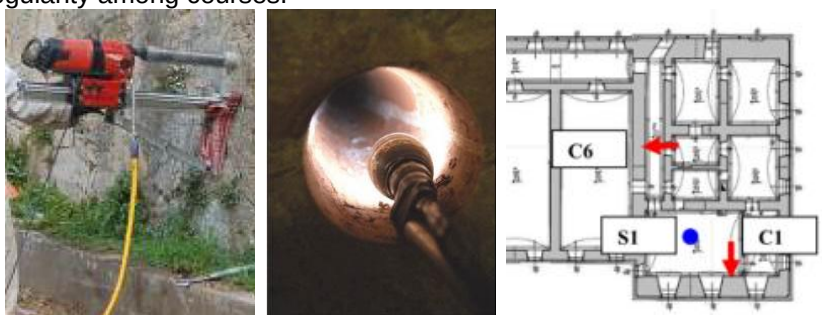


*Fig. 4.9 Coring machine (left) and video endoscopy(centre), test on the East tower (rigth)*

*Tab. 4.1 Coring number and results*

| Coring | Element | Mas. Type | Aggregation | Density | Regularity | Voids |
|---|---|---|---|---|---|---|
| C1 | Wall | 1 | High | High | High | No |
| C2 | Wall | 2 | High | High | High | No |
| C3 | Foundation | 3 | High | High | High | No |
| C4 | Foundation | 3 | High | High | High | No |
| C5 | Wall | 2 | High | High | High | No |
| C6 | Wall | 2 | High | High | High | No |
| C7 | Perimeter wall | 2 | High | High | High | No |
| C8 | Wall | 1 | High | High | High | No |
| C9a | Wall | 1 | High | High | High | No |
| C9b | Vault | 1 | High | High | High | No |
| C10 | Vault | 1 | High | High | High | No |

### 4.2.4 *Flat jacks*

In order to characterise the compressive behaviour of masonries by means of flat jack, as illustrated in § 3.3, 18 singles and 8 doubles tests were performed on the structure.

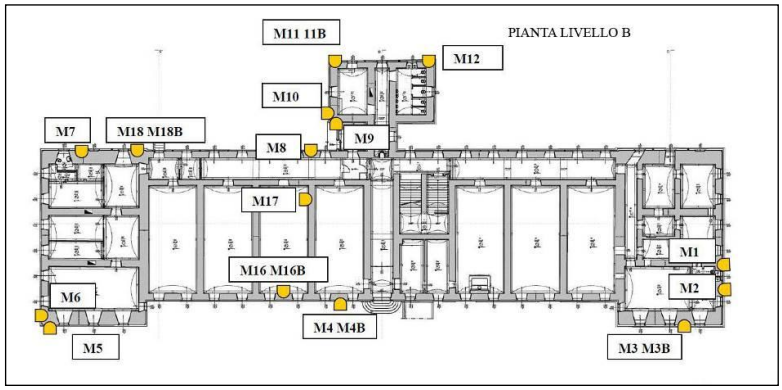


*Fig. 4.10 Location of single and double flat jacks (marked with letter B)*

The high number of single tests allows to understand the stress distribution on service loading. Fig. 4.10 shows the test location for the first floor in the castle and relative results are reported in Tab. 4.2. The reported figures of the single flat jack show low stresses as expected by considerably wall dimensions and from typical ranges of stress in historical masonry buildings. From the double flat jack is evident the masonry good quality. Considering analysis carried out on the database (see §3.3.13) the recent age of the building, together with the strategic use, correspond to high quality brickwork masonry.

*Tab. 4.2 Test numbers and results*

| Test N. | Location | Mas. type | $\sigma_v$ [MPa] | $E_{tang}$ [MPa] | Test N. | Location | Mas. type | $\sigma_v$ [MPa] | $E_{tang}$ [MPa] |
|---|---|---|---|---|---|---|---|---|---|
| M1 | External wall | 1 | 1.01 | - | M10 | External wall | 1 | 0.70 | - |
| M2 | External wall | 1 | 0.97 | - | M11 | External wall | 1 | 0.62 | 4672 |
| M3 | External wall | 1 | 1.10 | 3374 | M12 | External wall | 1 | 0.66 | - |
| M4 | External wall | 1 | 0.44 | 3035 | M13 | Internal wall | 2 | 0.62 | 4605 |
| M5 | External wall | 1 | 0.70 | - | M14 | Internal wall | 2 | 0.88 | 3183 |
| M6 | External wall | 1 | 0.62 | - | M15 | Internal wall | 2 | 0.84 | 3687 |
| M7 | External wall | 1 | 0.75 | - | M16 | Foundation | 3 | 0.35 | 1909 |
| M8 | External wall | 1 | 1.14 | - | M17 | Internal wall | 2 | 0.48 | - |
| M9 | External wall | 1 | 0.88 | - | M18 | Internal wall | 1 | 0.88 | 4812 |

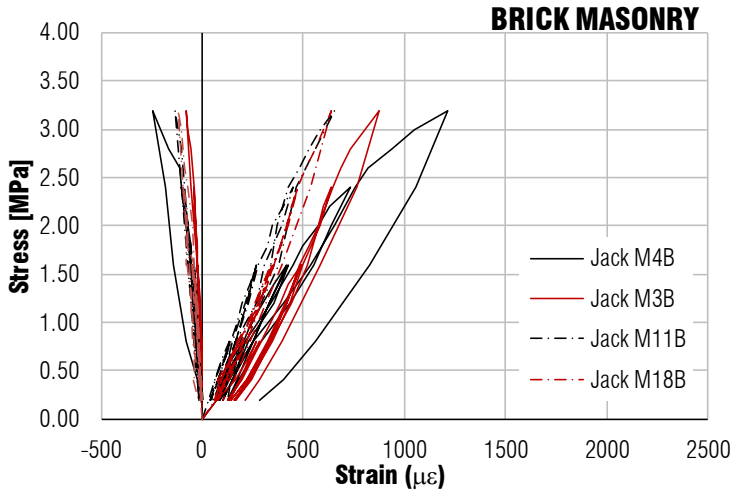


*Fig. 4.11 Average stress-strain curves for brick masonry*

Fig. 4.11 shows the average stress-strain curves of all the double flat jacks performed on brick masonry. The graph shows an almost linear behaviour until 3 MPa with limited deformation in both directions. The same good behaviour was

pointed out by tests on stone masonry (Fig. 4.12). The only test performed on foundations showed a lower quality

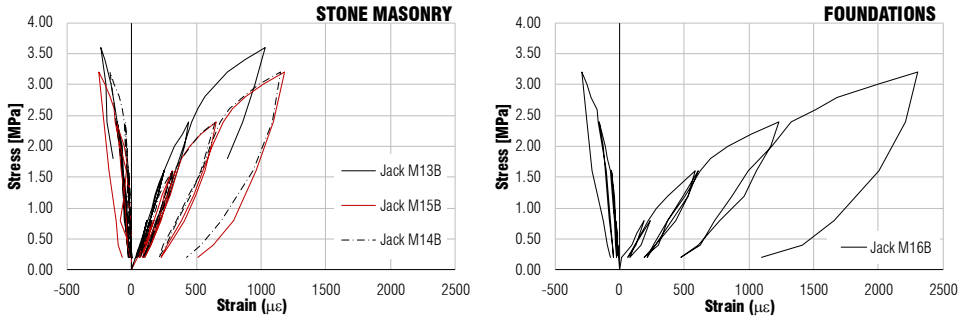


*Fig. 4.12 Average stress-strain curve for stone masonry (left) and foundations (right)*

According to outcomes of § 3.3.4, Fig. 4.13 shows the trend of tangent and secant moduli at each stress level. Masonry brick shows a more constant behaviour compared with other two. The difference between the two calculated moduli for each masonry type shows a constant behaviour that may confirm small damages of the tested specimens.

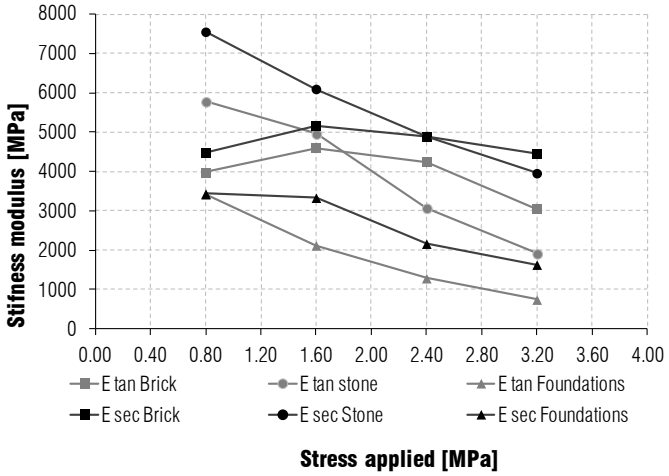


.

*Fig. 4.13 Tangent and Secant stiffness for each stress level*

The analysis of Poisson's coefficient by flat jacks could be affected by confinement. Nevertheless in literature Binda [2007] and guidelines [ASTM C1197:09 and RILEM MDT-05] suggest its calculation. Moreover the estimation of this value is suitable for FEM calculation. The coefficient was calculated at each cyclic peak as the ratio between horizontal and vertical deformation. For masonry types 1 and 3 $\nu$ was 0.11 and for type 2 was equal to 0.14.

*Tab. 4.3 Average vaules of elastic moduli*

| Masonry type | $E_{tang}$ [MPa] | $E_{sec}$ [MPa] | $f_{cmk}$ ACI [MPa] | $f_{cmk}$ EC 6 [MPa] | $f_{cmk}$ CIRC [MPa] | $f_{cmk}$ EXP [MPa] | $f_{cm,d}$ [MPa] |
|---|---|---|---|---|---|---|---|
| Brick | 3968 | 4744 | 5.70 | 4.00 | 4.80 | 3.20 | 2.20 |
| Stone | 3935 | 5624 | 5.60 | 3.90 | 4.58 | 3.20 | 2.10 |
| Foundation | 1890 | 2642 | 2.70 | 1.90 | 3.50 | 3.00 | 1.90 |

Average values of elastic moduli measured are reported in Tab. 4.3 and high moduli are founded.

In this practical example is possible to see the variability in estimation of mechanical properties, about stiffness but above all in terms of compressive strength. Referring at guidelines suggestion reported in § 2.2.1 the final value are reported in Tab. 4.3. For ACI according to eq. (2.1) and for EC6 according to eq. (2.2). Accounting for literature observations the use of the inverse equation to calculate masonry strength coefficient is too unconservative for lower value of the factor (for instance 413). The evaluation of elastic modulus by flat jack, even with a possible overestimation of 20%, lead to the upper bound of Tab. 2.1 limits. The calculated characteristic values are therefore the boundary average multiplied by the corrective factors (good mortar and stringcourses). About the design values the characteristic compressive strength of masonry should be divided by the material safety factor ($\gamma_m$ 2.0) and the knowledge factor (FC). Looking at ASCE [41-13] this value is 1.3 meanwhile for NTC08 it would be 1.20. Thanks to the cultural heritage approach of LL.GG.BB.CC [2010] the knowledge factor could be calculated adding four levels namely: complete geometrical survey (0), reconstruction of constructive phases (0.00), tests on mechanical parameters (0.06) and ground test (0.03) for a final FC equal to 1.09.

As is possible to understand form this short analysis, mechanical properties are significantly variable depending on the followed approach although the application of an extended number of tests. This underlines the need of further research in the field of existing masonry construction to provide an unified approach. On the other hand this highlights the need of an expert judgment as required by ISCARSAH [2005].

In this case study the adopted values are those derived from CIRC [2009] with the knowledge factor FC equal to 1.09. In conclusion the design strength (2.20 MPa for brick) is compared with the stress-strain curves of FJ. Form the comparison the adopted values seems adequate.

### 4.2.5 *Dynamic identification*

The seismic assessment of a structure relies on its dynamic behaviour in terms of global response. The correct understanding of such aspects is a crucial issue in the global analysis either for spectrum analysis or for static non linear analysis.

In particular the investigated issue concerns the in plane behaviour of diaphragms here made only by barrel vaults. The global effect of vaulted structures is not deeply studied. Some contribution came from Giresini [2014] and Rossi [2014] who tried to develop equivalent frame modelling. Indeed, usual simplifications of infinite rigid diaphragms for the floor rather than zero stiffness floors are not suitable for this case.

The dynamic acquisition was carried out by five setups for an overall number of 28 accelerometers (PCB 393 B12) displaced in both direction. Due to the structure extent and the relative small height the greatest part of instruments were placed on the last floor. The adopted methodology is an OMA with ambient vibration excitation. The modal extraction was performed by FFD. The elaboration pointed out the independent behaviour of some structural parts. All analysed mode shapes do not show a global mode. For this reason the analysis was divided among towers. Results are presented in § 4.3.4.

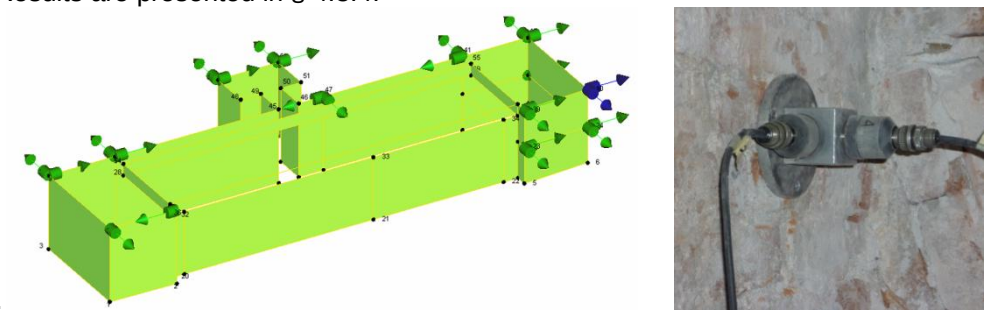

*Fig. 4.14 Sensors location on the castle (left) couple of PCB 393 B12 acceleormeters (right)*

## 4.3 DIAGNOSIS AND SAFETY EVALUATION

After the investigation phase, following the methodology suggested by ISCARSAH [2005], LLBBCC [2010] and presented in § 2.1 safety evaluations are presented. It is beyond the scope of this work to analyse in depth all structural

components and to focus on all structural verifications. The meaning is to highlight the problem accounted and to present the methodology.

### 4.3.1 *Static analysis*

Static analysis were carried out on all elements, masonry walls, stairs and obviously vault. Due to the high quality of masonry and thickness, all walls showed lower stresses and they do not present any problems. A similar conclusion was provided by thrust analysis of vaults. Fig. 4.15 shows the more stressed vault that for all load combinations presents a thrust line within the middle third therefore safe and without cracking.

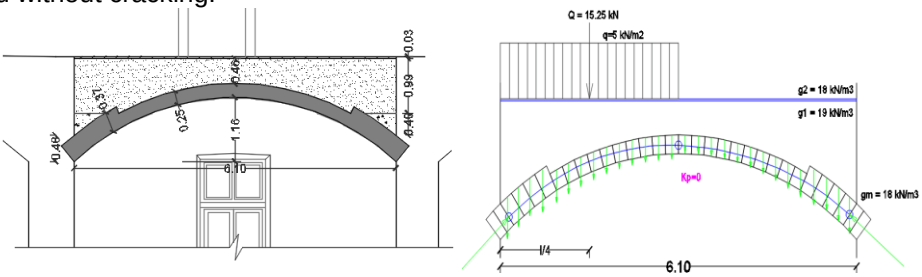


*Fig. 4.15 Static verification of vaults by thrust line analysis*

Some troubles were encountered in the analysis of thrust on abutments. Because of the flat shape of vaults, this horizontal force needs to be counteract by ties in order to avoid problems in bearing wall. This appeared clearly in the Northern tower where ties were cut. The reactivation of these devices was then an executed intervention during refurbishment works.

### 4.3.2 *Kinematic analysis*

After the static analysis, the local analysis on macro elements under seismic action was carried out. Fig. 4.16 shows an example of the overturning mechanisms considered. The monolithic behaviour of elements was guaranteed by the high masonry quality. Summarizing all results, some elements required the addition of ties to avoid the out-of-plane overturning that are designed in the refurbishment project.

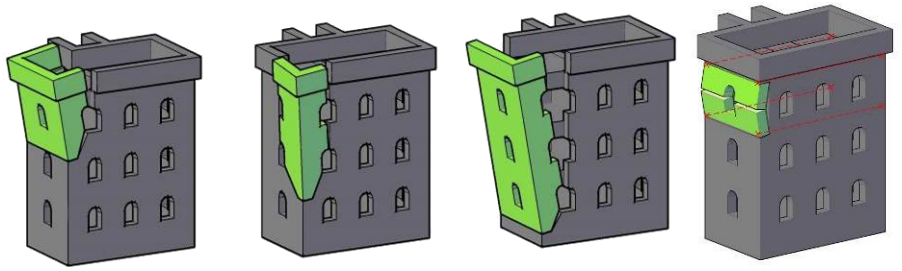

*Fig. 4.16 Kinematic analysis of macro elements*

### 4.3.3 *FEM - Static analysis*

The global Finite Element Model of the castle was developed with TNO DIANA 9.6 software. Fig. 4.17 and Fig. 4.18 show the mesh of the model with different colours according to the role and namely: external brick walls, internal stone masonry and vaults. The adopted finite elements were T15SH Q20SH, triangular and squared quadratic shell elements respectively. The mesh size has an average dimension of 0.3 m for walls and vaults.

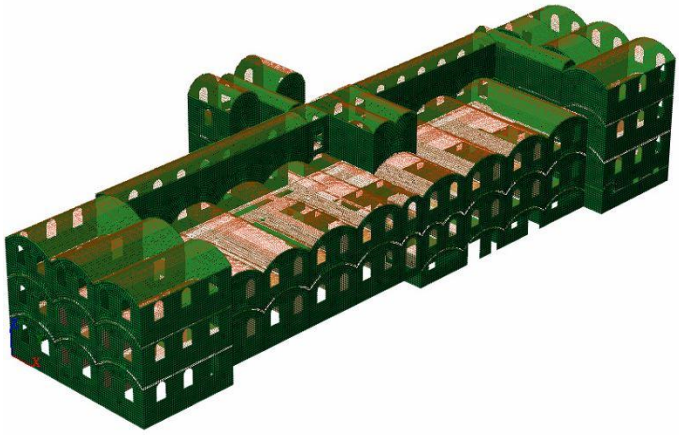

*Fig. 4.17 Global view of the FEM model*

*Fig. 4.18 External brick masonry walls (left) stone walls (centre) and vaulted system (right)*

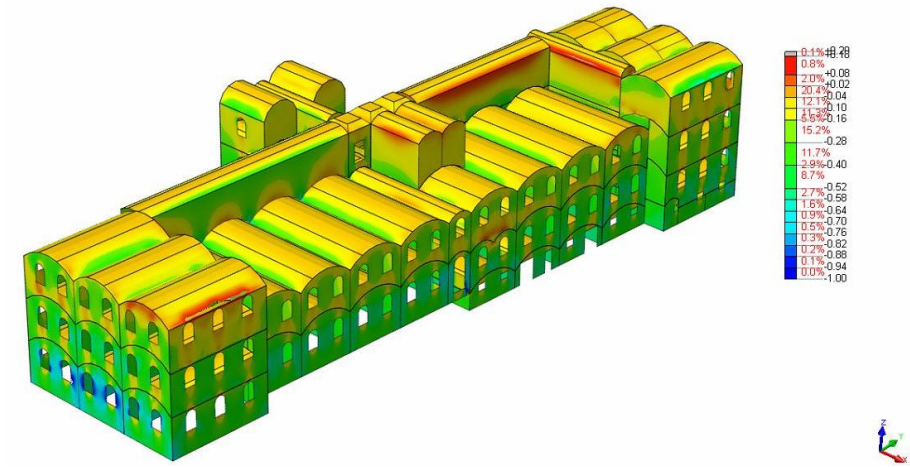


*Fig. 4.19 Vertical stresses under service loads*

Fig. 4.19 shows the first static calibration with dead and live loads on site during the flat jack testing campagin. Tab. 4.4 presents the comparison between values obtained with FEM and those measured on site by means of single flat jack. Even after an attempt of calibration, stresses on the model remains lower than measured. The average ratio between the two is 1.53 with a CoV of 14 %. The reason may be related to the linear connection bewteen vaults and walls. In fact, in linear model a complete connection could help loads to remains centred whitin the cross section. A calibration trial was also performed increasing loads on the structure. It results clearly that this was not the solution because to reach actual stresses loads were higher than rare SLS combination. According to ASTM [C1196:14] is not always possible to correlate single flat jack with the actual state stress.

*Tab. 4.4 Comparison between vertical local stresses measured with SFJ and FEM*

| Test N. | Location | Mas. type | $\sigma_{FJ}$ [MPa] | $\sigma_{FEM}$ [MPa] | Test N. | Location | Mas. type | $\sigma_{FJ}$ [MPa] | $\sigma_{FEM}$ [MPa] |
|---|---|---|---|---|---|---|---|---|---|
| M1 | Ext. wall | 1 | 1.01 | 0.57 | M7 | Ext. wall | 1 | 0.75 | 0.51 |
| M2 | Ext. wall | 1 | 0.97 | 0.55 | M8 | Ext. wall | 1 | 1.14 | 0.7 |
| M3 | Ext. wall | 1 | 1.10 | 0.60 | M9 | Ext. wall | 1 | 0.88 | 0.49 |
| M4 | Ext. wall | 1 | 0.44 | 0.32 | M10 | Ext. wall | 2 | 0.7 | 0.48 |
| M5 | Ext wall | 1 | 0.70 | 0.50 | M11 | Ext. wall | 2 | 0.62 | 0.49 |
| M6 | Ext. wall | 1 | 0.62 | 0.48 | M12 | Ext. wall | 2 | 0.66 | 0.49 |

### 4.3.4 *FEM - Modal analysis*

The dynamic identification and the calibration of the model was useful to underline the role of vaults in the global behaviour. The complete analyses of all setups in the Power Spectral Density on frequency domain pointed out an interesting observation on tests carried out with a high number of sensors. The sensor placement was designed on a FEM with infinite rigid diaphragms, that hypothesis gave global modes that better match the mode shape if located and connected globally. The whole analysis of the PSD does not provide clear peaks with clear associated mode shape. Only the substructuring in different structural portions of the castle proved to be effective.

Two outcomes are therefore drawn, to detect local modes a global analysis with many sensor proved to be ineffective because the increase of noises rather than meaningful contribution. The second aspects remarks the demand to operate in the analysis of vaulted structures by means of FE or equivalent frame elements which take into account the appropriate in plane stiffness of the vault.

Fig. 4.20 and Fig. 4.21 show the calibration of the global model. Starting from the flat jack values of stiffness the obtained elastic moduli were 2700 MPa and 2100

MPa for brick and stone masonry respectively. It is worth to notice that the moduli were lower whereas in general dynamic modulus should be higher than static ones.

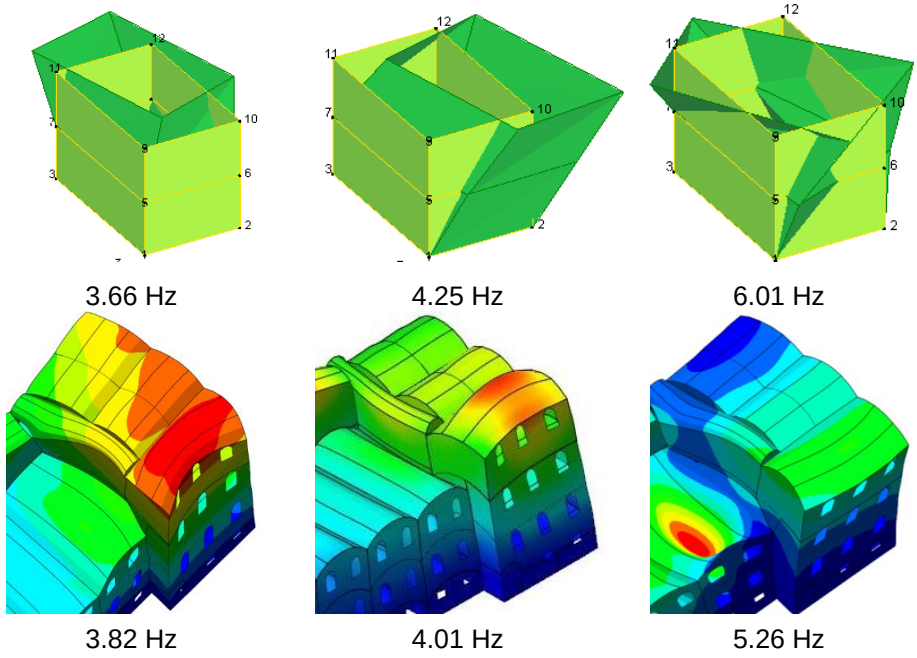


*Fig. 4.20 Comparison between modal extration and FEM analysis for the East tower*

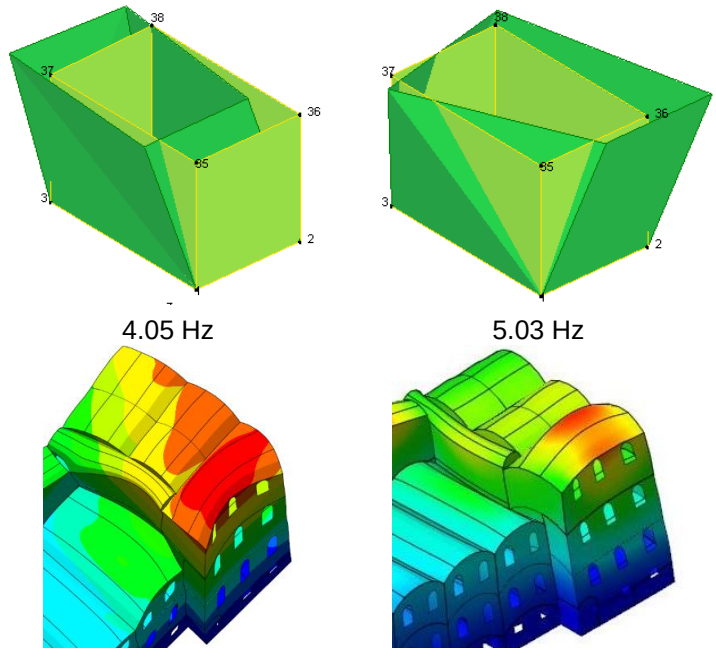


*Fig. 4.21 Comparison between modal extration and FEM analysis for the WEST tower*

The average error of the estimation was 0.3 % but the total absolute error is 22 %: Looking at the behaviour of errors varying elastic modulus, in the East tower, the relative distance between higher frequencies does not improve. Therefore model may improve its fitting by the introduction of other different materials or modifying connections among elements (i.e. vaults and walls).

The spectral response was performed by CQC combination and in all combinations. At least in lower levels the castle is fully safe.

### 4.3.5 *Global non linear static analysis (Pushover)*

To complete the seismic safety assessment of the castle a non linear static analysis was adopted. The approached used deal with an equivalent frame model implemented by 3MURI software. Fig. 4.22 shows the model used. As expected the analysis provide a good response of the structure in the East-West direction meanwhile in the transversal direction (North-South) only one case, for both force distributions (first mode and mass proportional) is not safe with the $\alpha_u$ equal to 0.91 and 0.80 respectively. For masonry existing structure could be still considered a high performance.

Despite good performances of the case studies some observations on the evaluation tools are reported. As highlighted in the dynamic analysis of the structure there is not a global behaviour which allows to recognise a SDOF system. The pushover analysis shows in this case its limits. Looking at Lopez [2004] other possibilities might fulfil the case study as for instance the N2 method. This underlines the need to develop and diffuse those methods in practice to better consider force distributions and MDOF.

Another aspect concerns the selection of the control point. Indeed it was observed that, with different local modes the selection of this point could severely change the final results.

The proposal for same future test is to provide capacity curves related to only some portion of structure keeping the model together in order to properly account of the mutual interaction. The portions, defined as structural units, may consider the three towers and the two central blocks.

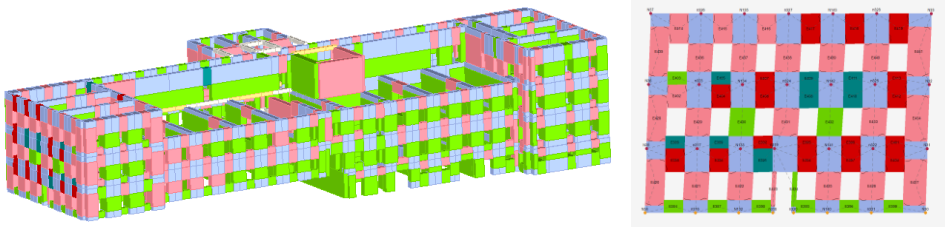

*Fig. 4.22 Overview of the equivalent frame model (left) and damage pattern of the western wall (right)*

### 4.3.6 *Conclusions e future works*

In the framework of the ProVaCI project the San Peter's Castle represents the simplest case, with less structural problems. Neverthless, the case study is here presented first of all to have information, investigation and material properties on the masonry which belong to vault of the experimental campaign and moreover to analyse and highlight the influence of vault on the global behaviour of the structure considering the in-plane behaviour of the structural element. Due to the wide presence on the Italian building stock (§ 2.4.1) of vaulted structure such aspects are relevant and interesting to deepen. The author wishes a further development also in this field.

Considerations on the non linear static analysis remarks how in the field of existing building is indeed crucial to develop instruments to analysis irregular structures that are the usual case.

In conclusion future comparisons with a pushover carried out with the FEM with both material and geometrical non linearity in order to control capacity curves and in particular the damage pattern with the equivalent frame models may provide interesting conclusion to the methodological analysis of irregular buildings or clusters. Also in the modelling of the structural global behaviour there are still to improve methodologies and tools.

# 5 TEST ON A VAULTED SYSTEM: ARCHES AND TIES

## 5.1 EXPERIMENTAL CAMPAIGN

The refurbishment project of the castle into a museum, which assumes for accessibility purposes the introduction of lift and security stairs, allows to perform a unique experimental campaign on one full scale historical vault. The campaign, aims to understand the behaviour of vaults in both unstrengthened (UR) and strengthened conditions. The chosen strengthening techniques were according to vaults previously tested in the laboratory of the University of Padova [Giradello 2012]. In following paragraphs the setup and the vaults preparation will be illustrated.

*Fig. 5.1 View of the tested vaults inside the castle.*

### 5.1.1 *Setup design*

The unconventional and innovative test onsite on a full scale vault required a dedicated design in terms of setup and procedures. The first requirement that the whole test had to fulfil was to avoid any damages on the existing structure designing a localized destructive test. In order to accomplish this, the necessary forces acting to reach failure were as much as possible limited. The width of the vault was thus defined of 80 cm. Moreover, according also with literature tests presented in previous chapters, the loading was located at the quarter to enhance the mechanism activations and providing an asymmetric load (Fig. 5.2). To limit disturbances on the structure three ties were installed to counteract the development of thrust during the test. The load on the vault was transferred by means of two hydraulic jacks in traction, controlled with electronic servovalves. Each jack was fixed to a cable linked to a counteract steel pipe which was inserted in steel sleeves previously prepared in walls (Fig. 5.3 above). The gained shear action on supports is hence balanced by the reaction force of the steel frame. Therefore the whole setup involves only small portions of existing masonry walls. In addition a further contribution against the thrust was provided by neighbour chambers with continuous vaults.

The use of cables and light steel pipes with joints were necessary to allow the manual movements of components indoor. The design was hence based on resistance criterion instead of stiffness one, usually adopted in laboratory.

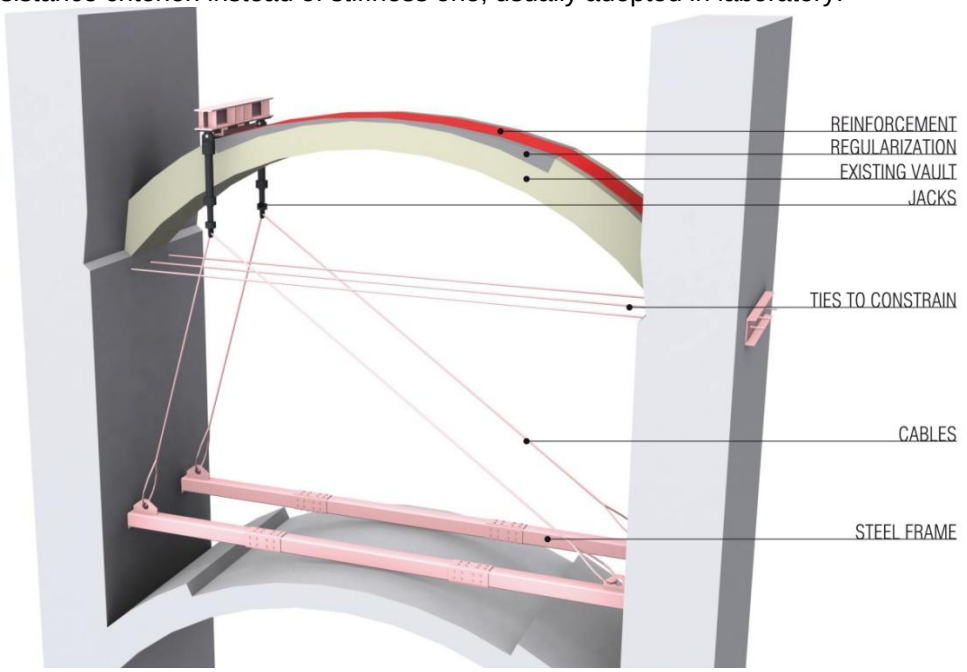


*Fig. 5.2 3D Reconstruction of the applied setup*

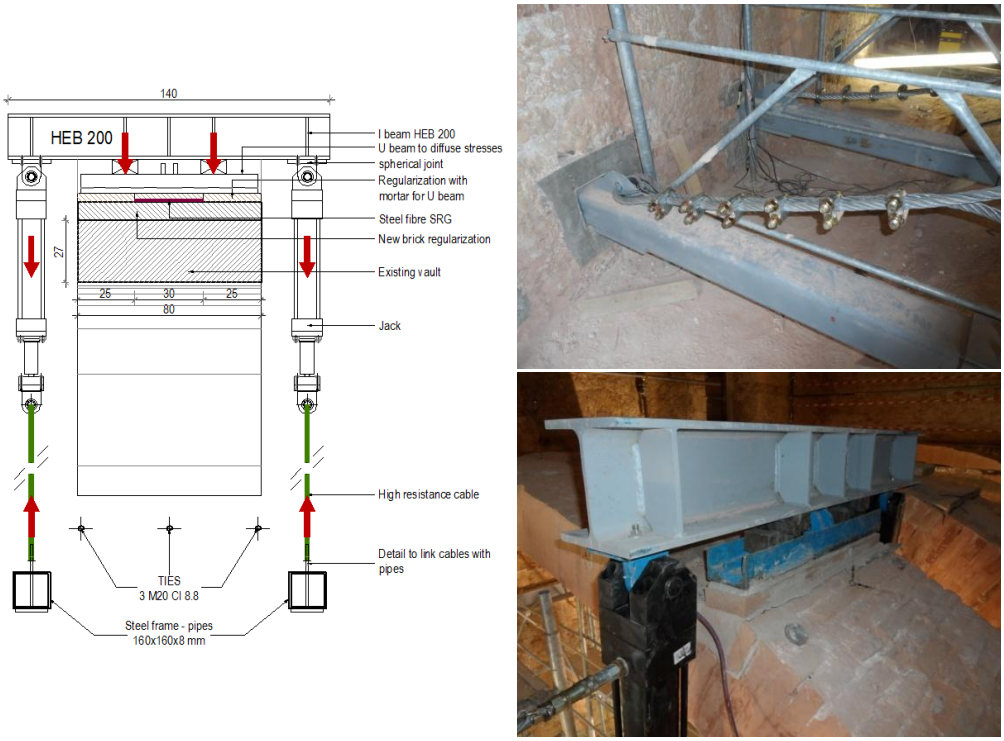


*Fig. 5.3 Drawing of the setup (left) Detail on cable link with steel pipe and wall (above) system of load application (below)*

The spherical hinges on the ends of the jacks were used to provide the axial force application. To ensure the uniform transfer of the load on the whole width of the structure, the force was applied by set of two beams - the I beam (HEB 200), which was placed over the U beam on the stiff separators (Fig. 5.3 right). Hence the load was applied in two point loads on quarters which diffuse on the whole width of the arch regardless the stiffness of I beam. The stiffness of the U beam was designed to uniformly distribute stresses on masonry.

The choice of cables tighten by hand before the test was together to the relevant decision to perform the test in force control instead of displacement control. In fact, the stiffness given by the two sides in case of cables was indeed different and in order to apply a symmetric action to the loading beam a force control was the solution. As a drawback the analysis of deep post peaks is impossible and once the maximum force is reached the realising of the load should be instantaneous to avoid any collapse.

To monitoring as deep as possible the response of the vault during the whole static test a series of sensors were fixed. This disposition was used for all vaults except the ones with diaphragms where there were slight variations.

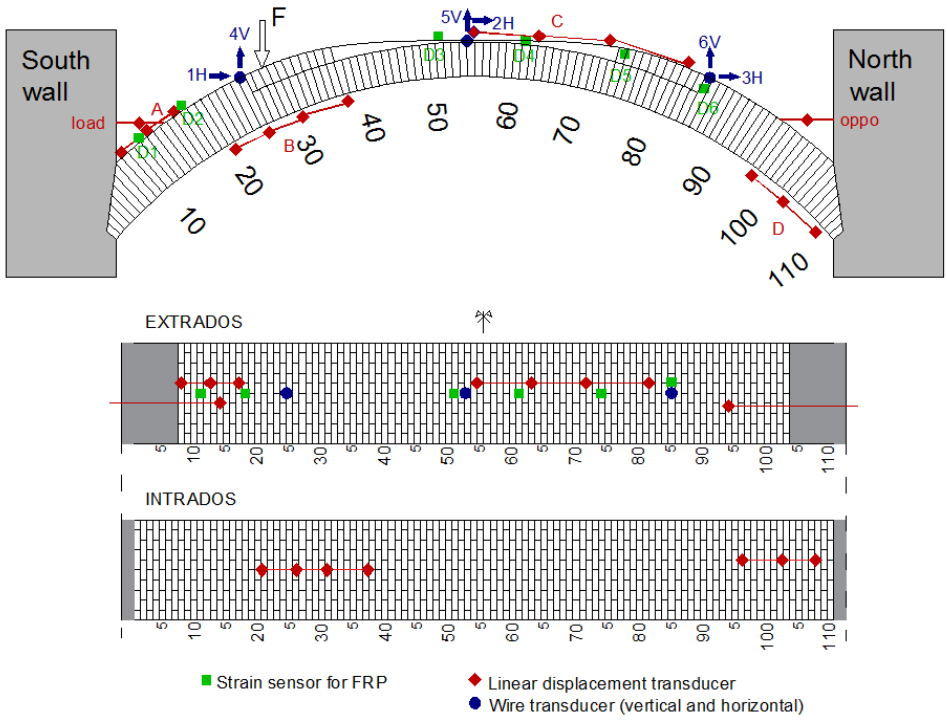


*Fig. 5.4 Sensors positions in tested vaults*

Fig. 5.4 describes the positions of sensors divided in three categories: wire transducers, linear displacement transducers and strain sensors.

Wire transducers (Fig. 5.5 left) aims to control the overall displacement of the vault with an external reference. Three couples were installed, one at the key stone (2H,5V) one at the loading point (1H,4V) and one at the opposite quarter (3H,6V). Vertical transducers were located on a pipe system meanwhile the horizontal ones on walls. In order to record the cracks opening at hinges, in the estimated positions, a series of rigid linear displacement transducers were adopted (Fig. 5.5 centre). The use of multiple sensors allows to eventually recording localized cracks. In case of strengthening, six strain sensors (Fig. 5.5 right), placed in stressed areas, were adopted to record fibres deformations. Those strain gauge sensors have a sensibility of ± 2.5 mV/V with a nominal range of ± 2.5 mm.

*Fig. 5.5 Wire trans. (left), linear displacement trans. (centre), strain sensor (right)*

### 5.1.2 *Vaults preparation*

By a detailed survey the vault results with a circular shape with a span of 5.6 m and with rise of 1.1 m for an angle of 100°. The vault thickness was higher in the support quarters and was equal to 42 cm; while in the middle part was equal to 27 cm. The arches were composed by 110 rows of brick with average dimensions of 55x130x275 mm with a slight decrease of 2 mm in the height to reduce radial bed joints.

In the first phase (Fig. 5.6) the vault was sliced with a circular saw with diamond blade in the central part whereas at the support a manual finishing was necessary (Fig. 5.7). Despite the difficulties in positioning, this cutting method guarantees a very accurate cut. Before the demolition of exceeding portions to work in more safety conditions all the preparation interventions were carried out.

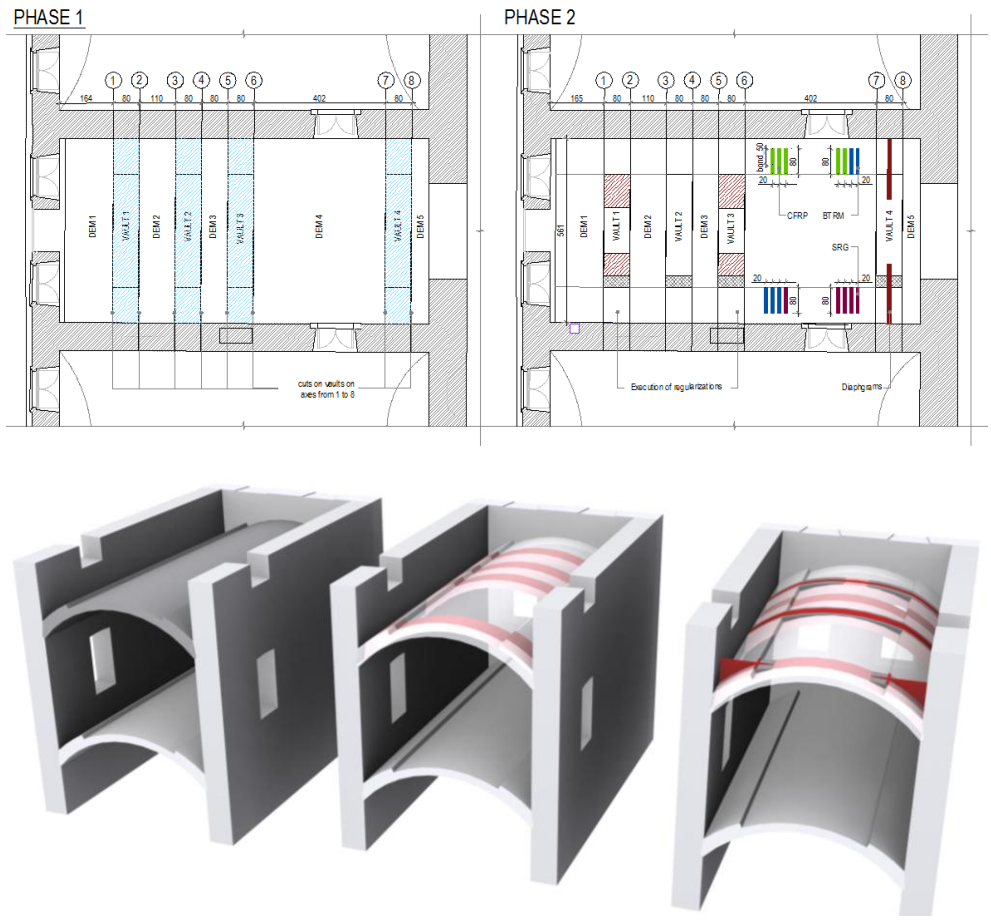


*Fig. 5.6 Phases executed in field*

*Fig. 5.7 Circular saw (left) and manual finishing (right)*

After the definition of vault separation, four portions were available. It has to be considered that typically unreinforced masonry vault fails by the activation of the four hinges mechanism activating rigid blocks. On the other hand it is interesting to understand if the strengthening interventions were also suitable to reinforce vaults already activated as frequently happened after earthquake strokes.

The tests on vaults were hence five, namely:

1. Unreinforced vault (UR) (vault 2-Fig. 5.6)
2. Vault strengthened with a central masonry diaphragms (DIA) (vault 4-Fig. 5.6)
3. Carbon Fibre Reinforced Polymer (CFRP), carbon fibre glued with epoxy resin (vault 1-Fig. 5.6)
4. Steel Reinforced Grout (SRG), steel fibre applied with mortar(vault 3-Fig. 5.6)
5. Basalt Textile Reinforced Mortar (BRTM), basalt net applied in the whole surface with mortar. (vault 2-Fig. 5.6)

The first operation was the surface cleaning with the removal of dust and weak mortar on surface obtaining a facing masonry (Fig. 5.8). It has to be noted how the historical texture present a rough surface in the magnitude of one centimetre. In case of strengthening with inorganic matrix as mortar this does not be problematic instead for CFRP the surface was abraded with diamond disk to obtain a smoother substrate (Fig. 5.8), moreover small gaps where filled with organic filler.

*Fig. 5.8 Cleaning and masonry surface, in red, area cleaned for CFRP application (right)*

*Fig. 5.9 Regularization for vaults strengthened with composites (left) and diaphragms (rigth)*

To apply fibres and avoiding any concave curvature, a regularization made with bricks was created in order to fillet the thicker part with the middle one (Fig. 5.9 left). Diaphragms were created 12 cm thick and at the same level with the load application point hence counteracting the two external quarters. During this phase the metallic sleeves for the steel frame were fixed and the holes for ties were drilled.

After the preparation of the unreinforced (UR) vault and the ones reinforced with the traditional intervention by means of diaphragms (DIA) the other three modern strengthening techniques, based on composites, were selected. In the current state of art, defining just three couples of fibres and matrixes is not an easy task.

The first typology was Carbon fibre applied with epoxy resin because is one of the most investigated and at the same time the most applied [Panizza 2010]. The increasing in using of mortar based systems for externally bonded strengthening of masonry and the possibility to compare the workability of the two systems in filed the selection went to steel fibres and to a distributed reinforcement as the basalt net which on lab behaved in a satisfactory way.

Finally, form a mechanical point of view in terms of stiffness and ultimate strain the three cover a wide range of properties. This is relevant in order to assess the influence, advantages and drawbacks of each system. The three type of fibres used are reported in Fig. 5.10.

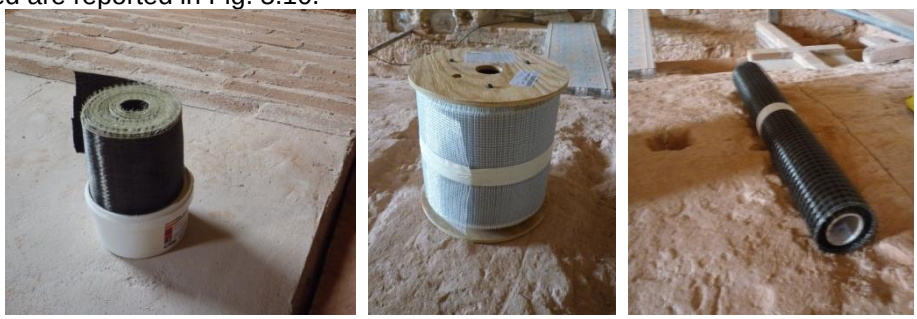

*Fig. 5.10 Fibres used, from the left: Carbon, Steel, Basalt net*

In order to properly install fibres a minimum width of 100 mm was accounted and thus CFRP was limited to this value. SRG was designed in order to be similar in terms of ultimate force ($E_f \cdot \varepsilon_{fu}$) and, due to the equal strain, also the same reinforced stiffness calculated as ($A_f \cdot E_f$) was reached for both. The same approach could not be applied with Basalt due to its lower resistance and stiffness value. According to Garmendia [2015] and to Giradello [2012], basalt was considered as a distributed reinforcement which has to involve the entire vault width.

The distribution of tapes in the width was design according CNR [DT 200] with equation (5.1). Due to the high ratio between thickness and width of the vault the formulation allows to use just one central tape that was adopted for both CFRP and SRG application. The final properties and geometrical features chosen are reported in Tab. 5.1.

$$p_f = 5 \cdot t + b_f \tag{5.1}$$

*Tab. 5.1 Composites properties from datasheet and adopted dimesions*

| | $t_f$ mm | $b_f$ mm | $E_f$ MPa | $\varepsilon_{fu}$ [%] | $F_u$ kN | $E_f A_f$ [$10^{-6}$] |
|---|---|---|---|---|---|---|
| **CFRP** | 0.170 | 100 | 240'000 | 1.50% | 61.20 | 4.08 |
| **SRG** | 0.084 | 250* | 190'000 | 1.50% | 59.85 | 3.99 |
| **BTRM** | 0.032 | 800 | 70'000 | 1.90% | 34.05 | 1.79 |

* the width correspond to 40 micro cords

Fibres have been applied according ACI provisions of [440-02R-8] about FRP material. After the abrasive operations, dust was carful removed before the application of primer uniformly distributed on the prepared surface (Fig. 5.11 left). The primer was cured for the time suggested by the manufacturer. After this a wet layup system was used firstly applying the resin and then the dry carbon fibres gently pressed by a rib roller into the uncured saturating resin (Fig. 5.11).

*Fig. 5.11 Primer application (left), fibre installation on matrix (centre, right)*

At the same moment an area of 300x1000 mm was prepared for pull-off tests and five strips 5 cm width and 80 cm long for shear test.

The application of SRG and BTRM was easier than CFRP from an executive point of view. After the surface preparation, which was not smoothed with circular saw as for CFRP, the vault was cleaned from dust and wetted with water to avoid water absorption from the mortar by the bricks substrate. Steel fibre and net were embedded with cement trowels into the mortar early laid out (Fig. 5.12 and Fig. 5.13). Once this operation was concluded an additional layer of mortar was spread to regularize and finish the surface. During the first hours of curing the surface was slightly wetted by means of nebulizer.

*Fig. 5.12 SRG installation, from the left: wetting, first layer and fibres inclusion*

*Fig. 5.13 Application of Basalt textile reinforcement with mortar*

The anchorage system on wall was different for each material but the anchorage length of 350 mm was guaranteed for all systems. Panizza [2015] pointed out an empiric linear law for the resistance of SRG anchorage with an ultimate axial force of 0.1 kN/mm. In this case two anchorages with this length allowed to reach the ultimate resistance of the fibre. For Carbon two tapes were inserted into a hole drilled with an external part of 300 mm overlapped with the fibre (Fig. 5.14) to avoid any debond between the two.

At the ends, the steel fibre was simply divided in parts and inserted into holes keeping the continuity with the external tape as shown in Fig. 5.12.

*Fig. 5.14 Details of the CFRP anchorage*

*Fig. 5.15 Details of the continuous anchorage of SRG fibre*

*Fig. 5.16 Steel anchorage for the Basalt net and injection of mortar based composites*

Holes were after injected with a lime based grout. The same steel anchorage was also applied in the Basalt vault because this material is not enough rigid to reach the hole end without developing a good adhesion with the injected grout.

In conclusion the use of mortar-based matrixes instead of resins gives more advantages in terms of workability like:

- mixing components, epoxy requires much care and skills in preparation;
- safety equipments, epoxy requires a special safety equipment with the respect of normal masons operations;

- primer or putty, to develop a good adhesion the organic reinforcement need the application of a primer;
- surface preparation, the application of carbon require a very smooth surface, easy to find in concrete applications. Masonry applications require a carefully smoothing operation.

## 5.2 PRELIMINARY CHARACTERIZATION

The following paragraph illustrates all preliminary tests carried out on-site and on laboratory to characterize some mechanical values. The tests carried out are related to both existing and new materials and also to their interaction.

The particular case of an existing vault not reconstructed in lab on one hand allows to test a real structure with actual historical materials, on the other hand does not allows a rigorous material characterizations of materials and structural elements (compressive tests of pillars, sliding test). To overcome this problem the same approach to an existing structure, with the use of NDT e MDT tests, was adopted.

All the materials, introduced for the strengthening intervention, were tested whereas only bricks were tested for the historical masonry because of the difficulties in mechanical on site testing of existing mortar. The overall behaviour has been detected by means of the double flat jacks carried out on the brick masonry wall of the castle. (see § 4.2.4). The connection between strengthening and the substrate were also performed.

### 5.2.1 *Bricks*

The tests on bricks were performed on new bricks (NB) and historical bricks (HB) gathered on site from the removed parts of the vault.

*Fig. 5.17 Specimens of new bricks (NB) (left), and historical bricks (HB) (right)*

With one brick three parameters where tested, compressive strength, flexural tensile strength and splitting tension.

The geometrical features of the historical bricks are less standardized than the new ones. The historical brick has an average dimension of 137x275 mm with a variation of ± 5 mm. The thickness is of 50 mm tapered for 2-3 mm on one side to improve the stereotomy in the vaults and reducing the bed joints dimension. The new brick has small variation in geometry due to the industrial technologies and it has a parallelepiped shape of 50x120x250 mm.

**TENSILE STRENGTH**

The tensile strength was tested according EN 771-1:2011 with a three bending test as shown in Fig. 5.18.

*Fig. 5.18 Three points test for the flexural tensile strenght after (L) and before the test (R)*

The formulation used for the flexural tensile strength is following and based on the measured $P_u$ which is the acting load.

$$f_{f,b} = \frac{3 \cdot P_u \cdot l_s}{2 \cdot b \cdot h^2} \tag{5.2}$$

where $l_s$ is the span between the two lower supports, $b$ and $h$ are respectively the width and the height of the brick height. The failure modes, with the exception of three specimens were normal to the brick surface.

The splitting test is according to EN 771-1:2011 and use an indirect measure of tensile strength. For a punctual line load the equation is eq. (5.3).

$$f_{s,b} = \frac{2 \cdot P_u}{\pi \cdot b \cdot h} \tag{5.3}$$

As is possible to notice from Fig. 5.19 the failure are according to the theoretical plan of failure. This happened for all the specimens.

*Fig. 5.19 Splitting test, the testing machine (left) and the brick failure (right)*

From the splitting failure it is clear, as shown in Fig. 5.20, how historic bricks are variable in the material due to variability in firing operations on kilns and in clay composition.

*Fig. 5.20 Differences among historical bricks*

The results of those tests are shown in Fig. 5.21 and summarized in Tab. 5.2.

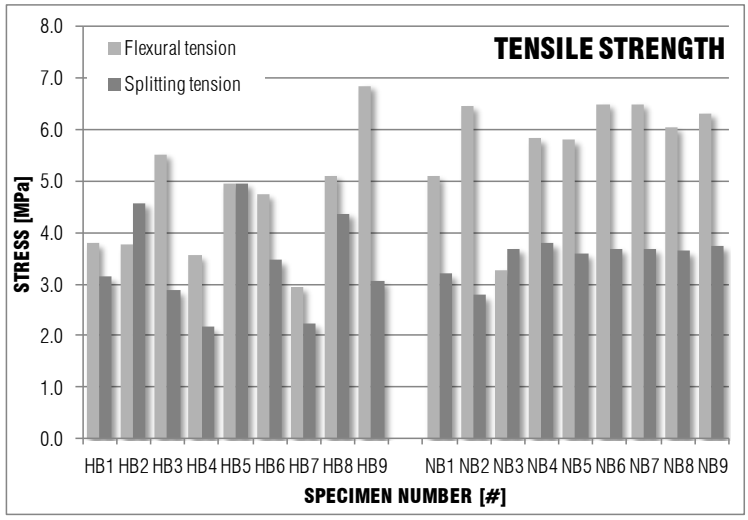


*Fig. 5.21 Tensile strength of brick with the two test methods*

**COMPRESSIVE STRENGTH**

The compressive strength is according to EN 772-1:2011.

$$f_{c,b} = \frac{P_u}{b \cdot l} \tag{5.4}$$

The observed failure with the typical double pyramid was observed in all the specimens. Results are shown in Fig. 5.22 and reported in Tab. 5.2.

*Fig. 5.22 Compressive test, the testing machine (left) and the typical brick failure (right)*

From Tab. 5.2 and form the histograms is possible to notice how the new elements chosen have mechanical characteristics similar to the existing bricks highlighting a good compatibility between the two. Flexural tension is in general higher than the splitting one. The first is approximately one fourth of the compressive values whereas the splitting is about the 15 % of $f_{c,b}$.

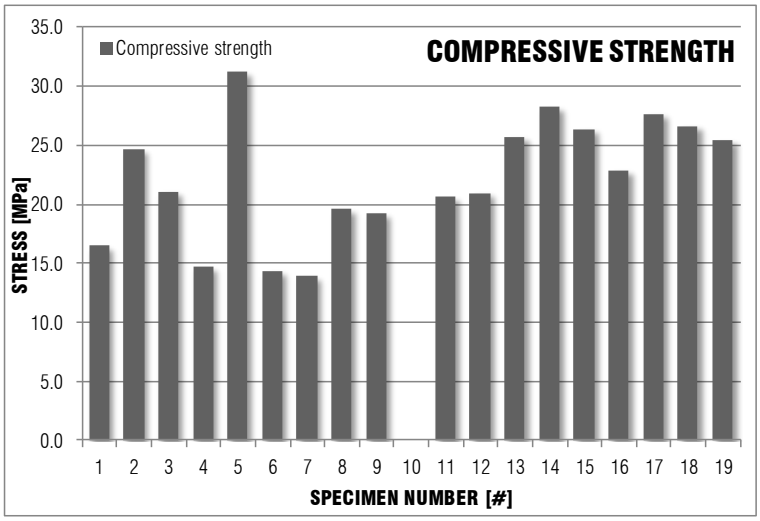


*Fig. 5.23 Compressive strength of specimens*

*Tab. 5.2 Tensile and Compressive resistance of bricks*

| | id | Tension Flexural [MPa] | Tension Splitting [MPa] | Compr. [MPa] | | id | Tension Flexural [MPa] | Tension Splitting [MPa] | Compr. [MPa] |
|---|---|---|---|---|---|---|---|---|---|
| Hisorical brick | HB1 | 3.80 | 3.15 | 16.46 | New brick | NB1 | 5.10 | 3.20 | 20.62 |
| | HB2* | 3.78 | 4.58 | 24.67 | | NB2 | 6.46 | 2.79 | 20.97 |
| | HB3 | 5.53 | 2.88 | 21.08 | | NB3* | 3.29 | 3.70 | 25.72 |
| | HB4 | 3.57 | 2.17 | 14.71 | | NB4 | 5.83 | 3.80 | 28.26 |
| | HB5 | 4.96 | 4.96 | 31.23 | | NB5 | 5.80 | 3.60 | 26.38 |
| | HB6 | 4.75 | 3.47 | 14.36 | | NB6 | 6.50 | 3.70 | 22.90 |
| | HB7* | 2.96 | 2.25 | 13.91 | | NB7 | 6.50 | 3.70 | 27.65 |
| | HB8 | 5.11 | 4.38 | 19.58 | | NB8 | 6.04 | 3.64 | 26.66 |
| | HB9 | 6.86 | 3.07 | 19.24 | | NB9 | 6.32 | 3.74 | 25.44 |
| | **AVG** | **4.59** | **3.43** | **19.47** | | **AVG** | **5.76** | **3.54** | **24.95** |
| | **CoV** | **26.1%** | **29.2%** | **29.1%** | | **CoV** | **17.9%** | **9.4%** | **11.2%** |

* specimens with a too inclined failure in the three point test

### 5.2.2 *Mortar*


*Fig. 5.24 Flexural testing of mortar prism (left), compressive test (centre) typical failure (right)*

The tests on mortar specimens were performed on prisms sampling with dimensions of 16x4x4 cm according to UNI EN 998:2010. The prisms were poured on site and cured for 30 days. For each specimen two measures of compressive stress and one of flexural strength were carried out (Fig. 5.24). All tests present the correct failure mode. Due to this type of test was not possible to have measures of the historical mortar. The results are reported in Tab. 5.3 and present good properties of the used mortar with an average compression strength of 16.4 MPa and a limited variation. This type of mortar was used to bond bricks in new masonry

element (i.e. regularization or diaphragm) and also as inorganic matrix for the FRCM (i.e. SRG, BTRM).

*Tab. 5.3 Mechanical characteristics of mortar*

| | $f_{t,mor}$ [MPa] | $f_{c,mor}$ [MPa] | |
|---|---|---|---|
| M01 | 1.93 | 17.17 | 15.63 |
| M02 | 2.02 | 16.68 | 16.25 |
| M03 | 1.90 | 16.00 | 16.86 |
| M04 | 1.81 | 16.49 | 16.49 |
| M05 | 1.81 | 16.92 | 16.37 |
| M06 | 1.76 | 16.06 | 16.25 |
| **AVG** | **1.87** | **16.43** | |
| **CoV** | **5.0%** | **2.6%** | |

### 5.2.3 *FRP*

The mechanical characterization of fibres was carried out by means of traction tests controlling the stress-strain behaviour of the specimens. In table Tab. 5.4 the results are reported comparing the characteristic provided in the manufactory's data sheet and those performed on laboratory. At least three specimens for each fibre have been tested.

The steel fibre shows a good agreement with properties reported in the datasheet with also a limited dispersion. Results also agree with tests performed on single micro cords [Girardello 2012]. The ultimate strength of Carbon reported in the datasheet clashes with the other two data and its calculation ($E_f$ times $\varepsilon_{fu}$) gives 3600 MPa. The so calculated value is close to the tested one instead the modulus and the ultimate strain are respectively higher and lower than expected with also a higher dispersion.

The Basalt strength by datasheet is almost one half of Carbon and after the laboratory tests the obtained value is about the 60% of the expected one. This might be slightly due to the specimen width (5 cm) too large to provide a uniform tension distribution, but mainly it shows of an overestimation in the datasheet of the ultimate strain. In all the laboratory test carried out the first fibre failed was the instrumented one and therefore this ensures the reliability of ultimate strain measurement which is 1.55%. Finally the indirect calculation of ultimate strength and elastic modulus, which agrees with the datasheet, differs by only the 1 % to the measured one. The measurements present also a reduced scatter.

*Tab. 5.4 Mechanical characteristic of FRP*

| | | $E_f$ [MPa] | $\sigma_{f,u}$ [MPa] | $\varepsilon_{f,u}$ [%] |
|---|---|---|---|---|
| Carbon | Data sheet | 240'000 | 4800* | 1.50% |
| | Tests AVG | 309'004 | 3500 | 1.21% |
| | Tests CoV | 42.8% | 17.9% | 11.5% |
| Steel | Data sheet | 190'000 | 2800 | 1.50% |
| | Tests AVG | 196'886 | 2989 | 1.72% |
| | Tests CoV | 1.5% | 6.6% | 11.1% |
| Basalt | Data sheet | 70'000 | 1700 | 1.90% |
| | Tests AVG | 66'680 | 1002 | 1.55% |
| | Tests CoV | 1.5% | 2.5% | 1.2% |

* inconsistent value, $E_f \cdot \varepsilon_f = 3600$ MPa

### 5.2.4 *On site pull off*

As reported in literature review the first test used to characterize the bond between the applied strengthening and the substrate is the pull-off according to [ASTM C1583], the test is also suggested by the Italian technical document [CNR DT-200] to check the execution of the intervention.

*Fig. 5.25 Preparation of specimens and cleaning (left-centre), test execution (right)*

The specimen preparation was carried out cutting the reinforcement and the substrate with a circular shape for CFRP and BTRM and after the dust removal the steel disk for the test was applied. In the case of steel fibre, due to their cutting resistance and to the micro cords disposition, the rotating saw could snag on it and thus, it was necessary to create an octagonal shape with a different saw (Fig. 5.28). A number of 12 tests were carried on for all the three types of strengthening and results are listed in Tab. 5.5.

*Tab. 5.5 Pull-off tensile strenght and failure mode for each fibre*

| ID | CFRP | | | SRG | | | BTRM | | |
|---|---|---|---|---|---|---|---|---|---|
| | Load [kN] | $f_{t,\,pull}$ [N/mm$^2$] | Fail. | Load [kN] | $f_{t,\,pull}$ [N/mm$^2$] | Fail. | Load [kN] | $f_{t,\,pull}$ [N/mm$^2$] | Fail. |
| P1 | 2.08 | 0.84 | A | 0.52 | 0.20 | B* | 1.64 | 0.67 | A* |
| P2 | 2.78 | 1.13 | A | 0.28 | 0.11 | B | 0.53 | 0.21 | A* |
| P3 | 2.60 | 1.06 | A | 0.69 | 0.27 | B | 1.29 | 0.52 | A/B |
| P4 | 1.44 | 0.59 | A* | 2.51 | 0.97 | B | 0.66 | 0.27 | A* |
| P5 | 2.84 | 1.15 | A | 2.16 | 0.83 | B | 0.58 | 0.24 | B |
| P6 | 1.11 | 0.45 | A* | 0.99 | 0.38 | B | 0.42 | 0.17 | B |
| P7 | 0.65 | 0.27 | A* | 2.46 | 0.95 | B | 0.78 | 0.32 | A |
| P8 | 3.71 | 1.51 | A | 0.22 | 0.08 | A* | 0.69 | 0.28 | A |
| P9 | 2.51 | 1.02 | A | 1.71 | 0.66 | B | 1.15 | 0.47 | A |
| P10 | 0.93 | 0.38 | A* | 1.93 | 0.74 | B | 0.71 | 0.29 | A |
| P11 | 3.79 | 1.54 | A | 0.31 | 0.12 | A* | 0.55 | 0.22 | B |
| P12 | 2.84 | 1.15 | A | 0.10 | 0.04 | A* | 1.19 | 0.48 | A* |
| **AVG** | **2.27** | **0.92** | | **1.16** | **0.44** | | **0.85** | **0.34** | |
| **CoV** | **46%** | **46%** | | **81%** | **81%** | | **45%** | **45%** | |

*test with larger area of joints fraction than block surface

From the columns of failure modes, also graphed in percentage terms in Fig. 5.26 (left) is possible to highlight the agreement with existing literature with all the epoxy bonded disks failed in the substrate. For the inorganic mortar the failure is different between the two fibres with a good percentage of failure A for BTRM (67%) instead for SRG the same percentage of tests (67%) failed in the interface between the two. Either failures C and D were not observed in the whole campaign that means a good permeation between matrix and fibre.

About the numerical figures, the lower values of CRFP are related to the cases in which the area friction was significantly involved by historical mortar with coherent lower tensile strength. The average value of CFRP test gives 0.92 MPa with a very scattered interval. About BTRM although the failure majority is A, the average value is lower because affected by B types. In fact, as long as the A failure reaches the highest values shown for carbon the interface become the weakest level and thus it fails before. SRG failures are more concentrated on failure B and even if it was expected from previous experiences the percentage is relevant compared with the basalt that has the same matrix. A possible reason could concerns the disturbance in sawing the material or the greater stiffness of the steel reinforcement that does not allow stress distribution.

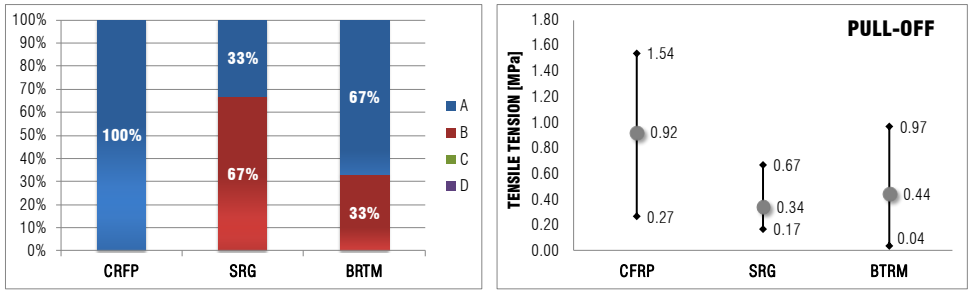


*Fig. 5.26 Percentage distribution of failure modes (left) of pull-off strenght interval (right)*

The CNR [DT-200] standard defines a minimum value of the tensile strength for the 80% of tests to accept the intervention. The value is the 10% of the substrate compressive strength. Considering the substrate as sole brick the limit is not reached by any test. It has to be taken into account, looking at Fig. 5.27 (left), that the test was performed on existing masonry with bed joints hence decreasing the guessed parameter although is clear that A failure was reached (right). This limitation might be more reliable if the tensile strength is measured, for example, using the test directly on the substrate, instead of using a guessed parameter.

*Fig. 5.27 Pull-off failures of CFRP*

Fig. 5.28 on the left shows the typical failure A which in field cases can involved relevant portion of mortar, on the right side of the figure, it is possible to see a B failure (specimens 10) that occurs directly on the cleaned surface of the brick.

*Fig. 5.28 Pull-off tests on SRG with A failure (left) and B failure (right)*

From the pull-off testing is possible to conclude that the organic matrix application always reaches the tensile strength on the substrate showing a good bond of the strengthening system instead in the application of inorganic matrix there are a significant number of failures within the interface.

This result does not mean a limited effectiveness of FRCM because it is expected that mortar (see Tab. 5.2 & Tab. 5.3) is the weakest link of the chain whereas the miss of failures between fibre and matrix represents a good fibre application. Finally the use of this test for checking quality execution needs a different application for FRCM.

### 5.2.5 *On site shear test*

Similarly to other mechanical characterizations, the analysis of bond behaviour on shear actions in the plane of the reinforcement was carried out onsite. The set-up adopted was based on proposal of the Italian standard and presented in literature review. In real application three problems raised. The masonry surface, especially in historical construction is quite rough with steps of about 1 cm, this provokes a more irregular application of the fibre and a load application less straight than the laboratory one. This is more problematic with fragile composites in the orthogonal direction (i.e. CFRP). The second problem was related to the test direction. Due to the mortar influence on the overall behaviour it was necessary to test the fibre orthogonal to bed joints. To overcome this problem the step given by the vault, which increases in thickness near supports, was used to counteract the jack traction force. Finally due to logistic reasons and time of execution a limited number of tests were carried out. To each application 5 shear tests was performed with one sheet of fibre 5 cm width.

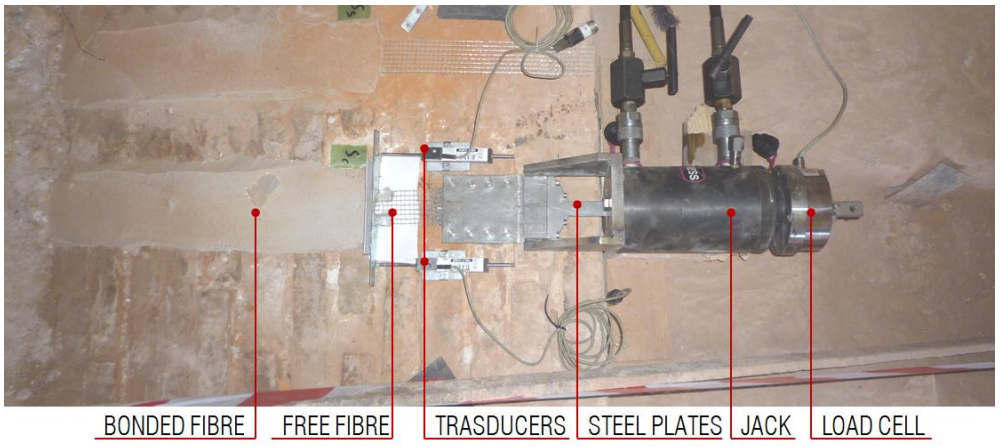


*Fig. 5.29 Set-up adopted onsite to test the in plane behaviour*

The possible variability in field testing, the greater errors commonly achieved on site, suggest choosing only one bond length of 300 mm. The fibre was applied longer and then precisely cut before the test. In addition to the normal applications in literature, also the displacement of the fibre at the loaded end was recorded by means of two linear position sensors located at the same distance to the fibre. Due to the manual control on jack the test was on force control. The set-up is shown in Fig. 5.29.

Fig. 5.30 (left) presents a typical curve recorded with also the calculated average displacement. Looking at the graph that summarises all tests (Fig. 5.30 Load displacement result of one test (left) all test on steel fibre (right)Fig. 5.30 right) on steel (continuous line) and basalt fibres (dashed line), the response curve demonstrate a good bond behaviour for the investigated length providing the rupture of fibres in all tests.

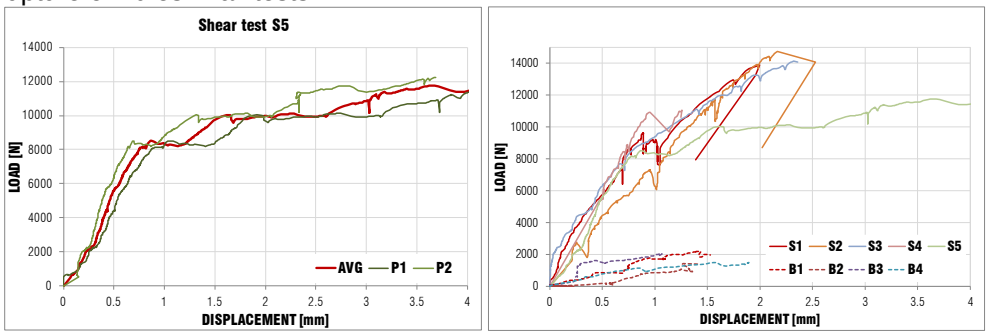


*Fig. 5.30 Load displacement result of one test (left) all test on steel fibre (right)*

The application of this test onsite, as presented in the Italian Standard [CNR DT-200] aims to check the quality of fibre application and the calculated bond length. Concerning these two aspects is possible to overcome that the prepared samples completely fulfil the requirements showing always the reinforcement rupture. Instead, compared with some literature results [de Felice 2014] the obtained curves present different behaviour, for instance SRG tests presented higher ultimate displacements whereas BRTM reached lower values of $\delta_u$ (Fig. 5.30 right). In SRG tests some frictional problems occurred in S2-S3-S4 thus reaching ultimate force slightly higher (10 %) than the maximum fibre strength reached in laboratory tests. The tensile strength showed by BRTM is according the test performed on lab.

Carbon, as for the lab applications, confirms its sensitivity to perpendicular actions. The onsite resin application to impregnate the free fibre did not perfectly meet the matrix used to bond the composite on the substrate thus creating a weak point near the loading point that lead to premature failure. For this reason, even if

the observed failures were in the fibres the results are not reliable and thus herein discarded.

*Tab. 5.6 Shear ultimate load and displacement of the test performed on steel fibre*

| SRG | | | | BTRM | | | |
|---|---|---|---|---|---|---|---|
| ID | Load [kN] | $\delta_u$ [N/mm²] | Fail. | ID | Load [kN] | $\delta_u$ [N/mm²] | Fail. |
| S1 | 13.88 | 2.00 | fibre | B1 | 2.21 | 1.43 | fibre |
| S2 | 14.72 | 2.53 | fibre | B2 | 1.42 | 1.27 | fibre |
| S3 | 14.13 | 2.40 | fibre | B3 | 2.06 | 1.06 | fibre |
| S4 | 11.05 | 1.34 | fibre | B4 | 1.45 | 1.90 | fibre |
| S5 | 12.24 | 5.54 | fibre | B5 | 1.39 | - | fibre |

After the test it was interesting, for SRG, to notice how the cracks occurred in the matrix involved very limited portions of bond length in the range between 5 and 10 cm. Unfortunately it was not possible to have strain measurements at different lengths.

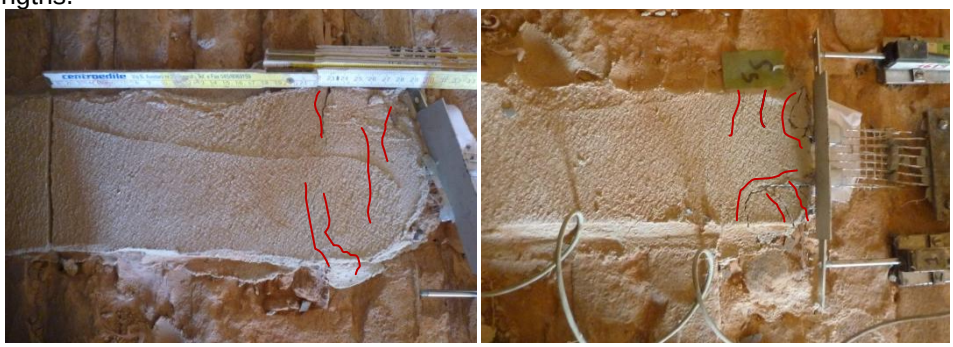

*Fig. 5.31 Cracks spreading in shear test on two specimens*

## 5.3 TEST RESULTS

In this paragraph are illustrated the results of the destructive test on full scale masonry vaults presented in this chapter. The test, carried on in force control, was cyclic with load steps of 2.5 kN each jack, moreover the measured weight of the setup portion above load cells was added to the overall load applied (3.51 kN). The load was applied in a fixed time, and in order to limit the test speed, beyond the tenth cycle the application was carried out in two steps, one reaching the load applied two cycle before and one for the last two steps (Fig. 5.32). The end of the

test was manually controlled looking at the vault displacement recognising a plateau phase or post peak behaviour more easy to reach in case of multiple cycles. The sudden release of the load in case of post peak allows to the vault to return, thanks to its selfweight on the initial equilibrium.

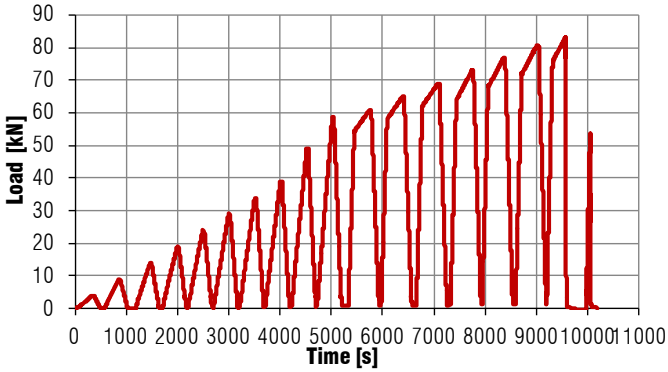


*Fig. 5.32 Diagram of loading history for SRG vault*

In this terms the graphs, later presented with the load displacement curve, have a completely different meaning than those presented in the chapter of material characterization because are describing the element behaviour. Due to the unique character of the test, and in particular of the loading set-up, was impossible to check the appearance of new cracks constantly due to safety reason. Vaults were approachable only with paused load.

### 5.3.1 *01-UR_ UNREINFORCED VAULT*

*Fig. 5.33 Unreinforced vault at moment of maximum load application*

The first test was performed on the reference vault without reinforcement. As expected the obtained failure was the activation of the four hinges mechanism (Fig. 5.33) that is also clearly visible from the damage pattern (Fig. 5.34).

Hinges B-C-D appeared in the mortar joints between bricks without damage on unit. The first crack appears in hinge A and was located on the extrados of the vault next to the wall on the side of loading point. The opening of this crack could be

enhanced by weak connection between the upper parts of the vault section and the load bearing wall. The next cracks appeared on the intrados in the surrounding of the load application point (B) – between bricks 28/29 and 31/32. The following crack was located on the opposite side than the loading point, on the intrados and it had diagonal path which started between bricks 100/101 on the one side and followed to the bricks 103/104 on the other. The last cracks to appear were located on the extrados next to the middle position between hinges B and C, between bricks 61/62 and 62/63.

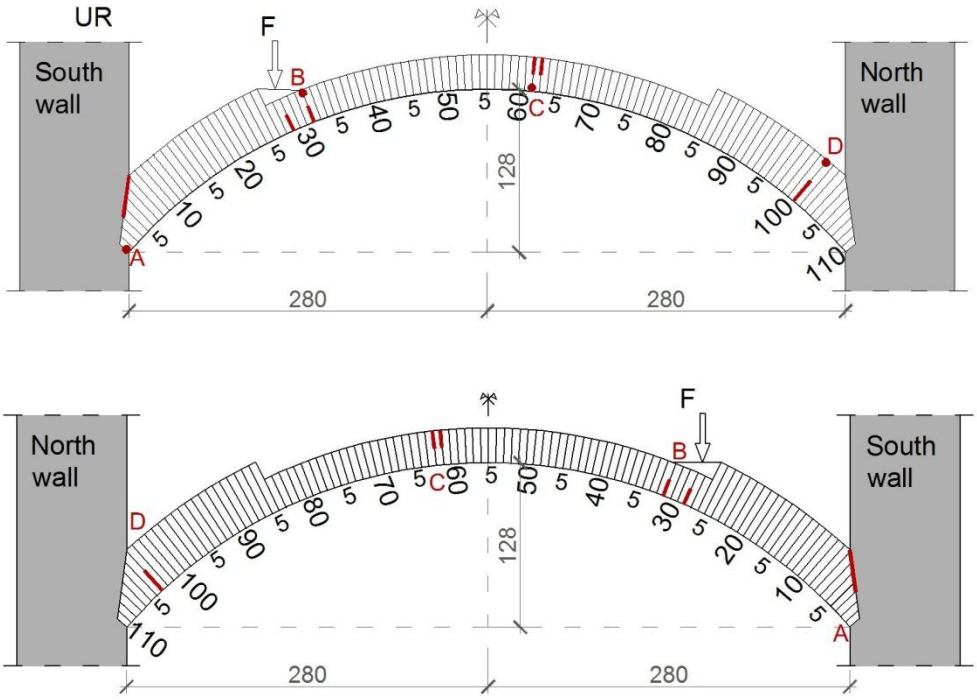


*Fig. 5.34 Crack pattern of the two frontal view of the UR vault*

*Fig. 5.35 Cracks in the Intrados hinges, B on the left and D on the right*

It is interesting to notice how hinge B that open under the loading application point involved the mortar detachment whereas the hinges D does not follow brick

courses because a stone moves up the thrust line and causes a movement of the hinge position (Fig. 5.35). This remarks the importance of geometry and stereotomy in the actual position of hinges and the vault behaviour in the depth.

The wall has two stringcourses in correspondence of the vault support; the first brick stringcourse involves the entire thickness of the wall and with a precise shape of bricks connects vaults of both sides with it (Fig. 5.36). Above this is present a stone stringcourse that is not connected with the third level of bricks used to increase the thickness of the vaults at springing. This highlights how the connection and the stereotomy among elements is relevant in masonry constructions.

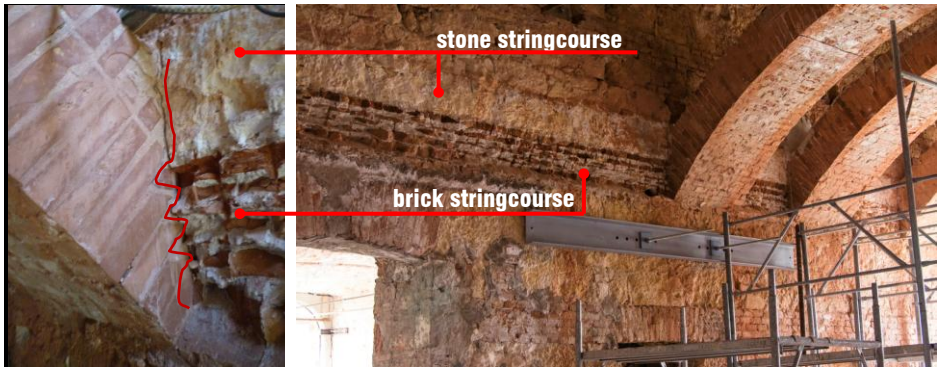


*Fig. 5.36 Detail of the stereotomy in supports*

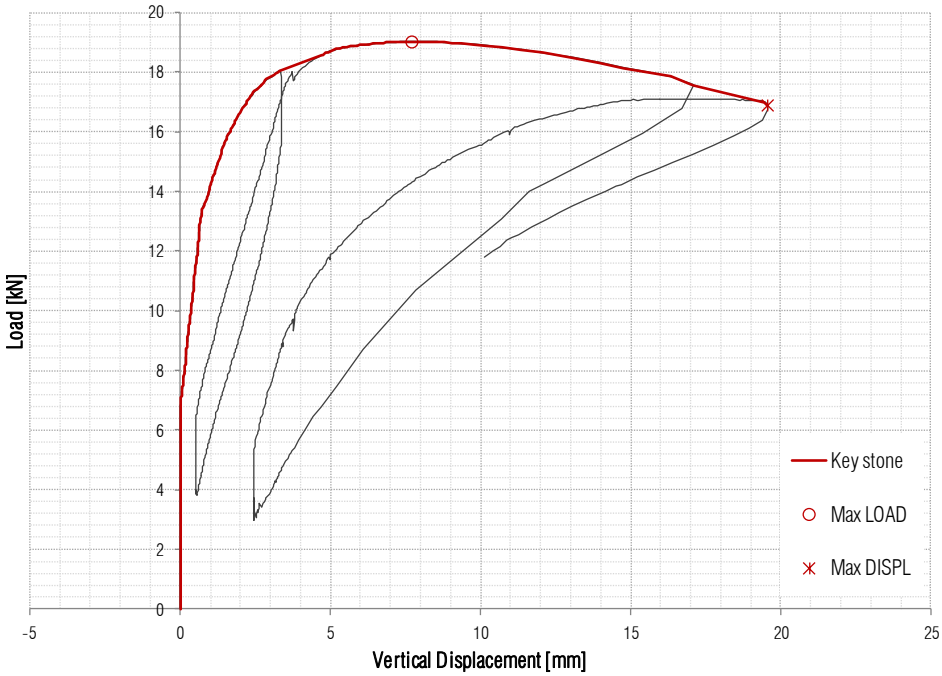


*Fig. 5.37 Load displacement cyclic and envelope curve of the key stone in vertical direction*

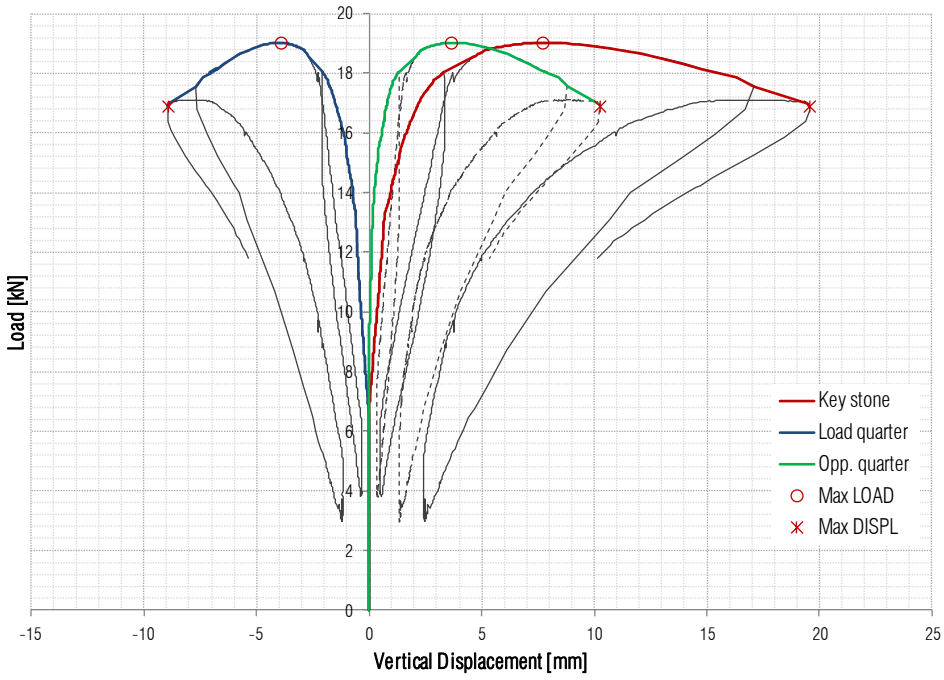


*Fig. 5.38 Load displacement curve of the measured points in vertical direction*

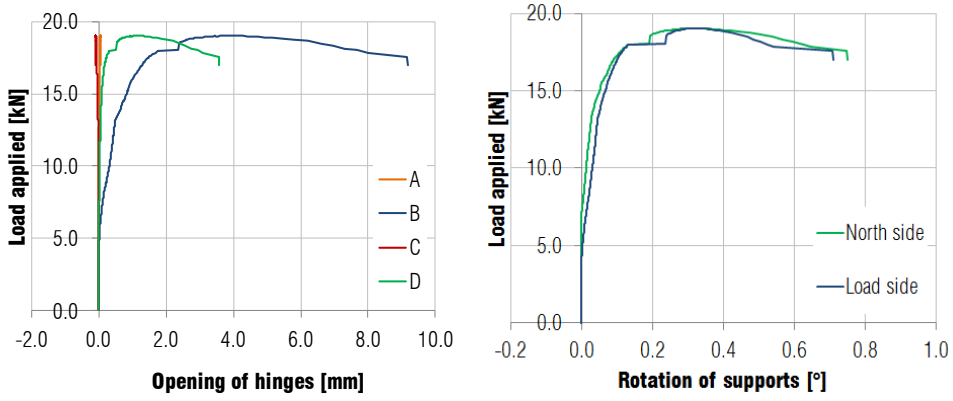


*Fig. 5.39 Hinges behaviour (left) and rotation of supports (right)*

Fig. 5.37 and Fig. 5.38 summarise the behaviour of the arch. Curves show, as expected, a first branch of loading with limited displacement (3 mm after 18 kN) while after the mechanism activation, that occurs at the maximum load 19.04 kN follows a post peak that requires lower load to develop displacements. The graph highlights also the mechanisms with keystone and north quarter which lifted. The displacement at the maximum load is limited to 7.69 mm in the keystone. All the data of force and displacement are reported in Tab. 5.8 and information on the hinges opening in Tab. 5.9. In conclusion Fig. 5.39 shows the magnitude of the hinges opening which, in particular under the load is significant. In case of C the

sensors had some problems in measurement instead the opening of hinges A is very difficult to measure with sensors on the vault (also in the other cases), an indirect measure of it is given by the rotation of supports in graph on the right. Hinges on supports shows a symmetrical behaviour.

### 5.3.2 *02-DIA_STRENGTHENED WITH DIAPHRAGMS*

*Fig. 5.40 Vault with diaphragms prior to collapse*

The vault strengthened with diaphragm walls presented much stiffer behaviour than the unreinforced one but less than composite reinforcements. In terms of failure mode this vault behaved as the UR with mechanism activation (Fig. 5.40). The stiffness of diaphragm in compression stuck the involved quarter moving the hinges position and this is also clear in Fig. 5.43 (green line) that demonstrate an almost fixed position of the northern quarter. Also Fig. 5.44 shows a very limited rotation of the portion near the support with the diaphragm.

The hinges position and their shorten span significantly increase the bearing load, and led to an almost simultaneous opening of hinges. The mechanism became more resistant but also more fragile, stressing the geometrical dependence of the ultimate load. The cracks were located (Fig. 5.41):on the support on the load side (A), starting from the extrados; on the intrados, under the point of force application (B), between bricks 31/32; on the extrados, close to the middle of the span between bricks 57/58 (C); and on the intrados between bricks 82/83(D). It is worth noticing, that due to the diaphragm walls, the location of hinges development, which usually appears next to the support on the side opposite to the force application, moved closer to the middle of the span, comparing to the unreinforced vault.

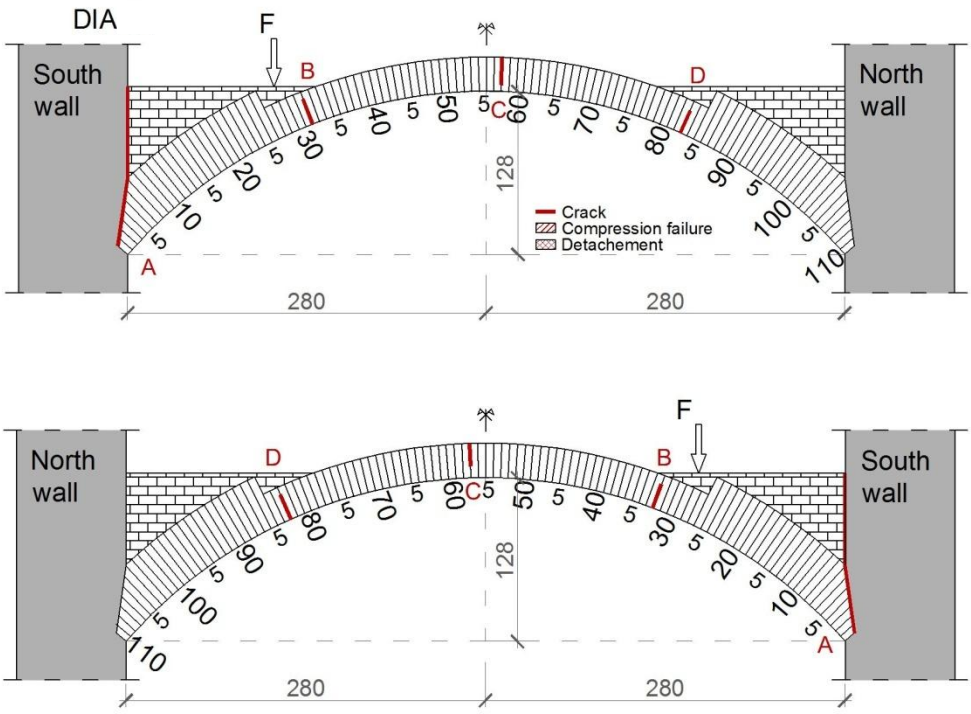


*Fig. 5.41 Crack pattern of the two frontal view of the DIA vault*

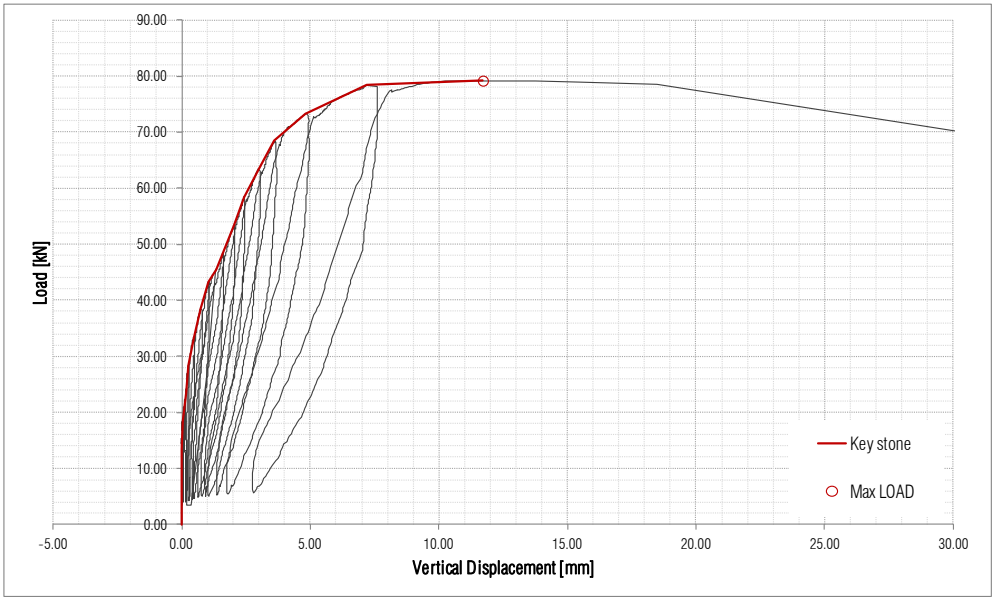


*Fig. 5.42 Load displacement cyclic and envelope curve of the key stone in vertical direction*

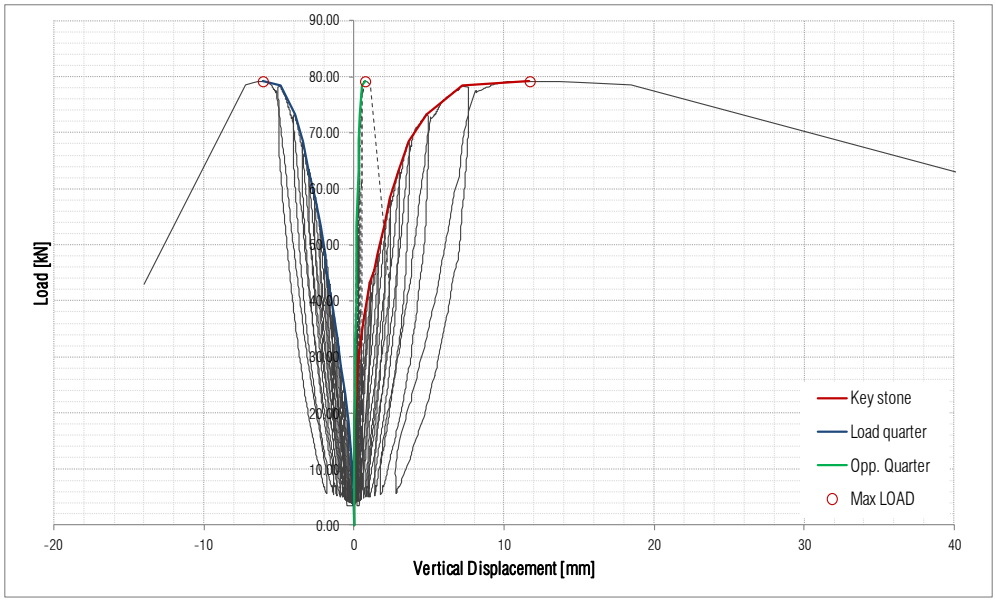


*Fig. 5.43 Load displacement curve of the measured points in vertical direction*

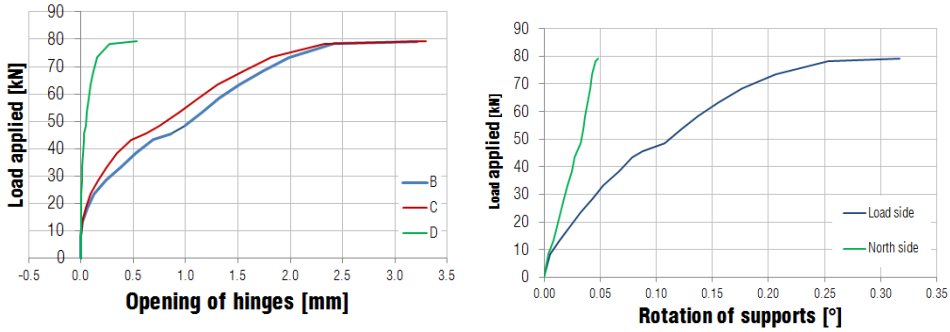


*Fig. 5.44 Hinges behaviour (left) and rotation of supports (right)*

The sensor placement was not correct for hinge D which is not accurately measured. Form Fig. 5.44 is relevant to notice the similar magnitude of hinges opening that is limited with the respect of UR situation and shows the brittle behaviour and the simultaneous opening. After the sudden activation (less than 1 sec) the vault collapsed. Fig. 5.45 shows this behaviour in time.

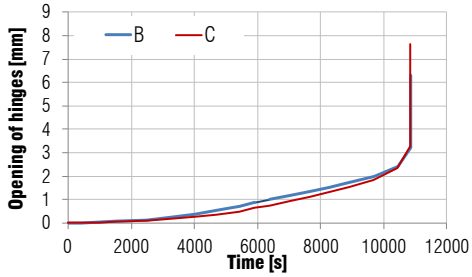


*Fig. 5.45 Development on time of hinges*

### 5.3.3 *03-CRFP_CARBON FIBRE REINFORCED POLYMER*

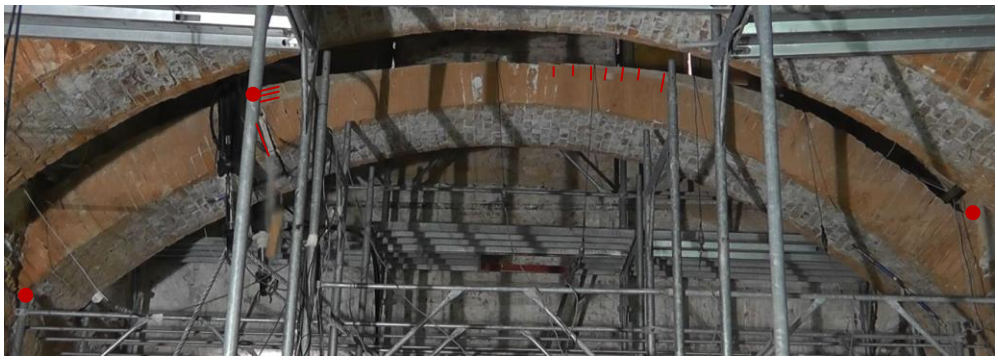

*Fig. 5.46 CFRP vault at the highest displacement*

The application of composites on vaults avoids a typical mechanism failure mode. The crack pattern of the vault strengthened with CFRP, showed not clear location of the hinge close to the middle of the span, what is characteristic for masonry vaults bounded on the extrados by external reinforcement. Those cracks are spreading between bricks 60 and 75 (Fig. 5.47), what prevent from precise localisation of the forth hinge.

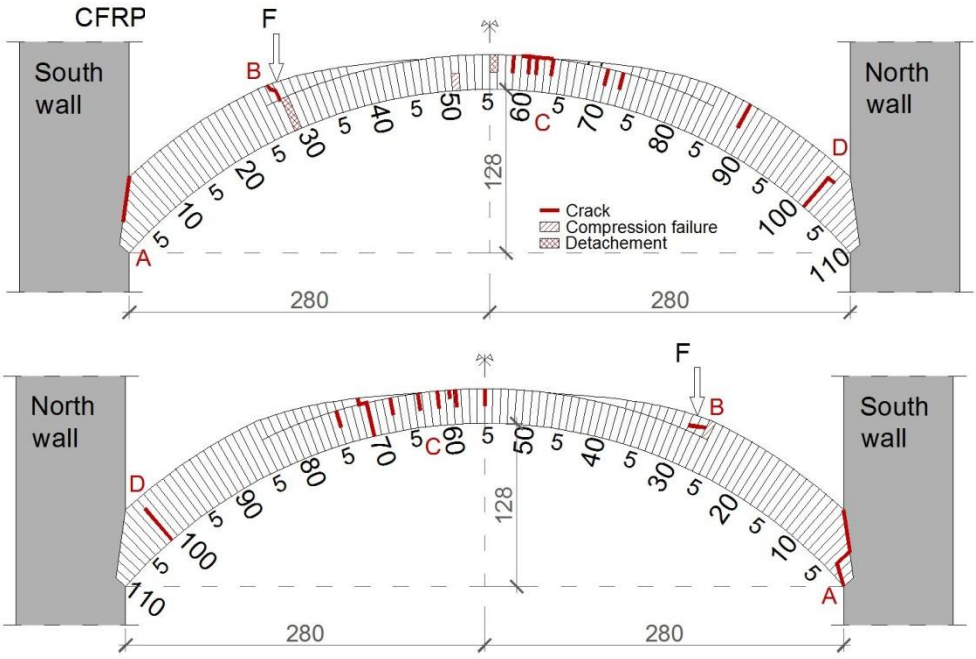


*Fig. 5.47 Crack pattern of the two frontal view of the CFRP vault*

The crack related to appearance of the hinge on the support, on south side, started to form the vault extrados and, after the detachment from the stone stringcourse, went through bricks toward the support with a remaining active part of about 4 cm (Fig. 5.48 left). When this crack occurs the CFRP started to work and to

bear tension. This tension detached the composite from the substrate that presented a slight curvature between the vault extrados and the anchor inclination (Fig. 5.48 right). For the strain measurement this happened at 1700 με which is not a very high strain. The crack related to the opening under the point of the force application (hinges B) appeared between bricks 30/31 on the intrados of the vault. This was the most stressed point, with a total opening of the crack of 24.33 mm (Fig. 5.52) that was enough to cause loose of one of the bricks on its selfweight from the row no. 29 (Fig. 5.49). This highlights the low value of tensile strength in mortar. When the maximum load was reached the major failure occurs on the loading point where was observed the masonry crushing due to compression (Fig. 5.49) that stopped the test. In the loading point also a sliding of the joint of about 12 mm occurred.

The creation of the hinge close to the northern support, on the opposite side than the force application, was revealed by appearance of the crack on the intrados of the vault, between the bricks 104/105 (D). The rotation of hinges seems symmetric according Fig. 5.52.

*Fig. 5.48 Crack opening in hinges A and CFRP debonding on anchorage*

*Fig. 5.49 Hinges B, sliding and loss of material (left) and masornry crushing (right)*

This vault reached a maximum load of 58.48 kN and with a ultimate displacement of 26.76mm. The magnitude of both, load and deflections, demonstrate a severe increase in performance of the strengthened vault.

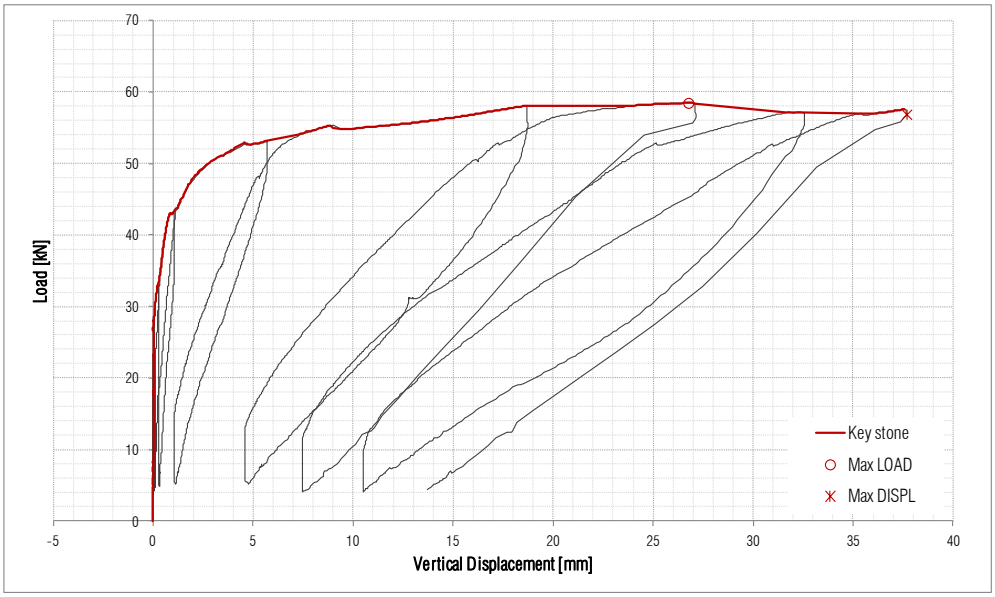


*Fig. 5.50 Load displacement cyclic and envelope curve of the key stone in vertical direction*

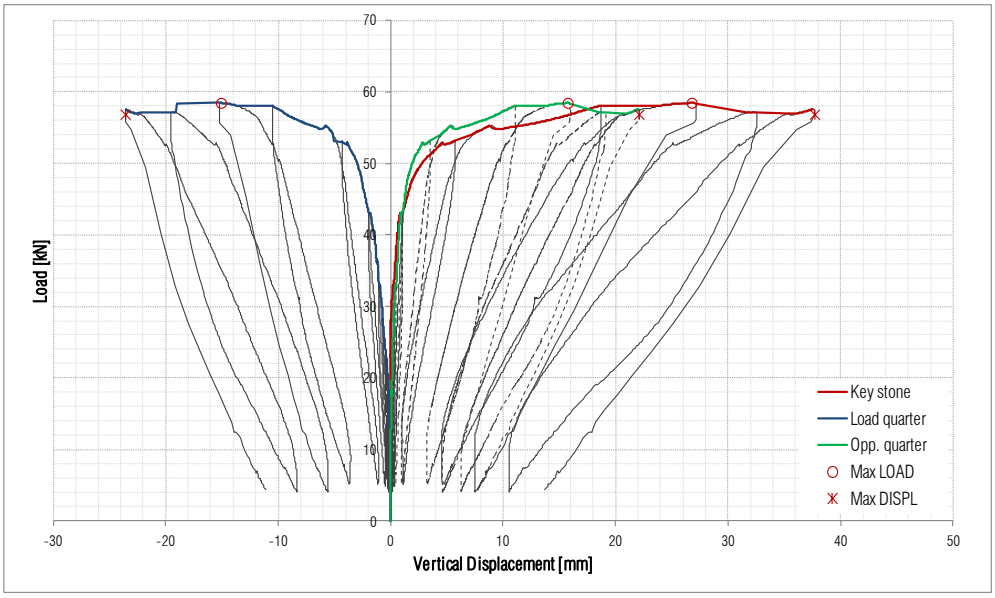


*Fig. 5.51 Load displacement curve of the measured points in vertical direction*

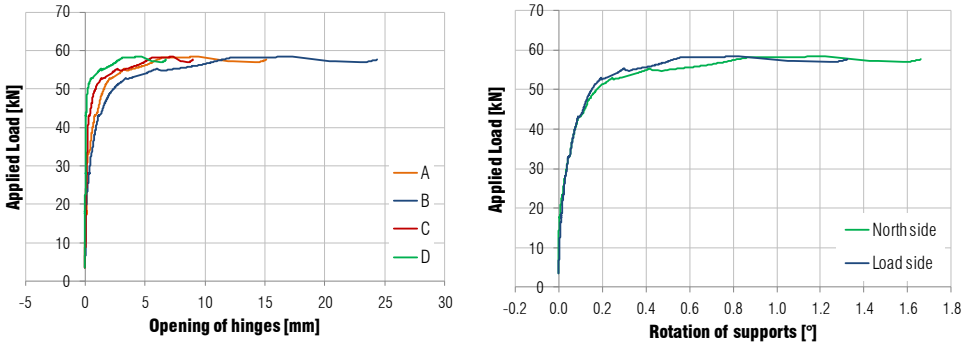


*Fig. 5.52 Hinges behaviour (left) and rotation of supports (right)*

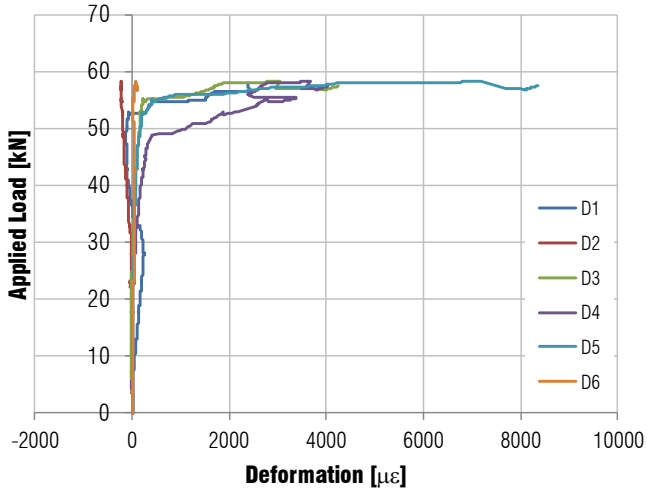


*Fig. 5.53 Strain measured in the reinforcement*


*Fig. 5.54 Cracks spreading due to composites application*

The aforementioned constrain played by composites in avoiding the hinges formation in C (between the load and the support) caused a spreading of cracks in a wider portion of the vault. This spreading occurred when the thrust line goes outside the masonry cross section activating the bending moment on the section. In

Fig. 5.53 the maximum strain recorded is by D5 and reached a strain of 0.83% (Tab. 5.10) whereas D4 achieved 0.4%. This deformation, according to the applied area and the mechanical characterization means a tensile force of 43.6 and 21.01 kN respectively. The estimated contribution of the anchorage before deboning was 8.93 kN. The use of a limited number of strain sensors do not allows to measure the maximum strain reached.

### 5.3.4 *04-SRG_STEEL REINFORCED GROUT*

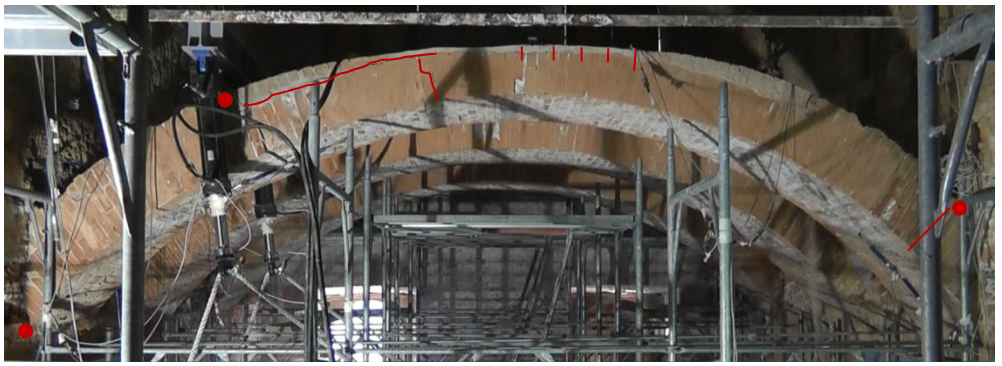

*Fig. 5.55 SRG vault after the reaching of the maximum displacement*

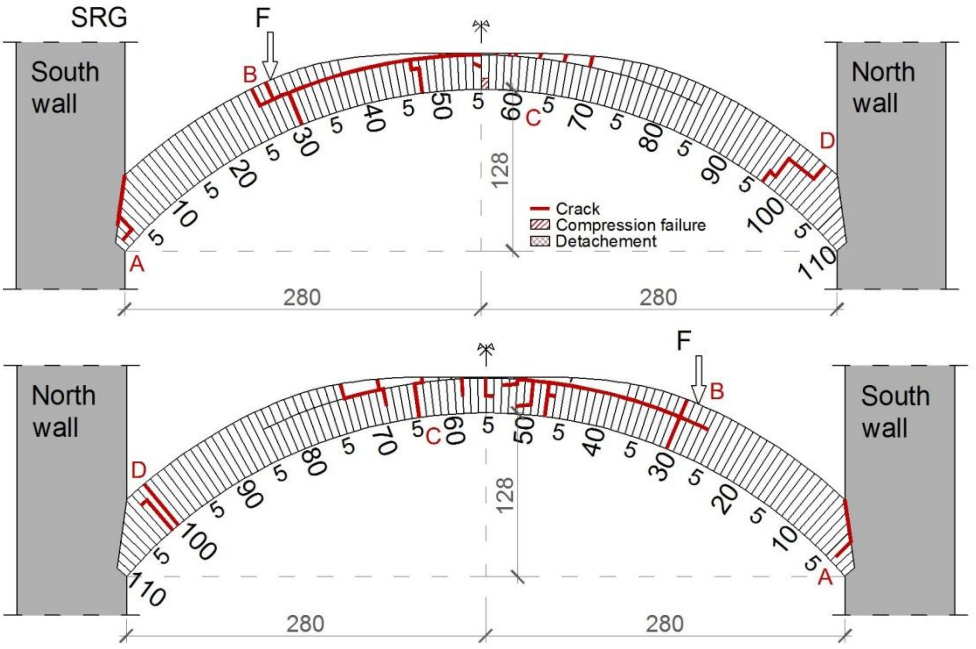


*Fig. 5.56 Crack pattern of the two frontal view of SRG vault*

The crack pattern of the vault strengthened with SRG presents a similar behaviour to the one strengthened with CFRP. The cracks on the extrados close to the middle of the span were spread between bricks 45 and 70 (Fig. 5.56). This

means even a more spreading with the respect of carbon fibres, and it could be justified by the higher ultimate load reached. As it was in the previous cases, the crack appeared on the extrados of the connection between the vault and the support wall on the side of the force application. In this case, only in the post peak branch a detachment occurred (Fig. 5.57). The presence of crazing in the mortar reveals a deep activation of the anchorage which highlights the efficacy of the proposed method of connection to support that develops almost the entire fibre capacity. The strain measurement (D1, see tab. Tab. 5.10) gives 1.74 % higher than the one reported in the datasheet and very close to the range measured on lab and close to the failure. Looking also at graph in Fig. 5.64 this was the position with the fibre higher contribution. It is worth to notice that strain measurements are recorded on the matrix displacements and are not related to strain gauges directly applied on the fibre. It is therefore possible that some sliding between fibre and mortar occurs, thus overestimating strain measures (see Fig. 2.16).

*Fig. 5.57 Debonding and diffusion of cracks in the anchorage on A (load side)*

*Fig. 5.58 Small sliding of joints under the loading point (left) and near hinge D (right)*

The crack under the force application formed on the intrados between bricks 30/31 and reached a significant opening (35.43 mm). Due to the increase of load, in the last cycle a sliding appeared in hinge D near brick 100 (Fig. 5.58 right) and it is also possible to recognise this event in a small force drop in the last loading cycle at the maximum force at about 45 mm of displacement (Fig. 5.61). A more exhaustive

graph is reported in Fig. 5.65 where, looking at the relative movement of the three measured points in horizontal and vertical direction is possible to recognise this sliding (dashed circle). Moreover another sliding occurred in hinge B under the load of about 1 cm of magnitude (Fig. 5.58) but this happened after the vault failure in the adjusting movement. The crack related to the creation of the hinge on the opposite side than the force application (D), had the diagonal character and formed from the bricks 96/97 on one side to the bricks 100/101 on the other.

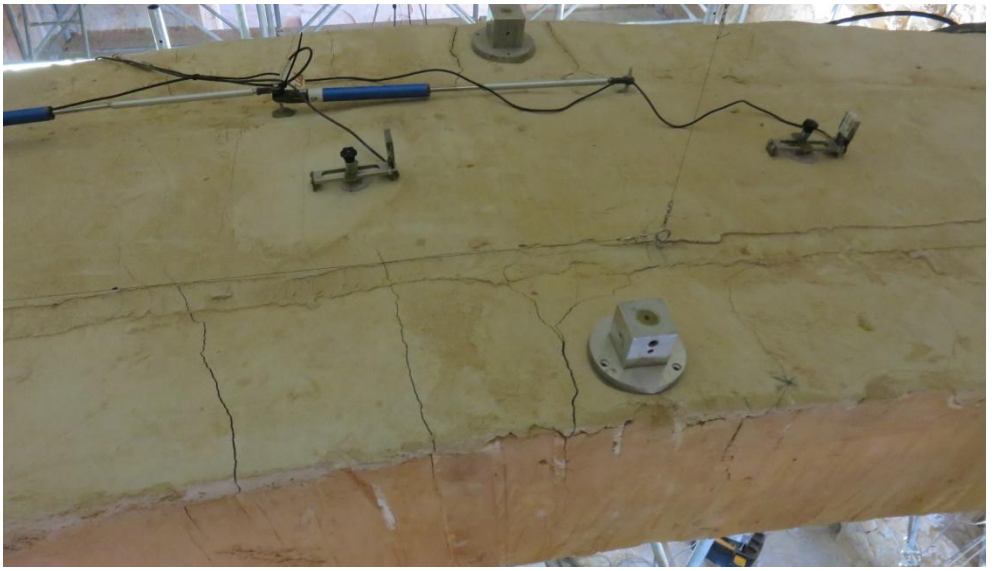

*Fig. 5.59 Crack diffiusion due to composites action*

*Fig. 5.60 Compressive failure of masonry beween the keystone and the loading point*

At the highest load (86.64 kN) the vault shows a good behaviour in diffusing cracks and involving masonry in compression (Fig. 5.59). In the last loading cycle still before reaching the highest load (34.6 kN) of response curve, the failure occurred due to the detachment of the regularization layer of the bricks on the side of the loading application (Fig. 5.60). In this case, although is not a common behaviour for arches, the failure involved the compression of masonry, not related

to material but to the structural element similarly to the compression failure of a two leaf masonry wall without transversals connections (see Fig. 2.2). This failure mode is clear in the longitudinal crack reported in Fig. 5.55 between the key stone and the loading point.

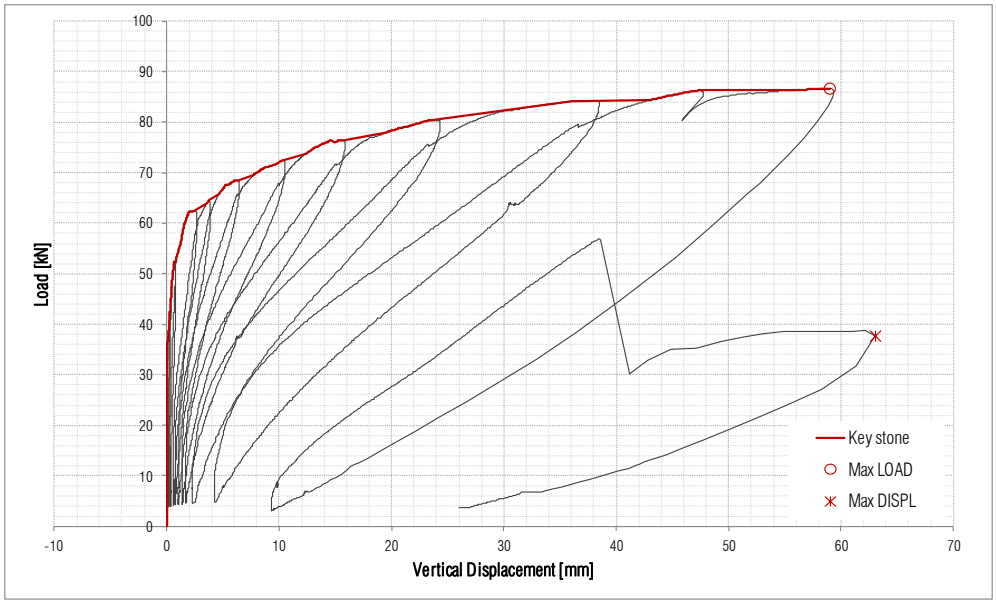


*Fig. 5.61 Load displacement cyclic and envelope curve of the key stone in vertical direction*

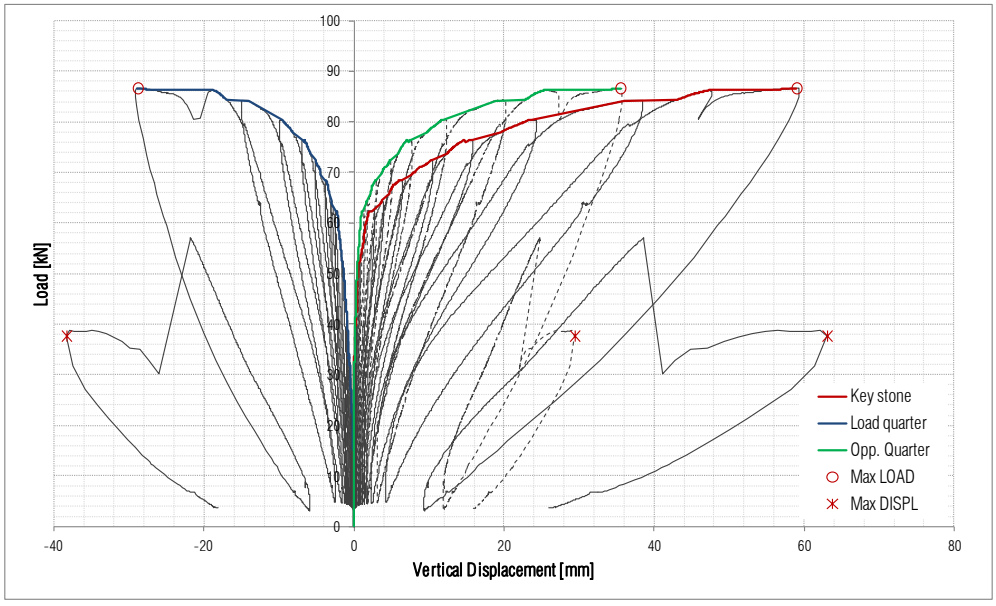


*Fig. 5.62 Load displacement curve of the measured points in vertical direction*

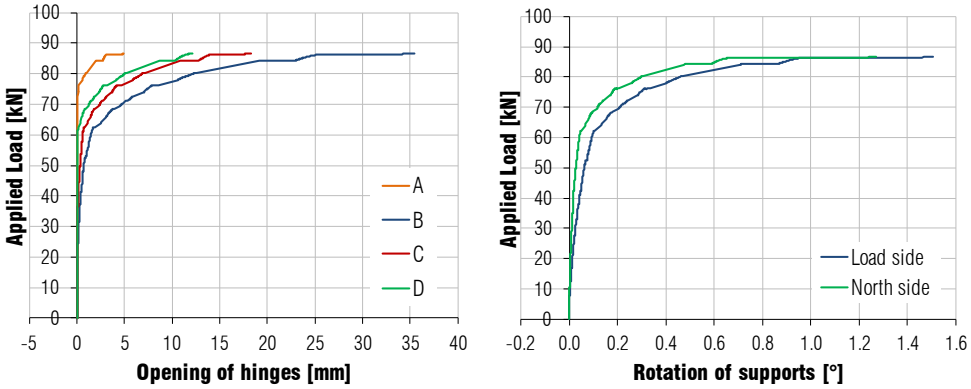


*Fig. 5.63 Hinges behaviour (left) and rotation of supports (right)*

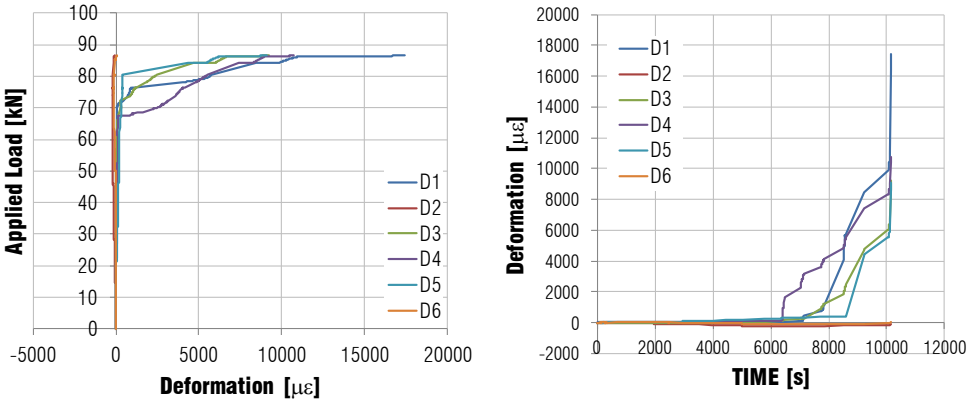


*Fig. 5.64 Strain measured in fibres (left) and its trend on time (right)*

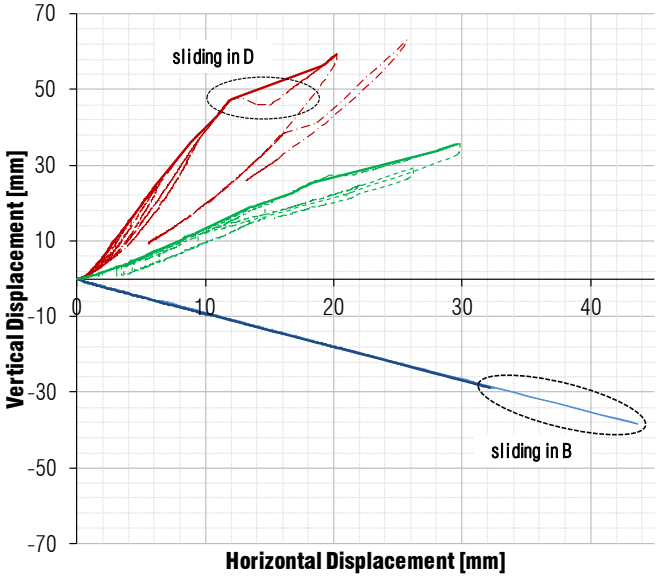


*Fig. 5.65 Reconstruction of movement in horizontal and vertical direction*

### 5.3.5 *05-BTRM_BASALT TEXTILE REINFORCED MORTAR*

The activation of a mechanism, which involves a rigid body motion without material deterioration permitted to reinforce the UR vault with a Basalt Textile Reinforced Mortar. Due to this kind of application, the cracks on the intrados were already present from the beginning of the test in the substrate.

*Fig. 5.66 BTRM vault at the maximum displacement*

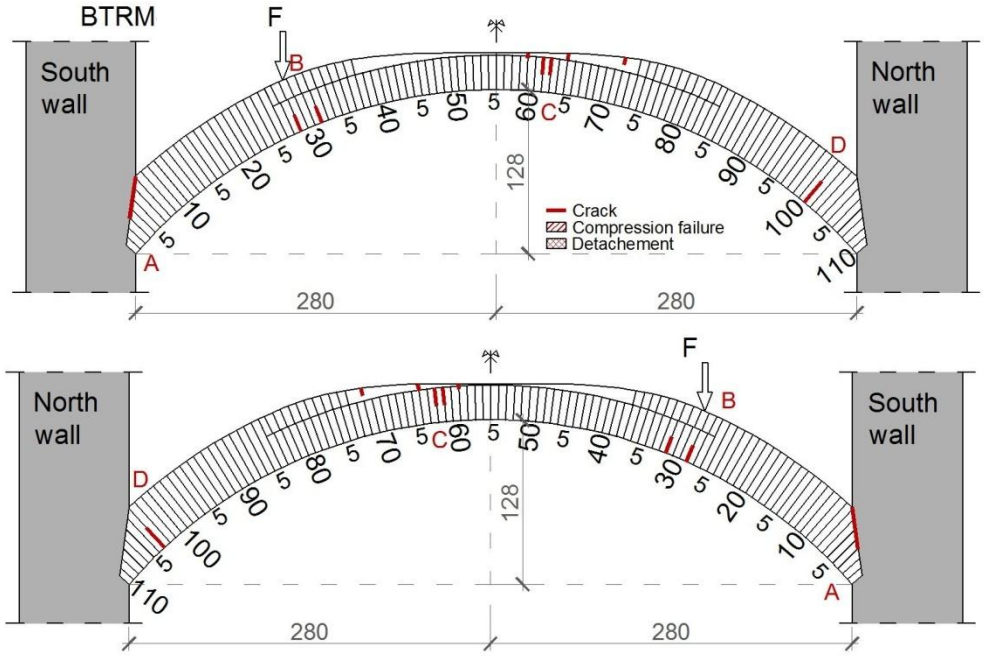


*Fig. 5.67 Crack pattern of the two frontal view of BTRM vault*

The deformation of this vault was defined by formerly created hinges what resulted in lack of appearance of new cracks on the intrados, reopening of the crack on the support on the side of the force application and formation of three new thin cracks on the extrados close to the middle of the span. The cracks on the intrados were located between the bricks 28/29, 31/32 and diagonally starting between

bricks 100/101 on the one side and following to the bricks 103/104 on the other (Fig. 5.67). The cracks which appeared in the BTMR were located between the bricks 59/60, 64/65 and 71/72 (Fig. 5.68).

*Fig. 5.68 Crack diffiusion in the texitile reinforced mortar*

In this case the load decrease of 3 kN in the reloading even with not evident damages but with an increasing deformation. This might be given by damage on the net inside the mortar that cautiously suggests stopping the test, also looking at previous experiences in literature [Giradello 2012, Garmendia 2015]. The strain records (Fig. 5.72) suggest a limited contribution of the reinforcement but in this case it has to be considered that cracks were lumped in few points.

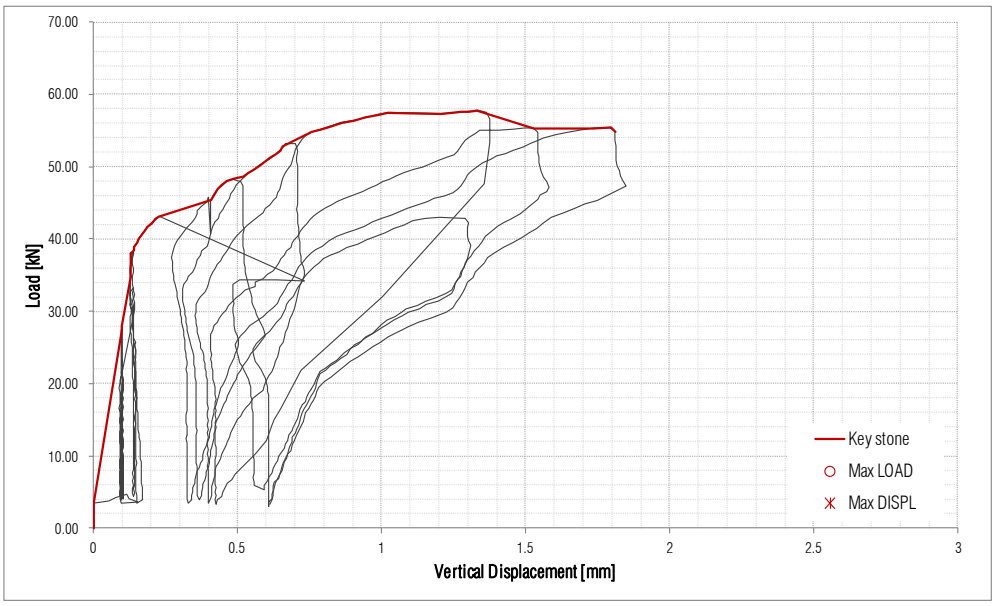


*Fig. 5.69 Load displacement cyclic and envelope curve of the key stone in vertical direction*

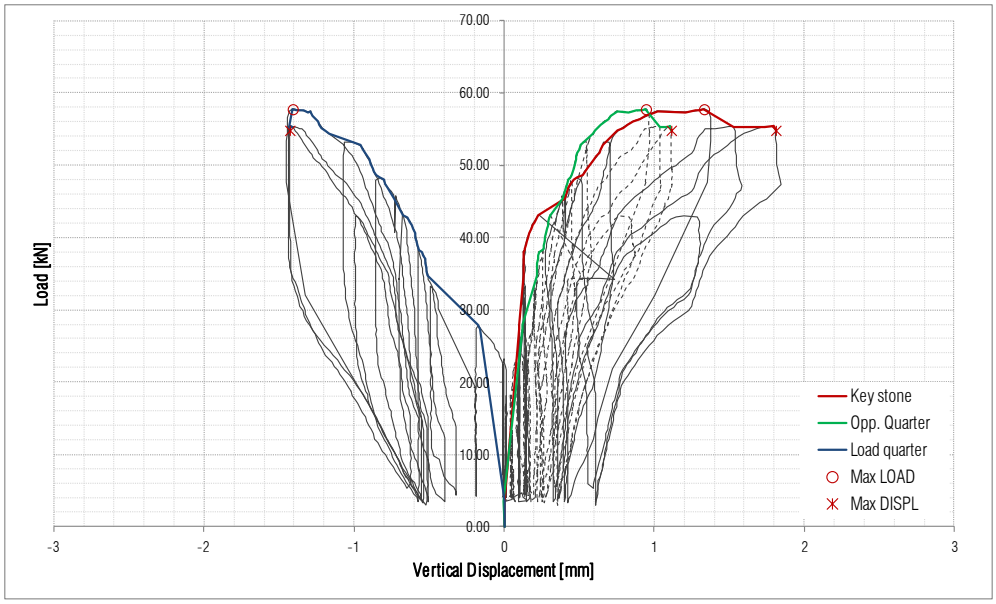


*Fig. 5.70 Load displacement curve of the measured points in vertical direction*

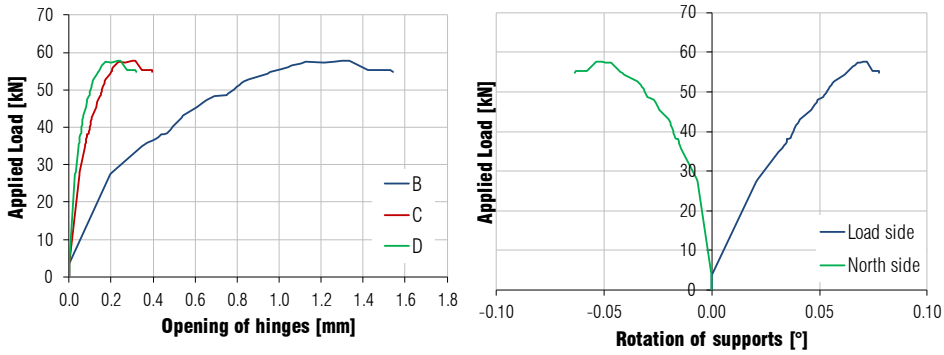


*Fig. 5.71 Hinges behaviour (left) and rotation of supports (right)*

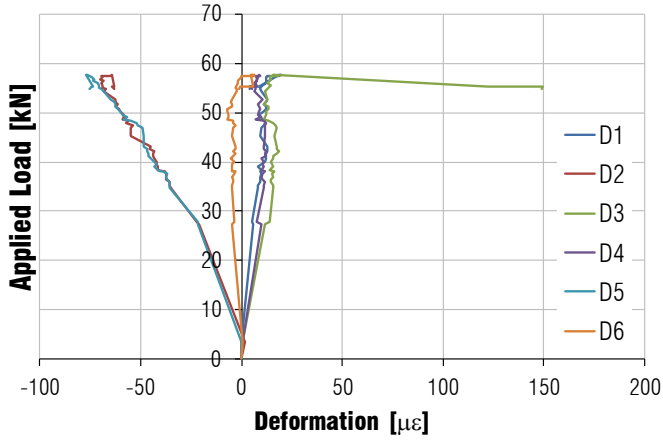


*Fig. 5.72 Strain measured in the net*

### 5.3.6 *Summary of static results*

In the following all the results are presented together in order to better describe and to be aware of relative magnitudes. Fig. 5.73 shows all curves obtained from static tests. All loads are related to the maximum vault strength although, due to load control is not possible to well analysis the post-peak behaviour. The first clear outcome concerns the effectiveness in increased strength of all reinforced vaults. EBR provides and confirms to be a valid option in resistance improvement. Moreover carbon and steel reinforces demonstrated also an enhanced ductility. Tab. 5.7 shows values of mutual comparison with the reference vault, the increase ratio of force and ultimate displacement, the failure mode and the other activated mechanisms.

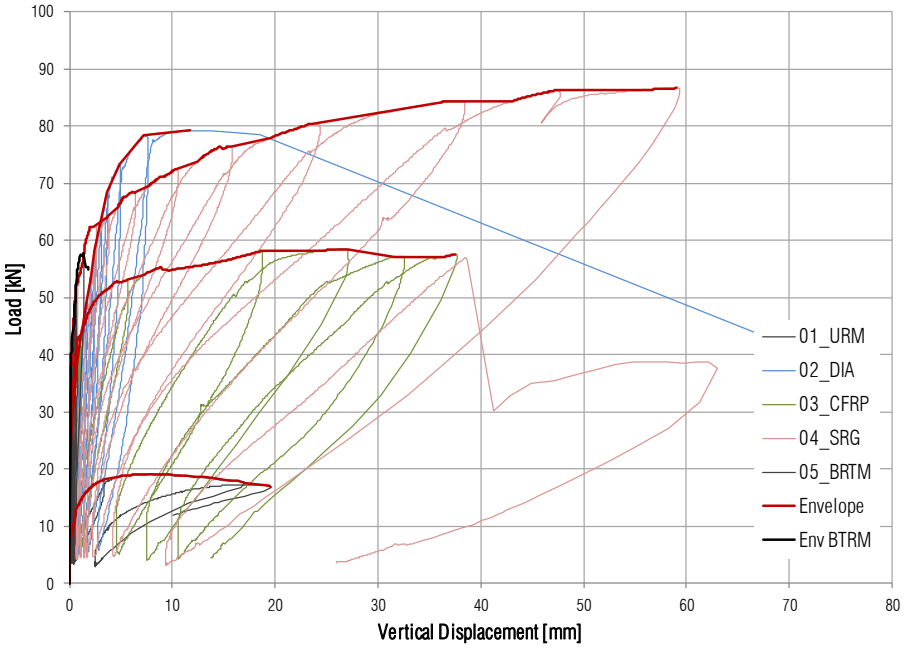


*Fig. 5.73 Load displacement curve of all tests*

*Tab. 5.7 Comparison among vaults main parameters*

| | $F_{max}$ | $F_{max}/F_{UR}$ | $\delta_{max}/\delta_{UR}$ | Failure | other |
|---|---|---|---|---|---|
| **01_URM** | 19.04 | - | - | M | - |
| **02_DIA** | 79.18 | 4.16 | 1.52 | M | - |
| **03_CFRP** | 58.48 | 3.07 | 3.48 | C | S-D |
| **04_SRG** | 86.64 | 4.55 | 7.67 | C | S |
| **05_BTRM** | 57.75 | 3.03 | 0.17 | M-F | - |

M - Mechanism; C - Crushing; S - Shear; F - Fibre rupture D- debonding

The most reliable comparison concerns each strengthening with the reference vaults instead comparison among strengthening has to be more cautious considering also other parameters ($E_f$,$A_f$,$\varepsilon_u$, etc). The major increase was recorded for the SRG vault with a maximum load of 86.6 kN (Tab. 5.8) with an overall increase ratio of 4.55 times UR and a correspondent displacement of almost 59 mm which is more than the double of all the other tests and more than 7.5 times UR. At the onset of cracks at a load of about 62.5 kN the displacement was 2.20 mm while at the maximum load the displacement was about 27 times. The same happens with the secant stiffness of the vault. Herein the data related to the onset of cracks are qualitatively identified because of the lack of a rigorous definition of such yielding loads. Neverless the first branch, before cracking is quite similar among all cases. These figures remark the good behaviour of SRG and its performance in terms of resistance and ductility. The second major increase of 4.15 times is related to the traditional intervention with diaphragms. In this case the overall load could not be directly compared with the other because the changing in hinges position gave a different distribution of the load which practically become at one third of the span and near to a rotational centre of the intermediate rigid block and this allowed such increase. As a drawback the traditional intervention remarks to be fragile and without ductility, therefore compared to UR mechanism the ductility of the element is seriously reduced.

From Tab. 5.9 is interesting to notice the magnitude reached in cracks. The hinges in the extrados (B-D), which does not involve composites, reached obviously high quantities. Moreover is confirmed that deformations are concentrated all in one joints or sometimes in two. Another observation is given to the spread hinge C where the composite is stitching it. The different magnitude could be directly related to the strain acting on reinforcements with comparable results than strain gauges.

About failure mode, although in two cases also sliding was activated the failure was in those cases related to masonry which implies the maximum increase achievable.

*Tab. 5.8 Load and vertical displacement at maximum resistance and displacement*

| | MAX LOAD | | | | MAX DISP | | | |
|---|---|---|---|---|---|---|---|---|
| | $F_{max}$ [kN] | $\delta_{k\text{-}v}$ [mm] | $\delta_{l\text{-}v}$ [mm] | $\delta_{q\text{-}v}$ [mm] | $F_{\delta,max}$ [kN] | $\delta_{k\text{-}v}$ [mm] | $\delta_{l\text{-}v}$ [mm] | $\delta_{q\text{-}v}$ [mm] |
| **01_URM** | 19.04 | 7.69 | -3.93 | 3.63 | 16.91 | 19.54 | -8.94 | 10.23 |
| **02_DIA** | 79.18 | 11.71 | -6.08 | 0.73 | 0.00 | - | - | - |
| **03_CFRP** | 58.48 | 26.76 | -15.09 | 15.73 | 56.88 | 37.67 | -23.60 | 22.07 |
| **04_SRG** | 86.64 | 58.99 | -28.64 | 35.50 | 37.65 | 63.05 | -38.36 | 29.41 |
| **05_BTRM** | 57.75 | 1.33 | -1.41 | 0.95 | 54.82 | 1.81 | -1.43 | 1.11 |

*Tab. 5.9 Maximum hinges opening in mm for each vault*

| | HINGES | | | | | |
|---|---|---|---|---|---|---|
| | A [mm] | B [mm] | C [mm] | D [mm] | L s [°] | N s [°] |
| **01_URM** | 8.20 | 9.20 | - | 3.58 | 0.71 | 0.75 |
| **02_DIA** | - | 3.21 | 3.29 | 0.53 | 0.32 | 0.05 |
| **03_CFRP** | 15.11 | 24.33 | 9.00 | 6.74 | 1.32 | 1.66 |
| **04_SRG** | 4.93 | 35.43 | 18.26 | 12.11 | 1.51 | 1.27 |
| **05_BTRM** | - | 1.54 | 0.40 | 0.32 | 0.08 | 0.00 |

Focusing on SRG strengthening vaults more detailed information can be given by Tab. 5.10 where the measured strains are reported. Comparing the conclusions drawn for hinges C the comparison between steel and carbon are confirmed. Indeed the maximum deformation recorded on carbon was 0.83 % against 1.07% of SRG. These strains might not be the highest values, mainly due to sensors position, but the overall trend confirms a lower effort of carbon. As reported in §5.3.3 the value of 0.17% in $D_1$ is related to the fibre debond on anchorage. This behaviour can be associated to stiffer behaviour of CFRP cross section which implies higher stresses in masonry and therefore stress concentrations. Indeed the failure occurs by masonry crushing. In conclusion, the fibre resistance , equal for carbon and steel, is not the only parameter which affects the whole response in agreement with some authors [Tirantafillou 1999, Valluzzi 2001].

The application of Basalt textile presents interesting confirmations of first literature observations [Girardello 2012, Garmendia 2015]. From the stress strain curvature is visible on one hand a high maximum load (close to carbon), which provides an increase of 3 times UR, and on the other hand a limited ultimate displacement. In terms of resistance the system provide to be effective but unfortunately, due to the type of test, is not possible to evaluate this behaviour more in depth. The system appears as a union of two fragile elements (basalt and mortar) which led to a fragile system as well. The initial higher stiffness can be related to the wider mortar application that drops after cracking. The limited deformation recorded on strain gauge is due to the sensor positions because this system lumped all deformations in three main cracks. Therefore Basalt confirms a small stress distribution within the net. The aforementioned observations on the stiffer behaviour are drawn also looking at the dynamic response (§6.2) hence confirming the outcome.

*Tab. 5.10 Maximum fibres deformations*

| FIBRES DEFORMATIONS | | | | | | |
|---|---|---|---|---|---|---|
| | $D_1$ ε [%] | $D_2$ ε [%] | $D_3$ ε [%] | $D_4$ ε [%] | $D_5$ ε [%] | $D_6$ ε [%] |
| **03_CFRP** | 0.17 | 0.00 | 0.43 | 0.40 | 0.83 | 0.01 |
| **04_SRG** | 1.74 | 0.00 | 0.92 | 1.07 | 0.91 | 0.01 |
| **05_BTRM** | 0.002 | 0.000 | 0.015 | 0.001 | 0.000 | 0.001 |

### 5.3.7 *Ties analysis during test execution*

The setup specifically designed for this test on vaults, as presented in §5.1.1, aims to avoid possible damages on the existing structure and to counteract the horizontal thrust, a series of three ties was arrange between supports (see Fig. 5.2). In order to monitoring their acting force one strain gauge for each tie was installed. By a tensile test on laboratory the specific correlation between strain and force has been carried out until 30 kN with a perfect linear behaviour. The ties young modulus was of 215'850 MPa with an area in the tested parts of 465 $mm^2$. Strain gauges were also applied in the ancient existing tie (Fig. 5.74 and Fig. 5.55 above) which remains onsite. Strain gauge were also applied in other ties on neighbour rooms but these are not herein presented because not interesting data or observations were pointed out. Finally due to the significant metals sensitiveness on temperature variations another reference strain gauge was applied on a free element to correct also the other sensors measurements. Unfortunately, due to hardware problems, records about UR and BTRM are not available.

*Fig. 5.74 Strain gauge applied on the existing tie (left) and on the setup ties (right)*

The records of all sensors were continuously recorded since the ties installation and the relative manual tightening. Because of the manual operation, ties have not same pretension and all reported strains consider only the variation occurred after fastening. In the data treatment temperature effects, which were not negligible during the entire day, were cleared.

Fig. 5.74 shows the total force in time acting in the three ties during tests. It is clear the time history applied to vaults and the good correlation between applied load and tension in ties. It is also evident the low action inside those elements for all cases. The interesting outcome form this graph concerns the stiffness behaviour of the whole systems.

Tab. 5.11 shows the main numerical results directly gathered as total maximum strain in setup ties and in the ancient tie, and also indirectly calculated entities such as maximum tension in setup ties $T_{max}$, total thrust of the vault $H_{max}$ and the ratio between the wall and the ties stiffness $k_w/k_t$.

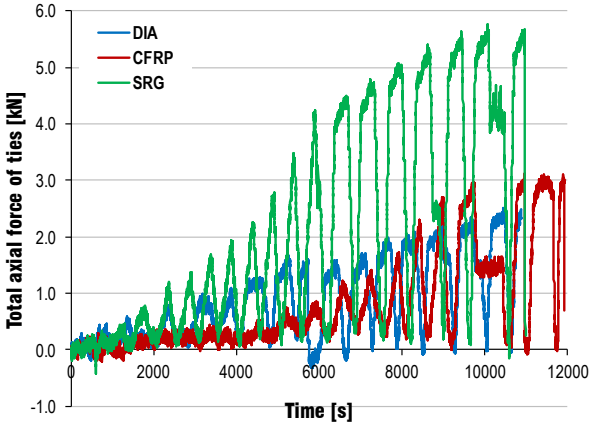


*Fig. 5.75 Axial load undergone in time by ties*

*Tab. 5.11 Results form strain monitoring of ties*

| | $T_{max}$ [kN] | $H_{max}$ [kN] | $k_w/k_t$ | $\varepsilon_{max}$ [με] | $\varepsilon_{Ancient}$ [με] |
|---|---|---|---|---|---|
| **02_DIA** | 2.51 | 77.2 | 29.7 | 25 | 13 |
| **03_CFRP** | 3.12 | 56.0 | 16.9 | 31 | 7 |
| **04_SRG** | 5.76 | 77.6 | 12.5 | 57 | 22 |

Considering the controlled conditions and the hinges identification with a good precision, in the order of few centimetres, a reasonably estimation of the thrust is possible. The only unknown concerns the bending moment of hinges A which for fix to pin conditions provide a maximum difference of 3 kN in H. Moreover, due to the pretension applied to setup ties, is herein assumed that displacement of wall and ties is the same.

Under such reasonable assumptions the obtained schematic structural system is presented in Fig. 5.76. Looking at the symmetric conditions of ties an average stiffness of both wall sides could be estimated imposing same displacements. The force R acting on walls is the wall stiffness $k_w$ times the displacement Δx meanwhile the tension T is $k_T$ times the same displacement. Considering that R is the difference between the estimated thrust H and the axial

tension T is possible to estimate by eq. (5.5) the relative magnitude of wall stiffness with the ties system.

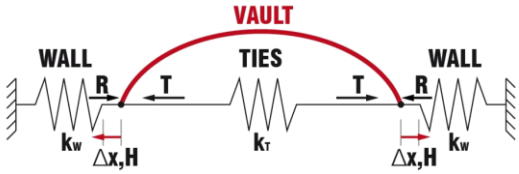


*Fig. 5.76 Schematic analysis of stiffness distribution*

$$k_w = \frac{(H-T)}{T} \cdot k_T \quad \rightarrow \quad k_w = \frac{(H-T)}{T} \cdot \frac{E \cdot A}{L} \tag{5.5}$$

Fig. 5.77 shows the ratio between the acting thrust and the axial tension in ties.

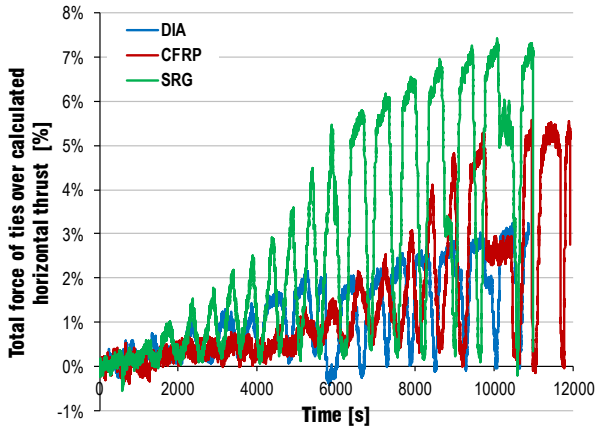


*Fig. 5.77 Tension acting on ties normalized on the calculated thrust*

From the presented data is possible to quantitatively notice how the wall stiffness varies in the room position probably due to the corner connection. The wall in the middle (SRG) is 12.5 stiffer than ties whereas near the corner is 16.9 times hence is clear an increased stiffness in wall of 35% due to the corner. The diaphragm vault, although located in similar position compared to CRFP, shows stiffness almost double. The hinge position and the thrust diffusion in diaphragm seems to engage more masonry walls. Moreover looking at the strain contribution of the ancient tie is evident how its effectiveness is higher in closer vaults.

In conclusion this example confirms Heyman's [1996] considerations on the actual state stress in masonry structures. Stiffness in uncracked conditions on the wall is substantially higher than common ties and stress distribution varies depending on several boundary conditions. In general the caution to apply setup ties to counteract the horizontal thrust was barely effective although necessary.

## 5.4 DYNAMIC IDENTIFICATION

The analysis of the dynamic behaviour of structural elements, before and after strengthening interventions helps to understand their effectiveness and the variation in mode shapes and frequencies. Moreover the execution of dynamic identification before and after destructive tests might be a promising tool in order to develop in future reliable procedures of damage detection as analysed in Ramos [2007] that has a wide diffusion in SHM.

### 5.4.1 *Test planning*

The test planning was decided looking at the best compromise between time costs and collected information. The experimental campaign on site needed to limit as much as possible the time involved in test. Moreover the OMA, due to the hypotheses mentioned in literature review, was performed only when the company stopped to work. Because of such restrictions, only one setup was defined.

To increase the effectiveness of the test and enlarge the number of identified modes, a large number of sensors were decided in a unique setup. The typical mode shapes of a vault involve especially the orthogonal direction of surface meanwhile the tangent direction is less engaged. Because the interesting is focus on vault the out of plane behaviour was neglected in models and tests. The cross section dimensions, squat with the respect of laboratory campaigns, and the strengthening location, only one strip in the middle, suggests to analyse torsion but with a limited number of sensors. Furthermore the analysis of mode highlights three mode of torsion in the first ten modes that involve a large movement on sensors. After these consideration on sensors placement a total number of 14 accelerometers where located orthogonal to the arch, two on supports and on each quarter whereas one by side in intermediate positions. That location allows to catch better flexural modes. Other two couples where located in the keystone to cover all directions.

Fig. 5.78 presents the application of sensors on the unreinforced vault and Fig. 5.79 shows the adopted setup scheme.

*Fig. 5.78 Accelerometers location in the UR vault*

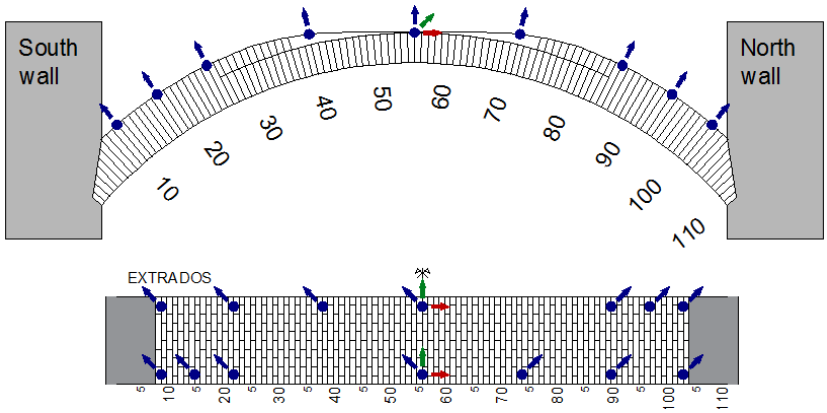


*Fig. 5.79 Accelerometers setup during the dynamic identification*

### 5.4.2 *Test equipment and excitation*

For each setup three ambient vibration tests and three records with hummer impact excitation were performed to obtain an average value. The estimated maximum frequency was lower than 150 Hz and it was decided to analyse the structure, using the Nyquist formulation, with a sampling frequency of 1000 Hz.

Accelerometers were piezoelectric sensors (PCB 393 B12) with a sensitivity of 10000mV/g, a resolution of 0.000008 grms and a frequency range (5%) between 0.15-1000 Hz. The adopted acquisition system was a NI PXI-1042Q platform with some embedded devices (NIPMA-1115;NI PCI-4472;NI PCI4472B; NI PCI-6220).


*Fig. 5.80 Acquisition system (NI PXI-1042Q) and accelerometer (PCB 393 B12)*

In order to improve the vault response and to better evaluate modal parameters, in addition to the ambient vibration an impact hammer excitation, random in space and time, was adopted. Although the white noise hypothesis is not herein fulfilled the methods provide effective results in many research Reynders [2006], Cantieni [2006], Ramos [2007]. In the present work this approach provides better result with EFDD than SSI where the performances were better with ambient vibration tests. Fig. 5.81 shows the analysis of one hammer record in time domain (left) and frequency domain (right). This graph points out how excitation source might be considered as a stationary Gaussian white noise stochastic process because the PSD function of the excitation is almost constant, at least in the range 0-150 Hz.

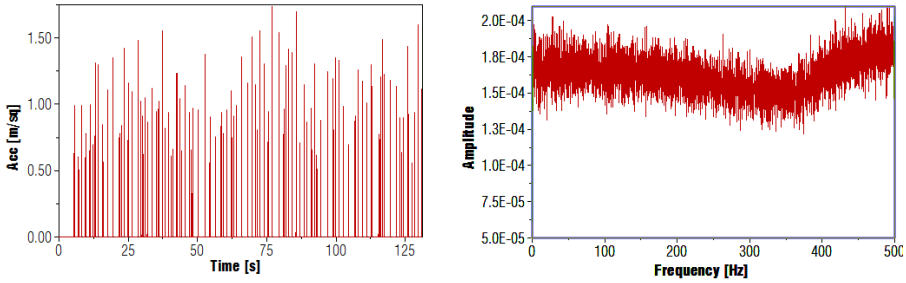


*Fig. 5.81 Hammer impulse in time domain (left) and frequency domain (right)*

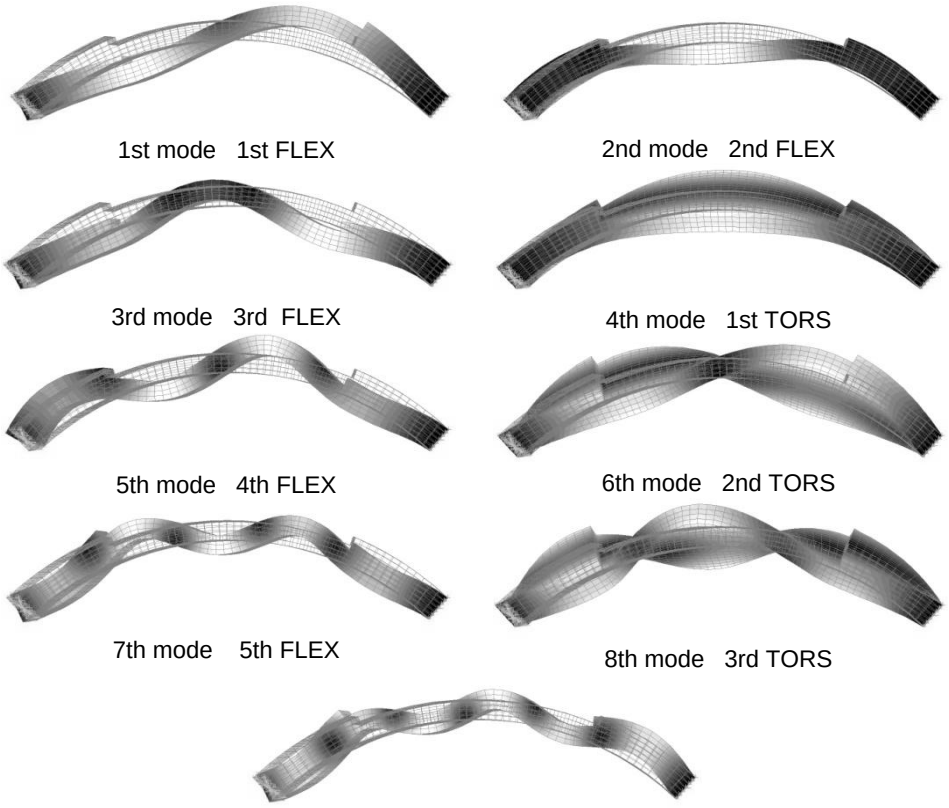


*Fig. 5.82 Vault mode shapes of the FEM*

A further step to achieve a good dynamic identification is to analyse a Finite Element Model (FEM) through a natural frequencies analysis. Results are reported in Fig. 5.82 where modes in depth direction are neglected and the first nine modes shown. The number of modes and the complexity of higher modes are usually difficult to identify. About 5th and 9th modes it has to be noted that accelerometer, at least the couples, are located near nodes and only four sensors are in antinodes. Such modes are then difficult to be analysed.

### 5.4.3 *Analysis and validation*

The modal extraction was performed with the software ARTeMIS and it was possible to recognise all the nine modes searched (Fig. 5.83). The higher flexural modes are more sensitive to the precise positioning of sensors and also to noise and disturbances. However it was possible to recognise them anyway even with a less excitation in the PSD, in particular for modes 5 and 9. The first step was to compare those modes with SSI and FDD finding the same results. It is only reported that EFFD with hammer provides a reduction of always less than 1.5% in frequencies than FFD extract in ambient vibration conditions. This might be associated to the vault activation. It is indeed known that excited structures decrease frequencies.

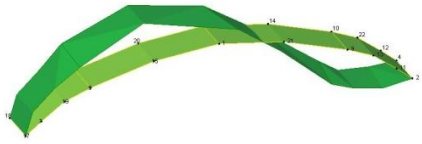

*1st mode 14.9 Hz 1st FLEX*

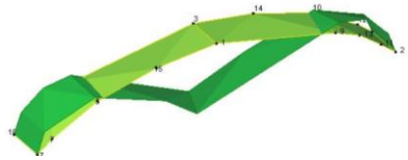

*2nd mode 28.4 Hz 2nd FLEX*

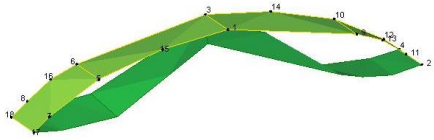

*3rd mode 38.3 Hz 3rd FLEX*

*4th mode 54.4 Hz 1st TORS*

*5th mode 58.1 Hz 4th FLEX*

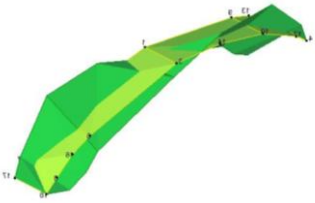

*6th mode 83.4 Hz 2nd TORS*

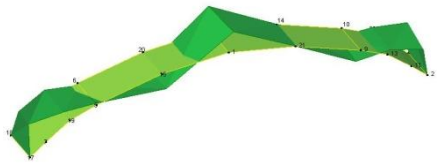

*7th mode 89.3 Hz 5th FLEX*

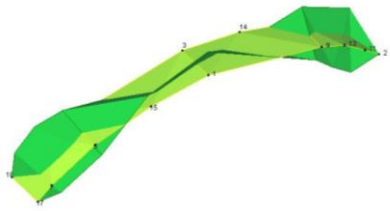

*8th mode 113.1 Hz 3rd TORS*

*9th mode 142.9 Hz 6th FLEX*

*Fig. 5.83 Identified mode shapes of the URM vault before the test with EFDD*

In order to validate and calibrate the FEM, a series of trial in boundary conditions and stiffness modulus have been carried out. The goal seek was the minimization of the overall error in frequencies estimation between the model and the experimental data.

In addition to the frequencies agreement the modal updating was carried on looking at the Modal Assurance Criterion (MAC) as suggested by Allemang [1983]. The MAC matrix is defined as in equation (5.6) where the vector product evaluates the agreement between eigenvectors of model A and B respectively. Once vectors are linearly independent MAC is 0 instead two parallel vectors imply MAC equal to 1.

$$\mathbf{MAC}_{(A,B)} = \frac{\left|\boldsymbol{\Phi}_{\mathbf{A}} \cdot \boldsymbol{\Phi}_{\mathbf{B}}^{\mathbf{T}}\right|^2}{\left|\boldsymbol{\Phi}_{\mathbf{A}} \cdot \boldsymbol{\Phi}_{\mathbf{A}}^{\mathbf{T}}\right| \cdot \left|\boldsymbol{\Phi}_{\mathbf{B}} \cdot \boldsymbol{\Phi}_{\mathbf{B}}^{\mathbf{T}}\right|} \tag{5.6}$$

*Tab. 5.12 Results after the model calibration*

| Mode number | EXP [Hz] | FEM [Hz] | Mode type | Ratio $f_{FEM}/f_{EXP}$ | ε [%] | MAC |
|---|---|---|---|---|---|---|
| 1st | 14.9 | 15.5 | I FLEX | 1.04 | 3.9% | 0.86 |
| 2nd | 28.4 | 28.2 | II FLEX | 0.99 | -0.6% | 0.92 |
| 3rd | 38.3 | 38.3 | III FLEX | 1.00 | -0.1% | 0.81 |
| 4th | 51.8 | 54.4 | I TORS | 1.05 | 4.9% | 0.80 |
| 5th | 58.1 | 57.6 | IV FLEX | 0.99 | -0.8% | 0.29 |
| 6th | 75.4 | 83.4 | II TORS | 1.11 | 10.5% | 0.75 |
| 7th | 78.7 | 89.3 | V FLEX | 1.13 | 13.5% | 0.72 |
| 8th | 109.7 | 113.1 | VI TORS | 1.03 | 3.1% | 0.91 |
| 9th | 142.9 | 123.2 | VI FLEX | 0.86 | -13.8% | 0.08 |

Tab. 5.12 shows the final figures obtained and some interesting conclusions were figured out. From the analysis of boundary conditions an hinges situation was adopted on supports with a good agreement of both MAC and frequencies. Moreover the observation made on static analysis on the role of stereotomy was confirmed also in the dynamic field. Indeed the thicker portion near the stone stringcourse (Fig. 5.36), may be due to existing cracking, does not play a significant role in constrains. For this reason in the model this part was leaved without constrains. On the left Fig. 5.84 shows the final agreement between model and experimental results with a very good agreement in 7 modes that is not common in existing masonry structures, on the right is reported on a graph view the MAC matrix that remarks the good agreement with the model.

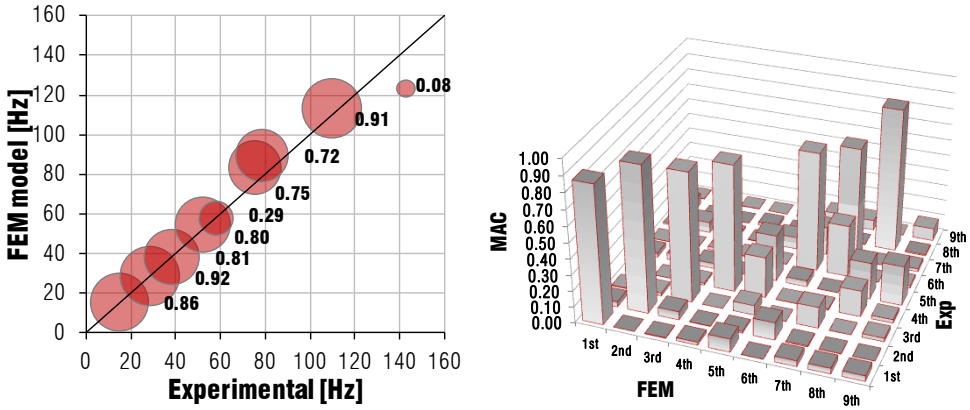


*Fig. 5.84 Models comparison in frequencies and MAC (left) graphic MAC matrix (right)*

In addition Tab. 5.13, which reports the numerical value of the MAC matrix, shows numerically the agreement. Is worth to notice how, as expected, the agreement with mode 5 and 9 is acceptable in frequency terms and by visual detection but eigenvectors are numerically different despite the increase of values on the diagonal term. This is associated to the non optimal sensor placement, and the increasing in disturbances in high frequency and antinodes location. Modes higher than the 5th have a limited mass participation (less than 4%).

*Tab. 5.13 Values of the MAC matrix*

| | | Experimental eigenvectors | | | | | | | | |
|---|---|---|---|---|---|---|---|---|---|---|
| | | 1st | 2nd | 3rd | 4th | 5th | 6th | 7th | 8th | 9th |
| FEM MODES | 1st | 0.86 | 0.00 | 0.00 | 0.02 | 0.08 | 0.00 | 0.04 | 0.04 | 0.03 |
| | 2nd | 0.03 | 0.92 | 0.05 | 0.00 | 0.01 | 0.11 | 0.01 | 0.00 | 0.00 |
| | 3rd | 0.00 | 0.02 | 0.81 | 0.00 | 0.06 | 0.00 | 0.13 | 0.00 | 0.02 |
| | 4th | 0.00 | 0.00 | 0.01 | 0.80 | 0.26 | 0.00 | 0.01 | 0.16 | 0.02 |
| | 5th | 0.03 | 0.04 | 0.03 | 0.00 | 0.29 | 0.04 | 0.00 | 0.23 | 0.25 |
| | 6th | 0.00 | 0.00 | 0.02 | 0.00 | 0.00 | 0.75 | 0.33 | 0.00 | 0.02 |
| | 7th | 0.01 | 0.07 | 0.01 | 0.00 | 0.08 | 0.18 | 0.72 | 0.00 | 0.02 |
| | 8th | 0.08 | 0.00 | 0.00 | 0.02 | 0.01 | 0.00 | 0.00 | 0.91 | 0.01 |
| | 9th | 0.00 | 0.02 | 0.00 | 0.00 | 0.00 | 0.07 | 0.06 | 0.00 | 0.08 |

In conclusion the model within a young modulus E of 1850 MPa and a density of 1800 kg/m$^3$ represents reliably the real vaults. About boundaries the model has a pin to pin condition limited to the brick portion on wall. From this value of stiffness some disagreement rises with results obtained from flat jack test which present values almost double (§ 4.2.4) than the one herein detected.

The dynamic analysis of each vault is directly reported in § 6.2.

# 6 VAULTS ANALYSIS

## 6.1 STATIC ANALYSIS

Before the analysis of the vaults global behaviour, some issues on models and strengthened cross sections will be pointed out in the following.

### 6.1.1 *Models issues*

As presented in the literature review the analysis of plain arches and vaults was deeply studied in the past with the development of reliable tools for the structural analysis. A further confirmation comes from the experimental campaign herein executed with the calculations presented later on. The crucial aspect which controls the activation of mechanism as failure is the substantial difference between tensile and compressive strength of masonry. This difference allows to neglect tensile contributions and to assume infinite the compressive strength, because generally significantly greater than the acting stress. Such hypotheses typically attributed to Heyman [1966] solve the problem by geometrical considerations and calculations of the acting forces by means of static or kinematic approach. The safety criterion is therefore separated from the mechanical properties of masonry eluding an indeed problematic question in the field of existing buildings.

It is also reminded the classification of possible strengthening interventions which operates on vaults (see §2.4.5 ). Despite interventions which act indirectly on the structural system bearing loads but without increasing the vault capacity, direct interventions aim to avoid the mechanisms activation.

Starting from these two observations on analysis and strengthening interventions the addition of elements bearing tensile efforts completely change the mechanical problem. On one hand to provide elements acting in tension avoids hinges formation and thus the mechanism failure, on the other hand the difference between the two stresses (tension and compression) become smaller and mechanical characteristics of material boost their influence. Among the four possible failures of vault and namely: mechanism, masonry crushing, tensile rupture and sliding; only the first does not actually deal with material properties.

Because of this changing in paradigm, the analysis of strengthened masonry vaults still needs a research deepening in: diagnostic tools to evaluate material properties, composites applications to understand working limits of strain, arch models to evaluate the complex interaction among curvature and combined compressive and bending action.

The first step here followed concern the analysis of constitutive laws of materials and the evaluation of the resistance domain.

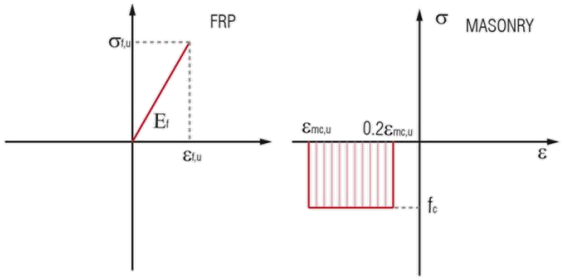


*Fig. 6.1 Adopted constitutive laws for FRP and masonry*

FRP linear behaviour is according to standards [CNRDT-200; ACI 440-7R-2012; ACI 549.4R-13 and FIB 14th 2011]. In literature [Triantafillou 1998, Valluzzi 2001, Briccoli Bati 2007] agree whit this assumption for FRP and in addition with [Hendry 1981] about considering a stress block law for masonry.

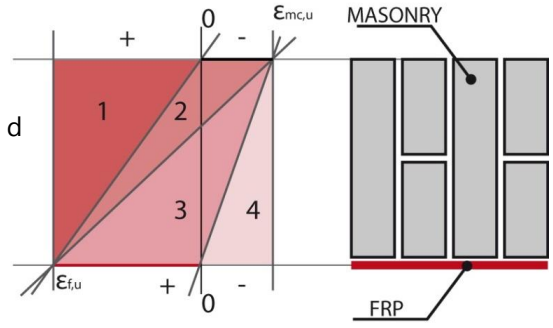


*Fig. 6.2 Stress-strain field of a strengthened masonry cross-section*

The first step is to analyse the strengthened cross resistance in terms of a combined normal and bending action according to the definition of state stress field. The creation of the domain, commonly adopted for concrete, is based on compatibility deformation of the section. With the hypothesis of plane deformations all combinations are considered as reported in Fig. 6.2 starting from complete traction to maximum compression. The imposed deformation provides for each position a couple of Normal and bending actions M. Filed definition is based on material strain threshold defined by constitutive laws (Fig. 6.1) and in particular:

1. Complete positive deformation, FRP acts according to the imposed deformation instead masonry is ineffective, FRP rupture;
2. A negative strain acts in masonry (compression) and FRP provides all the possible deformation, FRP rupture;
3. Masonry reach the maximum compressive strain and the FRP acts proportionally to the imposed deformation, Masonry crushing;
4. Strain is negative also in FRP zone and hence only masonry is effective, Masonry crushing.

A key turning point is the edge between fields 2 and 3 with the neutral axis position defined in eq. (6.1) with the following calculation of the associated couple of actions N and M (see eq. (6.2) and eq. (6.3)).

$$x_{2,3} = \frac{\varepsilon_{cm} \cdot d}{\varepsilon_{cm} + \varepsilon_{fu}} \tag{6.1}$$

$$N = C_m - T_f \quad \rightarrow \quad N = b\alpha f_m \beta_1 x - \varepsilon_{fu} E_f A_f \tag{6.2}$$

$$M = b\alpha f_m \beta_1 \beta_2 x^2 + \varepsilon_{fu} E_f A_f (d - x) \tag{6.3}$$

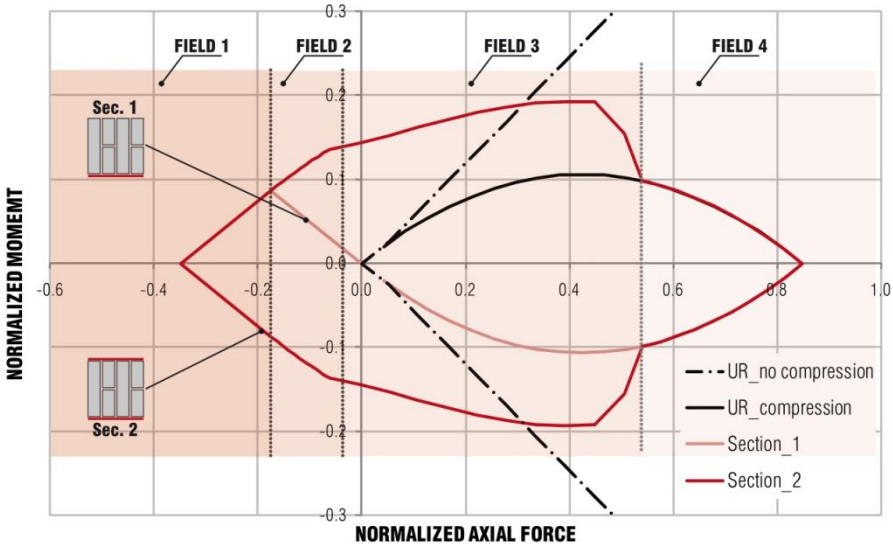


*Fig. 6.3 Resistance domains for different configurations and models*

To create resistance domains a Matlab® subroutine was created with four equations, one for each field. Fig. 6.3 shows in black domains of an unreinforced masonry section calculated according to Heyman [1996] in both conditions of infinite compressive strength (dashed line) and finite compressive strength (black continuous line). In red are reported results of the domain created with aforementioned criteria. The selection of a one side strengthening (for example only in vault extrados or intrados - Sec.1) provides for a maximum tensile action N, a bending moment due to the fibre ultimate traction times the lever arm of half section and moreover negative bending moments follow the unreinforced path. Section 2 (Fig. 6.3) instead behaves with a symmetrical domain which increase flexural resistance in both sides. A drawback of domains method concerns calculation efforts required to check the involved field and then the respective equation.

As shown in §2.4.4.1 Triantafillou's [1998] model (after called TRM), after applied on vault by Valluzzi [2001], develops a similar attempt but with limited controls on failure mode. The entity $\omega$ was introduced to normalize the area fraction of FRP on the masonry cross-section and to operate with a closed form. But, as highlight above, a closed form could be developed only within one field determined by one failure mode. In TRM there are not limitations for field 4 and lack of limits between fields 2 and 3. Indeed the first derivative of the domain's function has two zeros and it is not monotonically decreasing therefore with a convex portion (see Fig. 6.4). That minimum does not represent any physical meaning and it is evident only for small $\omega$ because increasing FRP area fraction that point moves to traction N (outside the TRM domain).

To figured out this anomalous behaviour is possible to find for each domain the turning point defined in eq. (6.1) calculating the associated N and M.

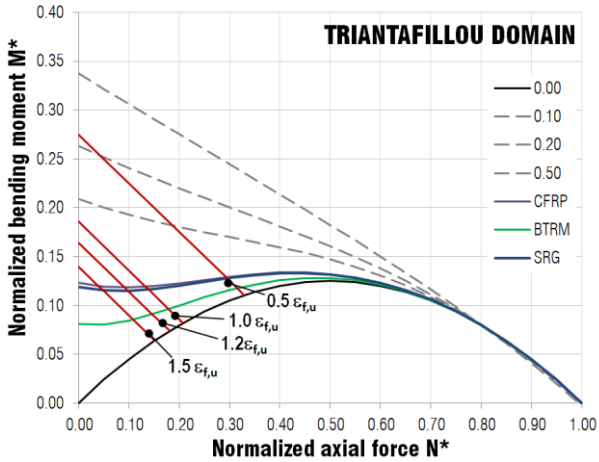


*Fig. 6.4 Triantafillou's domain with experimental applications (left) Foraboschi domain (right)*

Substituting eq. (6.1) and (2.15) into (6.2) and normalizing the axial force according (2.19), the boundary N* between field 2 and 3 is defined as:

$$N_{Ed}^{*} = \alpha\beta_1 \cdot \frac{1}{(1+\frac{\varepsilon_{f,u}}{\varepsilon_{m,u}})} - \omega\frac{\varepsilon_{f,u}}{\varepsilon_{m,u}} \tag{6.4}$$

Eq. (6.4) was used by TRM to define the $\omega_{lim}$ but with the inverse equation using the ultimate resistance axial force. This moves the problem on reinforce fraction, which is only indirectly related to failure mode, and surly not related to the whole domain. It is author's opinion to use N* as an action instead of a resistance and limiting the domain and not the reinforcement ratio. This appears clearly in Fig. 6.4 where for several values of the ultimate strain of FRP the N* on each domain was selected. The left hand of red thresholds is not still governed by crushing failure and hence by TRM domain. As reasonable the increasing of allowable strain in fibre increases the occurrence of masonry crushing. Fig. 6.4 shows also the domain of the TRM calculated in the experimental cases of this work (CFRP-SRG-BTRM).

The other model presented in literature review is by Foraboschi [2004], who seeks for a simply and efficacy descriptive model. In addition to considerations already drawn in § 2.4.4.1, Fig. 6.5 shows the adaptation of this model considering at least equilibrium equations for each acting N action the associated value M. Furthermore the minimum resistance between fibre and masonry failure are considered. The figure shows an acceptable agreement with the linearization in Filed 2 instead the limitation of masonry stress block in one third of the cross section does not allow a proper description of the domain beyond the 33 % of the ultimate strength. In the graph N* accounts also for $\beta_1$ equal to 1.

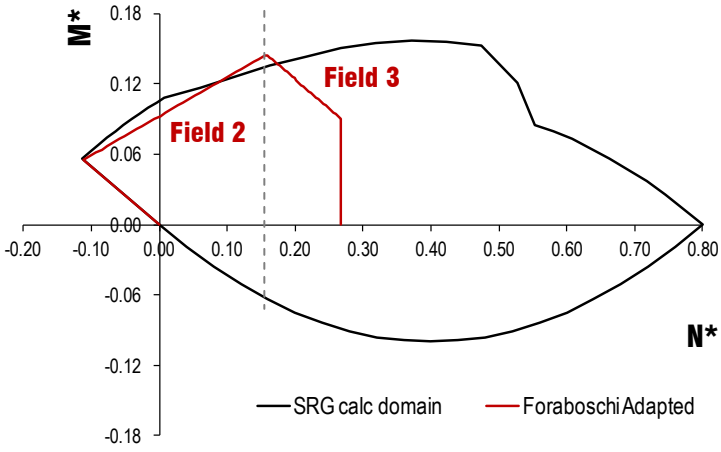


*Fig. 6.5 Adapted Foraboschi model to SRG vault*

The chosen analytical formulation of the domain, especially about the sole traction contribution of FRP, provides a sudden changing in behaviour of the strengthening path for values on the right side of the peak domain. Indeed, for high normal actions, FRP is ineffective and the cross section behaves has unreinforced.

After these observations a parametric analysis has been carried out varying several parameters affecting the overall resistance of the section.

Fig. 6.7 on the left shows the cross section domain calculated for EBR systems used in the experimental campaign. CFRP values are according experimental outcomes reported in §5.2.3. From the datasheet's values, due to the fibre design (see Tab. 5.4 ) carbon was equivalent to steel application. With the tested values, CFRP provides a smaller contribution than one stated by the manufacturer. On the left are plotted four domains with the only changing in fibre ultimate strain $\varepsilon_{f,u}$. Increasing the fibre deformation the overall strength increases. The same result is pointed out for the sole variation of $E_f$. Instead fixing the ultimate fibre stress ($E_f \cdot \varepsilon_{f,u}$) at 3000 MPa and changing simultaneously strain and stiffness (see Fig. 6.7 left) the overall contrition is not significantly different. The stiffer reinforcement provides in the worst position a smaller bending moment of 3 %. The same is highlighted by the influence analysis of the ultimate compressive strain of masonry that does not influence significantly the domain.

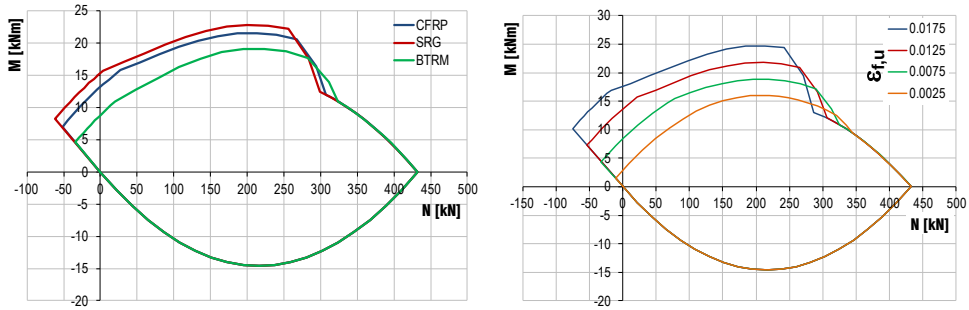


*Fig. 6.6 Cross section domain of experimental campaing (left) and influence evaluation of fibre ultimate strain $\varepsilon_{f,u}$ (right)*

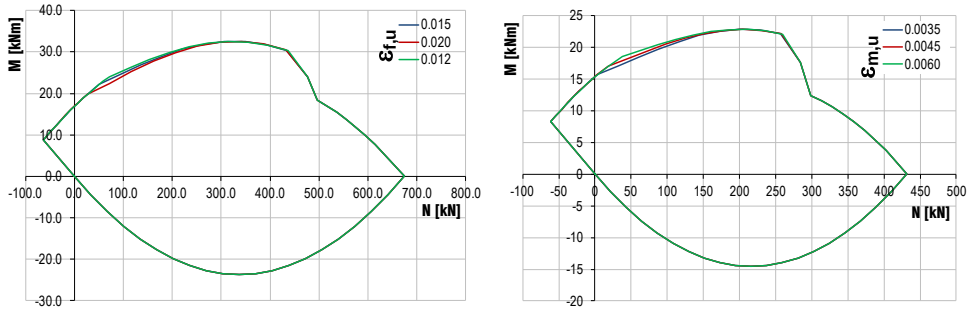


*Fig. 6.7 Influence of constant ultimate fibre stress (left), masonry ultimate strain (right)*

In conclusion, by the definition of resistance domain and the parametric evaluation is possible to figured out that reinforcing systems with same ultimate resistance could provides similar strengthening contributions. It has to be noted that ultimate strain means here the higher strain achievable in the reinforcement without compromising the overall structural element (similarly to concrete applications) whereas does not means directly fibre rupture.

### 6.1.2 *Bond issues*

In strengthening interventions with the EBR technique the bond behaviour plays indeed a crucial role affecting the overall strength of the reinforced structural element. Despite the improvement and the investigation of this behaviour is beyond the scope of this work, a comparison and some considerations on the available tools are herein presented.

The two standard approaches here examined concerns a fracture energy approach [CNR-DT 200:2012] (CNR200 in the following) and an allowable strain criterion [ACI 440.7R-2010, ACI 549.4-R-13] (ACI440 and ACI549 in the following). The first two standards refer to organic based composites meanwhile, to date, few mature guidelines and codes are available in the FRCM field. The aforementioned American standard (ACI 549) is here adopted and the Italian code adapted.

Starting from masonry properties, the fracture energy approach of CNR200 derives a maximum allowable stress in composites. Fracture energy is calculated according (6.5) where $f_{bm}$ and $f_{btm}$ are the compressive and the tensile strength of substrate respectively.

$$\Gamma_{Fd} = k_b \cdot k_G \cdot \sqrt{f_{bm} \cdot f_{btm}} \tag{6.5}$$

CNR200 suggests for the tensile brick strength the 10 % of the compressive one but this when there is lack of experimental data. It is worth to notice that in design application on existing structures the confidence factor FC must used. In case of masonry, the formulation should consider effects of mortar joints as presented in §2.2.2 but these effects are here neglected and energy is calculated on tested average features of brick (Tab. 5.2 ) and hence:

$$\sqrt{0.5(19.47 + 24.59) \cdot 0.5(3.43 + 3.54)} = 8.80\ N/mm^2 \tag{6.6}$$

Eq. (6.5) considered also the geometrical three-dimensional distribution of stresses with the $k_b$ coefficient expresses in eq. (6.7) where $b_f$ is the composite width and $b_m$ the active width on masonry. The previous formulation of the Italian

standard was similar to the FIB-14th [2011] formulation which gave no more a non dimensional quantity.

$$k_b = \sqrt{\frac{3 - b_f/b}{1 + b_f/b}} \tag{6.7}$$

The current formulation is more accurate and does not have numerical problem, and in particular when the width ratio is equal to 1 the coefficient is 1 as well. In the domain [0;1] the values lies between 1.73 and 1. CNR200 suggests $b_m$ equal to the width of the involved bricks. In practical terms, if bricks are usually about 25 cm and the minimum installed width of fibre is in the order of 10 cm the maximum value of $k_b$ is in the order of 1.45 meanwhile increasing fibre widths the coefficient tends to 1. The assumed values in the experimental case are shown in Tab. 6.1.

The main issue in the energy formulation is based on the $k_G$ empirical factor (in mm) which substantially affects the final stress value. For brick masonry the current given value is 0.031. Panizza [2010] after deep evaluations of experimental available results provides for sole bricks an average value of 0.105 ± 0.044 meanwhile Ceroni [2014] provides an mean $k_{G,m}$ value of 0.075 and a characteristic (0.05-percentile) $k_{G,k}$ value of 0.017. In conclusion this parameter is still under revision and it appears that for the characteristic figures, used for design purposes, it might be even lower than the current standard. For this application where empirical results are considered main values are assumed. All these data refers to FRP glued on site whereas there are still lack of information about mortar based application and further development are advisable. Looking at the experimental outcomes of Girardello [2012] on such systems the value of 0.031 seems suitable.

The stress allowable value is thus calculated according eq. (6.8) without any safety coefficient. The adopted values are presented in Tab. 6.2. In order to compare the American guidelines also the equivalent stain is calculated.

$$f_{fdd} = \frac{1}{\gamma_{f,d}} \cdot \sqrt{\frac{2 \cdot E_f \cdot \Gamma_{Fd}}{t_f}} \tag{6.8}$$

*Tab. 6.1 Assumed values in bond calculations*

| | $t_f$ | $b_f$ | $E_f$ | $\varepsilon_{fu}$ | $b_m$ | $\kappa_g$ | $\kappa_b$ | $\Gamma_{Fd}$ |
|---|---|---|---|---|---|---|---|---|
| | mm | mm | MPa | [%] | mm | [mm] | | [N/mm²] |
| **CFRP** | 0.170 | 100 | 309'000 | 1.20% | 275 | 0.031 | 1.390 | 0.379 |
| **SRG** | 0.084 | 250 | 196'800 | 1.50% | 275 | 0.031 | 1.047 | 0.285 |
| **BTRM** | 0.032 | 800 | 66'680 | 1.55% | 800 | 0.031 | 1.000 | 0.273 |

Fig. 6.8 shows the obtained values for the debonding stress calculated with the presented $k_G$ and the associated strain. Horizontal lines on the left refer to rupture strain, therefore for all three methods fibre rupture always occurs on basalt. In the other cases Panizza [2010] and Ceroni [2014] provide similar results, significantly higher than CNR200. It has to remind that proper values on mortar based composites are not available.

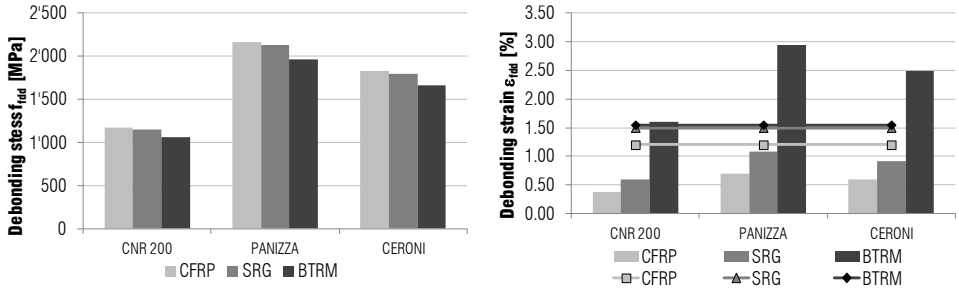


*Fig. 6.8 Calculated values of debonding stress (L) and strain (R) lines refes to rupture strains*

From facture energy and fibre properties the maximum shear stress and the optimal bond length are calculated according to CNR200 formulations reported in eq.(6.9) and (6.10) respectively.

$$f_{bd} = \frac{2 \cdot \Gamma_{Fd}}{s_u} \tag{6.9}$$

$$l_{ed} = \frac{1}{\gamma_{f,d} \cdot f_{bd}} \cdot \sqrt{\frac{\pi^2 \cdot E_f \cdot t_f \cdot \Gamma_{Fd}}{2}} \tag{6.10}$$

where $s_u$ is the ultimate slip in the $\tau$-s curve of the bond.

CNR200 provide 0.4 mm for bricks and the values in confirmed also by Valuzzi [2012] (see Fig. 2.15 right). In the case of mortar based systems there are not suggested values. In this case, looking at the behaviour of eq. (6.9) a guessed value of 0.6 mm is more conservative for such applications. About $l_{ed}$ its value is limited to a minimum of 150mm as a constructive detail.

Fig. 6.9 shows the calculated bond figures with more conservative results of CNR200 but in general with limited bond lengths. SRG and BTRM in situ test in shear §5.2.5 confirmed the observations on the effective length. It come out also that BTRM has shorter optimal bond lengths. Looking at eq. (6.10) the fibre modulus is at numerator and therefore lower modulus provide shorter bond length.

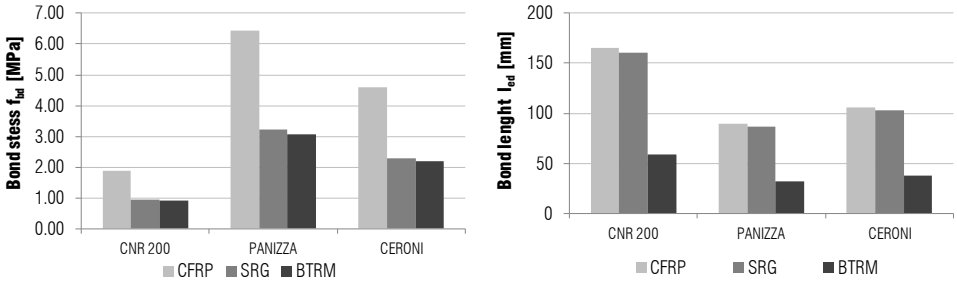


*Fig. 6.9 Calculated values of bond stress (L) and Bond length (R)*

In conclusion on vault application the sheet end debonding is unlikely, especially if there are anchorages. The standard indicates a possible increasing in stress for the intermediate debonding of a coefficient between 1 and 2 times $f_{fdd}$. CNR200 also indicates a limit of 1.5 considering the distance from the free end, in fact moving the range between 1.5 and 2.

The second approach examined is based on strain control and follows the American standard ACI440 for carbon application and ACI549 for FRCM. Also in this case the use of safety factors like $C_E$ (environmental coefficient) are not considered, moreover the American standard specifically refers to manufacturer data. Calculations are carried out for flexure-controlled failure modes. With eq. (6.11) is possible to calculate the effective strain and with eq.(6.12) the equivalent stress.

$$\varepsilon_{fe} = \kappa_m \cdot \varepsilon_{fu}^{*} \leq C_E \cdot \varepsilon_{fu}^{*} \tag{6.11}$$

$$f_{fe} = E_f \cdot \varepsilon_{fe} \tag{6.12}$$

where:

$\varepsilon_{fu}^{*}$ is the ultimate strain provided by the manufacturer.

$\kappa_m$ is 0.45 for EBR applications

To calculate the shear stress eq. (6.13) is used.

$$p_{fm} = n \cdot t_t \cdot f_{fe} \leq 260\ N/mm \tag{6.13}$$

where *n* is the number of plies.

The final value for CFRP becomes from the limitation of eq. (6.13) to $f_{fe}$ equal to 1529 MPa and $\varepsilon_{fe}$ equal to 0.64 %.

About FRCM, in case of flexure-controlled failure the standard provides a limit strain of 1.2%. The elastic modulus $E_f$ in eq. (6.12) is tensile modulus of elasticity of cracked FRCM that is here considered the modulus of the strip which is lower than the combination between mortar and fibres.

*Tab. 6.2 Calculated values for stresses in composites*

| | CERONI [2014] | | CNR200 | ACI | |
|---|---|---|---|---|---|
| | $f_{fdd,2}$ [N/mm²] | $\varepsilon_{fdd,2}$ [%] | $\varepsilon_{fdd,2}$ [%] | $f_{fd}$ [N/mm²] | $\varepsilon_{fd}$ [%] |
| **CFRP** | 2'739 | 0.89 | 0.57 | 1'529 | 0.64 |
| **SRG** | 2'698 | 1.37 | 0.88 | 2'280 | 1.20 |
| **BTRM** | 1'034 | 1.55 | 1.55 | 840 | 1.20 |

In conclusion, looking at the values calculated and reported in Tab. 6.2 it has to be noted that CNR200 is the most conservative, for FRP application. The adaptation on mortar based systems provides higher results even still conservative compared to ACI in SRG case instead under conservative for BTRM applications, controlled by fibre rupture.

Although with only three observations is pointless to draw any conclusion on bond models, at least in this case the Ceroni [2014] seems to be more effective. As already remarked all these models require more research an experimental data to be reliable. Also ACI 549, even if dedicated to FRCM, seems to need of further developments.

## 6.2 DYNAMIC DATA ANALYSIS

The analysis of the dynamic data acquired for each vaults in three conditions, pre and after intervention and pre and after damage provides some interesting outcomes. The DIA vault, with the introduction of stiff elements in only lateral quarters, completely change the dynamic behaviour and hence is not interesting to compare the pre and after strengthening intervention in this case where obviously in the strengthened case frequencies significantly increase. In particular the first flexural mode (28.57 Hz) overpasses in frequency the second flexural mode (25.44 Hz). The damage evaluation of DIA by the comparison between responses pre and after the test was unfeasible because of the vault collapse.

Tab. 6.3 shows the values obtained by dynamic identification; stars refer to torsion mode shape. The modal parameters for the undamaged condition are the same used for the model calibration in § 5.4.3.

Despite the first mode presents a strange increase in frequency, is possible to notice a frequency reduction after the test in the order of 4 % which is limited for monitoring purpose. Conversely damping notably increases in many modes

especially in first modes that involve motion in hinges and higher mass participation. Looking at MAC between the two, magnitudes are similar to model's calibration thus is not possible to detect any variation in mode shapes.

*Tab. 6.3 Dynamic results of UR vault*

| | URM | | | | | | |
|---|---|---|---|---|---|---|---|
| | PRE / AFTER TEST | | | | | | |
| | FREQ. [Hz] | DAMP. [%] | FREQ. [Hz] | DAMP. [%] | Freq. ratio | Damp. ratio | MAC |
| 1st | 14.9 | 2.0 | 16.1 | 5.3 | 1.08 | 2.67 | 0.86 |
| 2nd | 28.4 | 3.7 | 26.5 | 5.2 | 0.93 | 1.40 | 0.65 |
| 3rd | 38.3 | 4.7 | 35.3 | 4.2 | 0.92 | 0.89 | 0.94 |
| 4*th | 51.8 | 1.5 | 48.8 | 2.7 | 0.94 | 1.78 | 0.82 |
| 5th | 58.1 | - | 56.6 | - | 0.97 | - | 0.64 |
| 6*th | 75.4 | 1.6 | 73.7 | 2.2 | 0.98 | 1.38 | 0.83 |
| 7th | 78.7 | 0.9 | 78.2 | 1.4 | 0.99 | 1.54 | 0.68 |
| 8*th | 109.7 | 0.3 | 106.9 | - | 0.97 | - | 0.70 |
| 9th | 142.9 | 1.6 | 138.0 | 0.2 | 0.97 | 0.13 | 0.76 |

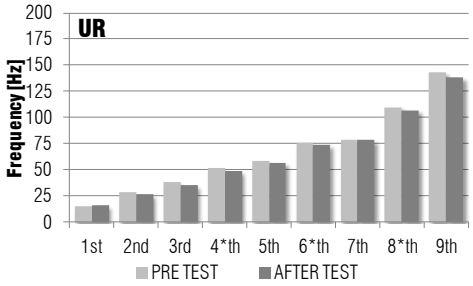


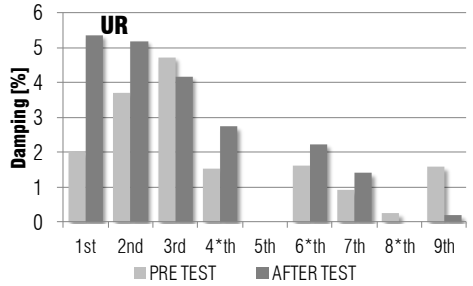


Tab. 6.4 shows the values obtained for the CFRP vault. In this case is possible to analyse the strengthening contribution which increases of 1.8 times the first mode. The stiffness increasing also caused by the geometrical distribution of the reinforcement, highlights major effects on the first mode whereas for higher modes the increasing has an average of 20 % (see Fig. 6.10). About damping ratio the third mode shows a wired increase whereas in general there is a reduction of the damping.

Damaged condition shows the highest variation in the first mode too with a frequency drop of 34%. Other modes have a frequency 0.80 times the initial one. The damping general increases but its trend is not homogeneous. The diagonal values of MAC, even for same mode shape presents lower values that are directly related to damages which changes mode shapes hence decreasing the mode correlation.

*Tab. 6.4 Dynamic results of CFRP vault*

| 02_CFRP | | | | | | | | | |
|---|---|---|---|---|---|---|---|---|---|
| | PRE / AFTER STR | | PRE / AFTER TEST | | | | | | |
| | Freq. ratio | Damp. ratio | FREQ. [Hz] | DAMP. [%] | FREQ. [Hz] | DAMP. [%] | Freq. ratio | Damp. ratio | MAC |
| 1st | 1.80 | 0.66 | 26.8 | 3.0 | 17.6 | 3.9 | 0.66 | 1.28 | 0.78 |
| 2nd | 1.08 | 1.13 | 30.8 | 3.3 | 28.4 | 2.7 | 0.92 | 0.83 | 0.71 |
| 3rd | 1.32 | 4.08 | 50.6 | 1.1 | 39.7 | 2.1 | 0.78 | 1.85 | 0.53 |
| 4*th | 1.04 | 0.86 | 53.9 | 1.8 | 44.3 | 3.3 | 0.82 | 1.84 | 0.85 |
| 5th | 1.31 | - | 75.9 | 1.8 | 60.6 | 2.5 | 0.80 | 1.35 | 0.77 |
| 6*th | 1.12 | 0.62 | 84.5 | 2.6 | 69.3 | 1.0 | 0.82 | 0.40 | 0.74 |
| 7th | 1.46 | 0.27 | 114.8 | 3.4 | 89.8 | 2.6 | 0.78 | 0.78 | 0.83 |
| 8*th | 1.25 | 0.12 | 136.9 | 2.0 | 107.6 | 2.1 | 0.79 | 1.05 | 0.90 |
| 9th | 1.04 | 0.73 | 149.2 | 2.1 | 116.7 | 2.3 | 0.78 | 1.08 | 0.49 |

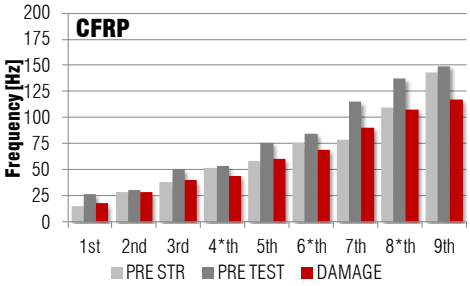


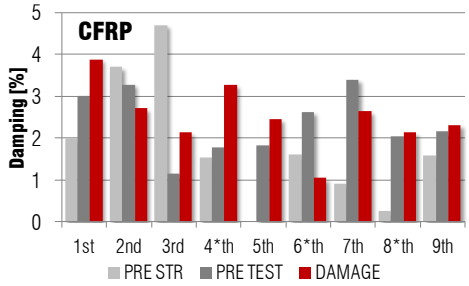


Tab. 6.5 and Tab. 6.6 show the dynamic response of SRG and BTRM vaults respectively, conclusions are drawn together later on.

*Tab. 6.5 Dynamic results of SRG vault*

| SRG | | | | | | | | | |
|---|---|---|---|---|---|---|---|---|---|
| | PRE / AFTER STR | | PRE / AFTER TEST | | | | | | |
| | Freq. ratio | Damp. ratio | FREQ. [Hz] | DAMP. [%] | FREQ. [Hz] | DAMP. [%] | Freq. ratio | Damp. ratio | MAC |
| 1st | 2.00 | 0.77 | 29.8 | 2.6 | 15.5 | 3.6 | 0.52 | 1.39 | 0.76 |
| 2nd | 1.23 | 1.47 | 34.9 | 2.5 | 23.3 | 3.5 | 0.67 | 1.42 | 0.51 |
| 3rd | 1.58 | 3.42 | 60.4 | 1.4 | 35.6 | 3.3 | 0.59 | 2.43 | 0.63 |
| 4*th | 1.24 | 0.84 | 64.4 | 1.8 | 41.1 | 2.4 | 0.64 | 1.31 | 0.83 |
| 5th | 1.52 | - | 88.2 | 0.6 | 46.4 | 2.8 | 0.53 | 4.61 | 0.46 |
| 6*th | 1.22 | 2.19 | 92.3 | 0.7 | 63.7 | 2.6 | 0.69 | 3.57 | 0.79 |
| 7th | 1.59 | 0.27 | 125.3 | 3.4 | 76.0 | 2.8 | 0.61 | 0.83 | 0.74 |
| 8*th | 1.42 | 0.12 | 155.3 | 2.0 | 93.4 | 2.1 | 0.60 | 1.06 | 0.86 |
| 9th | 1.18 | 0.85 | 168.7 | 1.8 | - | - | - | - | - |

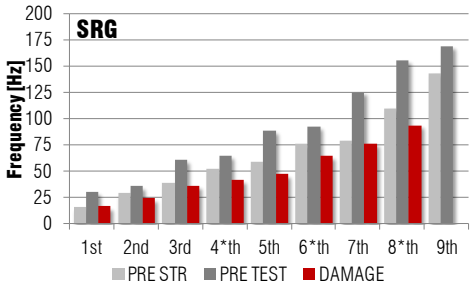


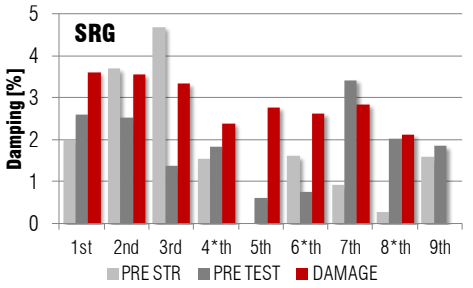


*Tab. 6.6 Dynamic results of BTRM vault*

| BTRM | | | | | | | | | |
|---|---|---|---|---|---|---|---|---|---|
| | PRE / AFTER STR | | PRE / AFTER TEST | | | | | | |
| | Freq. ratio | Damp. ratio | FREQ. [Hz] | DAMP. [%] | FREQ. [Hz] | DAMP. [%] | Freq. ratio | Damp. ratio | MAC |
| 1st | 2.33 | 0.81 | 34.7 | 2.5 | 30.0 | 3.6 | 0.87 | 1.45 | 0.41 |
| 2nd | 1.27 | 4.70 | 35.9 | 0.8 | 37.6 | - | 1.05 | - | 0.81 |
| 3rd | 1.65 | 10.56 | 63.2 | 0.4 | 63.5 | 2.0 | 1.00 | 4.47 | 0.53 |
| 4*th | 1.48 | 1.00 | 76.5 | 1.5 | 72.7 | 2.2 | 0.95 | 1.46 | 0.98 |
| 5th | - | - | - | - | 68.9 | 2.0 | | - | |
| 6*th | 1.38 | 2.87 | 103.9 | 0.6 | 104.2 | 2.7 | 1.00 | 4.84 | 0.64 |
| 7th | 1.92 | 1.91 | 151.3 | 0.5 | 130.6 | 2.5 | 0.86 | 5.19 | 0.64 |
| 8*th | 1.51 | 0.12 | 165.4 | 2.1 | 156.5 | 2.3 | 0.95 | 1.08 | 0.98 |
| 9th | 1.35 | 0.61 | 192.5 | 2.6 | 174.1 | 2.3 | 0.90 | 0.89 | 0.86 |

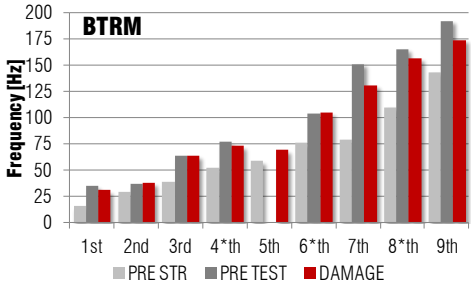


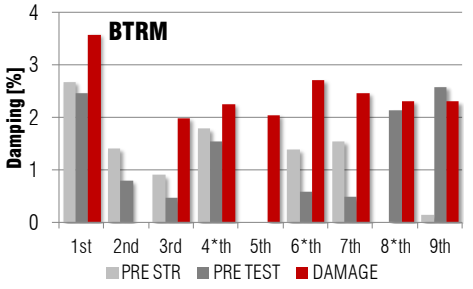


Fig. 6.10 presents an overview of the influence of strengthening on frequencies. The greatest increase is always related to the first mode which follows the shape of the four hinges mechanism. The most effective EBR action is against this global mode; instead higher modes are less increased in stiffness. Due to the fibres concentration in the middle of the cross section, the three modes in torsion (4th, 6th, 8th) are less affect by stiffening. It is also possible to recognise the different stiffness of each system. The diffuse intervention with basalts net, that

covers the entire vault surface, provides the highest increase; on the other hand carbon, that is limited to 10 cm, gives the minor contribution whereas SRG is in an intermediate solution and this is also clear in torsion modes. Such relationships in stiffness are confirmed also by static tests considering the modulus of the first elastic branch as reported in §5.3.6. In conclusion dynamic evaluation properly catches changing in stiffness according to static tests in the un-cracked situation.

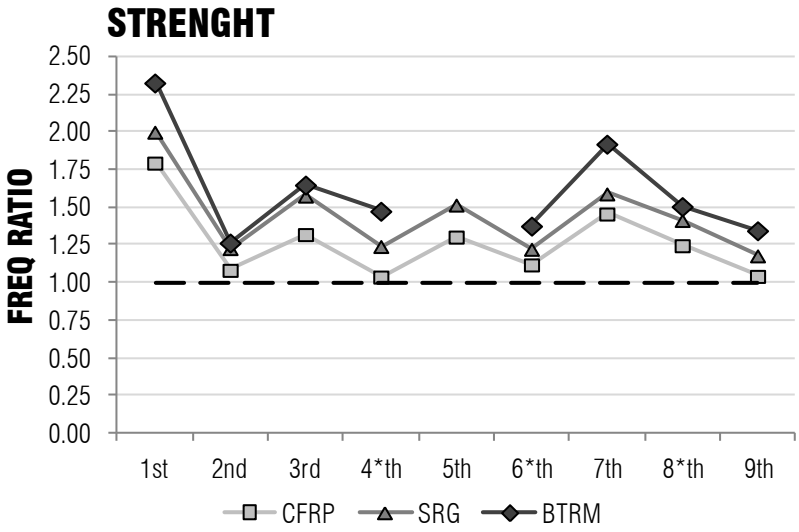


*Fig. 6.10 Frequency ratios due to strenghening intervention for all cases*

An overall analysis on variations in modal parameters after the damage occurrence is presented in Fig. 6.11. According to outcomes based on EBR interventions the frequency analysis provides reliable evaluations of the occurred damage in masonry elements. It is relevant to notice how the mechanism failure, which is lumped in four hinges, does not lead to frequency drops because related to rigid body motions. The average ratio in case of UR and BRTM vault lies around 0.95. The masonry crushing is instead more related to the rise of damage within the constitutive element and brings to stiffness variation and hence on frequency. The most damaged vault (SRG) which reached high deformations and spread cracking presents frequencies in the order of the 60% the undamaged conditions. For CFRP the ratio was 0.8. Also in this case the first mode is the most representative of the phenomena. Equal conclusions, with a theoretical damping increase, are not possible for damping where data are scattered and hence any conclusion was drawn.

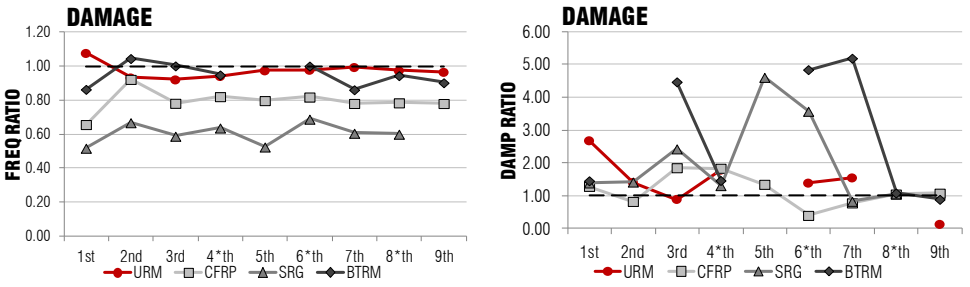


*Fig. 6.11 Frequency (left) and damping (rigth) ratio due to onset of damage of all cases*

Fig. 6.12 shows diagonal values of MAC matrix considering damaged condition. It is possible to conclude that, probably gained by the concentrated load in a quarter, damage is not detected only in frequency but also in variation of the mode shape. MAC values pointed out an increasing disagreement between modes pre and after tests. In order to remark this consideration the MAC matrix beyond the pre and after test (green bars in Fig. 6.12) was calculated as well between two damaged vaults (CFRP and SRG, red bars in Fig. 6.12) finding a better agreement. Despite the different damage degree the similar damage locations provide a similar behaviour demonstrating the changing also in mode shape.

Further developments could improve the mode shape analysis with the use of NMD [Gentile 2007] and COMAC [Allemang 1993] in order to better detect the damage magnitude and location.

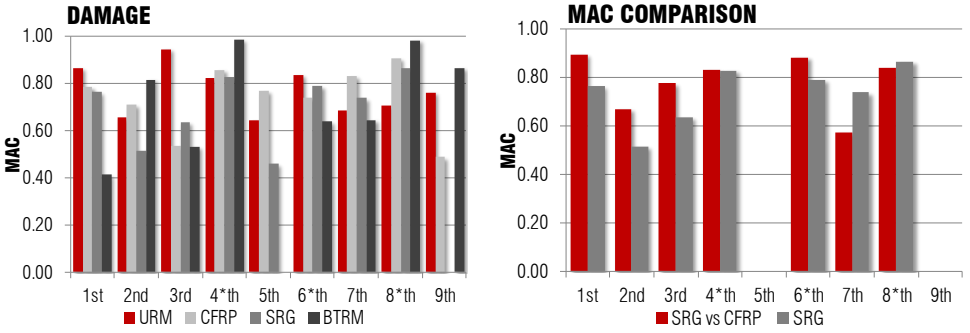


*Fig. 6.12 MAC value for each case pre and after damage (L), compared between vaults (R)*

In conclusion the NDT dynamic identification proves to be an effective tool in order to check both, quality of interventions and damages. It shows a good sensitiveness on damaged situation properly evaluating changed conditions. This confirms the key role and the promising imply of dynamic analysis in SHM. It worth to notice that refined systems are used in SHM because the damage degrees here evaluated are more severe and extent that what should be detected by a monitoring

system. Moreover this effort can be sustainable for bridges with a convenient number of dedicated sensors.

Use high number of sensors in one setup demonstrates also to be a valid option with the possibility to check a high number of modes otherwise difficult to be detected and controlled. The use of random impacts with hammer also improves the identification efficacy with good results. As drawback the awaited improvement in damping evaluation was not reached with this technique. It is also relevant to remind that EFDD with a damping estimation in frequency domain do not guarantee enough performances.

## 6.3 ANALYTICAL MODELS

### 6.3.1 *Limit analysis*

One of the greatest difficulties of kinematic analysis before the estimation of the critical load is the hinge positioning, which is indeed the crucial issue. Static assessment of bridges and the seismic assessment of entire buildings rely on this calculation method to figure out the critical multiplier of the structure. Neverless it is in general difficult to verify the real accuracy of calculation.

In the following, with the availability of experimental proofs, kinematic analysis and block analysis by RING will be compared. In this case all parameters were fixed and geometrical features are known. Moreover the joint position is defined by experimental observations and hence overcome this initial trouble. Anyway by means of FEM or thrust line analysis the joints position was confirmed. Fig. 6.13 shows the analysed four hinge mechanism. In order to fulfil the safe theorem the critical multiplier is the actual multiplier if and only if yield criteria are respected in all sections. Therefore the hinge regression should take into account.

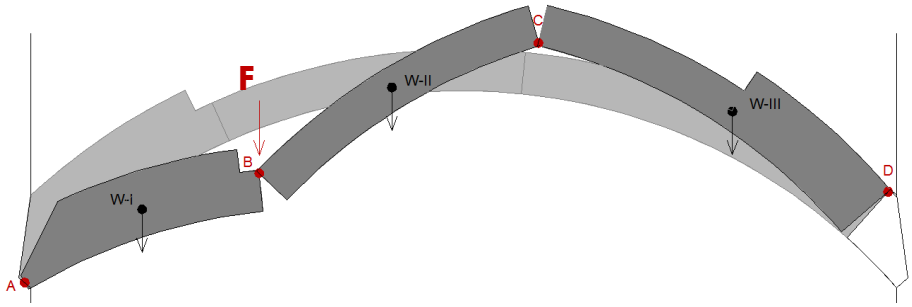


*Fig. 6.13 Considered four hinges failure mechanism*

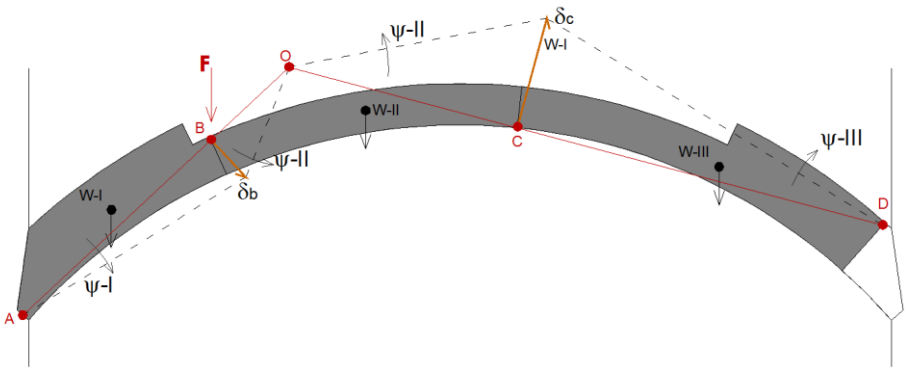


*Fig. 6.14 Used parameters to calculate virtual work*

According to the principle of virtual work once the total sum of virtual works by internal and external forces is null the system is in equilibrium (see eq. (6.14)).

$$\sum_{i=1}^{n} \mathbf{F}_i \cdot \boldsymbol{\delta}\mathbf{P}_i = 0 \tag{6.14}$$

The general definition of forces $\mathbf{F}_s$ can be divided, for the analysed case, in work of the selfweight and the work of the applied load F as:

$$\sum_{s=1}^{3} \mathbf{W}_i \cdot \boldsymbol{\delta}\mathbf{G}_i + \mathbf{F} \cdot \boldsymbol{\delta}\mathbf{B} = 0 \tag{6.15}$$

In order to define the virtual displacement the position of the rotation centre O is identified by the intersection of lines matching A and B and C and D respectively. The virtual displacement for each point follows eq. (6.16) where the angular vector $\boldsymbol{\psi}$ is different for each rigid body but all can be expressed as function of one arbitrary rotation.

$$\delta\mathbf{P} = \delta\mathbf{H} + \boldsymbol{\psi} \times \mathbf{HP} \tag{6.16}$$

In this particular case there are only vertical actions and hence the scalar product between virtual displacements and forces will further referred to vertical displacement. Considering the load acting on hinge B the resulting load is calculated according eq. (6.17).

$$F = \frac{\sum_{i=1}^{3} W_i \delta y_{g,i}}{\delta B_y} \tag{6.17}$$

The first analysis was carried out considering Heyman [1996] hypothesis of infinite compressive strength with values reported in Tab. 6.7 and Tab. 6.8 obtaining a critical load of 23.6 kN, 20 % higher than real one. It has to be considered that in flat arches, or when the rise is not high compared with thickness, the hinge regression within the vault thickness affects more severely the solution. Despite the

experimental comparison the first solution found could not be considered the exact solution because does not control yielding strengths. To point out the influence of hinge regression, the experimental load was reached with $f_m$ equal to 2.9 MPa and obtaining a critical load of 19.04 kN. This estimation was carried out by an implemented algorithm explained later on in § 6.3.3. Such solution highlights on one hand the role of strength evaluation but on the other hand remarks the power of the limit analysis and the uniqueness theorem.

*Tab. 6.7 Posistions of hinges, rotation centre and block centroids*

| | A [mm] | B [mm] | C [mm] | D [mm] | O [mm] | $G_1$ [mm] | $G_2$ [mm] | $G_3$ [mm] |
|---|---|---|---|---|---|---|---|---|
| X | 0 | 1185 | 3197 | 5598 | 1641 | 579 | 2249 | 4550 |
| Y | 0 | 1200 | 1259 | 638 | 1662 | 689 | 1290 | 971 |

*Tab. 6.8 Virtual work of blocks selfweight*

| | L [mm] | θ [rad] | P [kN] | $\delta_g$ [mm] | $P\delta_g$ [kNm] |
|---|---|---|---|---|---|
| Block I | 1686 | 1.0 | 9.01 | 579 | 5.22 |
| Block II | 2013 | -2.6 | 7.85 | -1582 | -12.42 |
| Block III | 2480 | 1.7 | 11.96 | -1766 | -21.13 |

According to da Porto [2007] the analysis was also extended to the capacity curve looking for the rotation which implies a null value of the un-stabilizing load and in this case equal to 5.30° for block 1. As control point, according to the other analyses, the key stone was used and an ultimate vertical displacement $d_k$ of 134 mm and horizontal of 44 mm of were calculated. The two calculated capacity curves are plotted in Fig. 6.31.

### 6.3.2 *Block analysis*

In addition to the kinematic analysis performed with the implemented algorithm a comparison was provided by kinematic analysis made with block discrete analysis according to Orduña [2003] and Gilbert [2007] by the academic software RING 3.0® (limtstate). The analysis was performed with a density of 1800 kg/m$^3$ consistently with other calculations, a friction coefficient of 0.6 and masonry strength of 3 MPa, due to the aforementioned consideration on hinges regression. The resulting critical load was of 19.1 kN.

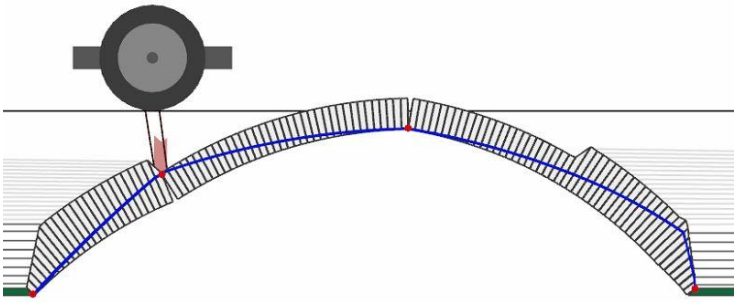

*Fig. 6.15 Kinematic analysis and thrust line in UR vault (RING)*

Values and hinges positions (see Fig. 6.15) agrees with those found by hand calculation by the implemented algorithm and experimentally observed. RING accounts for the friction coefficient affecting the overall response but neglecting cohesion. For this reason for low value of N a higher friction coefficient may appear. Tab. 6.9 shows the variation of the critical load depending on compressive strength and friction coefficient. It is worth to notice that the analysis, which check yield criteria properly varying the overall resistance. In any case for unreinforced vaults the two boundary limits are not very far.

*Tab. 6.9 Parametric analysis of critical loads varying strength and friction*

| $f_{cm}$ [MPa] | μ | | | |
|---|---|---|---|---|
| | **0.4** | **0.5** | **0.6** | **0.7** |
| **2** | 17.0 | 17.8 | 18.4 | 19.0 |
| **3** | 17.6 | 18.4 | 19.1 | 19.6 |
| **4** | 17.9 | 18.7 | 19.4 | 20.0 |
| **5** | 18.1 | 18.9 | 19.7 | 20.2 |

After the evaluation of the URM condition with satisfactorily results for both methods, the further step is to analyse the strengthen case.

Once again, the model definition in RING shows the greatest sensitivity to geometry. For instance the vaults thickness of bricks was entirely considered on support although in the real case brick were inside the wall, the span was hence considered looking at the intrados value. Moreover on the right hand the addition of a resistant material was necessary to simulate the wall influence. Once all these cautions were taken the model provides results consistent with actual mechanism observations and presented in Fig. 6.16.

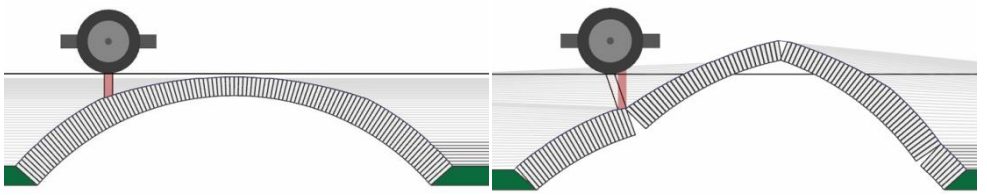

*Fig. 6.16 RING model for EBR strengthened vault, before (L) and after (R) the mechanism*

The used software is also suitable for reinforced cross section with ductile reinforcement as for example steel. The reason of this limitation is based on the definition of a fixed yielding force kept constant. To overcome this issues a proposed algorithm will be further presented but a parametric analysis was anyway performed to assess the possibility of use this tool in usual practice and it actually figured out to be a valuable solution.

The first studied parameter was the friction coefficient between 0.5 and 0.6 considering the outcomes of UR vault. As expected in reinforced cases the critical load is not affected by friction changing because the axial action becomes higher. The reinforcement was considered on the vault extrados with an ultimate tensile force and anchored on both supports.

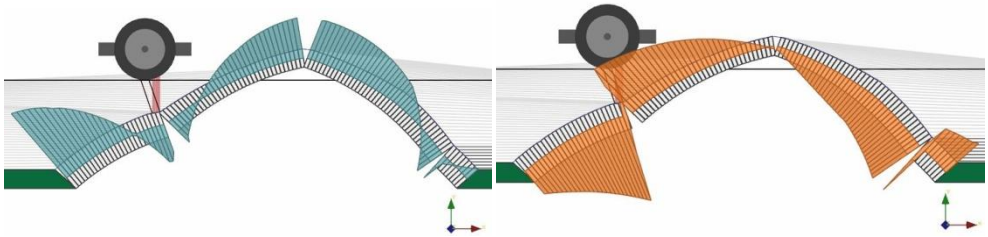

*Fig. 6.17 Bending moment diagram (left) and shear diagram (right)*

Tab. 6.10 shows critical loads F obtained varying material resistances namely masonry compressive strength $f_{cm}$ and the ultimate tensile action of FRP ($T_f$).

*Tab. 6.10 Critical load F of the strengthening vault for different values of T and $f_{cm}$*

| T | $f_{cm}$ [MPa] | | | | |
|---|---|---|---|---|---|
| [kN] | 2 | 3 | 4 | 5 | ∞ |
| 0 | 37.6 | 39.6 | 40.6 | 41.1 | 43.4 |
| 10 | 48.1 | 51.1 | 52.7 | 53.6 | 57.4 |
| 20 | 57.8 | 61.9 | 64.2 | 65.6 | 71.4 |
| 30 | 66.9 | 72.3 | 75.3 | 77.2 | 85.4 |
| 40 | 75.2 | 82.1 | 86.0 | 88.5 | 99.3 |
| 50 | 82.9 | 91.5 | 96.4 | 99.5 | 113.0 |
| 60 | 90.1 | 101.0 | 106.0 | 110.0 | 127.0 |
| 70 | 96.8 | 109.0 | 116.0 | 120.0 | 141.0 |
| 80 | 103.0 | 117.0 | 125.0 | 130.0 | 155.0 |

Table results are also plotted in Fig. 6.18 where is possible to observe failures depending on masonry with increased $T_f$. The variability showed by such results remarks indeed, for strengthened sections, the key role played by material properties. It is therefore crucial, to obtain reliable results to properly estimate mechanical properties of materials.

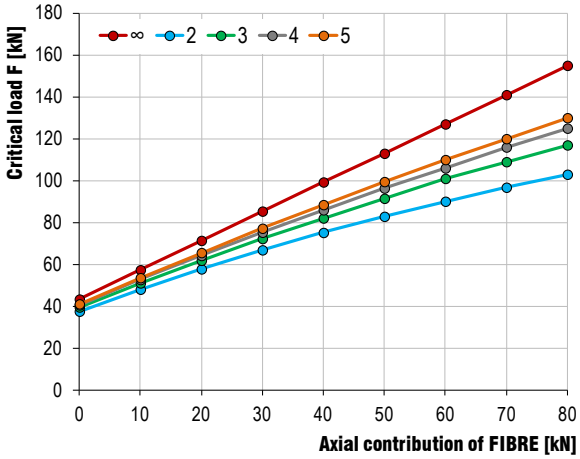


*Fig. 6.18 Evaluation of critical load depending on tensile action of FRP and $f_{cm}$*

Form the masonry compressive stress obtained in the UR vault the selected value is 3 MPa. It is worth to notice that only the addition of masonry regularization, that adjust steps on quarters, increases the ultimate vault capacity to 39.6 kN which is 2 times the initial resistance. By the proposed algorithm this value is confirmed and 41.1 kN was calculated. Such results point out the crucial contribution of construction details and care in masonry intervention. Unfortunately it was not possible to perform another test with this vault configuration to really proof the estimated increasing by experimental measurements. The increased ratio of ultimate resistance is therefore reduced for EBR application with the respect of Tab. 5.7 similarly to analytical outcomes.

For all the analysed cases, both bending moment M and normal action N where calculated. The ratio between them provides the eccentricity *e* which can be used as thrust line according [Rocà et al. 2007]. Fig. 6.19 shows, the thrust line position along bricks. The unreinforced vault (0 kN in purple) reach vault's edge in each hinges thus providing the critical load. It has to be noted that, at least in the unreinforced configuration, depending on compressive masonry strength thrust line could approach the edge to maximum a half of the stress block depending on acting N.

Form the limit analysis is also possible to confirm hinges position with the observed one. The addition of tensile strength allows thrust line beyond section edge. The anchorage on hinge A and fibre in hinge C permit significant increases of bending moment. According to outcomes pointed out with Fig. 6.18, major improvements are given by smaller tensile strength.

From the analysed curves is possible to estimate the FRP maximum stress corresponding to the experimental load. In case of SRG application, the ultimate

tensile force $T_f$ is 44.5 kN which provides a strain $\varepsilon_f$ of 1.08% very close to 1.07%, the maximum measured on fibre in $D_4$ (Tab. 5.10).

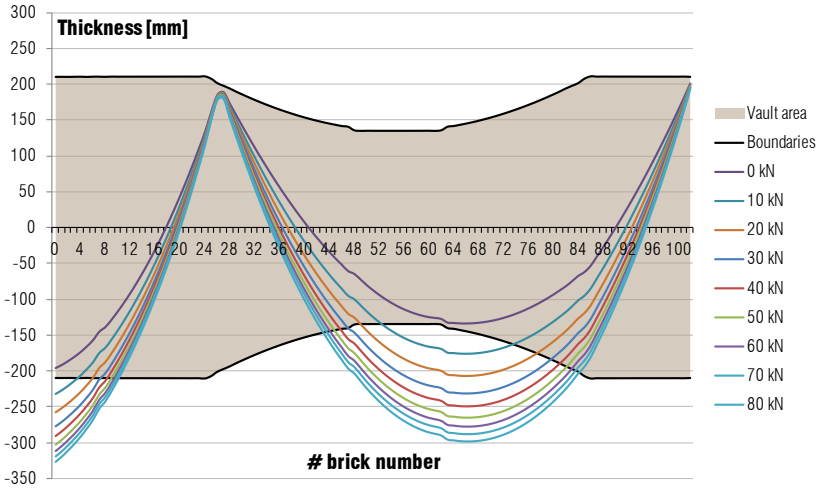


*Fig. 6.19 Eccentricity variation along bricks for several strengthening tension*

Once selected the tensile resistance of SRG a focus on actions are shown in Fig. 6.20 and Fig. 6.21. In the first image are reported N and M. The maximum bending moment is not reached in hinge C but in hinge on support (A). Moreover is clear, especially in axial force, that selfweight is significantly lower than the ultimate force.

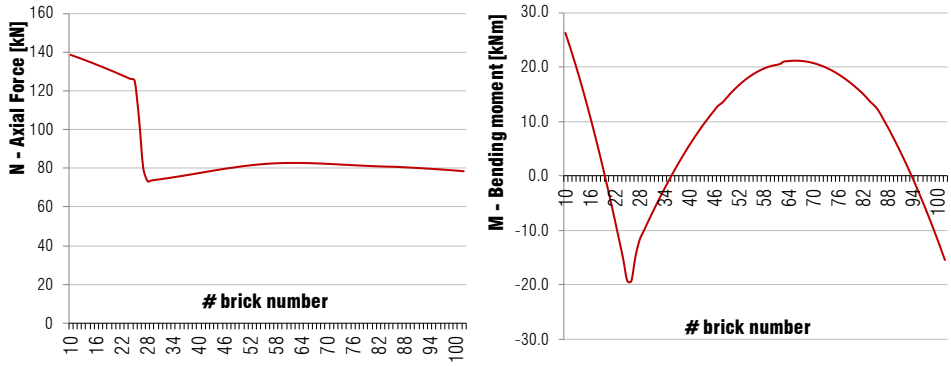


*Fig. 6.20 Variation of N (left) and M(right) along bricks for an SRG axial resistance of 44.5 kN*

Fig. 6.21, on the left, shows the shear action on joints. On the right is analysed the friction coefficient by the ratio between N and S on each joint. The coefficient should be calculated with the compressive component in the cross section and hence by C (see eq.(6.2)). The higher values of $\mu_{Ed}$ are inside red hatches which define portions with negative moment that does not involve FRP. In these sections N corresponds to C and therefore the presented friction coefficient is

correct. It is interesting to notice that, in addition to the loading point the worst joint is in support D due to the smaller N value. This outcome is also confirmed by experimental observation (see §5.3.4).

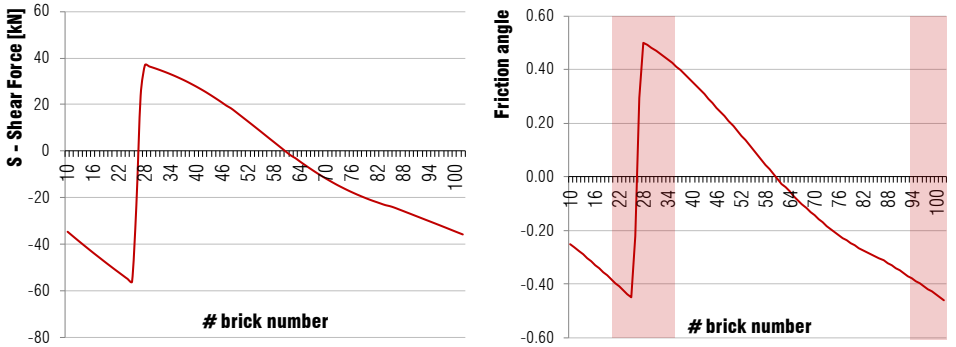


*Fig. 6.21 Variation of S (left) along bricks for an SRG axial resistance of 44.5 kN and activated friction coefficient (right)*

The analysis was then extended to all EBR vaults and the modified parameter was the $T_f$. According to eq. (6.2) $E_f$ and $A_f$ are known instead the effective strain $\varepsilon_{f,u}$ has to be defined (see Tab. 6.11). The ultimate critical load of the vault F was therefore calculated by different values of $\varepsilon_{f,u}$ based on bond issues (§ 6.1.2) and the experimental deformation measured.

Due to the evident FRP debonding in anchorage of CFRP vault, that contribution was neglected in calculations. Tab. 6.12 reports the obtained figures compared with experimental loads. Fig. 6.22 shows these results in a histogram.

Figures coming from CNR debonding load seem to better agree with the actual value. About BTRM the CNR adapted does not match the actual behaviour.

*Tab. 6.11 Table of ultimate strain and relative FRP ultimate action according three methods*

| | Ceroni | | CNR | | ACI | | EXP | |
|---|---|---|---|---|---|---|---|---|
| | T [kN] | $\varepsilon_f$ [%] | T [kN] | $\varepsilon_f$ [%] | T [kN] | $\varepsilon_f$ [%] | T [kN] | $\varepsilon_f$ [%] |
| **CFRP** | 46.6 | 0.89 | 29.9 | 0.57 | 33.5 | 0.64 | 43.6 | 0.83 |
| **SRG** | 54.7 | 1.37 | 35.2 | 0.88 | 47.9 | 1.20 | 42.7 | 1.07 |
| **BTRM** | 27.8 | 1.55 | 27.8 | 1.55 | 21.5 | 1.20 | - | - |

*Tab. 6.12 Table of estimated critical loads by presented methods*

| | Ceroni [kN] | CNR [kN] | ACI [kN] | $\varepsilon_{EXP}$ [kN] | $P_{EXP}$ [kN] |
|---|---|---|---|---|---|
| **CFRP** | 75.50 | 63.00 | 66.40 | 66.70 | **58.48** |
| **SRG** | 96.00 | 77.60 | 89.80 | 84.90 | **86.64** |
| **BTRM** | 70.10 | 70.10 | 63.50 | - | **57.75** |

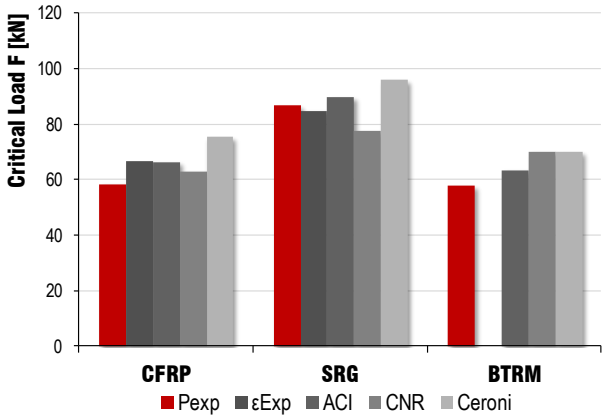


*Fig. 6.22 Evaluation of critical load for different methods compared with the experimental one*

About the vault reinforced with the traditional introduction of diaphragms the block analysis, as well as the kinematic analysis with the algorithm provide wrong results. Despite the position of hinges by RING (Fig. 6.23) agrees with test and the algorithm use those positions results are not reliable. This is probably due to particular position between hinges and load. It is shown in the kinematic scheme of Fig. 6.24 where the rotation centre O is very close to the load position and to hinge B. The load increasing provokes to increase hinges regression which can led to three hinges and therefore a labile (unstable) structure. Moreover the compression deformation can enhance the problem and lead to a snap-through failure that in masonry arches results in total failure. Unfortunately, the load position in this intervention returns sensitivity on uncertainties too high to be analysed in analytical terms.

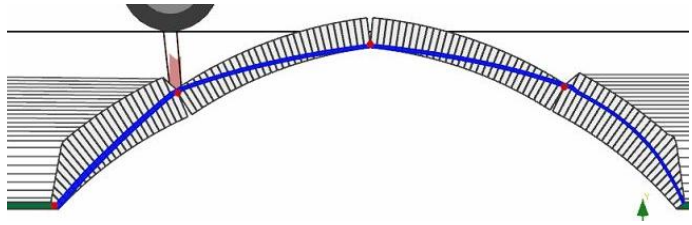

*Fig. 6.23 (left) and block analysis (right*

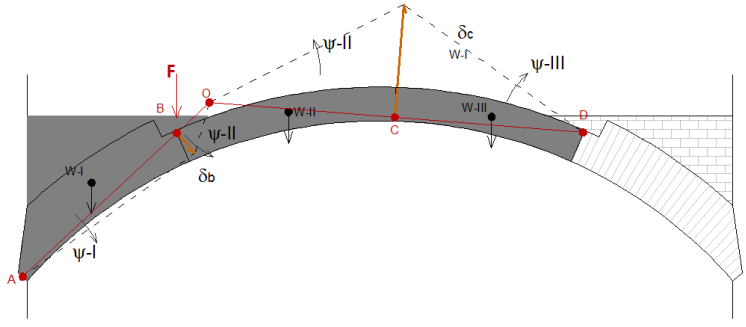


*Fig. 6.24 Diagram for the kinematic analysis of DIA vault)*

### 6.3.3 *Proposed algorithm*

Since Heyman [1996] developments, one of the most promising tools to analyse vaults is the kinematic analysis of four hinges mechanism in addition to the thrust line analysis. The first method requires iterative solutions, or prior analysis, to define hinges positions whereas the second requires iterative analysis to find the minimum thrust line. With the introduction of reinforcement both methods need an updating. As presented in literature review this need led to the formulation of some models especially concerning reinforced masonry with steel rebar. A method using the thrust line is suggested by Roca [2007], a modified four hinge mechanism which uses kinematic analysis by Chen [2007], a block analysis by Gilbert [2007] and an unbounded tendon model by D'Ambrisi [2013].

The aim of the proposed algorithm is a first attempt to overcome the differences introduced by FRP which results in hypotheses disagreement.

Experimental tests and models presented so far remarked the importance to consider:

i. finite compressive strength of masonry material
ii. FRP ultimate contribution

The presented literature models do not face, at least contemporarily:

iii. friction between FRP and masonry
iv. linear behaviour of FRP

For example Roca [2007], Chen [2007], and Gilbert [2007] neglect hypothesis *iv* whereas D'Ambrisi hypotheses *i* and *iii*.

The method relies on uniqueness theorem by means of lower and upper bound theorems and follows the flow chart drawn in Fig. 6.26. In order to be a simple method the critical load is defined by virtual work analysis which is faster than trust line. The first step is the definition of hinges positions that could be carried out iteratively, moving the initial position, or defined by other tools for instance thrust line of the unreinforced vaults or FEM analysis. All the aforementioned methods agree with experimental positions and therefore the hinges initial positions are herein defined.

A simple and fast way to estimate the critical load is the principle of virtual work. In the algorithm is defined as eq. (6.18)

$$\sum_{i=1}^{n} W_i \delta_i + \sum_{i=1}^{m} F_i \delta_i + \lambda \sum_{i=1}^{k} P_i \delta_i = \sum_{i=1}^{o} \Delta E_i \qquad (6.18)$$

where:

$W_i$ are vectors of dead loads

$F_i$ are vectors of live loads

$P_i$ are the estimated loads associated to a critical multiplier $\lambda$

$\Delta E_i$ are internal works provided by strengthening

$\delta_i$ is the associated relative virtual vector of displacement in each application points.

The estimation of $\lambda$ by this equation provides the critical multiplier by the upper bound therefore it could be greater or equal to the actual value. A problem that rises in FRP applications, where the reinforcement behaves linearly, is the definition of work. Indeed, with a fixed tensile force $T_f$ the energy provided by that elements can be evaluated as eq. (6.19) where the tensile force is multiplied by the virtual displacement.

$$\Delta E_i = T_f \cdot \Delta l_i \tag{6.19}$$

$$\Delta l_i = (\theta_i + \theta_{i+1}) \cdot (d - \beta_2 x) \tag{6.20}$$

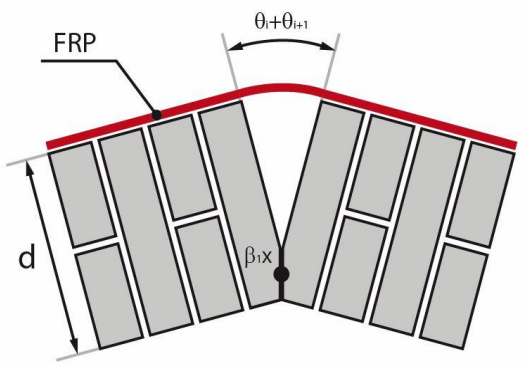


*Fig. 6.25 Hinge model for the calculation of virtual deformation*

In particular, in i-th hinge (see Fig. 6.25), the deformation $\Delta l_i$ of the reinforcement is provided by the distance to the pin centre times the internal rotation (eq. (6.20)). That angle is the sum of the virtual rotations of the two involved blocks. It has to be noted that actually the assumption of eq. (6.19) should be improved for linear material with the spring potential energy associated and defined in eq. (6.21) where the deformation $\Delta l_i$ is according eq.(6.20).

$$\Delta E_i = \frac{1}{2} \cdot \frac{E_f A_f}{L} \cdot \Delta {l_i}^2 \tag{6.21}$$

Although theoretically rigorous and correct, the problem in this equation concerns the spring axial stiffness, that in addition to known parameters as $E_f$ and

$A_f$ accounts for the length L which describes the distance between the two point involved. This quantity is very hard to define in terms of:

- actual bond behaviour, looking at few centimetres of experimental test (see Fig. 5.31),
- effective length of bond models (see §6.1.2),
- distance between two points with zero strain (Fig. 6.19).

In facts, crack opening involved a more spread portion and deformations are not lumped in one hinge. The length might be calculated similarly to concept of concrete beams where the EBR reinforcement is measured along the positive moment with the addition of two effective lengths at each end. It is advisable that future works may deepen this point defining a proper value of L but the variability of such quantity does not allow so far its reliable use. To date is thus used eq. (6.19) rather than eq. (6.21).

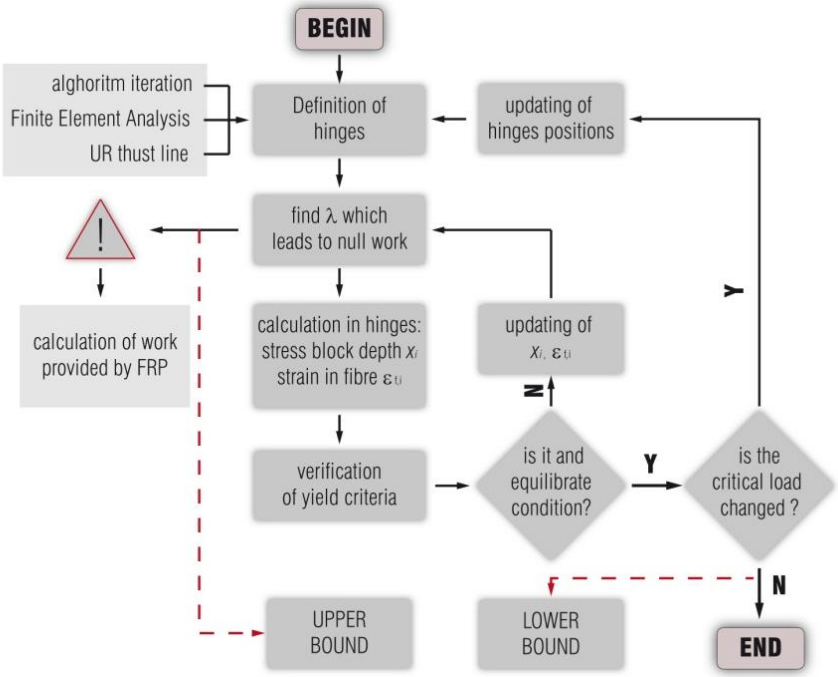


*Fig. 6.26 Schematic flow chart of the alghoritm*

Looking at the flow chart, once defined the critical load, the next step concerns the verification of yield criteria by the calculation of actions (M,N,S) in each hinge and the next evaluation of the stress block depth and fibre strain iteratively.

The iterative procedures starts from the ultimate value of $\varepsilon_{f,u}$ defined as parameter (allowable strain, rupture strain or debonding), than the stress block depth is calculated according eq. (6.2). This depth allows to find, by means of x, the

associated value of fibre strain $\varepsilon_f$. With this update values is possible to compare the two deformations, checking the ultimate strain and calculating a new load with the update the reinforcement work. After that a new value of critical load and of stress block depths will have found. The convergence criterion, which stops iterations, was fixed as difference between two subsequent values of x. Once the criterion is satisfy the equilibrated conditions are fulfilled. At this point the calculated values of x can provide the hinge regression (see Fig. 6.25) in each position. The new position can lead to a different value of the critical load. The procedure is therefore restarted with update positions. Here is implemented again a convergence criteria based on the difference in the critical load between two next steps.

Once the load is determined and yield criteria fulfilled the output is the final figure of the load. Fig. 6.27 shows the adopted concept to find the actual resistance value moving between lower and upper bound theorem. The yield criteria should be analysed in all cross sections and not only on hinges but, looking at resistance domain and actions (Fig. 6.19), bending moments are always higher in hinges whereas the axial stress N has limited variations in next cross section. This allows to state that the yield criteria are checked in worst sections.

In conclusion the algorithm it could be improved in numerical terms about convergence criteria and methods and also about the calculation of the FRP energy dissipation with the definition of the length L. Moreover further analysis on benchmark configuration will be performed. It has to be noted that to date the algorithm provides, because of the lower bound approach, a critical load equal or lower than the actual value and therefore on safety sides. The provide results seem promising even with the aforementioned simplification which results in minor errors compared to guess valued of L in eq. (6.21).

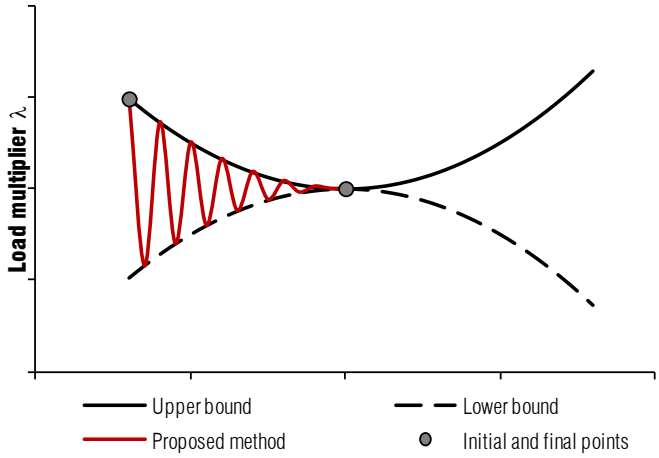


*Fig. 6.27 Theoretical appraoch to the actual solution*

The algorithm can be used also without strengthening. In this case the load becomes unique due to the correct estimation of virtual works. Tab. 6.13 shows the comparison for unreinforced vaults with block analysis performed with RING and by a meso-scale model with FEM (see pg. 240). Despite DIA case, next to snap-through configuration it is possible to conclude that the algorithm provide satisfactorily results.

*Tab. 6.13 Comparison between vaults calulated with different methods*

| | RING [kN] | proposed alghoritm [kN] | FEM [kN] | EXP [kN] |
|---|---|---|---|---|
| **UR** | 19.10 | 19.04 | 19.03 | 19.04 |
| **REGULARIZATION** | 39.60 | 41.10 | 43.13 | - |
| **DIA** | 36.10 | 35.10 | - | 79.18 |

Fig. 6.28 shows the trend among iterations of critical load and stress block depths on each hinge. The number of iterations is limited and depends on the magnitude of convergence criteria adopted. From the graph are clear the two cycles of yield criteria and the next hinges updating.

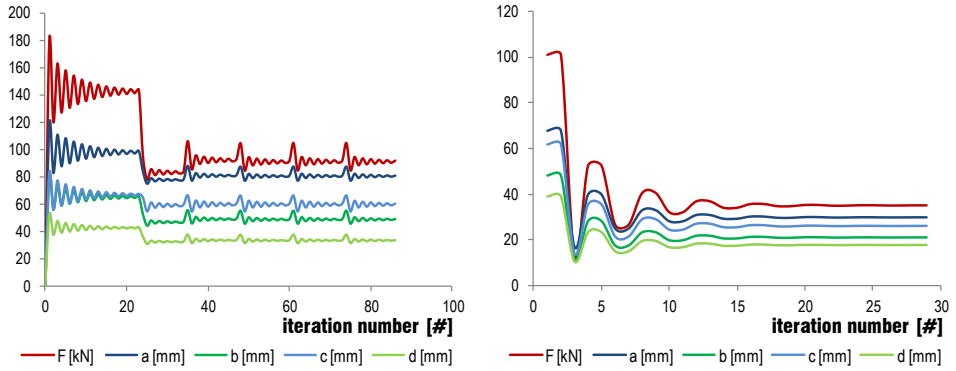


*Fig. 6.28 Convergence trend for the estimation of the critical load*

The proposed method was applied also to reinforced vaults and results are compared with RING solutions. Tab. 6.14 shows in the first two columns the input data namely: ultimate strain defined for the reinforcement and the masonry compressive strength. The critical load and effective strains are the output of the analysis. The related tensions in each hinge are reported to be compared with Ring output.

Fig. 6.29 shows the comparison for different tensile contribution of fibre for a $f_{cm}$ equal to 3 MPa. It clearly appears that there is a good agreement for firsts six

point. Indeed the implemented algorithm does not develop strains in fibre higher than 1.10% although this is not the ultimate strain in fibre. The maximum load is hence defined by masonry properties. The ratio between the two methods has an average 1.01 with a CoV of 5.28 % limited to values with similar tensions in fibre.

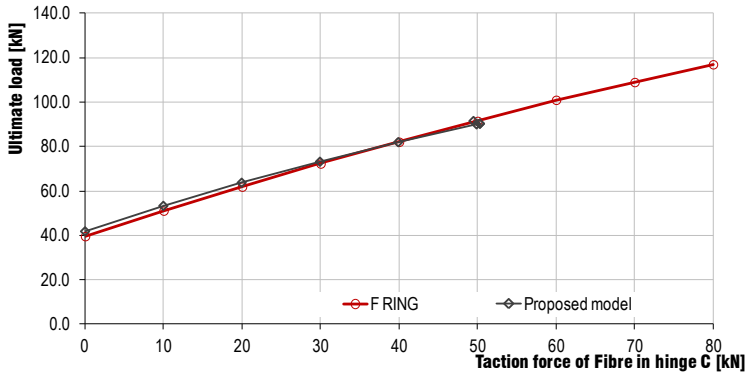


*Fig. 6.29 Comparison between Ring and model ultimate load ($f_{cm}$ 3 MPa)*

Fig. 6.30 explains better the behaviour with three cases with different compressive strengths. On Ring, a greater ultimate fibre strain (see Tab. 6.10) increases the ultimate load until fibre failure. In the algorithm instead, the effective strain $\varepsilon_f$ reach a maximum value in which masonry failure occurs. For example (see Tab. 6.14 and Fig. 6.30) for $f_{cm}$ 3MPa and $\varepsilon_{f,u}$ 2 %, the solution provide an ultimate load of 90 kN meanwhile the block analysis for steel elements provides 117 kN because in plastic material the tensile stress is independent from the developed strain.

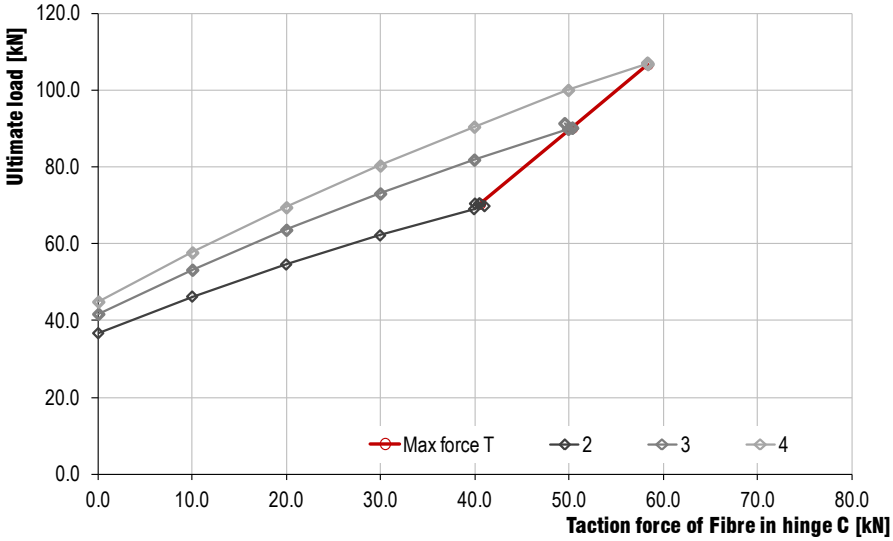


*Fig. 6.30 Ultimate load F for different allowable strain of fibre and $f_{cm}$*

The analysis stresses the demand on linear analysis on strain with FRP applications confirming the *iv* hypothesis (pg. 204). Moreover with the help of red line in Fig. 6.30 it is clear that for low masonry strength is not useful to seek for high ultimate strain in fibres. This in strengthening terms because no considerations on the ultimate displacement of the structural element are pointed out.

In conclusion the introduction of the algorithm appears an innovative idea to improve the analysis of vaults strengthened by EBR technique.

*Tab. 6.14 Comparison between the proposed algorithm and RING software*

| $\varepsilon_{f,u}$ | $f_m$ [MPa] | F [kN] | $\varepsilon_A$ | $\varepsilon_C$ | $T_A$ [kN] | $T_C$ [kN] | $T_{RING}$ [kN] | $F_{RING}$ [kN] | $F_{prod.}/F_{RING}$ |
|---|---|---|---|---|---|---|---|---|---|
| 0.000 | 2 | 36.70 | 0.0000 | 0.0000 | 0 | 0 | 0 | 37.6 | 0.98 |
| 0.003 | 2 | 46.25 | 0.0025 | 0.0025 | 10 | 10 | 10 | 48.1 | 0.96 |
| 0.005 | 2 | 54.61 | 0.0050 | 0.0050 | 20 | 20 | 20 | 57.8 | 0.94 |
| 0.008 | 2 | 62.19 | 0.0075 | 0.0075 | 30 | 30 | 30 | 66.9 | 0.93 |
| 0.010 | 2 | 69.02 | 0.0100 | 0.0100 | 40 | 40 | 40 | 75.2 | 0.92 |
| 0.013 | 2 | 69.81 | 0.0111 | 0.0103 | 44 | 41 | 50 | 82.9 | 0.84 |
| 0.015 | 2 | 70.47 | 0.0109 | 0.0102 | 44 | 40 | 60 | 90.1 | 0.78 |
| 0.018 | 2 | 70.47 | 0.0109 | 0.0102 | 44 | 41 | 70 | 96.8 | 0.73 |
| 0.020 | 2 | 70.53 | 0.0109 | 0.0101 | 44 | 40 | 80 | 103.0 | 0.68 |
| 0.000 | 3 | 41.77 | 0.0000 | 0.0000 | 0 | 0 | 0 | 39.6 | 1.05 |
| 0.003 | 3 | 53.25 | 0.0025 | 0.0025 | 10 | 10 | 10 | 51.1 | 1.04 |
| 0.005 | 3 | 63.67 | 0.0050 | 0.0050 | 20 | 20 | 20 | 61.9 | 1.03 |
| 0.008 | 3 | 73.14 | 0.0075 | 0.0075 | 30 | 30 | 30 | 72.3 | 1.01 |
| 0.010 | 3 | 81.95 | 0.0100 | 0.0100 | 40 | 40 | 40 | 82.1 | 1.00 |
| 0.013 | 3 | 89.96 | 0.0125 | 0.0125 | 50 | 50 | 50 | 91.5 | 0.98 |
| 0.015 | 3 | 90.26 | 0.0136 | 0.0126 | 54 | 50 | 60 | 101.0 | 0.89 |
| 0.018 | 3 | 90.28 | 0.0136 | 0.0126 | 54 | 50 | 70 | 109.0 | 0.83 |
| 0.020 | 3 | 91.46 | 0.0134 | 0.0124 | 53 | 49 | 80 | 117.0 | 0.78 |
| 0.000 | 4 | 44.95 | 0.0000 | 0.0000 | 0 | 0 | 0 | 40.6 | 1.11 |
| 0.003 | 4 | 57.76 | 0.0025 | 0.0025 | 10 | 10 | 10 | 52.7 | 1.10 |
| 0.005 | 4 | 69.53 | 0.0050 | 0.0050 | 20 | 20 | 20 | 64.2 | 1.08 |
| 0.008 | 4 | 80.41 | 0.0075 | 0.0075 | 30 | 30 | 30 | 75.3 | 1.07 |
| 0.010 | 4 | 90.54 | 0.0100 | 0.0100 | 40 | 40 | 40 | 86.0 | 1.05 |
| 0.013 | 4 | 100.12 | 0.0125 | 0.0125 | 50 | 50 | 50 | 96.4 | 1.04 |
| 0.015 | 4 | 106.83 | 0.0150 | 0.0146 | 60 | 58 | 60 | 106.0 | 1.01 |
| 0.018 | 4 | 107.16 | 0.0157 | 0.0146 | 63 | 58 | 70 | 116.0 | 0.92 |
| 0.020 | 4 | 107.21 | 0.0157 | 0.0146 | 63 | 58 | 80 | 125.0 | 0.86 |

### 6.3.4 *Comparisons*

After all the considerations on analytical models and looking at FEM outcomes drawn in the following paragraph, Fig. 6.31 summaries the calculated response for UR vault with several methods. This comparison allows to evaluate the usual assessments tools used in existing unreinforced masonry constructions in terms of static or seismic actions with the absolute advantage of actual experimental results.

The kinematic analysis evaluates the critical load that activates the mechanisms and defines only a value and not the associated displacement. The output ranges varies depending on masonry strength, moreover, with the proper value (3 MPa) a very good agreement has been found between RING analysis, the proposed algorithm, and the experimental results. This confirms that hinge regression is important and stresses the power of the simple kinematic analysis. Moreover, if a ultimate displacement calculation [da Porto 2007] is carried out it is possible to match with good agreement the post-peak experimental inclination (blue dash line).

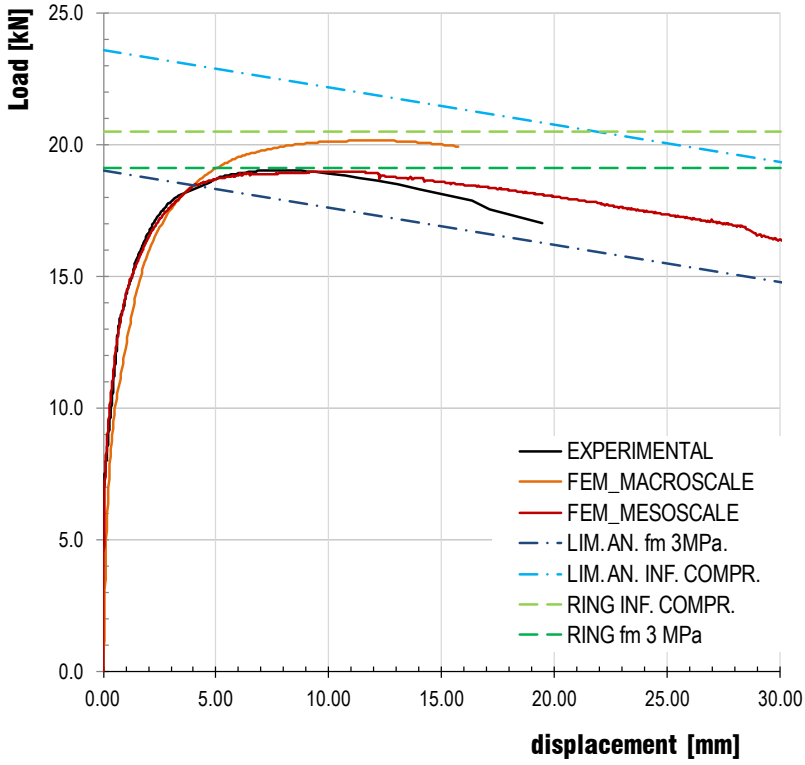


*Fig. 6.31 Summarizing results and comparisons among performed analyses*

From Finite Element response curves is possible to see how models can carefully describe the entire development of the response curve summarising linear and plastic analysis outcomes. Moreover integrations on each point of stress and strain allow a deep investigation of the structural element. In particular the meso scale model perfectly agrees with the actual response also with large deformations and describes accurately the crack pattern and experimental observations.

Conversely the FEM setup and configuration result from a tricky job on constitutive laws and materials which are composed by wide set of parameters. This accurate response thus is indisputable related to experimental observations and calibration.

In conclusion design calculations and the safety assessment is more reliable if based on simple and less sensitive approaches as well the limit analysis that demonstrates a good response also on the drawing of the capacity curve. At the same time, a careful FE modelling is essential to understand the proper behaviour and failure developments. The combined use of both approaches confirmed by means of experimental observation the methodological reliability.

## 6.4 FINITE ELEMENT MODELS

The implementation of Finite Element Models (FEM) of the experimental campaign is a versatile and interesting method to extend a research investigation. A combined experimental/numerical basis is the key to validate, extend and improve existing methods. Numerical simulations are fundamental to provide insight into the structural behaviour and to support the derivation of rational design rules. Nevertheless, the step towards the development of reliable and accurate numerical models cannot be performed without a thorough material description and a proper validation by comparison with experimental results.

As mentioned in the literature review, masonry could be modelled with three approaches depending on the mesh complexity. Herein two of them, namely the macro-scale and meso-scale modelling were selected. The first because of the wide use in common case for the neglect of masonry texture, and the second one to reach high accuracy. These cases help also to highlight advantages and drawbacks of both approaches. Moreover the use of EBR also implies to face the problem of bond modelling. In the following five models are illustrated:

- one model of the on-site shear test,

- two macro-scale models (UR and SRG),
- two meso-scale models (UR and SRG).

### 6.4.1 *Solution method*

The first common step of among all models was the selection of the most efficient parameters to perform analysis accounting for namely: solution method, iterative methods, convergence criteria, geometrical non linearity, load application, mesh sensitivity and boundary conditions.

The solution method was chosen in order to limit as much as possible time costs and model instability. The first was evaluated in the time consumed for each analysis and the second on the convergence lack. Fig. 6.32 shows, for a macro model of UR vault with plane stress elements the time cost of two solution methods (left) and three equilibrium iteration methods. Cholesky was chosen because shows to be more effective for the analysis but with limited advantage (7%). With more complex elements Parallel Direct Sparse method (PARADISO) provides better results.

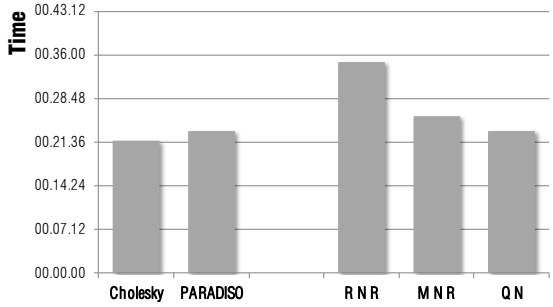


*Fig. 6.32 Time consuming analysis for macro-modelling*

About equilibrium iteration methods (Regular Newton Raphson, Modified Newton Raphson and Quasi Newton [DIANA 2012]) the difference are well known and based on the calculated inclination for the next iteration. The comparison provides better results for the Quasi-Newton method presented in Fig. 6.33 and with a convergence criteria based on energy. QN is based on secant inclination on the investigated curve. Analyses provide more problems with the first two methods meanwhile QN does not give any convergence lack showing higher robustness. High tolerance in energy criterion provides faster solutions but with wavering curves and more instability problems. On the other hand too small values raise as well problems in convergence and are more time consuming. Several attempts were made and a final value for conclusive solutions was chosen as $1x10^{-5}$.

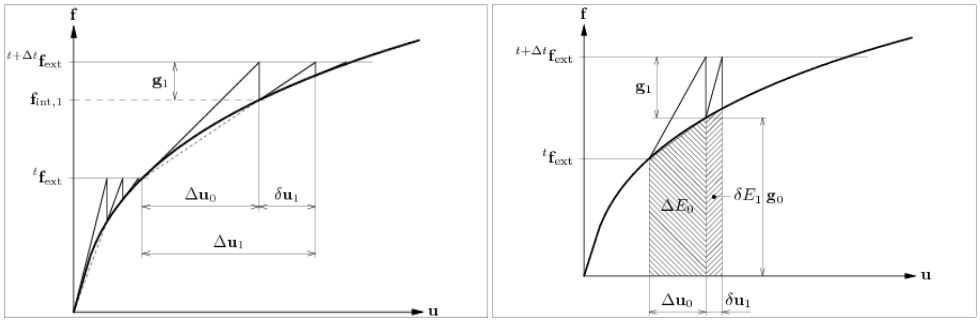


*Fig. 6.33 Quasi-Newton method (left) and convergence criteria (right)*

Another test was carried out about the relevance of geometrical non linearity. According to theoretical observations reported in §2.5.2 the capacity curve (load-displacement) of mechanisms could reasonably figured out with a geometric analysis (see also conclusions in §6.3.3). In fact, the use of the initial undeformed conditions does not provide reliable results in the plastic branch. Fig. 6.34 shows the comparison for the UR meso-scale model where is clear the ineffectiveness to describe the post peak behaviour by linear approach, instead the geometrical non linearity properly evaluates this actual phenomena.

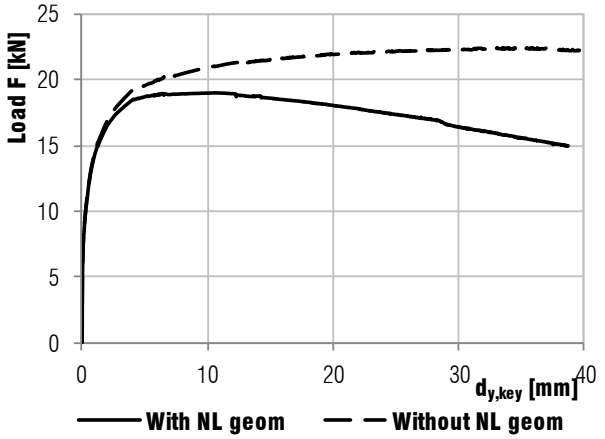


*Fig. 6.34 Evaluation on geometrical non linearity (UR meso-scale model)*

From the experimental point of view the load was applied in load control but the same attempt, also with arc-length criterion does not provide promising result. The load application on the model was therefore implemented by displacement control of the steel beam at the quarter.

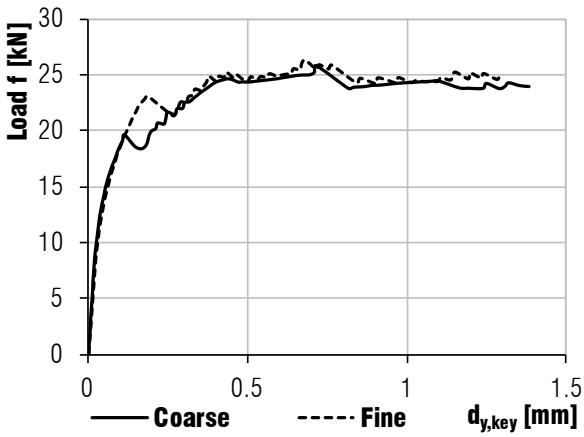


*Fig. 6.35 Evaluation of the mesh sensitivity*

Fig. 6.35 presents the evaluations carried on the mesh sensitivity. The effects are less relevant in this case compared with other parameters. The mesh regularity actively helps to reduce those troubles and a final mesh with rectangular elements 30x45 wide (Fine in Fig. 6.35) were selected, except portions near to supports. To obtain comparable results the same parameters were used among models. The mesh selection in the macro model is not problematic and easy to adapt instead in the meso-scale approach has substantial effects on the creation of elements.

The last setting concerns boundary condition (BC). As highlighted in §5.3.1 details in the stereotomy of supports are relevant. BC analysis looks at how accounts of this detail. About the tensile contribution of the stone portion, in the higher third (Fig. 6.36), both cases fixed and free were analysed. Moreover the same couple of models were tested with only pin nodes. The North support, opposite to the load application was considered fixed because even if cracked the contact works in compression.

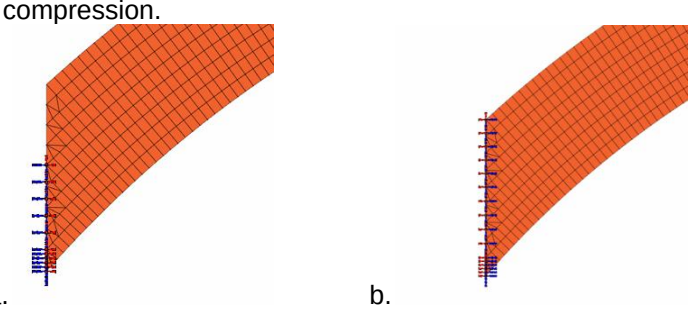

a. b.

*Fig. 6.36 Different models of BC: 2/3 fixed (a) (left) and all fixed (b) (right)*

From results there are not significant differences in the pin and fixed constrain of nodes, whereas the two cases presented in Fig. 6.36 show different results in stiffness and failure mode. (B) is stiffer than case (A) while the load was not significantly affected by this variation. The failure mode of (A), later presented in

models, perfectly agrees with the experimental observation whereas (B) configuration moves the hinge A in higher joints than observations.

### 6.4.2 *Type of elements*

The first choice in the finite element definition was the analysis of the out-of-plane direction. Although the observed response, in particular looking at hinges crack formation, varied in the vault depth (see §5.3), the model was considered with bi-dimensional elements. First of all for computational cost reasons, and then because the observed differences are indeed related to non uniform BC very complex to reproduce on a FEM. Some trials have been performed with shell elements where is possible to evaluate the out-of plane behaviour even with bi-dimensional elements but the response was analogous.

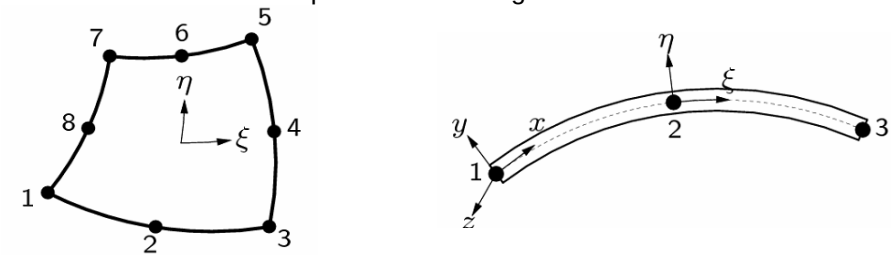


**CQ16M** **CL9BE**

*Fig. 6.37 Bi-dimensional and linear curved element used with Gauss axis*

The CQ16M element used for bricks is an eight-node quadrilateral isoperimetric plane stress element based on quadratic interpolation and Gauss integration. For irregular zones on supports a CT12M six-node triangular elements was selected. To model EBR the element adopted is CL9BE, a three node, two-dimensional class III beam element. The choice to use curved elements was necessary to consider the vault edges.

The interface element selected was necessary for meso-scale models and for the EBR applications to consider the matrix behaviour. The CL12I element was selected for both cases. It is an interface element between two lines in a two-dimensional configuration based on quadratic interpolation. The integration scheme is a 3 point Newton-Cotes. It is worth to notice that those elements require strict nodal definition to properly accounts of tensile direction.

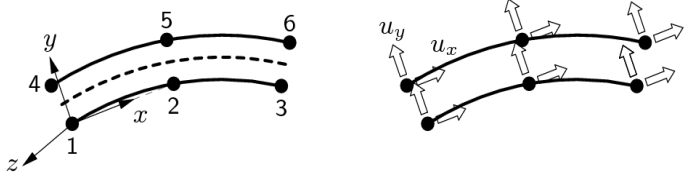


**CL12I** *topology (left) displacement (right*)

*Fig. 6.38 Topology and displacement of the CL12I interface*

Two constitutive non linear models were selected for mortar joints and matrix. The first one was a Coulomb Friction law with a tension cut-off (Fig. 6.39 left). This constitutive model provides the shear behaviour according to a friction law and an interface tensile failure whereas compressive resistance is infinite. This model was preferred to the combined crushing sliding cracking law of Lourenço [1997], which accounts also of compressive failure, because of the selected model has limited number of well known parameter. The compressive crushing, fundamental in such applications, as experimentally observed occurred on brick rather than mortar and thus was considered in unit mechanical properties. Lourenço [2007] values of compressive cap are in the order to 10 MPa for crushing, hence very high, and also for this reason the assumption of the crushing in units is acceptable.

The second law for fibre bond was linear in the normal direction and follows a multi-linear τ-s law user defined in shear as considered in experimental tests. Only this option of τ-s law in Diana allows softening. To have more accurate details and information see DIANA [2012].

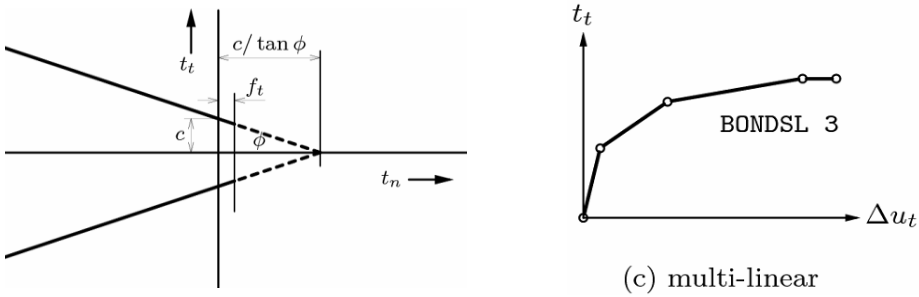


COULOMB FRICTION BOND-SLIP

*Fig. 6.39 Constitutive non linear model of interface for mortar joints (left) and EBR (right)*

### 6.4.3 *Bond analysis*

Once selected a bond-slip multi-linear law, the curve definition is a challenging issue also looking at considerations in §6.1.2. To obtain meaningful solutions the single lap shear test performed on-site on SRG strips was modelled. The adoption of a constitutive model which accounts for a softening branch better describe the actual shear behaviour with the movement, from the loading end toward the unloaded end, of the effective length. This is clear in model used for the calibration and presented in Fig. 6.40. At the initial stage (a) the active part is only in the strip begin. Increasing the load the maximum shear is reached in the loaded end and the softening parts is activated. In stages (b) and (c) all points on the peak left are in the softening part whereas points on the right are still in the elastic branch.

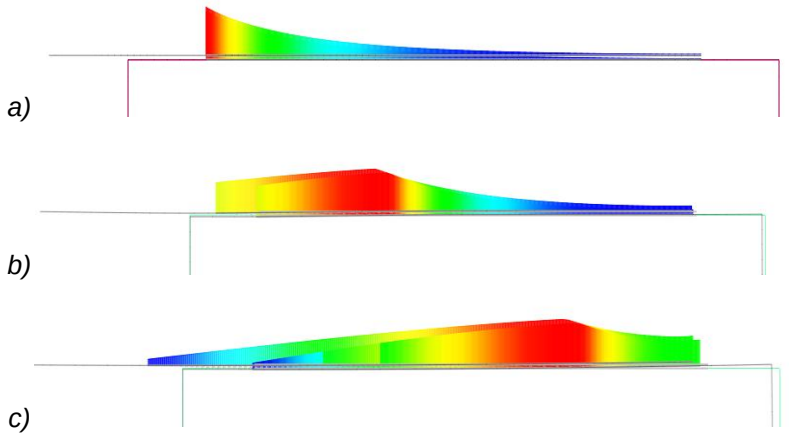


*Fig. 6.40 Distribution of shear stress at first step (a) after the reaching the maximum $\tau$ (b) (c)*

This trial follows the application of Ghiassi [2012b] but in that case more information from the experimental test was available. In the model here presented only the P-$\delta$ was available. Moreover the on-site measurements of $\delta$ are less accurate than laboratory test. Finally the failure of the test occurs on fibre and does not involved the shear failure, hence the load is a lower bound limit.

Among the several purposes in literature (Fig. 2.13) the bi-linear curve was selected because coherent with the experimental observations and at the same time with a low amount of parameters to define. It has to remind that also CNR200 adopt this law. The calibration was hence based on the sensitivity analysis, rather than the experimental test, by the variation of: maximum shear, ultimate slip, initial stiffness, fracture energy.

The first analysis looks at the variation of the ultimate slip, starting from CNR limit (0.4mm) and with the half (0.2) and the double of this value (0.8). The fixed fracture energy provide the relative maximum shear on the matrix. Fig. 6.41 shows the three laws (left) and the final response (right). A small ultimate slip provides high shear stresses, a stiff behaviour and reaches the maximum load for less displacement with also a shorter effective length. In the opposite condition the failure occurs before the activation of the effective length. It is possible to conclude that the actual test shows smaller stiffness than all cases but the behaviour, in terms of load and effective length are more closed to slips smaller than 0.4 mm.

The second trial accounts for the influence of the initial stiffness. CNR200 provide an analytical formulation for this but only in case of organic matrixes. Fig. 6.42 shows the influence of stiffness variation in case of same fracture energy and ultimate slip. From the load displacement behaviour is possible notice that despite the first branch, which shows stiffness variation, the overall behaviour is equivalent.

In conclusion the yielding slip was considered one tenth of the ultimate one but is not a relevant parameters.

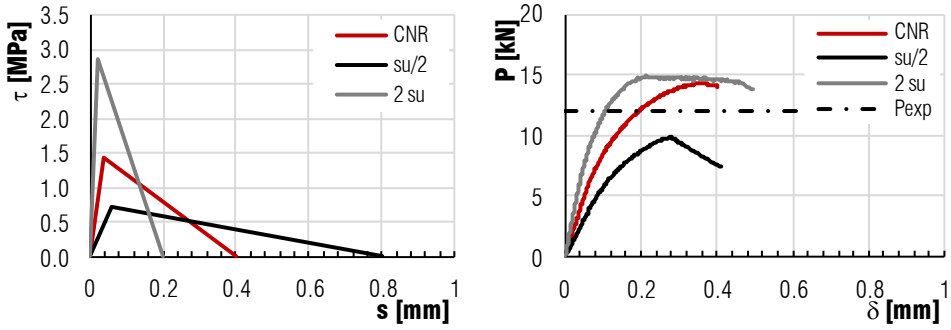


*Fig. 6.41 Influence of ultimate slip in the load displacement curve*

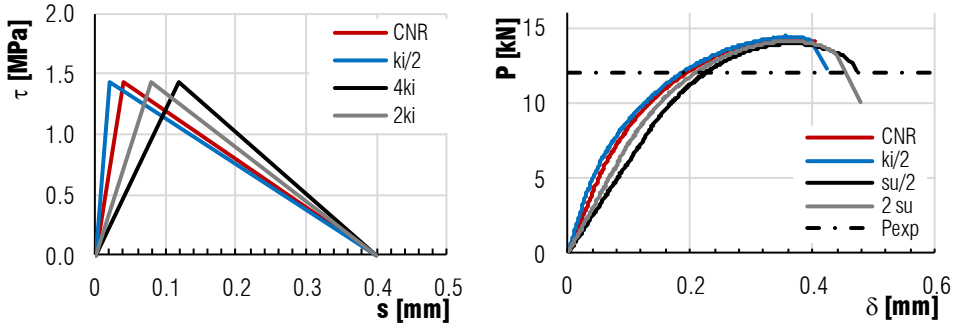


*Fig. 6.42 Influence of initial stiffness in the load displacement curve*

The last analysis looks at the changing in fracture energy according to calculation of § 6.1.2. In this case the shear stress was kept constant varying the ultimate slip. Fig. 6.43 presents higher ultimate loads increasing energy but it can be noted that Panizza does not reached the effective length. In conclusion is not possible to understand the real behaviour from the experimental test but, increasing energy, for same shear stress, the working length increases and thus for longer fibre anchorage the load increases as well. By the whole analysis Ceroni [2014] seems to be the better compromise.

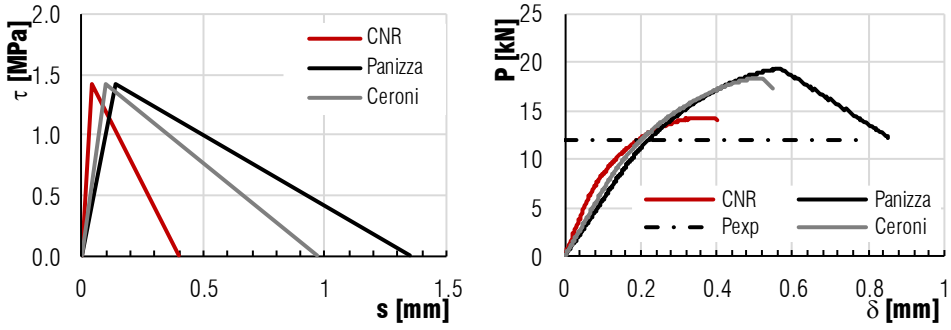


*Fig. 6.43 Influence of fracture energy in the load displacement curve*

### 6.4.4 *MACROSCALE Unreinforced vault*

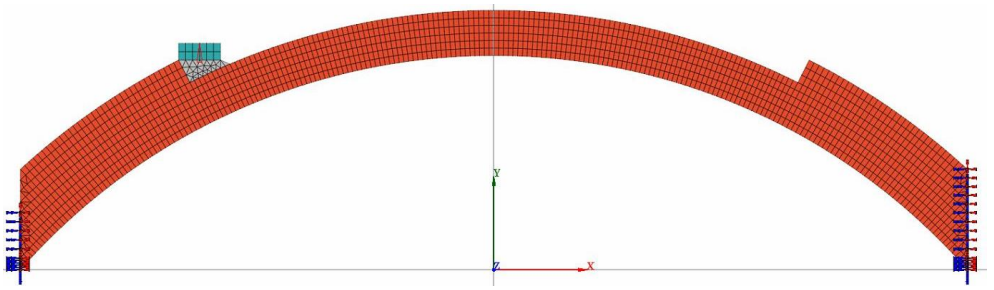

*Fig. 6.44 Frontal view of the mesh model*

The first global model created was the UR vault with a macro-model approach and all the common setting were already presented in previous paragraphs. In this model, the changed variables are material properties.

*Tab. 6.15 Masonry properties in FEM*

| | $E_m$ [N/mm²] | ρ [kg/m³] | ν | $f_c$ [N/mm²] | $f_t$ [N/mm²] | $G_c$ [N/mm] | $G_f$ [N/mm] |
|---|---|---|---|---|---|---|---|
| **Masonry** | 440 | 1800 | 0.11 | 1.67 | 0.084 | 2.672 | 0.0025 |

The final parameters adopted for masonry are reported in Tab. 6.15 and starts from the definition of the material for the global model of the castle from the Italian standard [NTC2008]. The tensile strength is 0.05 times the compressive one. To characterise the Total Strain Crack model (see pg. 74) the two softening curves were defined. In compression, a parabolic function was selected whereas after some trials with linear softening the exponential was selected. Compared to the linear function Exponential provides smoother results with also lower convergence problems for a small increase in computational costs.

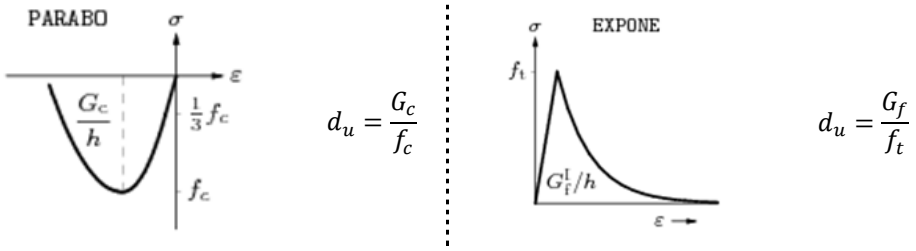


*Fig. 6.45 Constitutive model of non linear behaviour of masonry in compression (left) and tension (right)*

The parameter definition is based on fracture energy and tensile strength. To calculate the energy Lourenço [2009] tips were followed starting from the ductility index $d_u$ equal to 0.029 mm for tension, and $d_u$ 1.6 mm for compression. The Poisson's ratio of 0.11 refers to the elastic behaviour in FE and thus the measured value in flat jack tests was adopted. By the inverse calculation from the Italian parameters of elastic and shear moduli (Tab. 2.1) the obtained ratio is 0.5 but it accounts of cracked conditions and thus with higher values. The tensile strength

also agrees with Lourenço [2009] and Eurocode 6 [2005] as the tensile strength of mortar joints which lies between 0.1 and 0.2 MPa.

In order to evaluate the sensitivity of the model, some trials on the constitutive law have been carried out. The compressive parameters as $f_c$ and $G_c$ provides to does not affect the solution in their range of variability. As reasonably the tensile behaviour plays instead a more sensitive role. In particular in Fig. 6.46 are presented the differences in fracture energy variations highlighting, at least in the first part, a stiffer behaviour and also a higher first peak for great energies. It has also to be considered that the final value, for higher displacements seems to reach similar conclusions according also with Lourenço [2001] consideration (see **Fig. 2.73**) where $G_f$ deeply affects the peak behaviour rather than the plastic branch. Moreover, it is clear looking at values, that the behaviour is very stiffer compared to experimental results.

In conclusion tensile and compressive parameters were fixed on the initial values derived for experimental and when were not available from literature values.

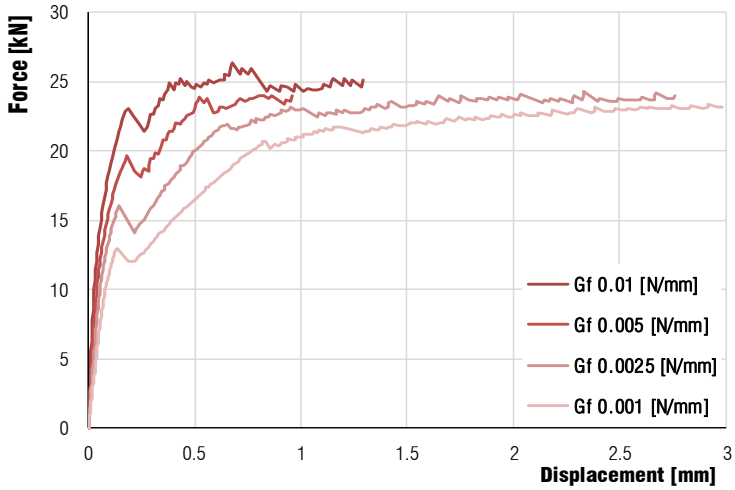


*Fig. 6.46 Sensitivity evaluation of the tensile fracture energy*

The last parameter studied concerns the masonry Young modulus starting from the flat jack outcomes § 0 and decreasing until 440 MPa which is an unrealistic value of modulus. Fig. 6.47 shows the comparison with the experimental curve and presents a too stiff behaviour until 1000 MPa. Also the value of 1800 MPa detected with dynamic test is not suitable. It is worth to notice, from a numerical point of view, thanks to consideration on masonry in §2.2.1, that if used the average value find by experimental results of $E_c$ equal to 413 $f_c$ might led to results low values of the modulus. This may be a confirmation of the difficult interpretation and usage of that figures. In this case the problem may rise from the assumption of a very low compressive strength.

In conclusion this remarks how with a macro model approach, although is possible to reach similar results with actual situations, displacements are not properly estimated with convenient materials parameters. This could be associated to deformations that in actual examples, lumped deformation in cracks and for this reason a meso-scale modelling could provide better results.

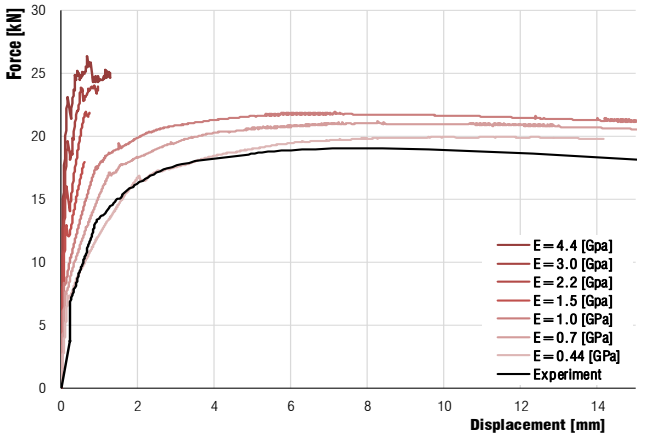


*Fig. 6.47 Sensitivity in F-$\delta$ graph of the Young elastic modulus*

Once defined with the calibration of the vertical displacement to extend the solution to the global behaviour the displacement of all monitored points are compared in Fig. 6.48. The solution, for high displacements become less stable because controlled by sole energy. The load quarter is stiffer in the experimental curve whereas the other quarters have the same response. This is confirming a non optimal description by the overall behaviour by the FEM.

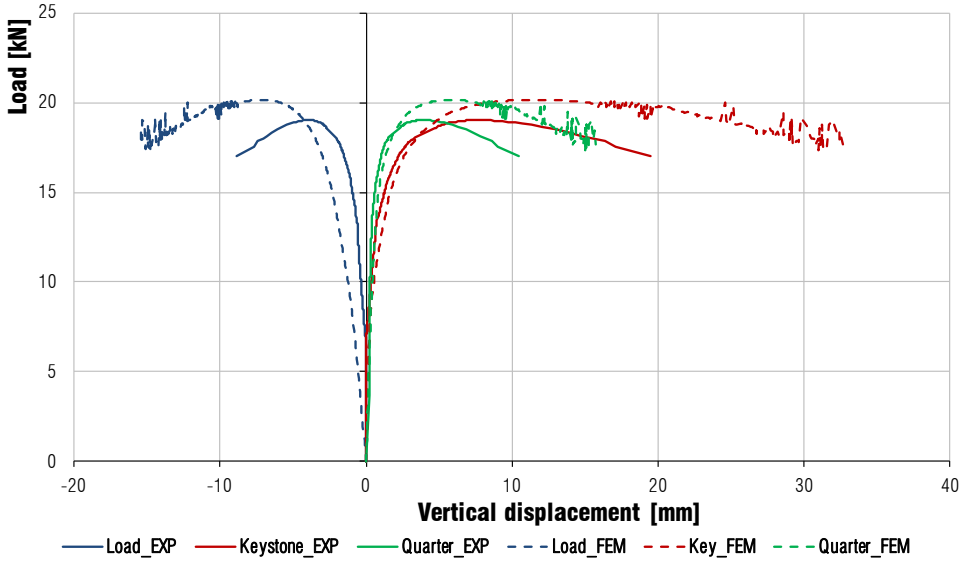


*Fig. 6.48 FEM comparison with experimental vertical displacement of UR vault*

Another comparison (see Fig. 6.49) is made on the hinge opening with the comparison of the wider crack located in B. In this case the facture energy and the softening behaviour seem to agree with the measured value with a positive solution for a macro model.

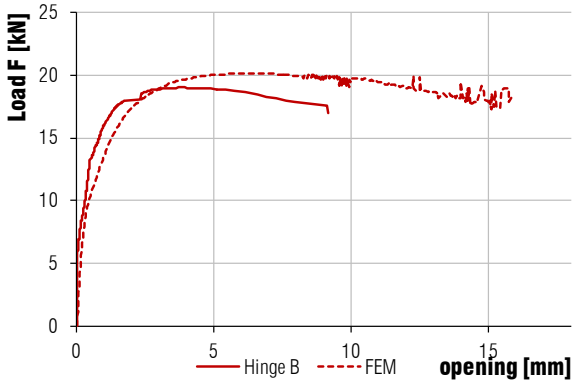


*Fig. 6.49 Comparison between FEM and experimental data of hinge B*

FEM is not only suitable for figures but is important also to analyse failure modes and damage locations as well as stresses distribution. For this purpose two stages of the loading history have been selected (see Fig. 6.50). All the presented configurations have deformations magnified of 5 times than calculated values to better represent the shape.

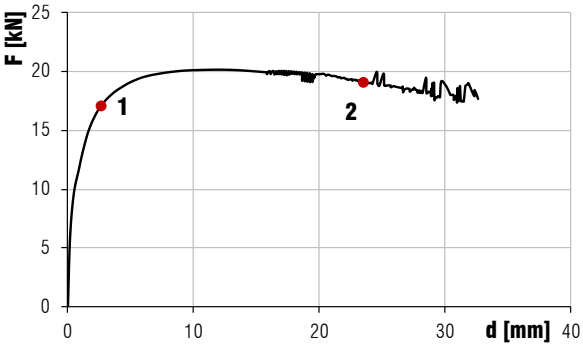


*Fig. 6.50 Stages definition in the results presentation*

From the principal strain distribution in tension, plotted in Fig. 6.51, is possible to observe an adequate representation of the actual hinges. In particular the hinge under the load (as shown in Fig. 6.49) and the two on supports are perfectly located and lumped in one position. The intermediate hinge C does not properly confirms experimental results with the formation of 3 cracks.

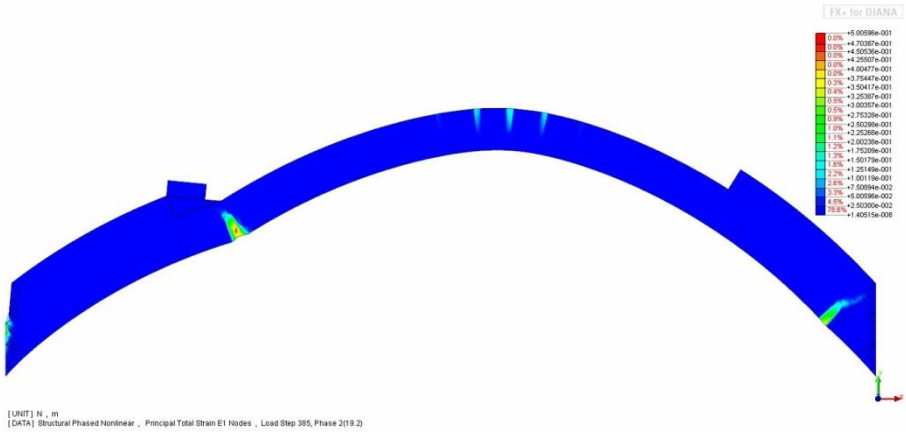


*Fig. 6.51 Stage 2 - Principal tensile strains*

A better understanding of this cracks spread becomes from the analysis of cracks distribution in Fig. 6.52 and Fig. 6.53 which refer to stage 1 and 2 respectively. Macro-model due to its smeared crack approach significantly enlarges the position of such damages with the respect of actual observations. Also about this topic, meso-scale models can better describe crack openings and distribution.

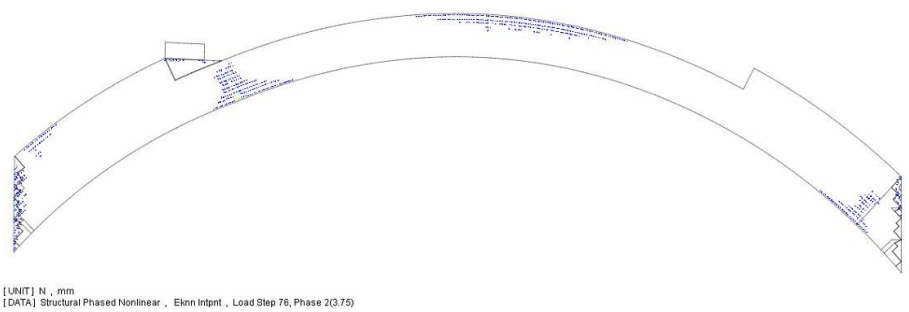


*Fig. 6.52 Crack pattern at stage 1*

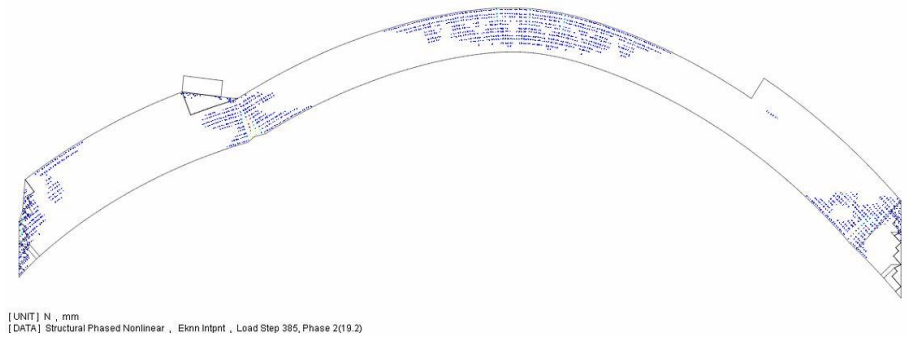


*Fig. 6.53 Crack pattern at stage 2*

The principal stresses distribution, Fig. 6.54, shows unloaded portions opposite to the hinge locations (in gray stresses higher than -0.01 MPa) and the location of higher stresses. From this is also possible to localize cracked section

that appears with the thrust line outside the middle third. The contour helps also to see the thrust line behaviour with limited variations in hinges and diffuse stresses in intermediate position. The maximum compressive stresses reached are limited at 0.8 MPa still an half of the imposed limit, confirming Heyman hypothesis of infinite compressive strength for URM vaults that fails for mechanism.

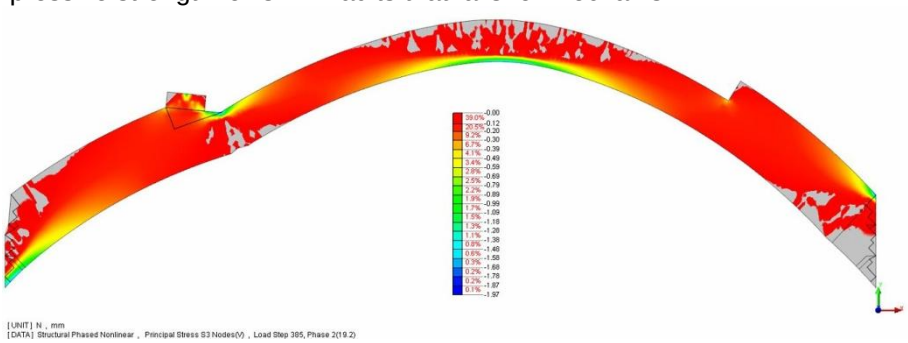

*Fig. 6.54 Stage 2 -Principal compression stresses in the range [0.01;2.00] MPa*

Finally, for model with low compression strengths in the last step of the analysis appears masonry crushing on the right side of the loading point. Although this is not the case of compressive failure this clue confirms the insight of stress distribution defining this portion as the critical one for compression failures as confirmed experimentally in strengthen vaults.

### 6.4.5 *MESOSCALE Unreinforced vault*

From the results of the Macro scale model, limits in the evaluation of displacements and also on maximum load were clear, while overall acceptable agreement with damages, failure modes and stress distribution was found. To achieve better results and to overcome these limits a meso-scale model was implemented. In this type of models a key aspect is the mesh definition between interface and other elements.

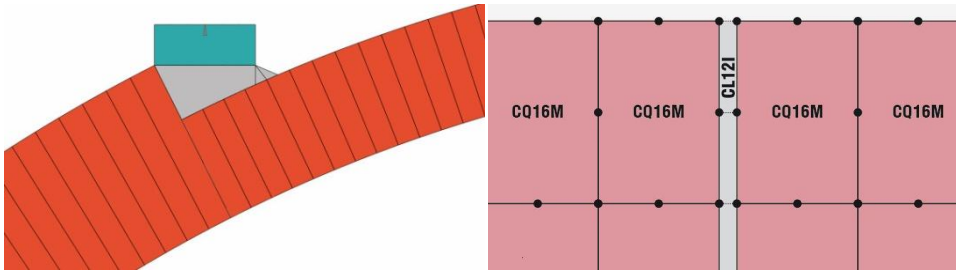


*Fig. 6.55 Elements of the micro model (left) and view of finite elements (right)*

Fig. 6.55 shows the simplified micro-modelling with the definition of unit and interface that accounts for mortar joints. A schematic view of nodes and element

implemented is drawn on the right. After the meshing all interface were collapsed in order to have zero thickness element.

The material definition of properties starts form unit and mortar. In the first case due to the interface constitutive model, not limited in compression, the compressive strength of unit was reduced to the overall resistance. The sensitivity analysis carried out and presented in Fig. 6.56 for compressive and tensile strength of units confirms negligible effects of these parameters mainly because failure mechanisms are related to mortar joints.

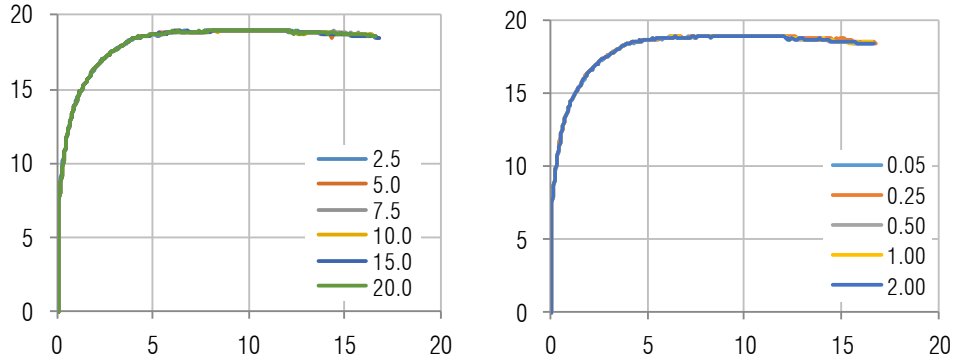


*Fig. 6.56 Sensitivity in F-$\delta$ graph of compressive $f_{c,u}$ (left) and tensile $f_{t,u}$(right) strength of unit*

A similar behaviour is given by the elastic modulus of units, starting form 2000 MPa, the identified dynamic modulus of whole masonry, to a value of 600 times the compressive strength (12'000 MPa). After such analyses is possible to recognize the limited influence of brick properties on the overall behaviour.

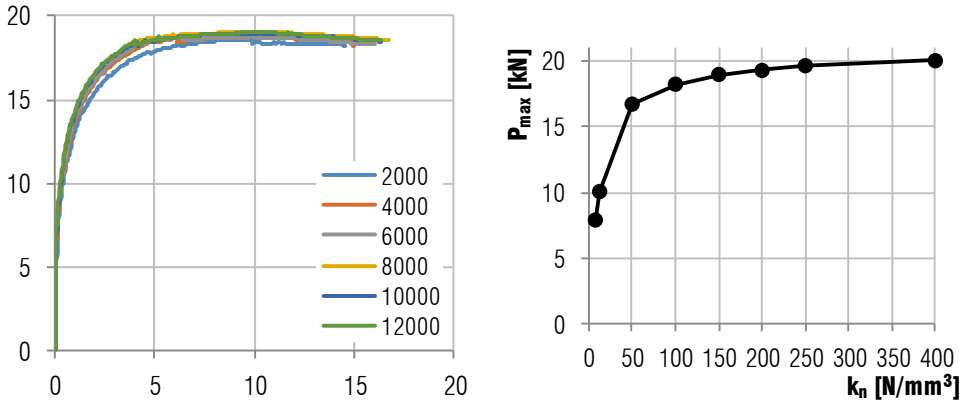


*Fig. 6.57 Sensitivity in F-$\delta$ graph of unit Elastic modulus $E_u$ (left)*
*variation of ultimate force for different interface normal stiffness $k_n$ (right)*

On the other hand, the characterization of the interface plays a crucial role in the final definition of the maximum load. Fig. 6.57 on the right shows the different maximum load calculated depending on the interface normal stiffness. Fig. 6.58 shows, in the F-$\delta$ graph the different behaviour of interface normal stiffness.

It is interesting to observe how the increase of $k_n$ lead to an asymptotic behaviour at a value close to 21 kN. That load was also determined from the limit analysis performed with infinite compressive strength (§6.3.1), therefore the use of high interfacial normal stiffness is equivalent to a limit analysis performed under Heyman [1996] hypotheses. In this case, due to the limited stress acting, as shown before, the compressive failure is never reached.

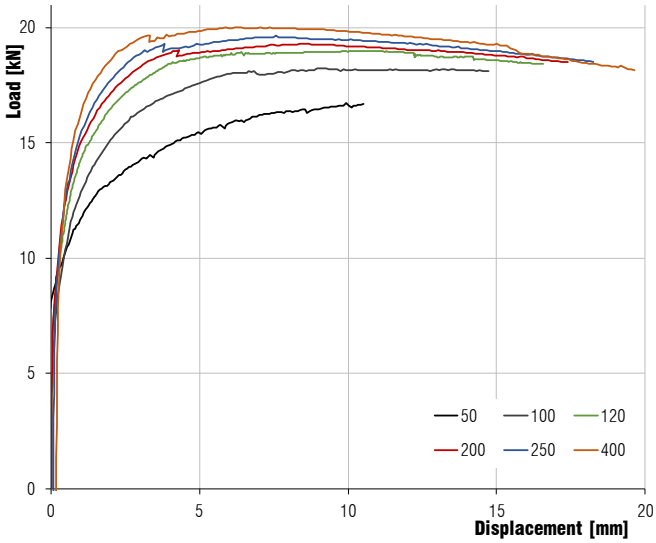


*Fig. 6.58 Sensitivity in F-$\delta$ graph of interface normal stiffness $k_n$*

Looking at the sensitivity analysis performed above, the unit mechanical properties do not affect significantly the overall behaviour. In Tab. 6.16 (above) are presented the used parameters. The Young modulus of unit is near the 400 $f_c$ times the compressive strength experimentally determined in §5.2.1. The value of $f_c$ was based on the flat jack test and by the limit analysis carried out in previous paragraphs. The facture energy values were calculated according Fig. 6.45 and the aforementioned $d_u$.

Mortar interface between bricks was instead sensitive to the parameters changing. In particular the stiffness values of interface were key parameters. Form an analytical point of view is possible to calculate the interface stiffness according eq. (6.22) but due to the on-site test is unfeasible to have the mortar elastic modulus. It was thus decided to directly evaluate $k_n$.

$$k_n = \frac{E_u \cdot E_m}{h_m \cdot (E_u - E_m)} \tag{6.22}$$

The modulus was calibrated with experimental test and provides 120 N/mm$^3$ and 60 N/mm$^3$ in the normal and tangent direction respectively. The obtained figures are according to Lourenço [1997] examples.

About the failure domain, the tensile cut-off was fixed at 0.1 N/mm$^2$ while the shear parameter of friction was according Heyman [1996] and the cohesion according to [Giradello 2012]. The selection of these figures could be tentative and are still not well defined in literature, for this reason a mutual comparison has been used for $f_t$ and $c$. Both values agree with Lourenço [1997] and with the experimental data carried out at UniPD and shown in § 2.2.1.

A special attention should be given to shear fraction angle. That values varying among authors (Lourenço [1997], Borri [2009]) and the two European and American standards provide for design purposes 0.4 and 0.45 respectively. It is herein used, for the effective acting coefficient 0.5. Moreover the sliding occurred in SRG vaults seems to agree with this value. In conclusion all the presented figures coming from similar considerations carried on the limit analysis.

*Tab. 6.16 Material properties of the meso-scale UR - FEM*

| | $E_m$ [N/mm$^2$] | $f_c$ [N/mm$^2$] | $f_t$ [N/mm$^2$] | $G_c$ [N/mm] | $G_f$ [N/mm] |
|---|---|---|---|---|---|
| **Unit** | 7200 | 3.0 | 0.2 | 4.800 | 0.01 |
| | $k_n$ [N/mm$^3$] | $k_s$ [N/mm$^3$] | $f_t$ [N/mm$^2$] | C [N/mm$^2$] | $\mu$ |
| **Mortar** | 120 | 60 | 0.1 | 0.17 | 0.5 |

The final output of the analysis is shown for the vertical displacements in Fig. 6.59. It is clear the good agreement achieved with the model in both displacements and maximum load. Also the plastic branch gives a similar trend. By the implementation of the meso-model the actual behaviour is represented and it is also possible to reach higher displacements than experimental results. Analogously to the physical case the meso model lumps in one mortar interface all the opening without damages in unit. The magnitude of displacement reached is considerable for FEM. The comparison between FEM and experimental results in both, vertical (Fig. 6.59) and horizontal (Fig. 6.60) positions, shows same differences highlighting the accuracy of the model also in the global behaviour. In horizontal measurements the effects of long horizontal wire sensors (2H and 3H) shows inactivity for small movements but for higher displacements the response become better. In this case is possible to analyse some portions without good sensors measurements by means of the FEM model.

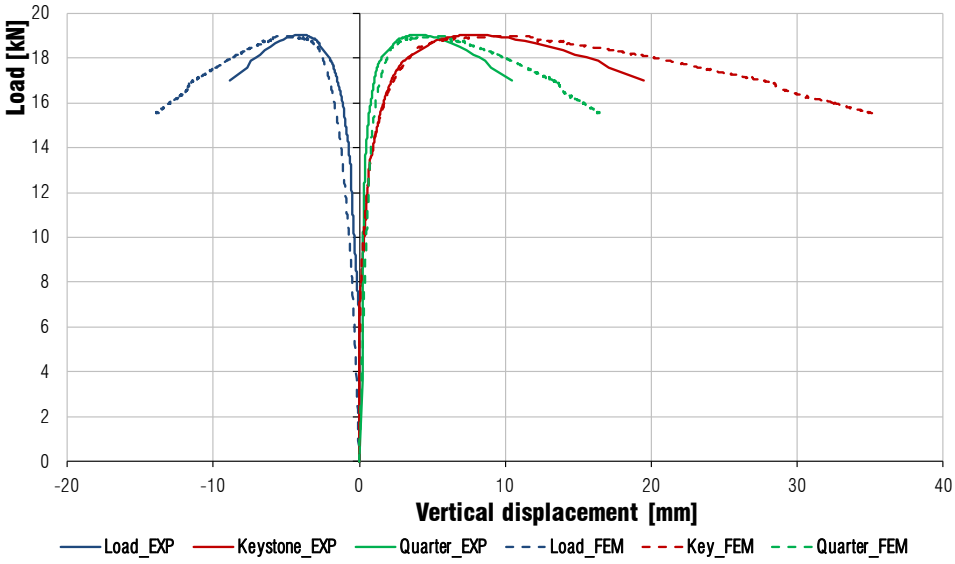


*Fig. 6.59 FEM comparison with experimental vertical displacement of UR vault*

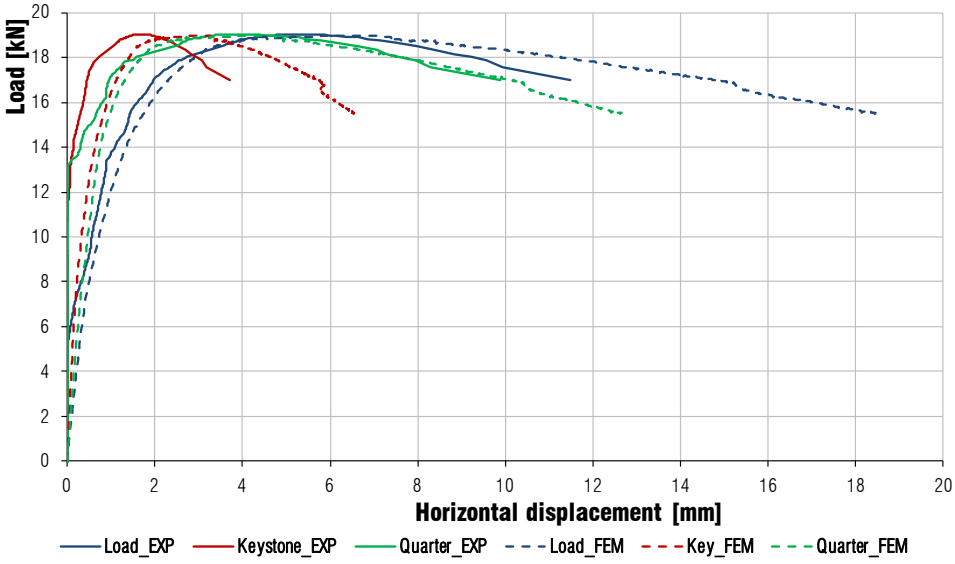


*Fig. 6.60 FEM comparison with the experimental horizontal movement of UR*

Like for the macro model the opening of hinge B was checked also in the meso model. Fig. 6.61 compares FEM and experimental measurements and shows a perfect agreement between the two solutions.

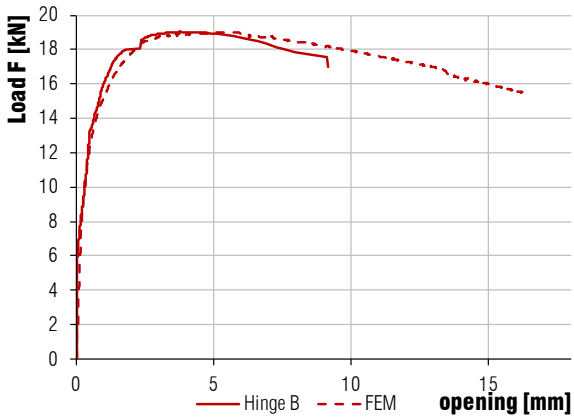


*Fig. 6.61 Comparison between FEM and experimental data of hinge B*

Once confirmed the reliability of the model in terms of numerical values of load and displacements, the analysis of mechanisms, failure modes and stress distribution are shown. The presented stages are represents in Fig. 6.62 below.

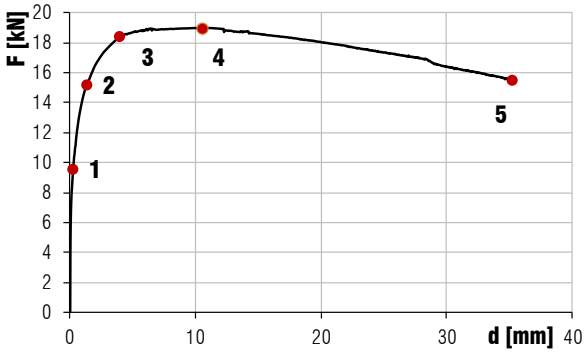


*Fig. 6.62 Stages definition in the results presentation*

Fig. 6.63 shows the development of normal contact stresses in compression for the five selected stage. At almost the half of the maximum load (stg 1) are clear the two hinges on the left A and B. Specifically, is clear the low contribution of the increased thickness on the left. With the increase of load (stg 2 and 3) up to the maximum the stress block appears evident in hinges. Indeed for lower load the stress distribution is constant instead in the mechanism activation the stress concentration is high. It is also interesting to notice at stages 4 and 5 the actual active length of the interface in the order of 3 cm. This length was also confirmed on-site where small cracks in joint appeared until 3-3.5 cm to the hinges edge. This outcome confirms that the effective hinge position is close to the section edge.

The opened joints perfectly agree with those observed onsite and reported in the crack pattern (see Fig. 5.34). The crack width reached in the last step 13.32 mm in B, 5.64 mm in C and 9.50 mm in D and for the step of maximum displacement

measured (see Tab. 5.9) the width is 9.49 mm in B, 7.94 mm in C and 5.16mm in D according to experimental results.

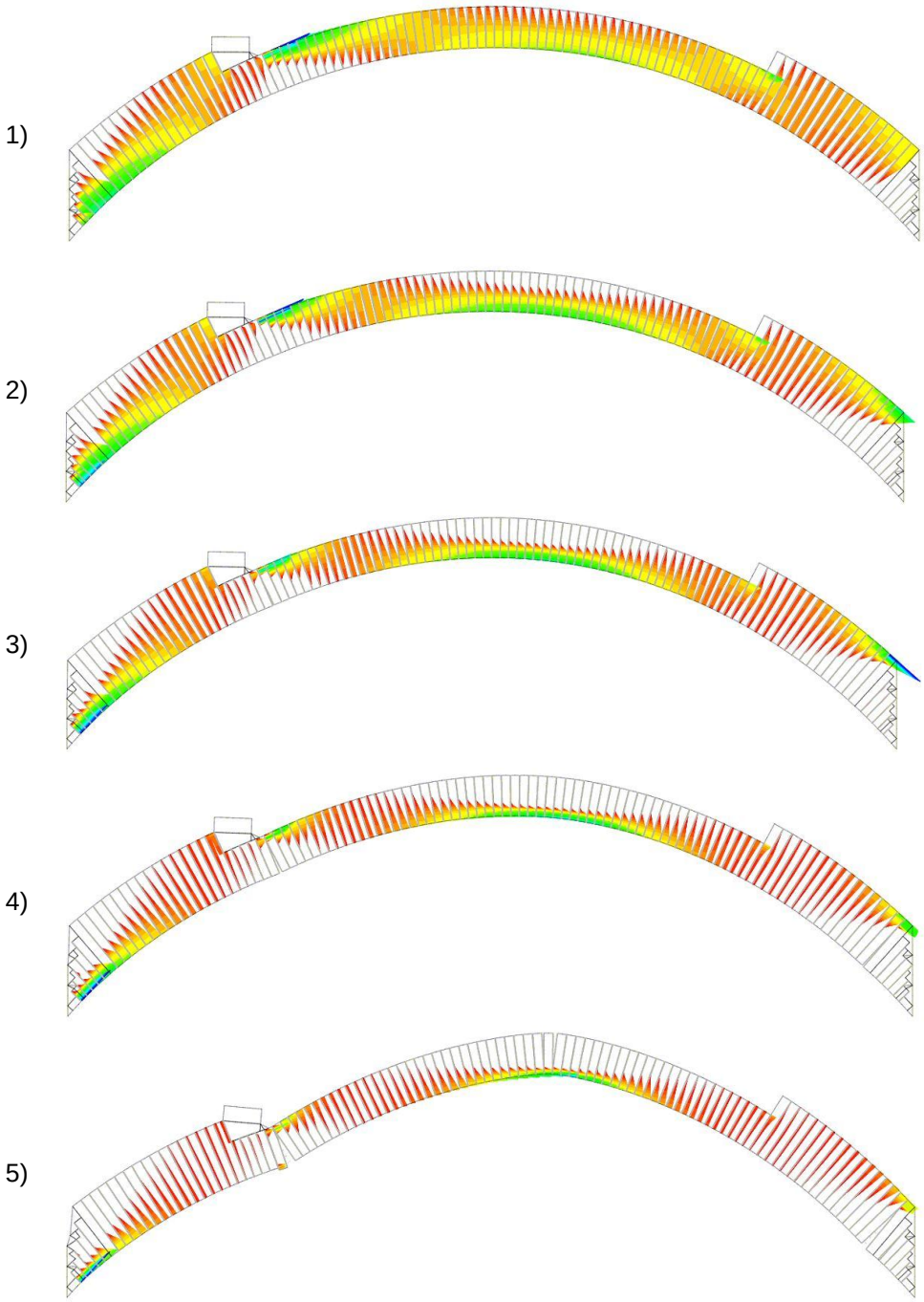


*Fig. 6.63 Normal stresses on interfaces for each stage*

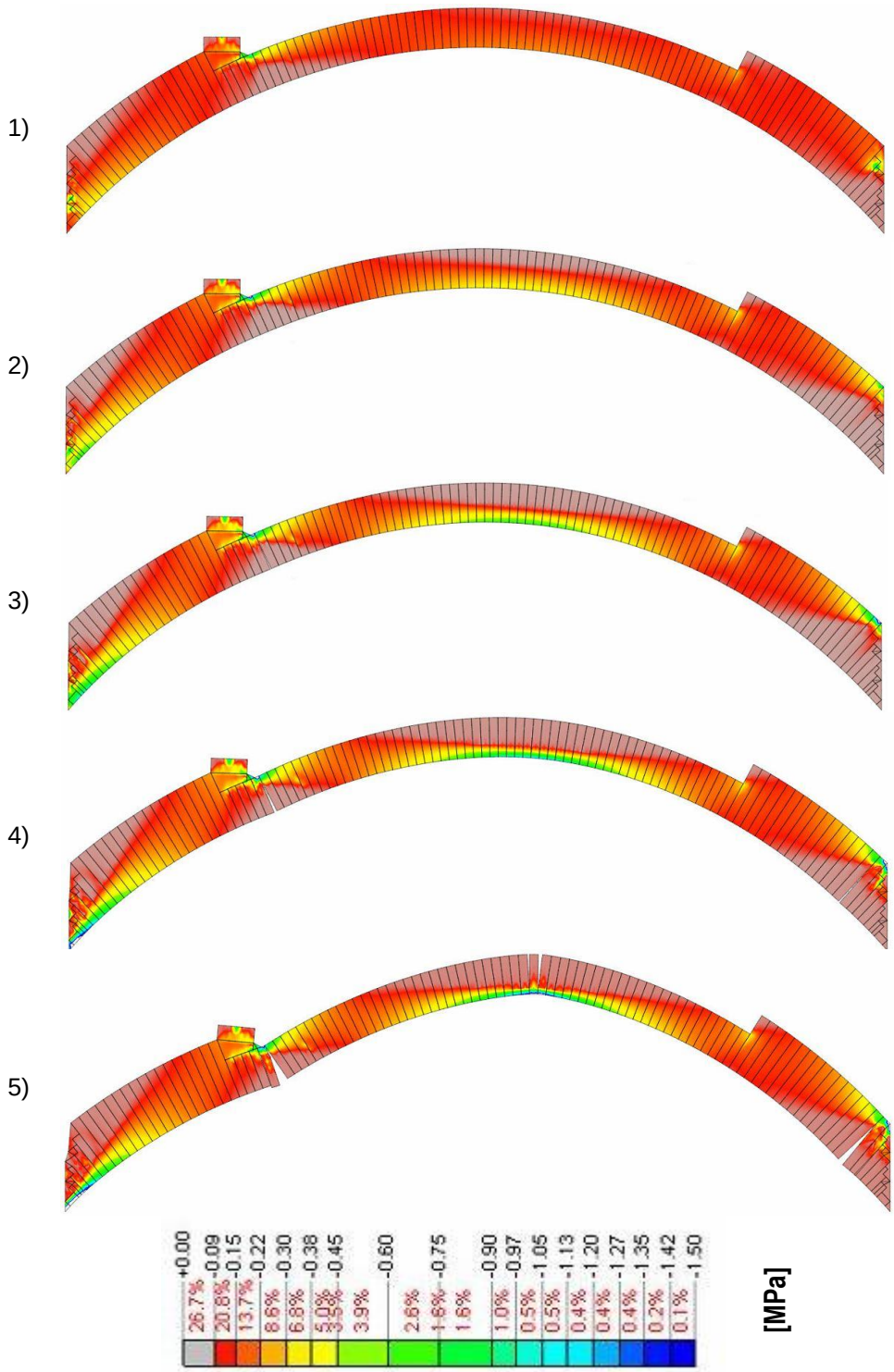


*Fig. 6.64 Principal compressive stress for each stage*

Looking at the compressive stress distribution, shown in Fig. 6.64 for each stage, the distribution is according to interface outcomes. In this case is also possible to observe the unload area, according to interfaces analysis. The magnitude of stresses is always lower than 1.50 MPa.

Another aspects, well known in literature of UR vault but evident with this powerful tool is the low area involved in stresses, the 77 % of vault has a principal stress lower than 0.30 MPa and the 92.3 % does not bears beyond of 0.45 MPa. Once again for UR vaults the most relevant parameter is geometry. It also worth to notice how thrust line goes outside the middle third (already in stage 1) for load significantly lower than the ultimate. The stress analysis also highlights the stress concentration in the step caused by the increasing in thickness in unit 86. A smoother changing of thickness will be advisable although in historic vaults is the most common arrangement.

A conclusive remarks concerns actions. In this case the action is well defined and known, but in real application is also an unknown. It was observed that the model is sensitive to load position and inclination. It is author's opinion that the achieved precision in state stress estimation is affected for practical design purposes by uncertainties on action. With the calibrated mode is now possible to test reliably all possible load distributions.

### 6.4.6 *MACROSCALE Reinforced vault*

The FE analysis was extended to the strengthening case for both approaches. The macro scale model follows indications and evaluations figured out in the unreinforced model and in particular about solution methods and equilibrium iterations. The solution was carried out with an energy convergence tolerance of $5x10^{-5}$ and a tolerance in displacement of 0.01 mm. The first outcome about this model concerns the increased effort required to converge, that specifically for the introduction of the interface in matrix, leads to some numerical troubles.

Tab. 6.17 shows the adopted constitutive law for masonry with elastic and non linear properties. About elastic modulus and compressive strength it is worth to notice that in this case properties comes from flat jack results. The non linear behaviour was defined according the aforementioned criteria about: curve type, energy calculation and ultimate displacement $d_u$ (see pg. 220).

In the strengthening model there is the introduction of a non linear interface related to the matrix as described in § 6.4.2 and 6.4.3. The linear properties are according Girardello [2012] and Basilio [2007]. A brief sensitivity analysis on these parameters seems not to affect significantly the output. Major attention was instead

given to τ-s curve and, thanks to the bond analysis carried out in § 6.4.3, the adopted curve was the one by Ceroni [2014] (gray line in Fig. 6.43).

The steel strip is modelled as a steel beam 0.084 mm thick and 250 mm width with a linear behaviour and a young modulus of 190'000 MPa.

*Tab. 6.17 Masonry properties and matrix elastic properties of interface*

| | $E_m$ [N/mm²] | $f_c$ [N/mm²] | $f_t$ [N/mm²] | $G_c$ [N/mm] | $G_f$ [N/mm] | $k_n$ [N/mm³] | $k_s$ [N/mm³] |
|---|---|---|---|---|---|---|---|
| **Masonry** | 4400 | 3.00 | 0.30 | 4.80 | 0.005 | - | - |
| **Matrix** | - | - | - | - | - | 80 | 100 |

Fig. 6.65 shows the comparison between the response curve and the FE model with a good agreement in terms of stiffness and trend. The analysis shows, for high displacements problem in convergence and therefore a maximum of 17 mm was reached. Nevertheless the model response is satisfactorily with the adopted material properties which are coherent with actual values.

Compared with the UR vault the macro-model in strengthened conditions provides better performances and a more accurate response. This might be related to the failure mode which does not involve a lumped deformation in hinge C.

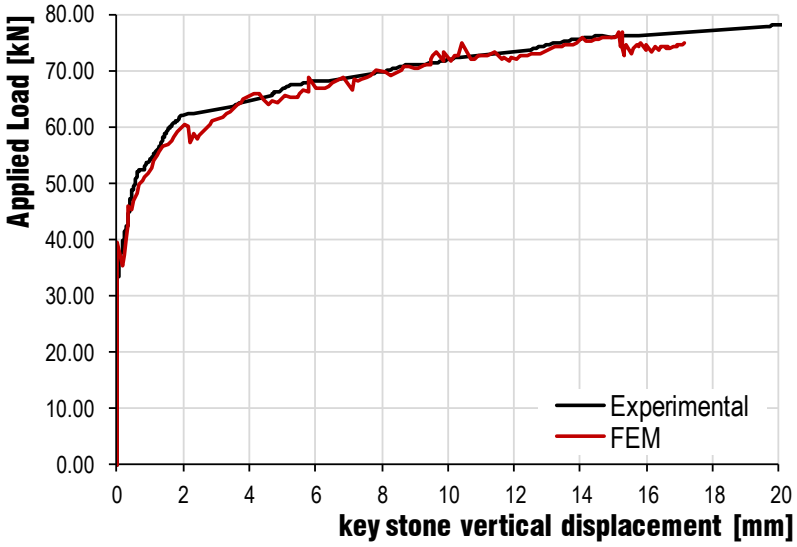


*Fig. 6.65 Comparison in load-displacement curves between experimental SRG and FEM*

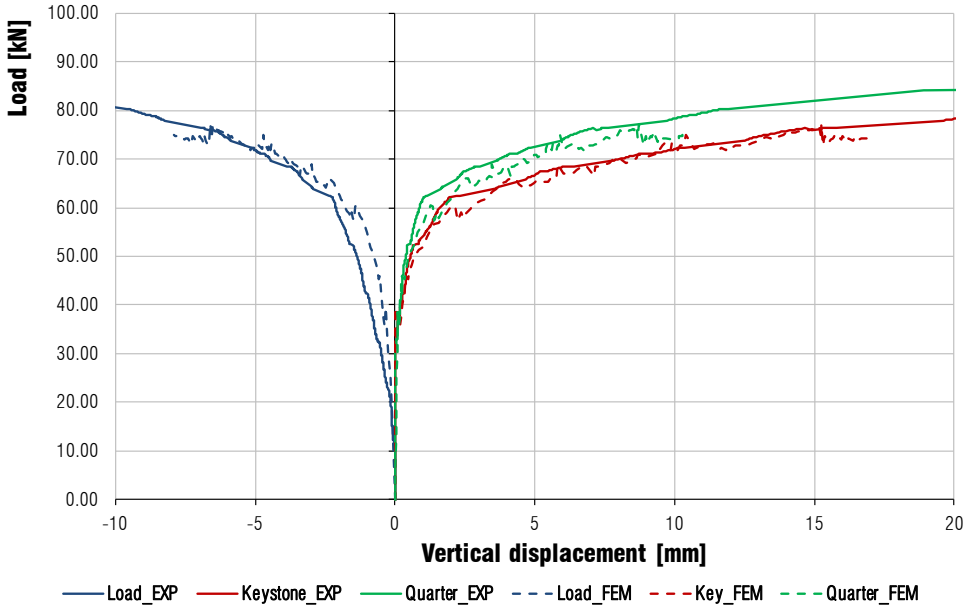


*Fig. 6.66 Model evaluation on vertical displacements of quarters*

Also Fig. 6.66, which shows the displacements comparison in each quarter, demonstrates an overall agreement with experimental results. In order to evaluate failures, stresses and the overall behaviour three stages are selected and reported in Fig. 6.67. Points are selected to represent a changing in the mechanical behaviour.

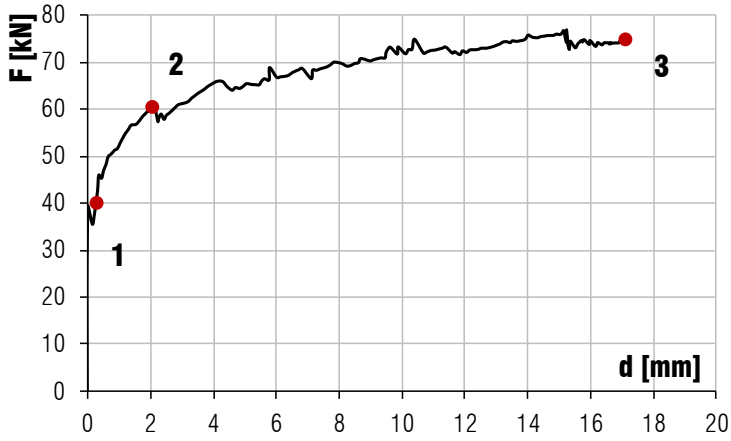


*Fig. 6.67 Comparison in load-displacement curves in keystone of test and FEM*

Principal tensile strains shown in Fig. 6.68 pointed out on stage one the onset of cracking under the loading point and on the closest support, and this explain the changing in stiffness. It has to be noted that this happen near 40 kN the estimated load of the unreinforced condition confirming again that outcome. Another stiffness changing appears on stage two and from strains plot the opening in hinge D and

first cracks on hinge C appears. Finally at stage 3 where the analysis ended the two hinges on extrados (B & D) shows an almost discrete hinges opening, also confirmed in Fig. 6.69 by the crack pattern. On the Southern support cracking are equivalent with experimental ones.

About hinge C the cracks spreading agrees with actual openings and is possible to observe the fibre influence also in the strain distribution near the vault's edge. Also the crack pattern highlights this effect.

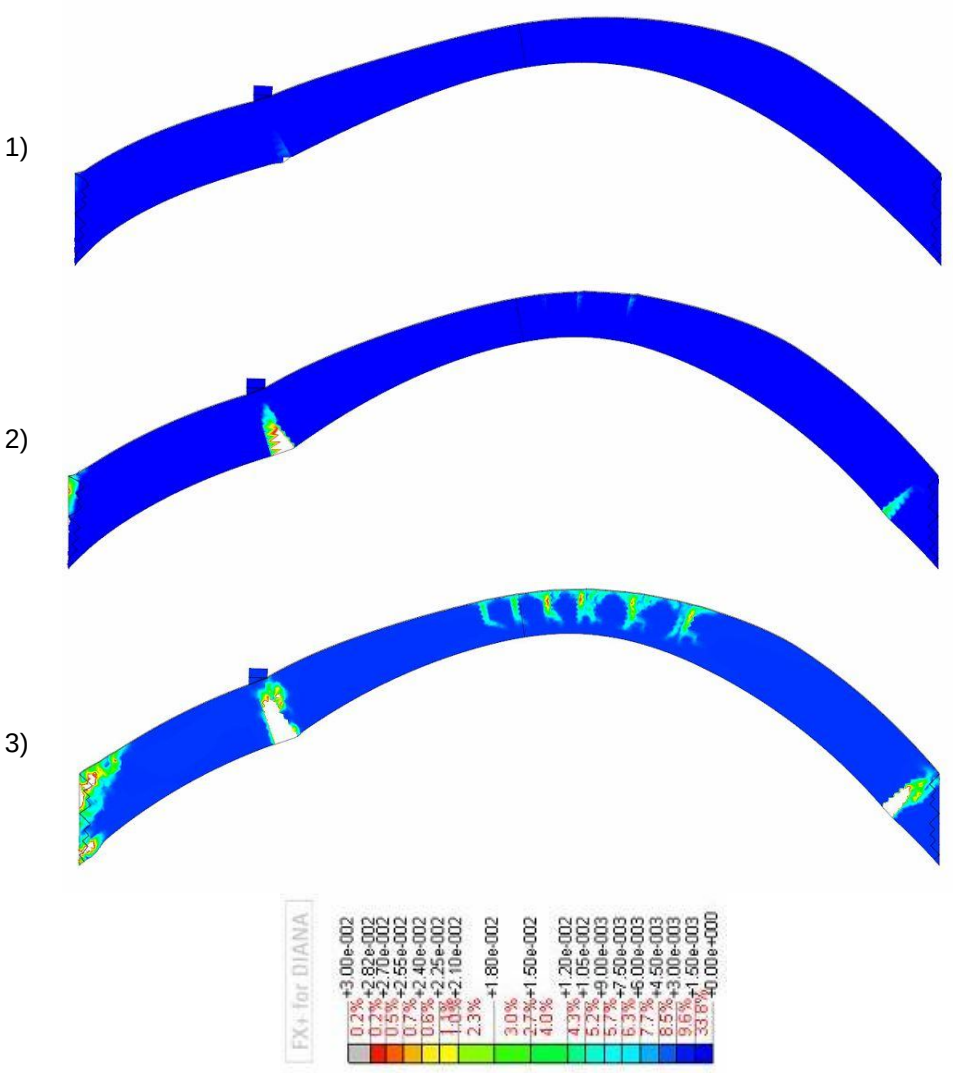


*Fig. 6.68 Principal tensile strains on each stage*

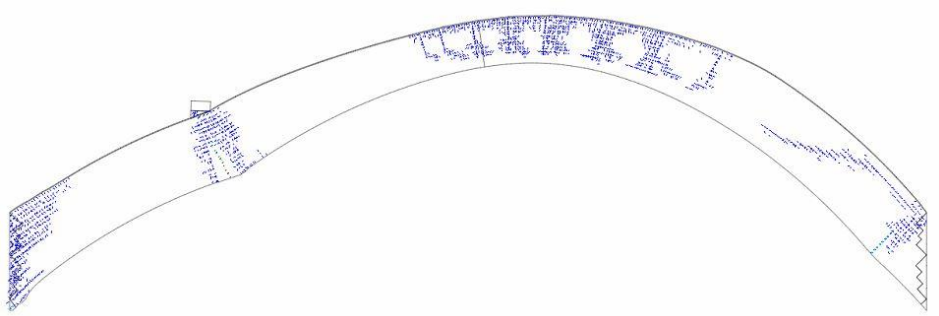

*Fig. 6.69 Crack pattern on stage 3*

1)

2)

3)

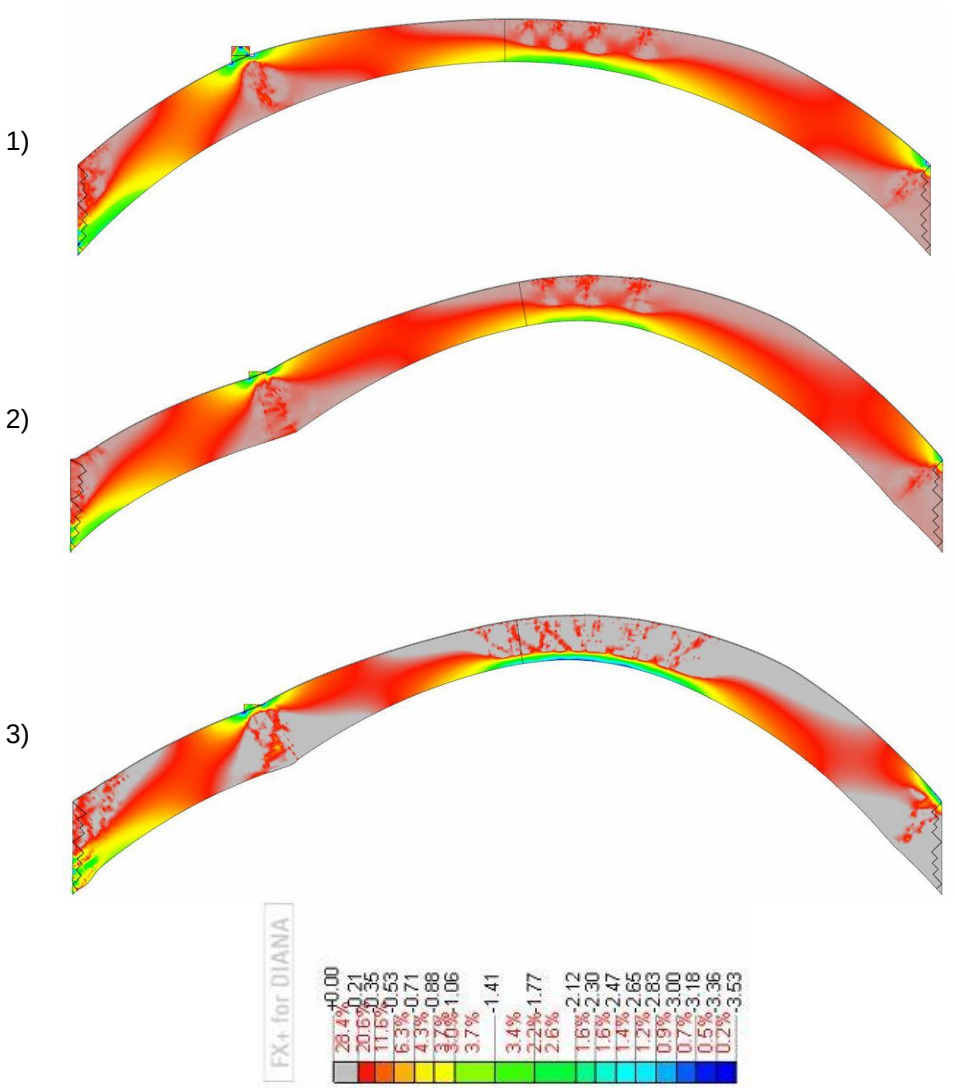


*Fig. 6.70 Principal compressive stress on each stage*

Fig. 6.70 shows the principal compressive stress distribution for each stage. As in the unreinforced vaults is clear that the thrust line behaves as a flow depending on the tension distribution in each cross section. In stage 1 is already possible to recognise unloaded areas which become more evident in further step.

Compared with UR cases stresses have higher figures in particular in hinges positions. In particular the third stage highlights the stress concentrations on the two extrados hinges. If in the CFRP case (see Fig. 5.49) the stress in hinges B results in masonry crushing according whit such observations, other two portions are critical. Indeed the two portions on the right of hinge B and on the left on hinge D due to the combined action of shear and stress could results in failure. Fig. 6.71 shows the critical portions (in yellow) directly on the mortar joint between the regularization and the original vault confirming the occurred failure in SRG. With a zoom on the failure Fig. 6.72 better explains this effect. The model provides a masonry failure on the D despite the actual observation in SRG. This is because in the model the weakness between the regularization is not considered.

Looking at stresses in intrados hinges, conversely to UR condition, C undergoes the greatest effort because of the smaller depth of the cross section.

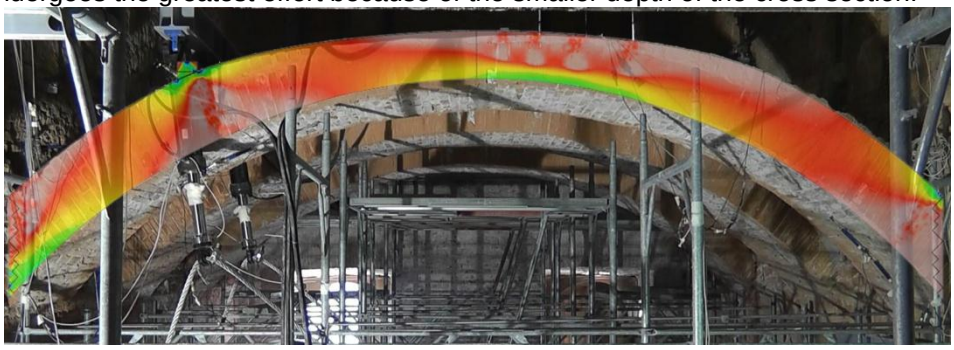

*Fig. 6.71 Principal compressive stress plotted on SRG vault*

*Fig. 6.72 Zoom on the failure*

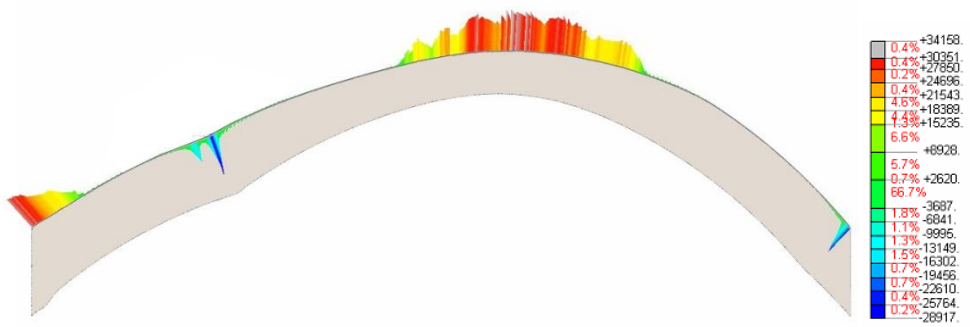


*Fig. 6.73 Tensile force developed in fibre on stage 3*

It is hence clear that failure rise in this case on masonry but some final conclusions are also drawn on fibre reinforcement. Fig. 6.73 shows the strain development within fibre to a maximum value of 30.4 kN. The strain behaviour and distribution agrees with measurement reported in Tab. 5.10 and figures as well for the reached load (75kN - see Fig. 5.64). A further comparison with the block analysis provides, for this tensile action an ultimate load of 72.7 kN very close to 74.93 kN provides by the FEM.

### 6.4.7 *MESOSCALE Reinforced vault*

The last model presented concerns the use of simplified micro modelling to the strengthen vaults. As already introduced, the nodes definition for interfaces is fundamental and in Fig. 6.74 are presented the finite elements used and the nodal interface definition. Because of that, a drawback of this approach in a model with 8278 nodes and 3146 elements is the meshing phase which is considerably time consuming.

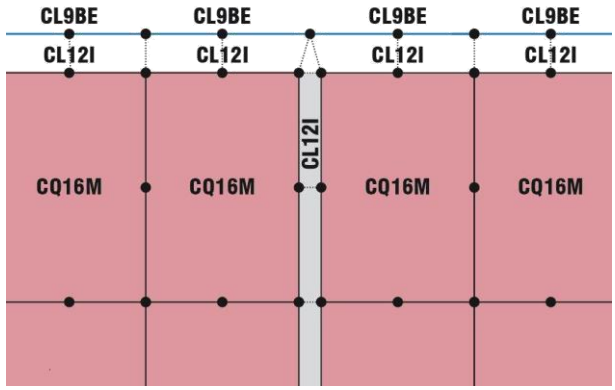


*Fig. 6.74 Elements definition and node*

The first step was to perform the analysis without the fibre contribution in order to estimate the ultimate load of the unreinforced vault with the introduction of the masonry regularization. In the load displacement graph plotted in Fig. 6.75 this

case is reported in gray. From this analysis a further confirmation of the UR meso model stability was confirmed with a reached displacement greater than 50 mm, and the maximum value reached agrees with figures of limit analysis (Tab. 6.13). The masonry geometrical regularization plays a significant role in increasing the ultimate load of about 2 times, confirming for UR conditions the importance of geometrical feature.

With the fibres introduction FEM presents an increased sensitivity to numerical aspect with more convergence problem. Fig. 6.75 shows in red the FEM load displacement curve related to the keystone in vertical direction (as for the other cases positive displacements are going up). The trend is very accurate compared with the experimental one although the ultimate displacement reached is in the order of 12 mm. This shortcoming is due to the wide series of nonlinearities associated to each material and interface.

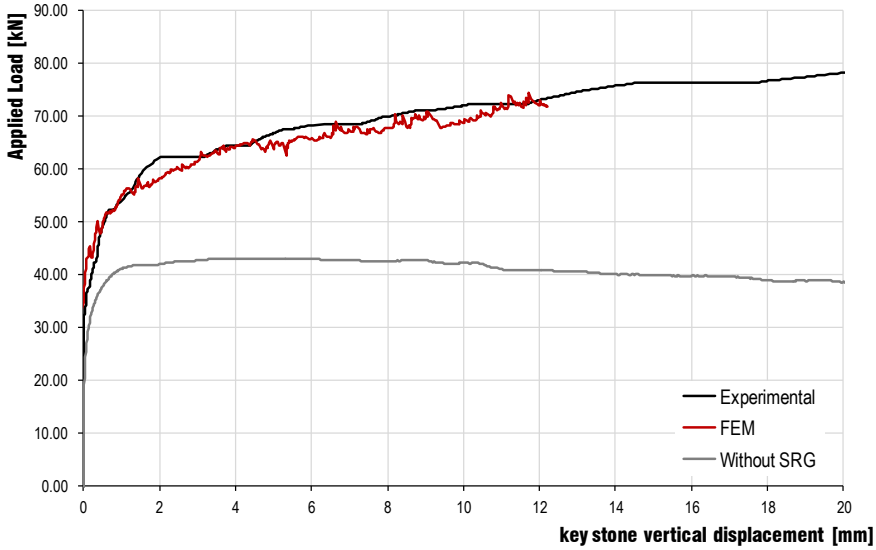


*Fig. 6.75 Comparison between load-displacement curve by experimental SRG and FEM*

According to the previous cases a sensitivity analysis of parameters was carried on. Among all parameters the most sensitive was the tensile mortar strength $f_{t,mor}$ considered in the interface parameters. Fig. 6.76 shows the curves obtained in each case. The most accurate one was $f_{t,mor}$ equal to 0.25 MPa. This increase might be related to the introduction of thicker portion of regularization in which the laboratory tests or mortar provide a tensile strength of 1.86 MPa. Such figure is not the measure of the interface failure because accounts for the tensile rupture within the mortar but it can give an insight.

Another property evaluated and modified to guarantee a better stability of the model was $f_{cm}$. Fig. 6.78 (left) shows the influence of the masonry compressive

strength that does not seem to influence the overall behaviour. The selected value of 6 MPa demonstrated the best results in terms of stability despite all three cases provide negligible differences. This aspect has to be carefully evaluated because the model is sensitive to $f_c$ in the load of peak position. Some trials with lower value (1-2 MPa) shows the typical masonry crushing in the vault with a sudden drop in the load displacement curve according to the observed behaviour (see e.g. Fig. 5.61). Therefore limitation in convergence stability does not allow to properly assessing this parameter which was surly higher than 3 MPa. The other parameters for masonry and interface have been hold to evaluate the effective contribution of the sole reinforcement.

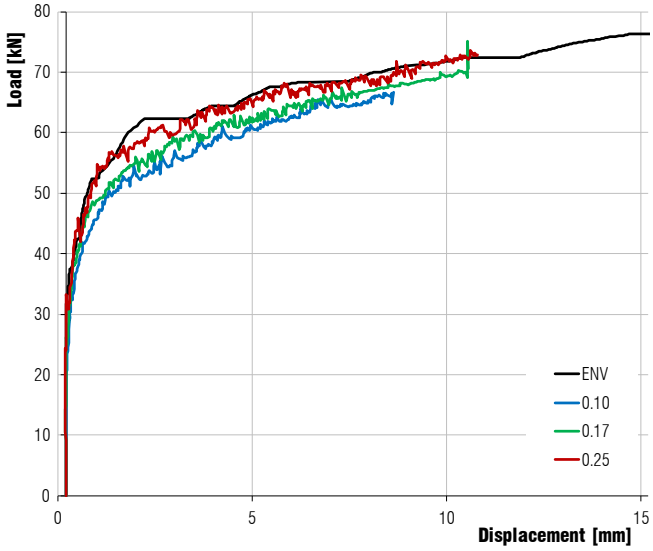


*Fig. 6.76 Sensitivity analysis on interface tensile strength $f_{t,mor}$ [MPa]*

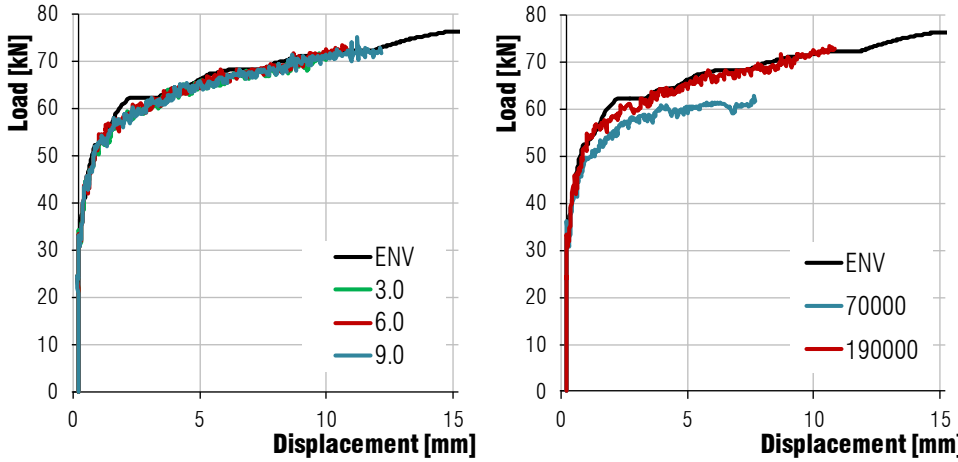


*Fig. 6.77 Sensitivity analysis on masonry compressive strength (L) fibre Young modulus (R)*

In Fig. 6.77 (right) are plotted two curves obtained with different young modulus of the fibre. As expected a lower value of the modulus presents a less stiff behaviour but is also worth to notice that a soft fibre (70.000 MPa) as the case of BRTM can express a very interesting contribution in terms of increased capacity, confirming that the experimental lower response observed is not related the net stiffness. Tab. 6.18 reports the final values selected for unit and mortar interface elements.

*Tab. 6.18 Material properties of masonry in the meso-scale SRG - FEM*

| | $E_m$ | $\upsilon$ | $f_{c,m}$ | $G_{c,m}$ | $f_{t,m}$ | $G_{f,m}$ |
|---|---|---|---|---|---|---|
| | MPa | | MPa | N/mm | MPa | N/mm |
| **Unit** | 7200 | 0.11 | 6.0 | 5.3 | 0.3 | 0.1 |
| | $k_n$ | $k_s$ | $f_{t,j}$ | $c$ | $\mu$ | $\psi$ |
| | N/mm | N/mm | MPa | MPa | | |
| **Mortar** | 120 | 60 | 0.25 | 0.2 | 0.5 | 0.01 |

Tab. 6.19 reports final values of the FRCM systems. The steel strip properties are according to the initial data. The constitutive law was defined linear because the model fails before for other aspects. More critical was the aspect related to the mortar-matrix interface. A sensitivity analysis on interface stiffness ($k_n$ and $k_s$) highlight a very negligible influence of this parameter shows similar results even with a magnitude of ten times lower. Probably this was already observed by other authors because in literature many works do not report such values. Instead, more relevant is the interface law. According to conclusions drawn in §6.4.3 and §6.4.6, the bond-slip law shows to be a valuable solution for the model. The adopted curve was the Cerroni's one reported in Fig. 6.43. A trial with lower fracture energy (1/2 times) provide a more spread shear stress along the fibre, reaching often the maximum stress but the overall behaviour remains similar.

*Tab. 6.19 Material properties of strengthening in the meso-scale SRG - FEM*

| **Steel Fibre** | | | **Mortar Matrix** | | |
|---|---|---|---|---|---|
| $E_m$ | $\rho_m$ | *type* | $k_n$ | $k_s$ | *Type* |
| MPa | kN/m$^3$ | | N/mm | N/mm | |
| 190000 | 7.85x10$^{-10}$ | linear elastic | 8 | 10 | bond-slip |

The overall response (see Fig. 6.75) provides a satisfactorily result that allows to extend observation in the whole model by means of the FEM. Fig. 6.78 plots the principal tensile strains and by the focus on hinge C deformations is possible to observe the crack positions which are spread in the same position as in the real case. The meso scale approach allows also to lump cracks in the interface among bricks as in actual behaviour whereas the entity of strains is limited within

units despite the right support where hinges A opened the cracks according to the experimentation.

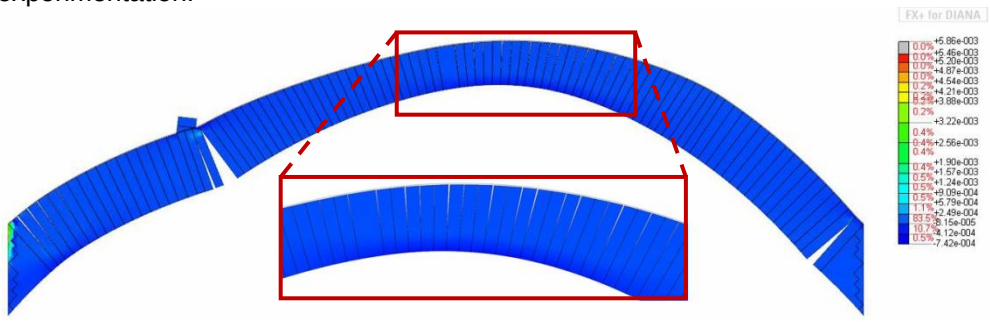


*Fig. 6.78 Principal tensile strain on the last step*

Fig. 6.79 shows the normal actions on joints interfaces highlighting the stress block behaviour. As in the case of UR meso-scale model, the normal tensile opening of joints shows a better agreement than macro-modelling. In hinges A and C is possible to see the contribution of the fibre in middle joints.

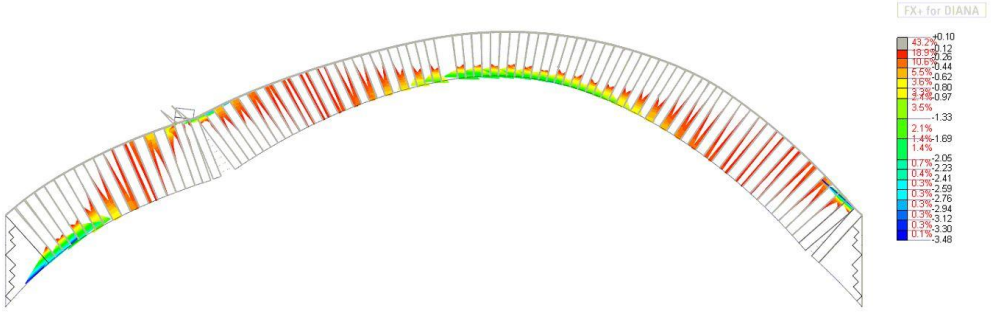


*Fig. 6.79 Normal stresses on mortar joints*

An additional view is provided by Fig. 6.80 that plots the principal compressive stresses into units. Results are similar to the macro model and it is interesting the analysis of compressive stresses compared with the thrust line. In particular when the line is inside the middle third, stresses are low and distribute. The contour confirms also the higher magnitudes in hinges and smaller thicknesses involved.

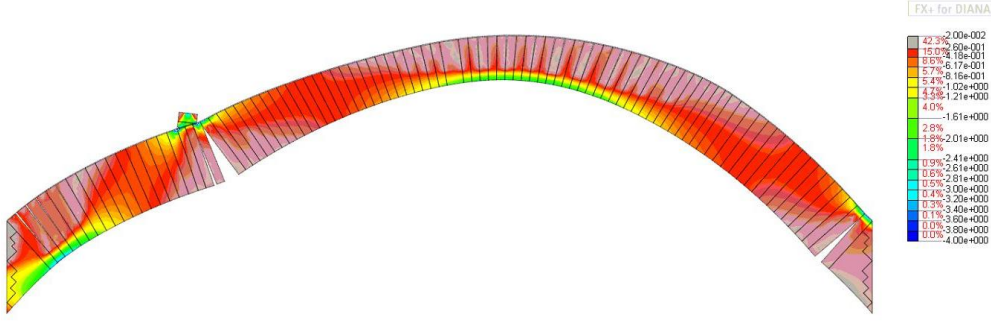


*Fig. 6.80 Principal compressive stress on the last step*

About the fibre action, the bond-slip law allows the end displacement of the fibre which relatively moves from the substrate increasing the internal normal strain. Fig. 6.81 plot the diagram of strains along the fibre. It is possible to notice the magnitude lower than actual observations. The behaviour and the distribution is instead according to experimental observations. The strain distribution in hinge A highlight the key contribution of the anchorage which provide a resisting bending moment higher than the central hinge C. Such considerations are confirmed by the shear stress contribution reported in § 6.4.6 where it appears clearly the effort migration between the substrate and the fibre.

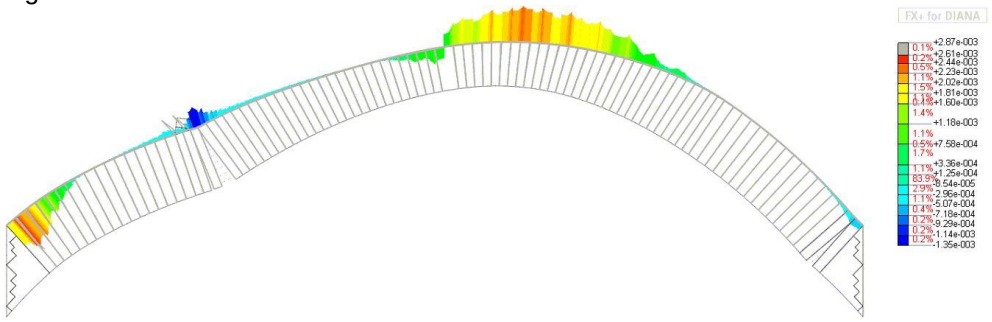


*Fig. 6.81 Strain development within the fibre*

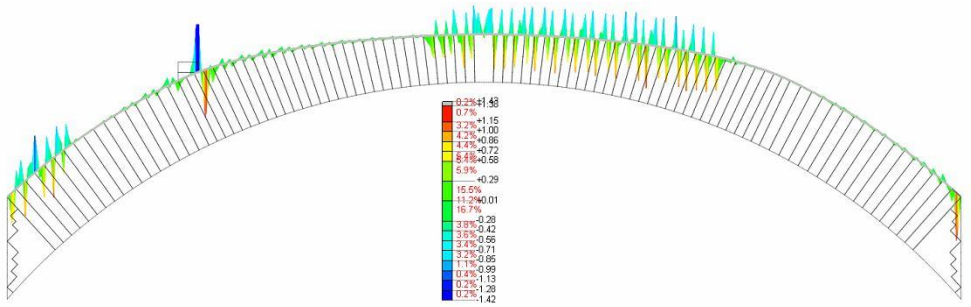

*Fig. 6.82 Shear stress of the reinforcement*

In conclusion, as often happen on FEM the meso-scale models have troubles in reaching high displacements and this require a further improvement of the model. Despite this problem, common also to the smeared crack approach, this simplified micro-modelling allows the best description of actual phenomena giving clear insights of the actual behaviour of this complex structural system.

It is also crucial to underline that despite the calibration of the model was carried out with experimental characterization numbers with a physical confirmation, their slight variation provides results significantly different in terms of load and displacement and this was pointed out during the modelling phase and the sensitivity analysis. This does not suggest this tool to the ultimate load prediction.

# 7 TEST AND ANALYSIS ON TIE RODS

## 7.1 RESERCH STRUCTURE

The creation of a database, presented in § 3.5.1, represents a suitable tools to focus the problem about the estimation of tensile action inside tie rods. In particular helps to design the experimental campaign.

The research, partially still ongoing, is organized as shown in Fig. 7.1. Three main steps were recognised and the research aims to combine those tools to provide, in each comparison, a valuable improvement or better understanding of the problem. The first comparison (A) has been carried out between numerical and analytical model. This comparison allows to simulate the experimentation and to preliminarily analyse the possible issues. Moreover it helps to highlight practical problem and differences between theoretical and practical behaviour. The step B is used to check numerical models but also to assess the FEM reliability. Finally the C step aims to understand the reliability on real cases of analytical models.

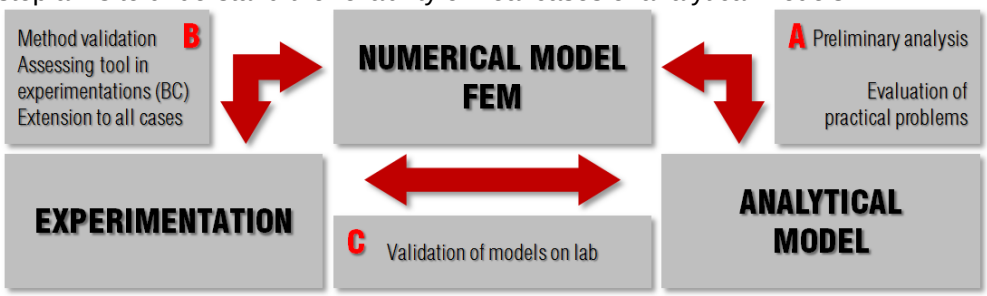


*Fig. 7.1 Schematic concept of the process adopted in this work*

## 7.2 EXPERIMENTAL CAMPAIGN

From the analysis carried out on typical ranges by the database (§ 3.5.1) six representative tie rods have been designed. Tab. 7.1 reports their geometrical features. Two lengths were selected according logistic aspects in the range of 4-5 m and 8-10 m. Moreover two areas were selected varying the section proportions in order to test two flexural stiffness for the same area.

*Tab. 7.1 Geometrical and mechanical features selected for the tests layout*

| Tie rods | length | E | Cross section | |
|---|---|---|---|---|
| | | | b | h |
| | [m] | [Gpa] | [mm] | [mm] |
| CAT 1 | 4.61 | 210 | 15 | 40 |
| CAT 2 | 4.61 | 210 | 20 | 30 |
| CAT 3 | 4.61 | 210 | 25 | 60 |
| CAT 4 | 4.61 | 210 | 30 | 50 |
| CAT 5 | 8.81 | 210 | 25 | 40 |
| CAT 6 | 8.81 | 210 | 30 | 50 |

The test setup is presented in Fig. 7.2. The tie-rod is connected in one side (left in figure) to a beam fixed to a reaction wall and in the other (right in figure) always to a beam which can be pushed by an hydraulic jack, this resulting in an axial force in the tie-rod measured by a load cell. The rod is connected to the beams through spherical hinges, thus obtaining almost perfect pinned constraints conditions.

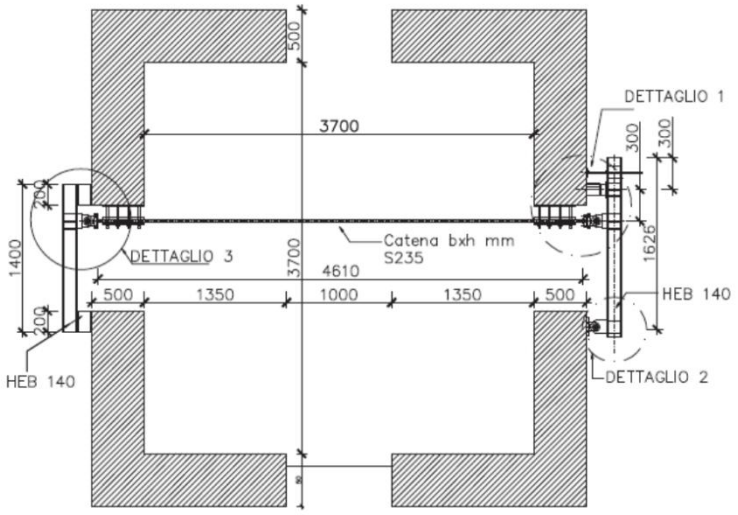


*Fig. 7.2 Design of the experimental setup with dimensions*

*Fig. 7.3 Connection end and spherical joints*

Fig. 7.3 shows the beam end connection with the beam which counteract on the wall. In yellow the jack which pushing on the reaction wall tightens the tie rod. The two black devices are the spherical nodes.

To obtain intermediate conditions between the pinned and totally clamped boundary conditions, a device composed by four steel plates which can constrain the tie by using nuts on threaded bars has been designed and showed in Fig. 7.4. The sequence of clamping, from the external to internal position, was able to confer an increasing rotational stiffness to ends. Experimental data confirmed that the tightening of all of the plates practically corresponds to fixed boundary conditions.

*Fig. 7.4 BC regulation device, frontal (left) and plan (right) view*

So far, a number of tests was carried out on a selected cross section/span combination (CAT1), with increasing axial force and different restraint conditions and specifically: five load steps, 0-20-40-60-80 kN, each of these in its turn considering six boundary configurations: pinned, clamped, and four intermediate conditions according to the tightening of each of the four plates.

The accelerometers to define the modal parameters – according to the Tullini [2008] proposed method – were installed at the span quarters, with two further

sensors placed close to ends (see Fig. 7.5). To the goal of the dynamic testing, a sampling frequency of 1000 Hz was selected, and both ambient vibration and impact excitation tests were carried out (3+3). Modal parameter extraction was carried out by means of commercial software (ARTEMIS) and proposed the resonant frequencies with the nodal amplitude of their related mode shapes.

The static approach was also adopted to measure the rotational stiffness of the boundary conditions. A point load, recorded by a load cell, was applied at the mid-span and the consequent deformations measured by three LVDTs placed in the loading point and 10 cm far from supports, this has been done for each boundary condition (Fig. 7.5).

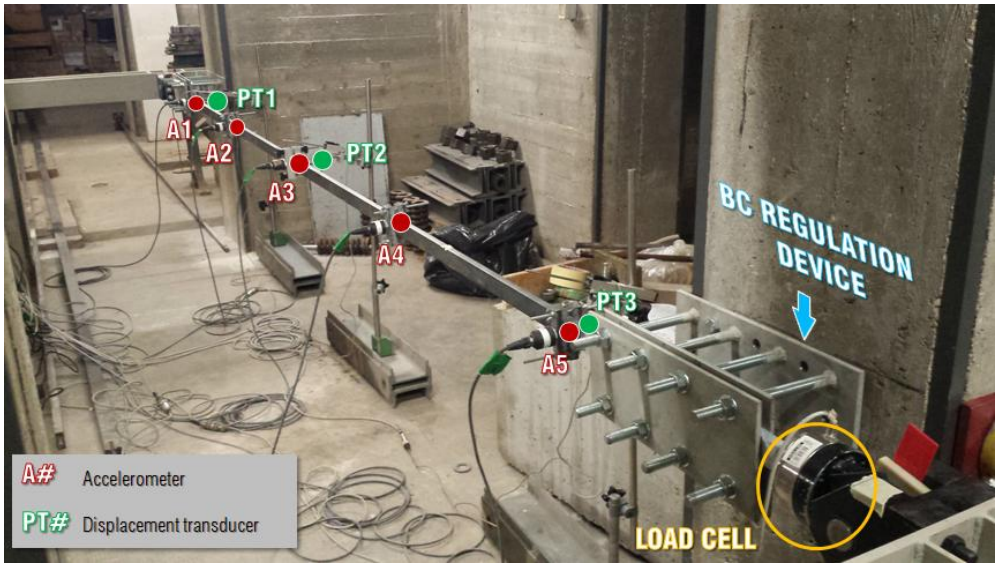


*Fig. 7.5 Experimental setup*

## 7.3 TEST RESULTS

In the laboratory experimentation the tensile action in the tie-rod was recorded by a 100 kN load cell (the same of CH5), whereas the stiffness of BC was calculated starting form a load. Fig. 7.6 shows an example of the measures carried out for a tensile action N in the tie of 20 kN and the relative displacement curve in the three positions (see Fig. 7.5) for a load applied in the mid-span.

This graphs allows to perform the static approach [Briccoli Bati 2001] and also to assess the BC stiffness.

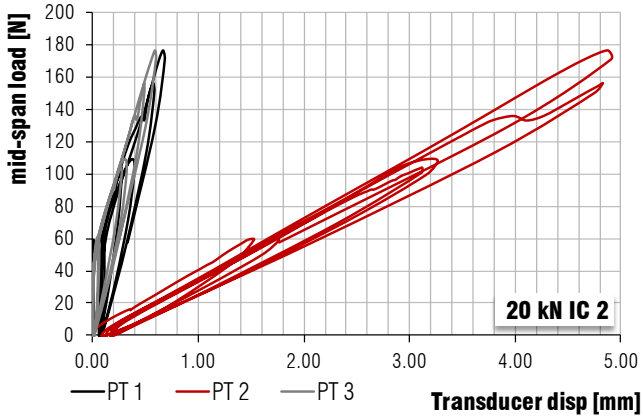


*Fig. 7.6 Load deflection graph to estimate the stiffness of BC*

Tab. 7.2 reports the dynamic results in 16 cases. The values reported are the average among the six records. The $CV_{mode}$ is the CoV calculated among the value of the eq. (2.9) left side for all the six measures. It is worth to notice that the CoV measured among records of each case provided figures in the order of 1% for the first frequency instead about the $CoV_{mode}$ the differences can reach very high value. In the following of the research this trouble will be reduced by a new execution of the test for high CoVs as is currently adopted in sonic test.

*Tab. 7.2 Test results with average frequencies and first mode shape amplitudes*

| ID TEST | BC | $f_1$ [Hz] | $f_2$ [Hz] | $f_3$ [Hz] | $v_1$ [#] | $v_2$ [#] | $v_3$ [#] | $CV_{mode}$ [%] | $v_1/v_3$ |
|---|---|---|---|---|---|---|---|---|---|
| 20KN_PP | PP | 8.30 | 17.09 | 27.34 | 0.44 | 0.76 | 0.48 | 20.62 | 0.93 |
| 20KN_PIC1 | IC1 | 10.25 | 22.46 | 37.60 | 0.47 | 0.75 | 0.47 | 0.98 | 0.99 |
| 20KN_PIC2 | IC2 | 9.77 | 21.00 | 34.67 | 0.47 | 0.75 | 0.47 | 0.67 | 0.99 |
| 20KN_PIC3 | IC3 | 9.28 | 19.90 | 32.59 | 0.47 | 0.75 | 0.47 | 1.35 | 0.98 |
| 20KN_PIC4 | IC4 | 8.79 | 18.68 | 30.40 | 0.50 | 0.68 | 0.52 | 22.96 | 0.98 |
| 20KN_FF | FF | 10.25 | 22.46 | 38.09 | 0.47 | 0.75 | 0.46 | 17.51 | 1.02 |
| 40KN_PP | PP | 10.74 | 21.97 | 33.69 | 0.45 | 0.75 | 0.48 | 37.69 | 0.95 |
| 40KN_PIC1 | IC1 | 13.31 | 27.95 | 44.92 | 0.49 | 0.71 | 0.50 | 17.43 | 0.99 |
| 40KN_PIC2 | IC2 | 12.57 | 26.25 | 41.99 | 0.49 | 0.72 | 0.49 | 10.85 | 0.99 |
| 40KN_PIC3 | IC3 | 12.21 | 24.78 | 37.96 | 0.48 | 0.74 | 0.48 | 0.13 | 1.00 |
| 40KN_PIC4 | IC4 | 11.47 | 23.80 | 37.35 | 0.48 | 0.73 | 0.49 | 4.85 | 0.99 |
| 40KN_FF | FF | 13.67 | 28.32 | 45.90 | 0.49 | 0.72 | 0.48 | 41.93 | 1.03 |
| 60KN_PP | PP | 12.70 | 25.39 | 39.06 | 0.48 | 0.73 | 0.49 | 60.20 | 0.97 |
| 60KN_FF | FF | 16.11 | 33.20 | 52.25 | 0.48 | 0.73 | 0.49 | 56.67 | 0.99 |
| 80KN_PP | PP | 14.16 | 28.81 | 43.46 | 0.40 | 0.57 | 0.40 | 89.59 | 0.98 |
| 80KN_FF | FF | 18.07 | 36.99 | 57.62 | 0.48 | 0.73 | 0.48 | 61.32 | 0.99 |

## 7.4 FINITE ELEMENT MODELS

### 7.4.1 *Preliminary analysis*

In the research the Finite Element Analysis has been used first of all in the preliminary phase to design the experimental test. This demonstrates that models can be useful also prior to tests. It has to be remind that the analysis, as reported in § 2.5.4, needs to take into account of the initial state stress in order to update the stiffness matrix. The experimental campaign designed and presented above, has been carried out by FEM analysis to analyse the reliability of models and to carried out some sensitivity analysis.

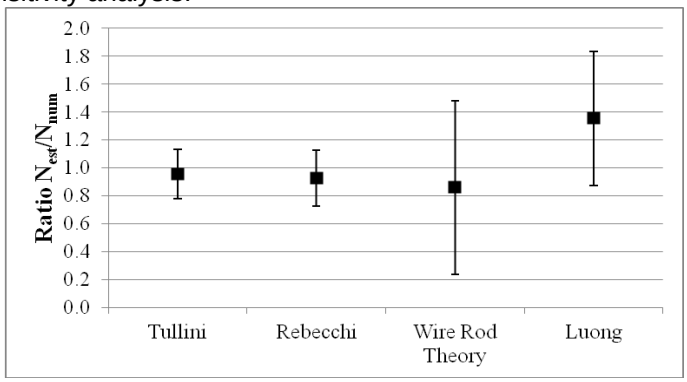


*Fig. 7.7 Average ratio of agreement between the estimated axial force by different methods and corresponding FE model numerical one.*

Fig. 7.7 summarises the variation range obtained by the application of analytical models to FEM results. The analysis indicated that the Luong [2010] method presents less dispersion with respect to the string theory, and that the Tullini method seems to be the quite well matching the FE predictions.

The analysis was carried out also in terms of different working rate and BC. About the influence of BC increasing the stiffness of supports the reliability decreased for the Luong method, while the Tullini one demonstrated not to be sensitive to this parameter. In this numerical analysis all models presented a slight error increase with the increase of axial stress.

In total 230 cases were analyses and each case is reported in Mosca [2015]. The sensitivity analysis highlights that the number of subdivisions in mesh should be greater than 8. Moreover the analysis of the rotational stiffness pointed out that for a BC higher than 1-2 times the beam flexural stiffness the connection can be considered as fixed.

Another sensitivity study was carried out using the MAC matrix (see pg. 176) where different BC and sensors positions were compared to pointed out the sensitivity to differences. In Tab. 7.3 are reported the diagonal values of each

evaluated case. The first (I) compare three accelerometers at quarter, in the second (II) two accelerometers are near supports and one central, the last (III) accounts for three accelerometers at quarters and two near ends.

*Tab. 7.3 Diagonal values of MAC evaluated on FEMs with pinned and clamped restraints*

| | Modes | | | | |
|---|---|---|---|---|---|
| | 1st | 2nd | 3rd | 4th | 5th |
| I | 0.987 | 1.000 | 0.979 | 0.667 | 0.169 |
| II | 0.973 | 1.000 | 0.899 | 1.000 | 0.084 |
| III | 0.974 | 0.998 | 0.906 | 0.432 | 0.001 |

Reasonably the sensitiveness increases with the number of sensors and covering many positions. In general the variation is small and the MAC can be considered a reliable tool only if it considers the first five modes where there are more differences in models. About sensors location, the position near the tie ends seems to be a sensitive position for a correct assessment of the actual rotational stiffness (II, Tab. 7.3). The choice of the number of sensors must then to balance the on-site efforts with the precision required.

These considerations are considered in the (A) branch (see Fig. 7.1) therefore a fundamental aspect rise in noises and precision. In facts positions close to ends are less involved in the vibration and for this reason more affected by noises and less precise in the measurement. In conclusion the author still recommends the position in quarters.

### 7.4.2 *FEM calibration*

In addition to the preliminary analysis the FEM was developed for all cases tested on laboratory.

Fig. 7.8 shows an example of the model where the intermediate conditions are considered (IC3 on the left and IC4 on the right). In the model the material properties were defined (Area 622 $mm^2$, E 210 GPa, $\rho$ 7850 $kg/m^3$, v 0.3) and the axial force in the tie-rod was measured. The only calibration was carried out about the axial stiffness of the axial spring associated to the regulation device.

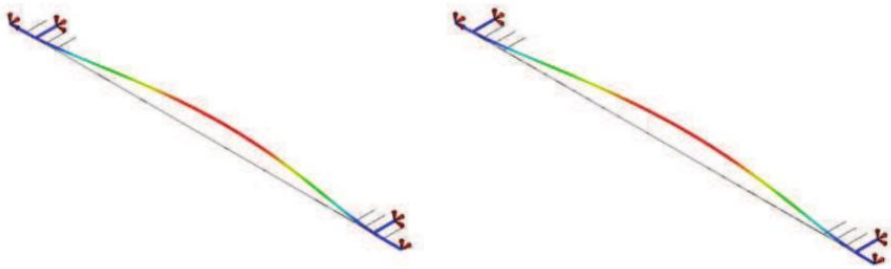

*Fig. 7.8 Diana model calibration of Intermadiate conditions (IC)*

After this the spring was moved in each position. Tab. 7.4 shows the FEM obtained value in frequency compared with those measured on lab. The agreement is good and with an average absolute error of 2.18 % and a standard deviation of 1.24%.

*Tab. 7.4 Comparison in frequency between Experimental figures and FEM*

| Mode Shape | IC1 | | IC2 | | IC3 | | IC4 | |
|---|---|---|---|---|---|---|---|---|
| N = 20 kN | $f_{Exp}$ [Hz] | $f_{FEM}$ [Hz] | $f_{Exp}$ [Hz] | $f_{FEM}$ [Hz] | $f_{Exp}$ [Hz] | $f_{FEM}$ [Hz] | $f_{Exp}$ [Hz] | $f_{FEM}$ [Hz] |
| 1 | 10.25 | 10.30 | 9.77 | 9.72 | 9.28 | 9.00 | 8.79 | 8.43 |
| 2 | 22.46 | 22.66 | 21.00 | 21.28 | 19.90 | 19.49 | 18.68 | 18.12 |
| 3 | 37.60 | 38.39 | 34.67 | 35.89 | 32.59 | 32.48 | 30.40 | 29.98 |

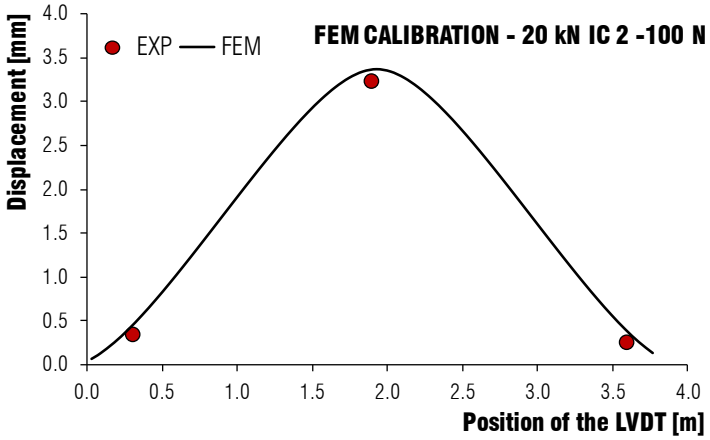


*Fig. 7.9 Comparision beteween FEM displ and experimental measurements*

Fig. 7.9 shows the comparison with the displacement measured on site (red dots), due to the application of the mid-span load, and the FEM deformation. All the comparisons are available in [Ramonda, 2015]. Moreover, the MAC matrix between tests and FEM was calculated with values equal to 1.00 on the diagonal and 0 in other positions.

From such comparisons some interesting conclusions are pointed out. The MAC, used also to analyse the FEM accuracy is order of magnitude less precise than transducer measurements. The comparison between numerical model and experiments (branch B Fig. 7.1) demonstrate that FEM is a valuable solution and that with a careful modelling is possible to obtain precise results. Because of that, when the precision requirement on the estimation is high, the author suggest to use a FEM model. The model may check both mode shape and high frequencies as suggested in the model of Amabili [2010] that could be suitable.

Finally this agreement allows to extend analytical evaluation and improvement on simulated campaign carried out by FEA to extend solutions.

## 7.5 ANALYTICAL MODELS

### 7.5.1 *Existing methods*

The last step (C in Fig. 7.1) concerns the evaluation of analytical model by means of the experimental campaign. The experimental campaign helped to confirm some analytical outcomes, to validate the FEM tools and to highlight some issues.

Despite the BC evaluation which is easy to set in static terms in controlled condition as in the laboratory, the static approach shown an excellent agreement with the measured load. In Tab. 7.5 these results are shown. Measures refer to pinned conditions.

*Tab. 7.5 Comparison between measured load and estimated*

| Exp [kN] | Briccoli Bati [2001] [kN] | Err [%] |
|---|---|---|
| 20.8 | 20.8 | 0.10 |
| 40.1 | 40.0 | -0.07 |
| 60.1 | 60.1 | 0.02 |
| 79.2 | 80.0 | 1.00 |

*Tab. 7.6 Results of first tests and comparison with estimations*

| ID TEST | BC | Exp [kN] | Tullini [kN] | Luong PP [kN] | Luong FF [kN] |
|---|---|---|---|---|---|
| 20KN_PP | PP | 20.1 | 20.6 | 28.5 | 18.3 |
| 20KN_PIC1 | IC1 | 20.4 | 18.2 | 26.6 | 15.9 |
| 20KN_PIC2 | IC2 | 20.1 | 18.4 | 26.9 | 16.3 |
| 20KN_PIC3 | IC3 | 20.5 | 19.0 | 26.9 | 16.2 |
| 20KN_PIC4 | IC4 | 20.5 | 17.9 | 25.9 | 15.3 |
| 20KN_FF | FF | 20.8 | 17.5 | 25.7 | 15.3 |
| 40KN_PP | PP | 40.0 | 37.7 | 49.6 | 36.5 |
| 40KN_PIC1 | IC1 | 40.4 | 43.4 | 46.4 | 32.7 |
| 40KN_PIC2 | IC2 | 40.4 | 41.5 | 46.3 | 32.6 |
| 40KN_PIC3 | IC3 | 40.3 | 37.9 | 48.2 | 34.6 |
| 40KN_PIC4 | IC4 | 40.2 | 37.8 | 45.8 | 32.0 |
| 40KN_FF | FF | 40.1 | 41.9 | 47.2 | 34.1 |
| 60KN_PP | PP | 60.0 | 60.2 | 68.9 | 54.3 |
| 60KN_FF | FF | 60.1 | 56.7 | 65.0 | 51.1 |
| 80KN_PP | PP | 80.1 | 89.6 | 86.4 | 70.4 |
| 80KN_FF | FF | 79.2 | 61.3 | 82.2 | 66.1 |

The dynamic approach seems to be less accurate compared with the static one as presented in Tab. 7.6, where the values estimated by dynamic models are reported.

It is relevant to notice that the Tullini method seems to be the more accurate one, estimating quite satisfactorily the measured load. The increasing in stiffness of BC shows an increase error in estimation. This disagrees with the considerations made for FEM where it seems to do not affect the response. Looking at the overall response, the advantage to evaluate the mode shapes and hence to define correctly the boundary conditions, significantly improve the quality of results for the Luong method, with a difference of about 10÷15 kN in the evaluation of the tensile force depending on the BC. Looking at $CoV_{mode}$ (Tab. 7.2) it is possible to notice that significant errors in estimation of mode shape amplitude lead to higher error in the estimation of the axial force N.

Summarizing results of Tab. 7.6 the Tullini method give an average estimation of 0.96 the real value and a CoV of 9.4 % that could be considered enough accurate for onsite measures. At the same time the estimation of Luong has an average of 1.2 of overestimation for pin-pin with a CoV of 8.7 % and another boundary of 0.83 with a CoV of 6.6 %.

In Fig. 7.10 the estimations are presented and it become clear the presence of two boundaries (dashed lines) given by Luong method instead Tullini well estimate real values.

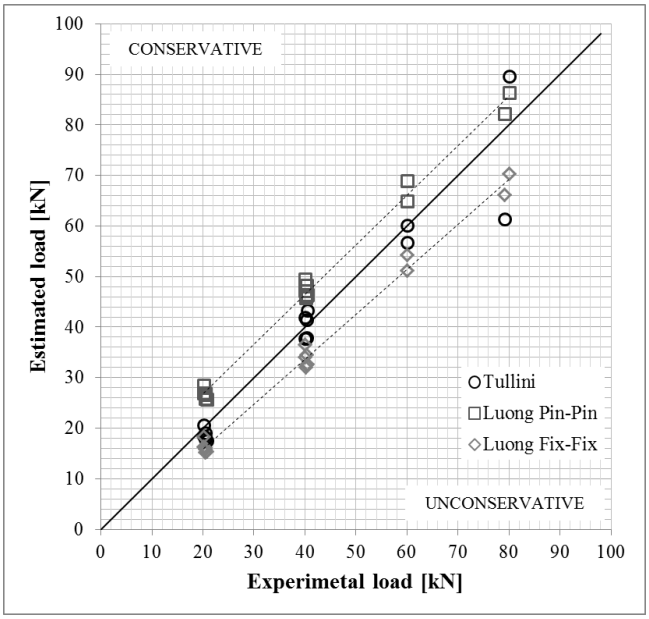


*Fig. 7.10 Experimental load vs estimated load of each models.*
*Dashed line shows the average boundaries of Luong method [Cescatti, 2016a]*

It has to be stressed that it was noted in the highest step (80kN) a relevant error also in the Tullini's method, comparable with the error of other models. The experimental campaign helped to highlight that real applications of Tullini are affected by measurement and sensor positioning. Whereas mode shapes of FEM are exact, the estimation of the mode shape by means of identification techniques are affected to actual position of sensors which require to be carefully positioned.

Analysing the Tullini's method form a theoretical point of view, starting from eq. 37), and calculating for a determinate n the left hand of eq. (2.9) varying $\lambda$ the obtained curves are reported in Fig. 7.11. It is also possible, to determine the field in which each eigenvector is defined.

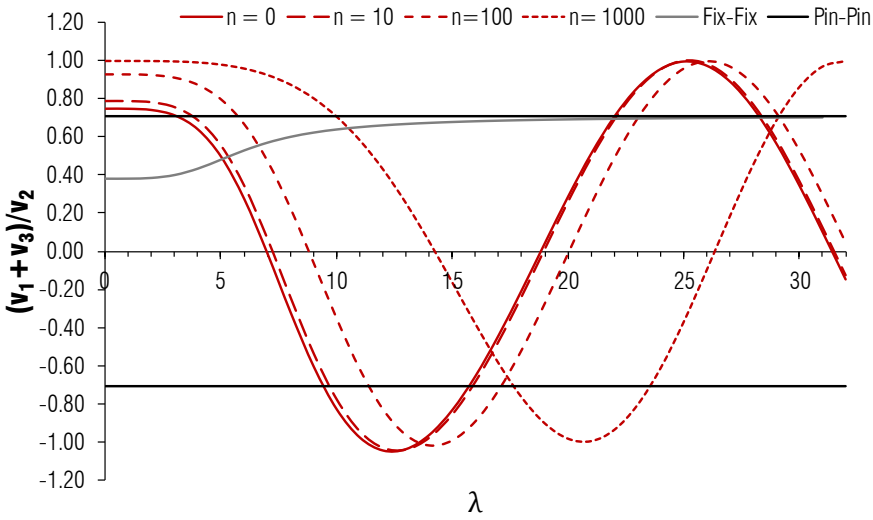


*Fig. 7.11 Lines of axial tensions for the Tullini method*

The model provides to be very rigorous form an analytical point of view. The experimental campaign helps to recognise the drawbacks that rise in the practical application. In particular the ID shows a very good performance in estimation of frequencies whereas error increases for the evaluation of eigenvectors. In this framework it is therefore advisable to work with both quantities to improve the method.

The study carried out indicated a decrease of influence played by BC with the increase of the axial force. On the contrary the estimation reliability seems to decrease. As a first consequence of this, all methods referring to the string theory, even with the advantages of the simplicity, considering just one frequency, proved not to be reliable.

The approach by means of numerical models demonstrates to be more time consuming and less rigorous from a theoretical point of view but, with an

appropriate calibration (e.g. an increasing number of sensors, like 5 or more) it gives reliable results, and according to the consideration above mentioned these methods less suffer the noises and disturbances of experimental tests.

To approach the problem in the modal domain (Tullini's method) demonstrated to be a valid option with good results and less effort. The drawbacks of this technique are related to eigenvectors that require a mandatory number of accelerometers, (at least three) and hence more on-site operations. Moreover it needs to measure the modal amplitudes, which means the needs of good instrumentation. Despite these minor problems is possible to conclude that this should be considered the standard method of estimation.

The static approach demonstrated to be a valid option with reliable results in pinned conditions. More evaluation in BC will be done but overall errors are very small. However, the static method is less suitable than the dynamic one in real cases on site due to difficulties in positioning LVDTs. Moreover it requires the installation of strain gauges that on one hand need more time in application and on the other hand they are more invasive due to the removal of coating than accelerometer positioning.

### 7.5.2 *Proposal and development*

The development of tests that should be performed on sites looks to improve the reliability but to simplify as well. It is indeed relevant to purpose methods which provide different precision levels depending on efforts in order to allow the practitioner to select the test balancing efforts and results.

During tests has been noted that the ratio between the modal amplitude on external quarters (last column Tab. 7.2) has an average of 0.99 and a CoV of 2.45 %. As remarked above the needs of three sensors increase the time involved on site, especially where tie-rods needs spider crane or scaffolding to be reached, for instance in churches. The idea here was to analysis the model reliability only with two accelerometers, one on in the mid-span and one on an external quarter. This can be done by the hypothesis of symmetry between the two ends. This modifies the eq.**(2.9)** in eq. (7.1).

$$\frac{2 \cdot \nu_1}{\nu_2} = \frac{1 + 2\cos(q_1/4) \cdot \cos(q_2/4)}{\cos(q_1/4) + \cos\mathrm{h}(q_2/4)} \tag{7.1}$$

The analysis of the ratio between $v_1$ and $v_3$ was also extended to the whole database to assess its variability. It was possible to observe a variation of the ratio but this was also related to the variability of modal amplitude as remarked in Tab.

7.1. From this is possible to pointed out that is very important the care of sensor position and signal acquisition, as well as of sensors number.

Another aspect concerns the sensitivity to asymmetric conditions of the original proposal. The left hand of eq. (2.9) calculates an average among the two, hence it provides for sure better results than only one value but still does not face rigorously the problem. On the other hand it should be care of the user to adopt three accelerometers when there are clearly asymmetric conditions. The worst values in the database were found for cloister's ties where in one side the tie-rod goes into the wall and on the other into a column. The results still confirms the laboratory outcomes.

The test on lab of this new proposal provides indeed an average ratio in the prediction of 0.94 and a CoV of 12 % with the respect of three accelerometers where the average 0.98 was with a CoV of 9%.

Fig. 7.12 shows estimations made by the proposed adoption of two sensors and results seem correctly estimated.

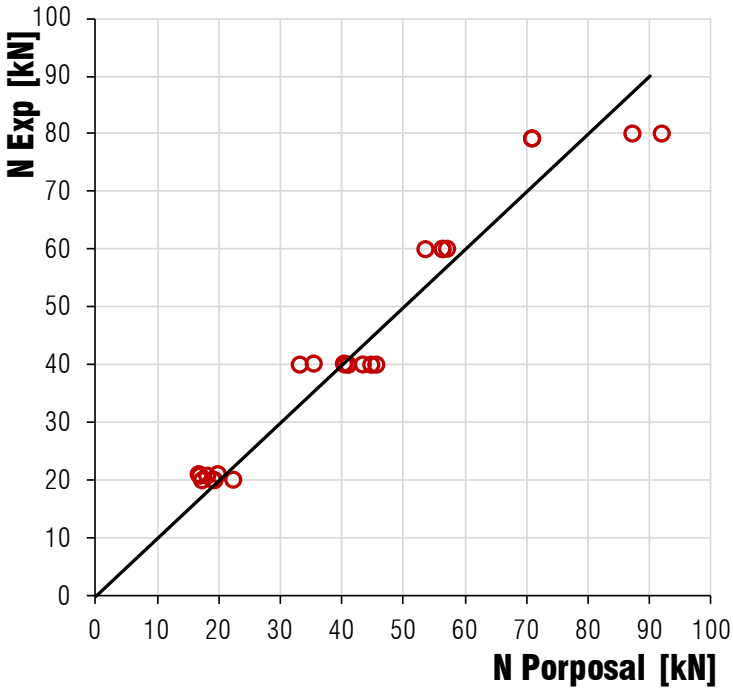


*Fig. 7.12 Estimated value with the proposal vs experimental measures*

In conclusion depending on the balance between efforts and accuracy it is possible to adopt different methods. In any case for on-site application the dynamic methods are more suitable.

The most accurate method is the numerical identification of the tie-rods, similarly to the proposal of Amabili [2010], this is also the most time consuming. In

the middle there is the Tullini [2008] proposal with three accelerometers whereas the model that requires less effort is the one here proposed. It accuracy is in the order of 12 % even very high for usual NDT tests.

In future works it will be necessary to focus on simply models based also on frequencies of higher modes that are easier to detect from an instrumental point of views and require fewer instruments. A possibility can come from the analysis of this proposed model including higher modes although first attempts still do not provide satisfactorily results.

# 8 CONCLUSIONS

The work carried out throughout the whole thesis pointed out several outcomes among all the phases of the current methodology in the structural assessment of existing buildings. Moreover the possibility to analyse these steps in real cases allowed to evaluate the development of the entire methodology.

In this framework, it is crucial to remark the need of testing, or when possible monitoring, in continuous control of further phases as modelling and intervention. In the presented cases indeed the application of tests, NDT and MDT, was fundamental to achieve reliable results according to current guidelines. Another aspect is related to the critical judgment capacity to moving between phases. A preliminary analysis on the literature showed limits and needs of the actual state of art. In addition to the vault diffusion in buildings, a first elaboration of the data collected after earthquake strokes highlights vaults as the mechanisms with the highest seismic risk. From the review of analytical models implemented for vaults it is clear that the strengthen case is not only a geometrical problem but involved the stress-strain distribution. This distribution in curved elements is not linear according to Navier formulation but a study on typical ranges of vaults and bridges figured out a small influence of this aspect that can be neglected.

In the following conclusions are reported according to the objectives reported for each tasks in introduction (§ 1.2).

## 8.1 INFORMATION AND INVESTIGATION

The knowledge phases, focused in CH 3, demonstrated to be a compulsory step in the assessment of building actual behaviour. Moreover the gathering of three datasets helps significantly to the scope.

i. Sonic tests, by the development of the presented algorithm, have been updated and improved in time costs and thanks to the automatic estimation of flight time provides more accurate and objective pulse velocity. The quantitative meaning confirms to be weak compared with DT tests an ineffective for double flat jacks. Instead, from a qualitative point of view, the analysis of pulse velocity underlines to be a useful tool. The comparison between typologies and velocities figured out some representative ranges that could be divided at least in three judgments namely: lower, medium and high quality. The quality detection is necessary to extend tests on the whole building and to recognise possible material vulnerabilities which can results in crumbling.

ii. The collection of a wide dataset was significant also in the case of Double Flat Jacks. The possibility to compare a total number of 103 tests, performed uniformly, allows to drawn some conclusion. First of all the analysis carried out on brickwork masonry remarks the high variability in mechanical properties and the influence of many parameters as the building typology and the construction period. The study was also focused on the test procedure an interpretation. About the first the use of a continuous acquisition together with a cyclic test allows to gather a noticeable number of data on site that can be compared among them. It was possible to recognise the secant modulus in unloading phase like the most stable parameter which can be purposed as reference value. This does not means that this modulus can be directly compared with the Young modulus, as correctly defined in the axial test, but at least could represent an objective value useful to be compared among test and proposed in standard. The use of areas defined in the stress-strain field in addition to stiffness modulus may also be a valuable solution.

iii. The thrust analysis on vaults showed a complex distribution of forces based on stiffness in indeterminate conditions, in this case was possible to assess the different contribution of the bearing walls thanks to tie rods measurement but this pointed out as well the

trouble in thrust appraisal that remarks the necessity of reliable methods in the estimation of the tension acting in ties in usual conditions.

The dataset collected and the experimental campaign carried out within this work demonstrates that, if modelled with the explained criteria and carefully calibrated, the FEM provides accurate and reliable results and this method is suggested when high accuracy is needed. Although the static approach presents high precisions it does not appear a suitable solution because many errors are possible on sites due to the delicate procedure. Nevertheless in many case on-site the required precision is lower and hence dynamic analytical methods demonstrate to be more suitable. This work figured out the Tullini method as the most rigorous and precise (AVG 0.98 and CoV 9 %) but the outcome is a proposal of modification with only two accelerometers that reduces the 30% of on-site operations and increases the CoV of only 3%. In conclusion mode shape methods (as Tullini) are more powerful theoretically, because the precision in BC estimation, but on the other hand are more affected by sensors features like: position accuracy and quality.

## 8.2 DIAGNOSIS AND SAFETY EVALUATION

Together with experimental applications the field of analysis was focused in the work and it was possible to drawn some conclusions. The availability of experimental results allows not only to compare different computational methods among them, as usually observed for building analysis, but to have a comparison with real responses. The followed approach has a methodological meaning concerning the capacity evaluation and not related to the action and therefore it can be applied to static or seismic actions. Different conclusions are drawn for UR and strengthened elements.

In the framework of the actual methodology, for UR masonry elements, the tricky point concerns the mechanisms identification, from this point of view the thrust analysis but in particular the FEM model can accurately predict the hinge position. The analysis carried out highlighted the sensitiveness to constructive details which reveals to be not details in the behaviour. In addition, actual situations

may present a crack pattern which has to be carefully read in order to recognise the actual mechanism. In particular on arches the critical load can be accurately estimated by FEA, DEM, block analysis and kinematic analysis according to Heyman conclusions (Fig. 8.1 left).

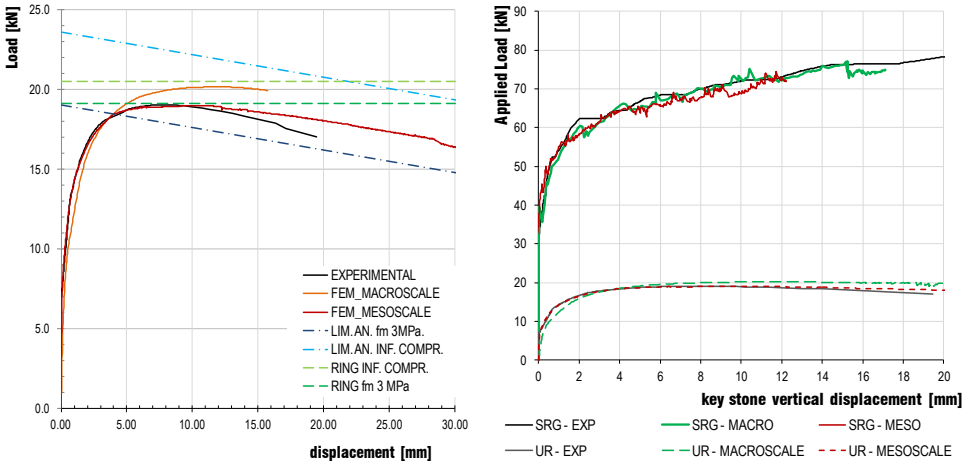


*Fig. 8.1 Comparison among numerical tools in UR (left) and among FEM models (right)*

It has to notice that finite elements showed a good agreement with the actual curves (Fig. 8.1 right) in both approaches macro and simplified micro modelling but it was possible after some studies and calibrations. Indeed it was the method that better describes actual observations and demonstrates its power. The meso scale model was very accurate in the description of the crack pattern, in crack width and in force displacement curve. With the respect of UR, strengthening models accounting for more non linearity pointed out increased numerical problems in convergence. As drawback FE models show a serious sensitivity on the many parameters needed to perform the analysis. It is author's opinion that finite element analysis is very useful to understand the structural behaviour, failure modes and to generalized results but is not suitable to a blind prediction of the ultimate load of the assessed structure or element. Moreover the finite element models provide, especially in macro modelling, limited displacements compared with real capacity curves. This must be carefully evaluated and could be dangerous in the evaluation of non linear static analysis where, according to Newmark [1982] outcomes, the controlled parameter is the ultimate displacement of a control point.

The kinematic analysis proved to be accurate and reliable in the analysis of the peak load and in the inclination of the post peak behaviour typically considered in the capacity curve (Fig. 8.1 left). The method is hence suitable in the non linear analysis with the evaluation of displacements. Another outcome is related to the

hinge regression which highlights to influence the critical load. It is hence advisable to consider this parameter also in the kinematic analysis in order to fulfil the yield criterion of the uniqueness theorem. The compressive strength of the material hence influences the critical load even if not dramatically. The influence is higher in flat arches in which the ratio thickness over span is higher. Finally load conditions closed to snap-though phenomena are still difficult to assess as figured out in the DIA case. In general applications on existing buildings of a combined use of FEM and limit analysis can be consider as reliable.

The role of strength properties, $f_{cm}$ and $\varepsilon_{fu}$ becomes crucial in reinforced conditions. In this field it appears clearly the influence of strength in the critical load. Many efforts are still need in the research of the actual behaviour of strengthened arches and in particular concerning the ultimate allowable strain of the fibre. According to other FRP applications [Cescatti 2012] it should be recognise a maximum strain which can develop all bearing mechanisms in the cross-section. This value seems to agree with the intermediate detachment CNR [DT-200:2012] and to 1.2 % according ACI [549.4-R-13] for FRCM applications but many studies are needed.

In this work a simplified numerical method has been proposed in order to account for the strengthening intervention. Despite the block analysis (RING) provides good results the linear elastic behaviour of FRP is not accounted. The method, moving between upper and lower bound theorems, provides the ultimate load capacity of the strengthened vault with better accuracy and limiting the maximum load achievable as describe in §6.3.3.

## 8.3 DECISION ON INTERVENTIONS

After the analysis on material characterization the research moved on the structural element level by the selection of vault systems. The analysis looks at the vault behaviour out of plain for unreinforced and reinforced configuration but to the behaviour in plane as well. The system is also completed by the analysis in tie-rods.

During the installation phase some simply practical observations were pointed out in terms of workability (see § 5.1.2) and economical issues. The first concerns the irregularity of historical masonry arrangements which requires significant effort in regularization and cleaning for carbon applications while mortar based composites are more suitable and are more close to normal masons

applications compared with resin work. Form an economic point of view the estimation carried out (about material based on the manufacturer) showed for area unit a convenience of mortar based application whereas, considering the area installed SRG and CFRP are quite similar instead basalt is the most expensive solution (Tab. 8.1). The prices related to work should be considered relatively and not in absolute terms because can change in different geographic areas. As explained in § 2.1 in the intervention design, costs are only one among many parameters to evalute. Neverthless it appers appropriate to reports information also in this field.

*Tab. 8.1 Economic evaluation of EBR interventions*

| | $b_f$ | Work | Material | | Total | |
|---|---|---|---|---|---|---|
| | [m] | [€/m$^2$] | [€/m$^2$] | [€/m] | [€/m$^2$] | [€/m] |
| **CFRP** | 0.10 | € 65.18 | € 125.90 | € 12.59 | € 191.08 | € 19.11 |
| **SRG** | 0.25 | € 37.61 | € 55.68 | € 13.92 | € 93.29 | € 23.32 |
| **BTRM** | 0.80 | € 35.23 | € 23.98 | € 19.19 | € 59.21 | € 47.37 |

The preliminary tests execution on composites figured out a qualitative meaning of pull-off where results were spread and the comparison with shear test is not affordable. The variability is related to surface preparation but also to the test position because of mortar joint and to the specimen cut. The main advantage of the test, which is simple and cheap, concerns the failure mode that should be considered separately between organic and inorganic matrixes. According to current guidelines for the first case, the failure in the substrate (A) proves the intervention effectiveness and the proper installation. For inorganic resins the failure B occurs more frequently and it is difficult to assess the quality with this test. Surely the system ineffectiveness, usually due to a too high strip density compared with matrix is proved by the occurrence of failure C. The onsite execution of shear-test demonstrates to be a valuable solution to control the system effectiveness. If in one hand figures are more difficult to interpret compared with a laboratory test, especially about slip, on the other the failure mode for a predetermined bond length proves numerically the overall shear strength of the anchorage. Both inorganic systems demonstrated to develop the entire fibre strength.

The tests performed on five full scale historical masonry vaults are an innovative solution with the design of a dedicated setup and which provide first results form an actual structure not reconstructed. The experimental campaign highlights the influence of structural details in stereotomy and connections on the overall behaviour, moreover the regularization intervention with masonry proved the

importance of geometry with a double ultimate load. The traditional intervention with diaphragms showed a very fragile behaviour increasing the ultimate load by the hinges movement but, once activated, the mechanism led to collapse. Conversely EBR strengthening technique on the extrados confirmed to be an optimal solution.

Form the load bearing capacity the minimum increase was of 3 times and maximum of 4.55 times. A large increasing was observed also in displacement capacity but with different behaviour among reinforcements. The basalt net showed a limited displacement even lower than UR whereas steel, grouted in mortar as well, exhibit an ultimate displacement of 7.67 times the UR. The ductility was significantly higher in SRG and very limited for BTRM. Both systems with inorganic matrix show a stiffer behaviour prior the onset of cracking with the respect of organic applications (CFRP). In general these outcomes are according to observations carried out on laboratory [Girardello 2012]. Considering an equal strength and stiffness between CRFP and SRG the latter pointed out better results. Carbon showed debond on the support and led before to masonry crushing. The basalt net, although as explained was not the best strengthening technique, demonstrated the effectiveness of EBR interventions applied on vaults where the mechanism was already activated as often happend after earthquakes. EBR proved to be a very effective strengthening intervention, its efficacy could be higher for slender vaults.

The observed failure modes confirm literature outcomes with the activation of the flexural mechanism inside the arch. This changing involves directly the strength of each material. For carbon and steel application the failure involved the masonry crushing. It is hence reached the maximum load bearing capacity of the element. It has to be noted that this failure involves directly a material damage whereas the rigid body mechanisms dissipation is related to the selfweight effects and hence potentially it could bear the maximum effort infinite times instead the masonry crushing led to the total loss of the original element. Form the conservation point of view this has to be considered. However, about conservation, the application of FRCM (without cement) proved to be less invasive and more compatible in physical and chemical terms with the respect of FRP, allowing also a better removability.

Efficient anchorages, for instance with the strip continuity in SRG, demonstrated to be an important detail in the extrados strengthening because decrease the possibility of shear failure but especially because provide another significant contribution in the hinge on supports with an overall increases of the ultimate strength. Finally a proper anchorage, as reported for unbonded tendons, may helps in the avoiding of the mechanisms increasing the tensile action in the reinforcement due to the perpendicular movement.

The case study in the framework of ProVaCI research project here presented was not problematic and pointed out good qualities of the structure in terms of material and global behaviour. However it was an extraordinary opportunity to analyse the behaviour of vault out-of-plane and in-plane at the building scale. The major outcome confirms the demand of a proper modelling and it will be suitable to develop and calibrate equivalent elements in order to reduce computational costs here necessary to the overall calibration. In addition the deep knowledge phase carried out in this real application confirms the difficulty to provide a unique and numerical description of material characteristics and hence remark the demand to combine many tests.

## 8.4 MONITORING

The dynamic analysis proved to be an effective and powerful tool to evaluate the stiffness increasing due to intervention and could be used to control the intervention efficacy by a NDT method. The identification also showed to be reliable in the reveal the rise of damage, especially about frequencies, demonstrating its value in SHM application. In case of monitoring of course many other factors are involved and the detection should be made with less damage than in this case but however the approach demonstrated its power. The damage detection was more focused on material degradation while the activation of the mechanism does not report same drops in frequencies. Damping information does not exhibit reliable results but this can also be associated to the identification technique. The analysis of MAC between the vault pre and after the test shows a variation in the mode shape due to the rise of damage and a deeper analysis could lead to promising results. In conclusion the methodology adopted proves to be excellent with the use of many accelerometers and with the random impact excitation. It was indeed possible to identify nine modes and to obtain, in the comparison with FEM model, very good results in frequency agreement and MAC matrix.

## 8.5 FUTURE WORKS

In the following are summarized according to each task herein faced the future works relevant in the author's opinion.

**Information and investigation**: the common wish for all tests is to extend all the three datasets with a large amount of future data.

i. Future works concerning sonic tests should try to improve the tomographic elaboration and acquisition in order to achieve better results in terms of time costs and accuracy. The time or frequency domains of pulse signal might provide further information on masonry quality but few works are available so far.
ii. About flat jacks it will be interesting to research and evaluate a multi parametric approach at least combining results with tests on mortar. Finally some considerations and analysis have to be pointed out to correlate the effective relationship between the elastic Young modulus which cannot be detected flat jacks and secant stiffness in unloading phase.
iii. In the estimation of axial tension in ties, future works should focus on the combined use of higher modes and mode shapes in order to reduce the error related to only one mode shape without increasing sensors.

**Diagnosis and safety evaluation:**

At the local level, future work would analyse and enlarge conclusions provided to similar vaults tested in different ways as for instance the cases of Garmendia [2015] (static test), Girardello [2013] (cyclic tests) and Giamundo [2014] (shaking table tests).

At the global level the comparison between models it will be interesting if scaled on the whole castle by means of the two available modes presented in § 4.3.

**Decision on interventions**:

A further experimental study should be provided in the measurement of deformations, especialy in FRCM application because it was difficult to correlate actual fibre deformations with those measured on the inorganic matrix that could not account for inner slip of strips.

Future works on **monitoring** should focus deeply on the characterization of the mode shapes to improve the damage localisation, once it is recognise. There are already some examples in literature; the application on this case with many acceleormeters could help to evalute such approaches.

## REFERENCES


Abrams D.P., Epperson G.S.; [1989]; *Non destructive evaluation of masonry buildings*, Advanced Construction Technology Center, Doc. n. 89-26-03, Urbana Illinois, October.

Adam, J. P. [1984]. *L'arte di costruire presso i romani. Materiali e tecniche.* Longanesi, Milan. (in IT).

Allemang R. J., Brown D. L.; [1983] *A Correlation Coefficient for Modal Vector Analysis,* 1st Int. Modal Analysis Conference, 247-261.

Amabili M., Carra S., Collini L., Garziera R. Panno A.; [2010]; *Estimation of tensile force in tie-rods using a frequency-based identification method*, Journal of Sound and Vibration, n.329 (11): pp. 2057-2067.

Anania L, Badalà A., D'Agata G. [2013]; *The post strengthening of the masonry vaults by the Ω-Wrap technique based on the use of C-FRP*, Journal of Construction and Building Materials, n. 47: pp 1053-1068.

Badalà A., Cuomo M, D'Agata G.; [2008] *Analisi limite di volte a botte rinforzate con CFRP,* XVII Convegno Italiano di Meccanica Computazionale – GIMC2008, Alghero, (Italy). (in IT)

Barlow W.H.; [1846]. *On the existence (practically) of the line of equal horizontal thrust in arches, and the mode of determining it by geometrical construction.* Minutes and Proceedings of the Institution of Civil Engineers, n. 5: pp.162–182.

Basilio I. S.; [2007]; *Strengthening of arched masonry structures with composite materials*, University of Minho, PhD Thesis, Portugal.

Bathe K. J.; [1992]; *Finite element procedures in engineering analysis* Prentice-Hall, New Jersey, USA.

Beconcini M. L.; [1996]; *Un metodo pratico per la determinazione del tiro nelle catene*. Costruire in laterizio, n. 54: pp. 229-301.

Belluzzi O.; [1941] *Scienza delle costruzioni*, Ed. Zanichelli, Bologna, Italy.

Binda L., Lenzi G., Saisi A.; [1998]; *NDE of masonry structures: use of radar tests for the characterisation of stone masonries,* Int. Journal of NDT&E n. 31(6): pp. 411-419.

Binda L., Gambarotta L., Lagomarsino S., Modena C., [1999]; *A multilevel approach to the damage assessment and seismic improvement of masonry buildings in*

*Italy*. Seismic damage to masonry buildings, Balkema, Rotterdam, Netherlands.

Binda L.; [2005]; *Investigation for the diagnosis of historic buildings: application at different scales*, 2nd Seminar on conservations, University of Porto, 12-14 October, Portugal.

Binda L., Cantini L., Cardani G., Saisi A., Tiraboschi C.; [2007]; *Use of Flat-Jack and sonic tests for the qualification of historic masonry*. 10th North American Masonry Conference, 3-7 June, St. Luis, Missouri, USA.

Binda L, Saisi A. ; [2009a] *Application of NDTs to the diagnosis of Historical Structures.* Conference on Non-Destructive Testing in Civil Engineering, 30th June - 3rd July, Nantes, France.

Binda, L., Borri, A., Cardani, G., Doglioni, F., [2009b]. ReLUIS 2005-2008. *"Scheda qualità muraria: relazione finale e linee guida per la compilazione della scheda di valutazione della qualità muraria".* Tecnical report

Blondel François [1683], *Course d'Architecture, 2* vols., Paris, (in FR) (reported also in Heyman [1996]).

Bolza J.; [1853]; *Documents of the project for the St. Peter Castle*. Kriegsarchive, Wien

Borri A., Avorio A., Cangi G., 1999. *Riparazione e consolidamento degli edifici in muratura.* In Regione dell'Umbria - Gurrieri F. (a cura di), Manuale per la riabilitazione e la ricostruzione post-sismica degli edifici, DEI - Tipografia del Genio Civile, Roma (in IT).

Borri A., Castori G., Corradi M., Grazini A., Casadei P., Giannantoni A.; [2006]; *SRP/SRG: sperimentazione e applicazioni per il miglioramento sismico ed il consolidamento degli edifici in muratura*, Proceedings of the Conference on Wonder Masonry 2006, 6th April, Florence, pp.193-206, Italy (in IT).

Borri A., Casadei P., Castori G., Hammond J.; [2009]; *Strengthening of brick masonry arches with externally bonded steel reinforced composites,* Journal of Composites for construction, n.13: pp. 468-475.

Borri A., Paci G., De Maria A.; [2011]; *Resistenza a taglio delle murature: prove diagonali e correlazione con l'Indice di Qualità Muraria IQM*. ANDIS 2011, Bari, Italy. (in IT)

Borri A., Castori G., Corradi M.;[2011b]; *Intrados strengthening of brick masonry arches with composite materials*, Composites: Part B. n. 42 pp 1164-1172.

Bosiljkov V. Tomazevic M, Binda L., Tedeschi C., Saisi A., Zanzi L., da Porto F., Modena C. and Valluzzi M.V. [2004]; Combined in-situ test for the

assessment of historic masonry structures in seismic regions. Int. Conference on Structural Analysis of Historical Construction, 10-13November, 2004, Padova, Italy.

Briccoli Bati S., Tonietti, U.; [1993]: *Determinazione dello sforzo nelle catene metalliche di vecchi edifici*. Nat. Conf. Prove non Distruttive Monitoraggio Diagnostica, Ferrara. (in IT).

Briccoli Bati S., Rovero L.; [2000]; *Consolidation of masonry arches with carbon fiber reinforced plastics,* 12th Brick & Block Masonry Conference, 25-28 June, Madrid, Spain.

Briccoli Bati S., Tonietti U.; [2001]; *Experimental Methods for estimating in situ tensile force in tie-rods*. Journal of Engineering Mechanics, n. 127(12): pp. 1275-1283.

Briccoli Bati S., Rovero L., Tonietti U.; [2007]; *Strengthening masonry arches with composites materials* Journal of Composites for Construction, n.11(1): pp. 33-41.

Briccoli Bati S., Rovero L.; [2007a]; *Towards a methodology for estimating strength and collapse mechanism in masonry arches strengthened with fibre reinforced polymer applied on external surfaces*; RILEM Materials and Structures, n. 41(7): pp. 1291–1306.

Brincker R., Zhang L., Andersen P.; [2001]; *Modal identification of output-only systems using frequency domain decomposition*, Smart Materials and Structures, n. 10: pp. 441-445.

Brownjohn J.M.W., Magalhaes F., Caetano E., Cunha A. [2010] *Ambient vibration re-testing and operational modal analysis of the Humber Bridge*, Engineering Structures, n. 32(8): pp. 2003-2018.

Caetano E. [2000]; Dynamic of Cable-stayed Bridges: Experimental Assessment of Cable-Structure Interaction, Engineering Faculty of University of Porto, PhD Thesis, Portugal.

Cangi G. (2012). *Manuale del recupero strutturale e antisismico*. DEI, Roma. (in IT)

Cantieni R.; [2006]; *Office floor vibrations: modal parameter identification and vibration monitoring*, ISMA 2006, 18-20 September, Leuven, Belgium, pp. 2937-2948.

Carbonara G.; [1996]; *Restauro Architettonico*, UTET, Torino, Italy. (in IT)

Cardani G, Valluzzi M.R., Panizza M., Binda L.; [2015]; *In-situ evaluation of composites-to-masonry bond in a natural aggressive environment*. 12th North American Masonry Conference, 17-20 May, Denver, Colorado.

Carloni C., Focacci F.; [2016]; *FRP-masonry interfacial debonding: An energy balance approach to determine the influence of the mortar joints*, Europ. Journal of Mechanics A/Solids, n. 55. pp. 1722-133.

Casarin F.; [2006]; *Structural assessment and seismic vulnerability analysis of a complex historical building*, Univeristy of Trento, PhD Thesis, Italy.

Castigliano C.A.P.; [1879]; Théorie de l'équilibre des systèmes élastiques et ses applications. Augusto Federico Negro, Turin (in FR).

Castori G. [2006], *Strengthening of masonry elements with innovative composite laminates*, University of Perugia, PhD Thesis, Italy.

Ceravolo R., Zanotti Fragonara L., Abbiati G.; [2010]; *Relazione: Identificazione dinamica. Realizzazione e taratura del modello della chiesa di S. Caterina in Casate Monferrato*. Politecnico di Torino, Torino, 2010 (in IT).

Ceravolo R., Matta E., Quattrone A., Zanotti Fragonara L.; [2013]; *Identificazione dinamica sperimentale di edifici strategici sotto sisma.* XV Convegno ANIDIS 30th June 4th July, Padova, Italy (in IT).

Cerroni F. Ferracuti B., Pecce M., Savoia M.; [2014]; *Assessment of a bond strength model for FRP reinforcement externally bonded over masonry blocks*, Journal of Composites: Part B, n. 61: pp. 147-161.

Cescatti E., Deiana R., Rosato L., Modena C.; [2015]. *Evaluation of injection intervention on real case in a medieval complex.* 12th North American Masonry Conference, 17-20 May, Denver, Colorado.

Cescatti E.; [2012]; Behaviour of RC beams strengthened in shear with NSM FRP reinforcement, MSc Thesis, University of Padova, Italy.

Cescatti E., Campostini G., Donà M., Rosato L., Bettiol G. Valluzzi M.R. and Modena C; [2015b]; *Applicazione delle metodologie integrate sviluppate per siti urbani,* Pro.Va.Ci. Project. Deliverable 7.2 (in IT).

Cescatti E., Lorenzoni F., Rosato L., Valluzzi M.R. and Modena C; [2015c]; *Applicazione delle metodologie integrate sviluppate, in particolar modo in relazione all'analisi di vulnerabilità sismica, per siti archeologici* Pro.Va.Ci. Project. Deliverable 7.3 (in IT).

Cescatti E., da Porto F., Modena C, Casarin F.; [2016a]; *Ties in historical constructions: typical features and laboratory tests,* 10th Int. Conference on Structural Analysis of Historical Constructions, 13-15 September, Leuven, Belgium. (in press)

Cescatti E., Dalla Benetta M., Modena C., Casarin F.; [2016b] *Analysis and evaluations of flat jack test on a wide existing masonry buildings sample*, 16th Int. Brick & Block Masonry Conference, 26-30 June, Padova, Italy. (in press)

Chen Y., Ashour A.F., Garrity S.W.; [2007]; *Modified four-hinge mechanism analysis for masonry arches strengthened with near-surface reinforcement;* Journal of Engineering Structures, n. 29: pp 1864-1871.

Chopra A.K. [2001]; *Dynamics of Structures, Theory and Applications to Earthquake Engineering*, Second Edition, Prentice Hall, New Jersey USA.

da Porto F., Valluzzi M.R., Modena C; [2003]; *Use of sonic tomography for the diagnosis and the control of intervention in historic masonry buildings*, Proceedings BB 85-CD, International Symposium Non-Destructive Testing in Civil Engineering, 16-19 September, Berlin, Germany.

da Porto F., Franchetti P., Grendene M., Ranzato M., Valluzzi M.R., Modena C.; [2007]; *Structural capacity of masonry arch bridges to horizontal loads.* 5th International Conference on Arch Bridges, 12-14 September, Madeira, Portugal.

da Porto F, Silva B., Catarina C. & Modena C.; [2012]; *Macro-Scale Analysis of Damage to Churches after Earthquake in Abruzzo (Italy) on April 6*; Journal of Earthquake Engineering, n. 16: pp 739-758.

Dalla Benetta M.; [2012]; *Qualificazione di murature storiche: procedure sperimentali in sito e calibrazione in laboratorio*, Phd Thesis, University of Padova, Italy (in IT)

Dardano D., Miranda J. C., Persichetti B., Valvo, P.; [2005]; *Un metodo per la determinazione del tiro nelle catene mediate identificazione dinamica*. 11th Conf. Naz. Prove non Distruttive, Monitoraggio e Diagnostica, Milano. (in IT)

D'Ayala D., Speranza E.; [2003]; *Definition of collapse mechanisms and seismic vulnerability of historic masonry buildings*. Journal of Earthquake Spectra, n. 19: pp. 479-509.

de Lorenzis L., Zavarise G.; [2009]; *Interfacial stress analysis and prediction of debonding for a thin plate bonded to a curved substrate*. Journal of Non-Linear Mechanics, n. 44: pp. 358-370.

de Felice G., De Stantis S., Garmendia L., Ghiassi B, Larringa P., Lourenço P., Oliverira D., Paolacci F., Papanicolaou C.; [2014]; *Mortar-based systems for externally bonded strengthening of masonry;* Journal of Materials and Structures, n. 47: pp. 2021–2037.

Doglioni, F., Moretti, A. and Petrini V.; [1994]. *Le chiese ed il terremoto*. ed. LINT, Trieste, Italy. (in IT)

Drougkas A., Roca P., Molins C. [2015] *Numerical prediction of the behaviour, strength and elasticity of masonry in compression,* Journal of Engineering Structures, n. 90: pp. 15-28.

Faiella D., Manfredini G., Rossi P.P.; ;[1983] *In situ flat jack tests: analysis of results and critical assessment* Int. symposium in situ test testing, Vol 2. Paris.

Ferrario L., Marini A., Riva P., Giuriani E.; [2008] ; ReLUIS 2005-2008 deliverable, *Allegato 3a.2-UR11-12 " tecniche di rinforzo per strutture voltate in muratura soggette ad azione sismica"* (in IT).

Ferrario L., Marini A., Riva P., Giuriani E.; [2010] *Proportioning criteria for traditional and innovative extrados techniques for the strengthening of barrel vaulted structures subjected to rocking of the abutments,* journal of Civil Engineering and Architecture Vol 4 n 26. ISSN 1934-7359.

Feenstra P.H.; [1993]; *Computational aspects of biaxial stress in plain and reinforced concrete*, University of Delft, PhD Thesis.

Foraboschi P. [2001] *Strength assessment of masonry arch retrofitted using composite reinforcements* Journal of British Masonry Society, n. 15(1): pp. 17–25.

Foraboschi P. [2004] *Strengthening of Masonry Arches with Fiber-Reinforced Polymer Strips* Journal of Composites for Construction, n. 8(3): pp. 191-202.

Galilei G.; [1638]; *Discorsi e dimostrazioni matematiche intorno a due nuove scienze attinenti alla meccanica e ai moti locali*. Leida, Belgium. (in IT)

Garmendia L.; [2010]; *Rehabilitation of masonry arches by a compatible and minimally invasive strengthening system,* University of Bilbao, PhD Thesis Spain.

Garmendia L., Larrinaga P., San-Mateos R., San-José J.T.; [2015]; *Strengthening masonry vaults with organic and inorganic composites: An experimental approach*. Journal of materials and design. n. 85: pp. 102-114.

Garzera R., Collini L., [2009]; *Identificazione della tensione nelle catene di edifici storici mediante analisi modale,* AIPnD 15-17th October, Rome. (in IT)

Gentile C. Saisi A.; [2004] Dynamic-based F.E. model updating to evaluate damage in masonry towers, Proc. 4 th Int. Seminar on Structural Analysis of Historical Constructions, 10-12 Padova 2004: pp 439–449.

Gentile C., Gallino N.; [2007]; *Ambient vibration-based investigation of the "Victory" arch bridge*, 5th International Conference on Arch Bridges, 12-14 September, Madeira, Portugal.

Gentile C., Saisi A., Cabboi A.; [2015]; *Structural Identification of a Masonry Tower Based on Operational Modal Analysis*, Int. Journal of Architectural Heritage: Conservation, Analysis, and Restoration, n. 9(2): pp. 98-110.

Ghiassi B., Silva M.M.M, Marcari G.,Oliveira D., Lourenço P. [2012]; *Moisture effects on the bond strength of FRP-masonry elements*, 6th Conference on FRP Composites in Civil. Engineering CICE, 13-15 June, Rome, Italy.

Ghiassi B, Macari G., Oliveira D., Lourenço P.B.; [2012b]; *Numerical analysis of bond behavior between masonry bricks and composite materials,* Journal of Engineering Structures, n.43: pp 210-220.

Giamundo V., Lignola G.P., Maddaloni G., da Porto F., Prota A., Manfredi G.; [2014]; *Shaking table test for seismic assessment of a full scale clay brick masonry vault.* Journal of Earthquake Engineering and Structural Dynamics.

Gilbert M. [2007]; *Limit analysis applied to masonry arch bridges: state-of-the-art and recent developments*. 5th International Conference on Arch Bridges, 12-14 September, Madeira, Portugal.

Girardello P.; [2013]; Rinforzo di volte in muratura con materiali compositi innovativi. University of Brescia, PhD Thesis (in IT)

Giresini L., Butenweg C., Andreini M., De Falco A., Sassu M..; [2014]; *Numerical calibration of a macro-element for vaulted systems in historic churches.* 9th Int. Conference on Structural Analysis of Historical Construction, 14-17 October, Mexico City, Mexico.

Giuffré A.; [1990]; *Letture sulla meccanica delle murature storiche,* Kappa Ed., Bologna, Italy. (in IT)

Giuffré A.; [1993] *Sicurezza e conservazione nei centri storici. Il caso di Ortigia,* Laterza Ed., Bari, Italy (in IT)

Giuffré A., [2010]; *Leggendo il libro delle antiche architetture. Aspetti statici del restauro saggi 1985-1997.* Ed. Cangemi, Roma, Italy (in IT)

Grinzato E. Petracca A., Morisi C., Bison P., Cadelano G., Milano L., Mannella A.; [2009]; *Valutazione del rischio sismico assistita dalla termografia IR,* Edilizia, n. 161 pp 35-36 (in IT).

Grünthal, G. [1998] *European Macroseismic Scale 1998 - EMS98;* Cahiers du Centre Européen de Géodynamique et de Séismologie 15, Centre Européen de Géodynamique et de Séismologie, Luxembourg, p. 99.

Guadagnini M., Serbescu A., Palmieri A., Matthys S., Billotta A., Nigro E., Ceroni F., Czaderski C., Olia S., Szabo Z., Balazs G., Mazzotti C.; [2012]; *Round Robin test on the bond behaviour of externally bonded FRP system to concrete.* 6th Conference on FRP Composites in Civil. Engineering CICE, June 13-15, Rome, Italy.

Gvozdev A.A.; [1960]; *The determination of the value of collapse load for statically indeterminate systems undergoing plastic deformation*. International Journal of Mechanical Sciences, n.1: pp. 322-35.

Hendry A. W.; [1981]; *Structural masonry*, 1st Ed. MacMillan Press, Basingstoke, UK.

Heyman J. [1966]; *The stone skeleton*; Int. Journal of Solid Structures, n.2: pp. 274-279.

Heyman J.; [1995]; *The stone skeleton. Structural engineering of masonry architecture,* Cambridge University Press. Cambridge.

Heyman J.; [1996]; *Arches, Vaults and Buttresses: Masonry Structures and their Engineering,* Variorum, Aldershot, Great Britain.

Hilsdorf H.K.; [1969]; *Investigation into the failure mechanism of brick masonry loaded in axial compression*. Proc. International Conference on Masonry Structural Systems, Texas, pp. 34-41.

Hojdys L, Krajewski P [2012]; *Experimental tests on strengthened and unstrengthened masonry vault with backfill,* Journal of Heritage Conservation n. 32: pp. 105-108.

Huerta S.; [2001]; *Mechanics of masonry vaults: The equilibrium approach*, Historical Constructions. Possibilities of numerical and experimental techniques, Lourenço & Roca ed., pp. 47-70, ISBN 972 8692 01 3

Keersmaekers R., Van Rickstal F., Van Gemert D.; [2004]; Geo-electrical techniques as a non-destructive appliance for restoration purposes, Int. Conference on Structural Analysis of Historical Construction, 10-13 November, Padova, Italy.

Khoo C.L. and Hendry A.W. 1973. *A failure criterion for brickwork in axial compression*, 3rd International Masonry Conference, Essen, pp. 139-145.

Lagomarsino S., Brencich A., Bussolino F., Moretti, A., Pagnini, L. C. Podestà, S. [1997]; *Una nuova metodologia per il rilievo del danno alle chiese: prime considerazioni sui meccanismi attivati dal sisma*. Ingegneria Sismica, n. 3: pp. 70-82. (in IT).

Lagomarsino, S. and Podestà, S.; [2004]; *Seismic vulnerability of ancient churches: I. Damage assessment and emergency planning*; Earthquake Spectra, n. 20: pp. 377–394.

Lagomarsino S., Calderini C.; [2005]; *The dynamical identification of the tensile force in ancient tie-rods,* Journal of Engineering Structures, n. 27: 846–856.

Lancaster L.C.; [2005]; *Concrete vaulted construction in Imperial Rome*, Cambridge University press, Cambridge, UK.

Liu K, Wu Y-F.; [2012]; *Analytical identification of bond–slip relationship of EB-FRP joints*, Journal of Composites Part B: Engineering, n. 43: pp. 1955-1963.

Lopez M.A. M.; [2004]; *A review of existing pushover methods for 2-D reinforced concrete Buildings,* Rose school, Pavia, Thesis.

Lourenço P.B.; [1996]; *Computational strategies for masonry structures*, University of Deft, PhD Thesis.

Lourenço P.B., Rots J.G.; [1997]; *Multisurface Interface model for analysis of masonry structures,* Journal of Engineering Mechanics, n.123: pp. 660-668.

Lourenço P.B.; [2001]; *Analysis of historical constructions: From thrust-lines to advanced simulations,* Historical Constructions, P.B. Lourenço, P. Roca (Eds.), Guimarães, pp. 91-116.

Lourenço P.B.; [2002]; *Computations on historic masonry structures*, Journal of structural engineering and materials, n. 4: pp. 301-319.

Lourenço, P.B.; [2009]. *Recent advances in masonry modeling: micromodelling and homogenisation*. In: U. A. M. H. Galvanetto, ed. Multiscale Modeling in Solid Mechanics: Computational Approaches. London: Imperial College Press.

Lourenço P.B.; Abrams D. P., Mendes N., Costa A.A. Campos Costa A.; [2015]; *Challenges in modeling out-of-plane seismic response of existing masonry builgings,* 12th North American Masonry Conference, 17-20 May, Denver, Colorado.

Lu X.Z., Teng. L.P., Ye L.P., Jiang J.J.;[2005]; *Bond-slip models for FRP/sheet/plates bonded to concrete*. Journal of Engineering Structures n.27: pp. 920-937.

Luong T.; [2010]; *Identification of the tensile force in tie-rods using modal analysis tests*, Guimaraes, Portugal SAHC Master Thesis.

Maier L.B., Rossi P.P., Landriani G.S; [1983]; *Diagnostic analysis of masonry buildings*. 8 p. 1983. in 1st ASBE Symposium, 29-30 September, Venice, Italy.

Magenes G., Bolognini D., Braggio C.; [2000]; *Metodi semplificati per l'analisi sismica non lineare di edifici in muratura,* CNR-GNDT, Roma, Italy. (in IT)

Mastrodicasa S.; [1981]; *Dissesti statici delle strutture edilizie*. Ulrico Hoepli, Milano (in IT)

Mazzon N. [2010], *Influence of Grout Injection on the Dynamic Behaviour of Stone Masonry Buildings,* University of Padova, PhD Thesis.

Milani G., Fedele R., Lourenço P, Basilio I.; [2014]; *Experimental and numerical FE analyses of curved masonry prisms and arches reinforced with FRP materials.* 9th Int. Conference on Structural Analysis of Historical Construction, 14-17 October, Mexico City, Mexico.

Meier U.; [1992]: *Carbon Fiber-Reinforced Polymers: Modern Materials in Bridge Engineering;* Structural Engineering International, pp. 7–12.

Melbourne C., Wang J. [2007]. *A new masonry arch assessment strategy (SMART)*, 5th International Conference on Arch Bridges, 12-14 September, Madeira, Portugal.

Méry E.; [1840]; Mémoire sur l'équilibre des voûtes en breceau, *Annales des Ponts et Chaussées,* I sér, I sem, n.19: pp. 50-70.

Modena C., Rossi P.P., Zonta D.; [1997]; *Static and dynamic investigation on the roman amphitethatre (Arena) in Verona*, Intern. Colloquium IABSE, May 1997, Bergamo.

Modena C., [2008]; *Aspetti strutturali: normativa in campo nazionale e internazionale,* in «Kermes. La rivista del restauro », XXI, n. 71: pp. 99-108 (in IT)

Modena, C., Casarin, F., da Porto, F., Garbin, E., Mazzon, N., Munari, M., Panizza, M. and Valluzzi, M. R.; [2009] *Structural interventions on historical masonry buildings: review of Eurocode 8 provisions in the light of the Italian experience*. In Quali prospettive per l'Eurocodice 8 alla luce delle esperienze italiane – Workshop Reluis-UNI, Naples (Italy).

Modena C, da Porto F., Bettiol G., Giarretton M.; [2012]; *Edilizia storica monumentale - Salvaguardia degli edifici di interesse storico-artistico nell'emergenza post-sisma;* Progettazione sismica, n. 3: pp. 211-221. (in IT)

Modena C., da Porto F., Valluzzi M.R.; [2012a]; *Conservazione del patrimonio architettonico e sicurezza sismica: insegnamenti dalle recenti esperienze italiane,* Materiali e strutture n. 1-2, Ed. Quasar, Roma (in IT)

Mosca L.; [2015]; *Metodi Dinamici sperimentali e numerici per la stima dello sforzo assiale in catene esistenti,* MSc Thesis. (in IT)

Newmark N.M., Hall W.J.; [1982]; *Earthquake spectra and design* Earthquake Engineering Research Institute, Berkeley, California, USA.

Niker [2012] Deliverable 9.4 *Report on the use of monitoring as knowledge based assessment and early warning tool. UniPD.*

Niker [2012] Deliverable 9.5 *Report on real case studies with definition of strategies for control of adequacy and quality level of interventions.* UPC

Navier C.L. M. H.; [1824] *Résumé des leçons données à l'Ecole des Ponts et Chaussées, sur l'application de la mécanique a l'établissement des constructions et des machines.* Paris; Saint-Venant, Paris 1864, Critical edn. (in FR)

Olivito R. S., Zuccarello F. A.; [2008]; *Quality control and monitoring of FRP application to masonry structures.* Strain, Blackwell Publishing Ltd, n. 45: pp. 340-348.

Orduña Bustamante A.; [2003]; *Seismic Assessment of Ancient Masonry Structures by Rigid Blocks Limit Analysis*; University of Minho, PhD Thesis.

Page A.W. [1981] *The biaxial compressive strength of brick masonry*. Proc. Institution of Civil Engineering, part 2, n. 71: pp. 893-906

Panizza M.; [2010]; *FRP strengthening of masonry arches: analysis of local mechanisms and global behaviour*. University of Padova, PhD Thesis.

Panizza M., Garbin E., Valluzzi M.R., Modena C.; [2012]; *Experimental investigation on bond of FRP/SRP applied to masonry prism*, 6th Conference on FRP Composites in Civil. Engineering CICE, 13-15 June, Rome, Italy.

Panizza M., Giradello P., Garbin E., Valluzzi M.R., Cardani G., Dalla Benetta M., Casadei P.; [2015] *On-site pull-out tests of steel anchor spikes applied to brickwork masonry 2015*, Key Engineering Materials n.624: pp 266-274.

Papanicolaou CG, Triantafillou TC, Karlos K, Papathanasiou M; [2007] *Textile-reinforced mortar (TRM) versus FRP as strengthening material of URM walls: in-plane cyclic loading.* Journal of Material Structure n. 40: pp. 1081–1097.

Park S, Choi A., Oh S.T, Stubbs N., Song H.C.; [2006] *Identification of the tensile force in high-tension bars using modal sensitivities,* Journal of Solids and Structures n. 43: pp. 3185–3196.

Peng C.Y.; [1987]; *Generalized modal identification of linear and nonlinear dynamic systems,* PhD Thesis, California Institute of Technology, USA.

Pérez-Gracia V., Caselles J.O., Clapés J., Martinez G., Osorio R.; [2013]; *Non-destructive analysis in cultural heritage buildings: Evaluating the Mallorca cathedral supporting structures*, NDT & E International, Vol. 59, pp 40-47,

Peeters B., De Roeck G.; [1999]; *Reference-Based Stochastic Subspace Identification for Output-Only Modal Analysis*. Mechanical Systems and Signal Processing, n. 13(6): pp. 855-878.

Pisani M.; [2008]; *Consolidamento delle strutture,* Ed, Ulrico Hoepli, Milano. (in IT)

Prota A, Marcari G, Fabbrocino G, Manfredi G, Aldea C; [2006] *Experimental in-plane behavior of tuff masonry strengthened with cementitious matrix-grid composites,* Journal of Composite Construction, n. 10: pp 223–233.

Poleni G.; [1748]; *Memorie istoriche della gran cupola del Tempio Vaticano*, Stamperia del seminario, Padova. (in IT).

Paulay, T., M.J.N. Priestley; [1992] *Seismic Design of Reinforced Concrete and Masonry Buildings*, Ed. J. Wiley, New York.

Ramos J. L.F.; [2007]; *Damage Identification on Masonry Structures Based on Vibration Signatures;* University of Minho; PhD Thesis.

Ramonda L.G.; [2015]; *Dynamic procedures to estimate the axial force in historical ties*, University of Padova, SAHC Master Thesis.

Rankine W. J. M.; [1858]; *A manual of applied mechanics,* Charles Griffin, London.

Rebecchi G., Tullini N., Laudiero F.; [2013]; *Estimate of the axial force in slender beams with unknown boundary conditions using one flexural mode shape*, Journal of Sound and Vibration, n. 332 (18): pp. 4122-4135.

Reinhardt H.W., Cornelissen H.A.W., Hordijk D.A., [1986] *Tensile tests and failure analysis of concrete*, Journal of Structural Engineering n. 112: pp. 2462-2477.

Reynders E., De Roeck G.; [2006]; *Reference-Based Combined Deterministic-Stochastic Subspace*, ISMA 2006, 18-20 September, Leuven, Belgium, pp. 3035-3046.

Ricamato M.; [2007]; *Numerical and experimental analysis of masonry arches strengthened with FRP materials;* University of Cassino; PhD Thesis.

RING® LimitState; [2015]; User manual.

Riva G., Bettio C., Modena C.; [2003]; *Valutazioni quantitative di caratteristiche meccaniche di murature in pietra mediante prove non distruttive.* Materiali e Strutture, problemi di conservazione. Anno I, nr 1. (in IT)

Roca P., Lopez-Almansa F., Miquel J., Hanganu A.; [2007]; *Limit analysis of reinforced masonry vaults*, Journal of Engineering Structures, n. 29: pp. 431–439.

Rossi M, Calderini C., Lagomarsino S. Milani G. [2014] *Seismic response of masonry vaulted structures: experimental and numerical modelling*, 9th Int. Masonry Conference, 7-9 July, Guimaraes, Portugal.

Rossi P.P.; [1985]; *Flat jack tests for the analysis of mechanical behaviour of brick masonry structures*, 7th Int. Brick masonry Conference, 17-20 February, Melbourne, Australia.

Rossi P.P.; [1987]; *Recent developments of the flat jack tests on masonry structures*, workshop Italy-USA, 18-29 August.

Rots J.G.; [1988] *Computational modeling of concrete fracture*, University of Deft, PhD Thesis.

Rubiò B.; [1912]; *Conferencia acerca de los conceptos organicos, mecanicos y constructivos de la Catedral de Mallorca*. Anuario de la Asociacion de Arquitectos de Cataluna, pp. 87-140.

Silva B., Dalla Benetta M., da Porto F., Valluzzi M.R; [2014] *Compression and sonic tests to assess the effectiveness of grout ingection on three-leaf stone masonry walls;* Journal of Architectural Heritage, n. 8: pp. 408-435.

Shaker F.J.; [1975] *Effect of axial load on mode shapes and frequencies of beams*, NASA Technical note (NASA TND-8109).

Straub H.; [1952]; *A History of Civil Engineering,* Leonard Hill, London.

Tao Y., Stratford T.J., Chen J.F.; [2011]; *Behaviour of a masonry arch bridge repaired using fibre-reinforced polymer composites*, Journal of Engineering Structures, 33 pp 1594-1606.

TNO DIANA®; [2015]; Documentation, User's manual - Realise 9.6.

Triantafillou, T. C., [1998a] *Strengthening of masonry structures using epoxy-bonded FRP laminates*, Journal of Composite for Construction, n. 2(2): pp 96–104.

Triantafillou, T. C., [1998b] *Errata for '**Strengthening of masonry structures using epoxy-bonded FRP laminates'*, Journal of Composite for Construction, n.2(4) : pp 203.

Tullini N., Laudiero, F. [2008] *Dynamic identification of beam axial loads using one flexural mode shape,* Journal of Sound and Vibration, n.318: pp. 131-147.

Valluzzi M.R.; [2000]; *Comportamento meccanico di murature storiche consolidate con materiali e tecniche a base di calce.* University of Padova, PhD Thesis. (in IT).

Valluzzi M.R., Valdemarca M., Modena C.; [2001]; *Behaviour of brick masonry vaults strengthened by FRP laminates,* Journal of composites for construction, n.5: pp. 163-169.

Valluzzi M.R.; [2003] *Consolidamento e recupero delle murature*, Collana Scientifica. Reficere, a cura del Prof. C. R. Romeo, Faenza Ed. (in IT)

Valluzzi M.R., Garbin E., Panizza M, Binda L., Tedeschi C.;[2011] *Moisture and Temperature Influence on FRP Masonry Bonding*. Conference on Durability of Building Materials and Components, 12th-15th April, Porto, Portugal.

Valluzzi M.R., Oliveira D. V., Caratelli A., Castori G., Corradi M., de Felice G., Garbin E., Garcia D., Garmendia L., Grande E., Ianniruberto U., Kwiecien A., Leone M., Lignola G.P., Lourenço P., Malena M., Micelli F., Panizza M., Papanicolaou C.G., Prota A., Sacco E., Triantafillou T., Viskovic A., Zajac B., Zuccarino G. Round Robin; [2012]; *Test for composite-to-brick shear bond characterization*, Journal of Material and Structures n.45. pp. 1761-1791.

Valluzzi M.R., Modena C., de Felice G.;[2014]; *Current practice and open issues in strengthening historical buildings with composites* Journal of Materials and Structures, n.47: pp 1971–1985.

van der Pluijm R.; [1992]; *Material properties of masonry and its components under tension and shear,* 6th Canadian Masonry Symposium, eds. V.V. Neis, Saskatoon, Saskatchewan, Canada, pp. 675-686.

Venice Charter; [1964]; *International Charter for the Conservation and Restoration of Monuments and Sites*. II International Congress of Architects and Technicians of Historic Monuments, 31 May, Venice.

Vignoli A., Boschi S, Modena C., Cescatti E.; [2016]; *In-situ mechanical characterization of existing masonry typologies: a research project in Italy finalized to update the structural codes*, 16th Int. Brick & Block Masonry Conference, June 26-30, Padova, Italy. (in press)

Vincenzi L.; [2007]; *Identificazione dinamica delle caratteristiche modali e delle proprietà meccaniche di strutture mediante algoritmi di ottimizzazione.* University of Bologna, PhD Thesis. (in IT)

Viollet-le-Duc, Eugene E. 1854–1868. *Dictionnaire raisonnée de l'Architecture Française du XI au XVI siécle.* Paris: A.Morel (in French).

Watkin D.; [1996] *History of Western Architecture - Second Edition*, Laurence King Ltd, London.

Zampieri P.; [2013]; *Simplified seismic vulnerability assessment of masonry arch bridges,* University of Trento, PhD Thesis.

**TECHNICAL DOCUMENTATION**

ACI 440.7R-2010; [2010]; *Guide for the Design and Construction of Externally Bonded Fiber-Reinforced Polymer Systems for Strengthening Unreinforced Masonry Structures,* American Concrete Institute, Michigan, USA.

ACI 530-08 [2008]; *Building Code requirements for Masonry structures.* American Concrete Institute, Michigan, USA.

ACI 549.4-R-13 [2013]; *Guide to Design and Construction of Externally Bonded FRCM Systems for Repair and Strengthening Concrete and Masonry Structures*, American Concrete Institute, Michigan, USA.

ASCE 41-13; [2014] *Seismic Evaluation and Retrofit of Existing Buildings*. American Society of Civil Engineers, Reston, Virgina.

ASTM C1196:14; [2009]; *Standard Test Method for In Situ Compressive Stress Within Solid Unit Masonry Estimated Using the Flatjack measurements,* ASTM International, West Conshohocken, PA, USA.

ASTM C1197:14a; [1991], *Standard Test Method for In Situ measurement of masonry deformability properties using the flatjack method*, ASTM International, West Conshohocken, PA, USA.

ASTM C1583/C1583M-13; [2013] *Standard Test Method for Tensile Strength of Concrete Surfaces and the Bond Strength or Tensile Strength of Concrete Repair and Overlay Materials by Direct Tension (Pull-off Method)*, ASTM International, West Conshohocken, PA, USA.

CNR-DT 200 R1/2012 [2012], *Istruzioni per la progettazione, l'esecuzione ed il controllo di interventi di consolidamento statico mediante l'utilizzo di compositi fibrorinfozati.* Consiglio nazionale delle ricerche. *(in Italian)*

CNR-DT 212/2013 [2013], *Istruzioni per la valutazione affidabilistica della sicurezza sismica di Edifici Esistenti.* Consiglio nazionale delle ricerche. (in IT)

C.S.LL.PP. 24/07/2009; [2009]; Linee guida per la Progettazione, l'esecuzione ed il Collaudo di Interventi di Rinforzo di strutture di c.a., c.a.p e murarie mediante FRP. (in IT)

EN 771-1:2011 [2011], Specification for masonry units - Part 1: Clay masonry units.

EN 1996 [2005]; *Eurocode 6 - Design of masonry structures;* CEN standards.

EN 1998 [2005]; *Eurocose 8 - Design of structures for earthquake resistance;* CEN standards.

FIB 14th; [2011];. *Last draft bulletin 14th*. Federation International du Beton, Technical report, fibTG9.3-EBR Bulletin 14-th. Unpublished.

ISCARSAH- ICOMOS, [2005]; *Recommendation for the analysis and restoration of structures of architectural heritage*. Barcelona.

ISO 13882; [2010]; *Bases for design of structures -- Assessment of existing structures*, International Organization for Standardization, Geneva, CH.

LL.GG.BB.CC. [2010] Guidelines for evaluation and mitigation of seismic risk to cultural heritage, Ministry for Cultural Heritage and Activities, Rome.

RILEM MDT-04; [2004]. *In-situ stress tests based on the flat jack* Reccomendation MDT.4, RILEM TC 177-MDT: 'Masonry durability and on-site testing'.

RILEM MDT-05; [2004]. *In situ stress strain behaviour tests based on the flat jack.* Reccomendation MDT.5, RILEM TC 177-MDT: 'Masonry durability and on-site testing'.